Design, Development and Nanoparticle based delivery of Topoisomerase II beta poisoning derivatives of Ferrocene
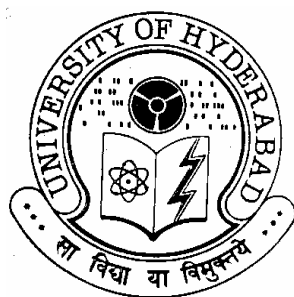
A thesis submitted for the degree of

DOCTOR OF PHILOSOPHY

by
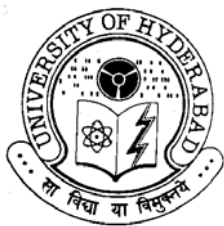
A.D. SAI KRISHNA

Department of Biochemistry

School of Life Sciences

University of Hyderabad

Hyderabad- 500 046, A.P., INDIA.

February 2008

University of Hyderabad

School of Life Sciences

Department of Biochemistry
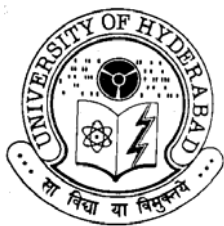
Hyderabad- 500 046, (A.P.), INDIA.

DECLARATION

I hereby declare that the work presented in my thesis is entirely original and was carried out by me in the Department of Biochemistry, University of Hyderabad, under the supervision of Prof. Anand K. Kondapi. I further declare that this has not been submitted before for the award of degree or diploma from any Institute or University.

Date   A.D.Sai Krishna

Prof.Anand K. Kondapi

University of Hyderabad

School of Life Sciences

Department of Biochemistry

Hyderabad- 500 046, (A.P.), INDIA.

CERTIFICATE

This it to certify that thesis entitled **"Design, Development and Nanoparticle based delivery of Topoisomerase II beta poisoning derivatives of Ferrocene"** submitted to the University of Hyderabad by Mr. **A.D. Sai Krishna** for the degree of Doctor of Philosophy, is based on the studies carried out by him under my supervision. This work has not been submitted before for the award of degree or diploma from any University or Institution.

Prof.Anand K.Kondapi

Supervisor

Head, Department of Biochemistry

Dean, School of Life Sciences

Date:

Sai Krishna

ABBREVIATIONS:

ATP	Adenosine triphosphate
Kbp	Kilo base pairs
BSA	Bovine serum albumin
DNA	Deoxy ribonucleic acid
EDTA	N,N ethylene diamine tetra acetic acid
KDa	Kilo Dalton
Min	Minutes
μl	Micro liter
μg	Micro gram
PAGE	Poly acrylamide gel electrophoresis
SDS	Sodium dodecyl sulphate
Topo II	Topoisomerase II
Tris	Tris(hydroxy methyl) aminomethane
LB	Luria bertani
Ct DNA	Calf thymus DNA
TEMED	Tetramethyl ethylene diamine
Ppt	Precipitate
BCIP	5-bromo-4-chloro-3-indoyl phosphate
DMSO	Dimethyl sulphoxide
m-AMSA	n-[4-(9-acridinylamino)-3-methoxy phenyl] methanesulfonamide
mg	Milligram
μm	Micro molar
Tm	Melting temperature
UV	Ultra violet
Aza fecp/aza	Azalactone ferrocene
Thio fecp/ thio	Thiomorpholide amido methyl ferrocene
Fecp	Ferrocene
m-AMSA	Amasacrine
ZH5	Zajdela Ascitic Hepatoma cells
AFP	Alpha feto protein
RITC	Rhodamine isothiocyanate

S-100	Sepharose-100
MTT	(3-(4,5-Dimethylthiazol-2-yl)-2,5-diphenyltetrazolium bromide)
HSD	Honestly Significant Differences
Anova	Analysis of variance
TfR	Transferrin receptor
RBC	Red blood cell
SEM	Scanning electron microscope
TEM	Transmission electron microscope
AFM	Atomic force microscope
nm	Nano meter
PBS	Phosphate buffer saline
3D	Three dimension
rpm	Rotations per minutes
HCl	Hydrochloric acid
H_2SO_4	Sulphuric acid
DMSO	Dimethyl sulphoxide
IR	Infra red spectroscopy
NMR	Nuclear magnetic resonance
r^2	Correlation coefficient
r^2cv	Cross validated Correlation coefficient
PRESS	Predicted sum of squares
QSAR	Quantitative structure activity relationship
S	Supercoiled form
R	Relaxed form
^{32}P	γ phosphate labeled ATP
Lk	linking number
Tw	number of twists or turns of the double helix
PFA	Paraformaldehyde fixation
NADH	Nicotinamide adenine dinucleotide
LDH	Lacatate dehydrogenase
PNPP	Para nitro phenyl phosphate
DTT	Dithio theritol
PCA	Principle component regression

PLS	Partial least square
MFA	Molecular field analysis
RSA	Receptor shape analysis
GFA	Genetic function approximation
Topo	Topoisomerase
TCA	Trichloro acetic acid
G/PLS	Genetic partial least squares

Contents

CHAPTER I

INTRODUCTION

DNA Topology

One of the most striking features of DNA is the intertwining of the two complementary strands of the double helix (1). Discovery of these characteristics led to the immediate recognition that biological processes such as replication would be severely affected by the topological state of the genetic material (2).

DNA in all species ranging from bacteria to humans is globally underwound (i.e., negatively supercoiled) (3-6). This underwinding makes it easier to separate complementary DNA strands from one another and greatly facilitates initiation of replication and the assembly of replication forks. Once the fork begins to travel along the DNA template, however, the deleterious effects of topology manifest themselves (Figure 1). Since helicases separate, but do not unwind the two strands of the double helix, fork movement results in acute over winding (i.e., positive supercoiling) of the DNA ahead of the replication machinery (3, 5-7). This over winding has two major consequences. First, it increases the difficulty of separating duplex DNA into individual strands. Therefore, accumulation of positive super coils presents a formidable block to fork movement (5, 7-11). Second, DNA overwinding ahead of the fork leads to a compensatory underwinding behind the replication machinery. If the replisome rotates around the helical axis of the DNA, this underwinding allows some of the torsional stress in the pre-replicated DNA to be translated to the newly replicated daughter molecules in the form of precatenanes (Figure 1) (6, 7, and 11). If these precatenanes are not resolved, they ultimately lead to the formation of duplex daughter chromosomes.

The supercoiling induced by underwinding is therefore defined as negative supercoiling. Conversely, under some conditions DNA can be over wound, resulting in

positive supercoiling (12). Note that the twisting path taken by the axis of the DNA helix when the DNA is underwound (negative supercoiling) is the mirror image of that taken when the DNA is overwound (positive supercoiling). Supercoiling is not a random process; the path of the supercoiling is largely prescribed by the torsional strain imparted to the DNA by decreasing or increasing the linking number relative to B-DNA. Linking number can be changed by 1 by breaking one DNA strand, rotating one of the ends 360 about the unbroken strand, and rejoining the broken ends. This change has no effect on the number of base pairs or the number of atoms in the circular DNA molecule. Two forms of a circular DNA that differ only in a topological property such as linking number are referred to as topoisomerase. Linking number can be broken down into two structural components called writhe (Wr) and twist (Tw) (13). These are more difficult to describe than linking number, but writhe is a measure of the coiling of the helix axis and twist as determining the local twisting or spatial relationship of neighboring base pairs. When the linking number changes, some of the resulting strain is usually compensated for by writhe (supercoiling) and some by changes in twist, giving rise to the equation

$$Lk = Tw + Wr$$

Tw and Wr need not be integers. Twist and writhe are geometric rather than topological properties, because they may be changed by deformation of a closed-circular DNA molecule

Topoisomerases Catalyze Changes in the Linking Number of DNA

DNA supercoiling is a precisely regulated process that influences many aspects of DNA metabolism. Every cell has enzymes with the sole function of underwinding and/or relaxing DNA. The enzymes that increase or decrease the extent of DNA underwinding are topoisomerases; changing the linking number of DNA. These enzymes play an especially important role in processes such as replication and chromosomal remodelling. There are two

Figure 1.1

Reactions catalysed by type II DNA topoisomerases
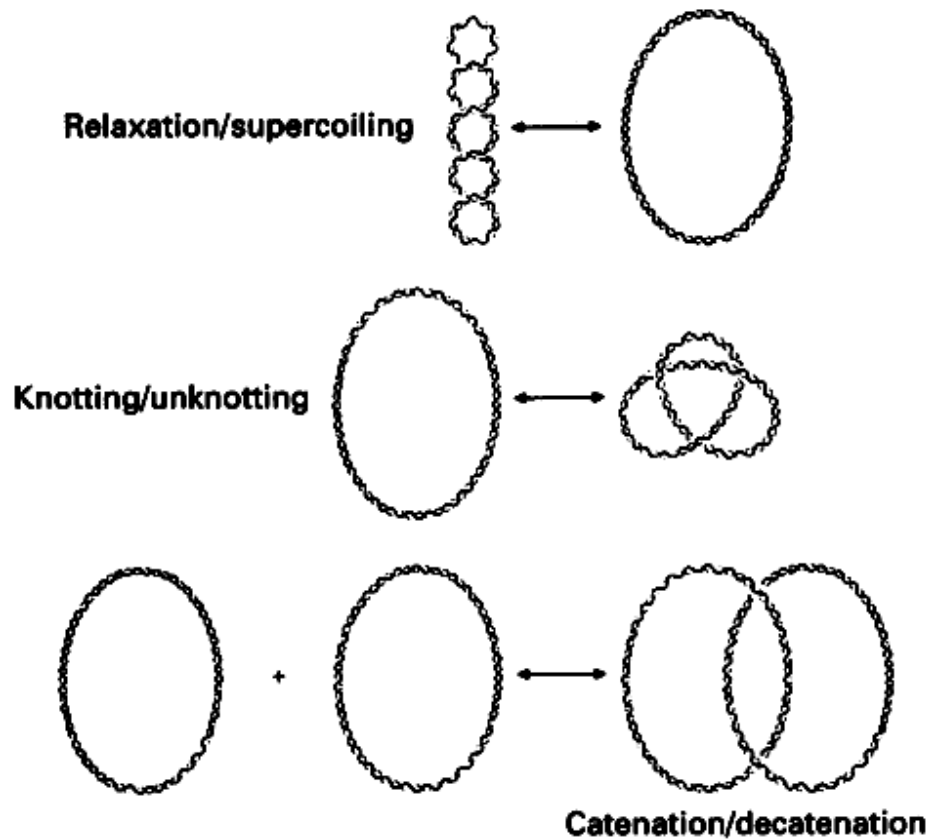
All of these reactions can be catalysed by certain classes of type II enzymes; however, the promotion of DNA supercoiling is unique to bacterial DNA gyrases (for negative supercoiling, as shown) and reverse gyrases (for positive supercoiling, not shown). (16)

classes of topoisomerases. Type I topoisomerases act by transiently breaking one of the two DNA strands, passing the unbroken strand through the break, and rejoining the broken ends; they change Lk in increments of 1(14). Type II topoisomerases break both DNA strands and change Lk in increments of 2 (Fig 1.1) (15). The effects of these enzymes can be demonstrated using agarose gel electrophoresis. A population of identical plasmid DNAs with the same linking number migrates as a discrete band during electrophoresis. Topoisomerase with Lk values differing by as little as 1 can be separated by this method, so changes in linking number induced by topoisomerases are readily detected. Various topoisomerases from different sources were presented in Table 1.1

DNA Topoisomerases

The topological state of DNA in the cell is modulated by enzymes known as topoisomerases (5, 7, 17-21). These ubiquitous enzymes regulate DNA over-and underwinding, and remove knots and tangles from the genetic material by creating transient breaks in the sugar-phosphate backbone of the double-helix (5, 7, 17-23). Topoisomerases maintain genomic integrity during this process by forming covalent attachments between their active site tyrosyl residues and the terminal DNA phosphates generated during the cleavage reaction (7, 17, 20, 21). This covalent linkage is the hallmark characteristic of all DNA topoisomerases. The actions of these enzymes allow the progression of virtually all metabolic events in the cell.

Table 1.1

Topoisomerase II Classification (25)

Name	Class	Organism	Special Features
Topoisomerase (ω protein)	I	E. coli.	Relaxes only negatively supercoiled DNA
Topoisomerase III	I	E coli.	Involved in chromosome stability and plasmid segregation
DNA gyrase	II	E. coli.	Introduces negative supercoiling. Required for chromosome replication/segregation
Topoisomerase IV	II	E coli.	No supercoiling activity. Required for chromosome segregation/cell division
Reverse gyrase	I	Various thermophilic bacteria	Introduces positive supercoiling
Topoisomerase I	I	S. cerevisiae	Relaxes negatively and positively supercoiled DNA
Topoisomerase II	II	S. cerevisiae	No supercoiling activity. Essential for chromosome segregation
Topoisomerase III	I	S. cerevisiae	Recombination function
Topoisomerase I	I	Human	Relaxes negatively and positively supercoiled DNA
Topoisomerase IIα	II	Human	No supercoiling activity.
Topoisomerase IIβ	II	Human	No supercoiling activity.

Topoisomerase II

Type II topoisomerases act by generating a transient double-stranded DNA breaks, followed by a double-stranded DNA passage event (19-21,25). Consequently, these enzymes are able to remove superhelical twists from DNA and resolve knotted or tangled duplex molecules. Type II topoisomerases are required for replication, recombination, chromosome segregation, and proper chromosome condensation and decondensation (5,7, 22,17-21).

Topoisomerase II isoforms

Whereas lower eukaryotes such as yeast and Drosophila encode only a single type II topoisomerase (26,27), vertebrate species express two discrete forms of the enzyme, topoisomerase II α and II β (19,23,28,29). These enzymes display a high degree of amino acid sequence identity (~70%) and similar enzymological characteristics. However, they differ in their protomer molecular and masses (170 vs. 180 kDa, respectively) and are encoded by separate genes (19, 23, 30). Either topoisomerase II α or β can complement the loss of topoisomerase II in yeast (31-33), but the two enzymes have distinct patterns of expression and physiological functions in vertebrate cells.

Topoisomerase II α is upregulated dramatically during cell proliferation and is tightly associated with mitotic chromosomes (18, 34-37). In contrast, expression of the β isoform is independent of proliferative status and the enzyme dissociates from chromosomes during mitosis (18,30,34,38). Thus, topoisomerase II α is believed to be the isoform that functions in growth-dependent processes, such as DNA replication and chromosome segregation (7,18)

Topoisomerase II Domain Structure

The primary structures of topoisomerase II α and β are very similar and based on the amino acid sequence comparisons with DNA gyrase (the best characterized prokaryotic type II topoisomerase) each topoisomerase II monomer can be divided into three distinct domains (Fig. 1.2) (5,19,20,23,30,41).

N-terminal domain: The N-terminal domain (first ~670 amino acids) of topoisomerase II is homologous to the β-subunit of DNA gyrase (GyrB). This portion of the enzyme contains the site of ATP binding and hydrolysis (19, 23, 42). Crystal structures of this domain recently were solved for yeast topoisomerase II (43) and human topoisomerase II α (44).

Central domain: The central domain (amino acids ~671-1200) of topoisomerase II is homologous to the A-subunit of DNA gyrase (GyrA) (19,23,45). This portion of the enzyme contains the active site tyrosine (amino acid 805 of topoisomerase II α and 821 of topoisomerase II β) required for DNA cleavage and religation. A crystal structure for this domain in the absence of a DNA substrate was solved for yeast topoisomerase II (46).

C-terminal domain: The C-terminal domain (amino acids ~1201-1521 for topoisomerase IIα and ~1201-1621 for topoisomerase II β) is highly variable among species and between the two human isoforms. This domain contains both nuclear localization sequences (47-53) and sites of phosphorylation (47, 54-56). Recent studies implicated C-terminal of protein in an intriguing and important role in the recognition of DNA geometry (54-60).

Figure 1.2:

Domain structures of topoisomerase II enzymes from prokaryotes and eukaryotes (16)

A schematic representation of the domain structure of one prokaryotic (E coli DNA gyrase) and four eukaryotic topoisomerase II enzymes is shown. DNA gyrase consists of two polypeptides, GyrB (left) and GyrA (right), while all eukaryotic forms are single polypeptide chains. The number of amino acid residues in each protein is indicated on the right. The N-terminal ATP binding domain is shown in light red. The ATP-binding region of E coli GyrB for which X-ray crystallographic data exists is indicated. The central DNA binding and DNA breakage/reunion domain is an open box. The C-terminal domain is grey. Additional notable features are: (1) A short N-terminal extension of unknown function in the S. pombe and human enzymes shown with black; (2) A horizontally hatched box denoting two amino acid motifs: EGDSA... PLRGK (single letter amino acid code) defining a conserved region in all type II topoisomerases; (3) The active-site tyrosine residue denoted by a black vertical line labeled Y; (4) putative nuclear localization signals denoted by red vertical lines labeled NLS. The domain boundaries have been defined by reference to protease-sensitive sites within the E coli or S. cerevisiae proteins. The DNA gyrase subunits each contain a preferred trypsin cleavage site, following arginine 393 (R393) in GyrB and arginine 571 (R571) in GyrA, marked by black arrowheads labeled TRY. The S. cerevisiae enzyme has two preferred sites for V8 proteinase digestion, after glutamate 410 (E410) and around residue 1200, marked by the black arrowheads labeled V8-A and V8-C, respectively. The third V8 cleavage site (V8-B*, at glutamate 680) is conditional upon ATP binding to the enzyme.

Figure 1.2

Domain structures of topoisomerase II enzymes from prokaryotes and eukaryotes
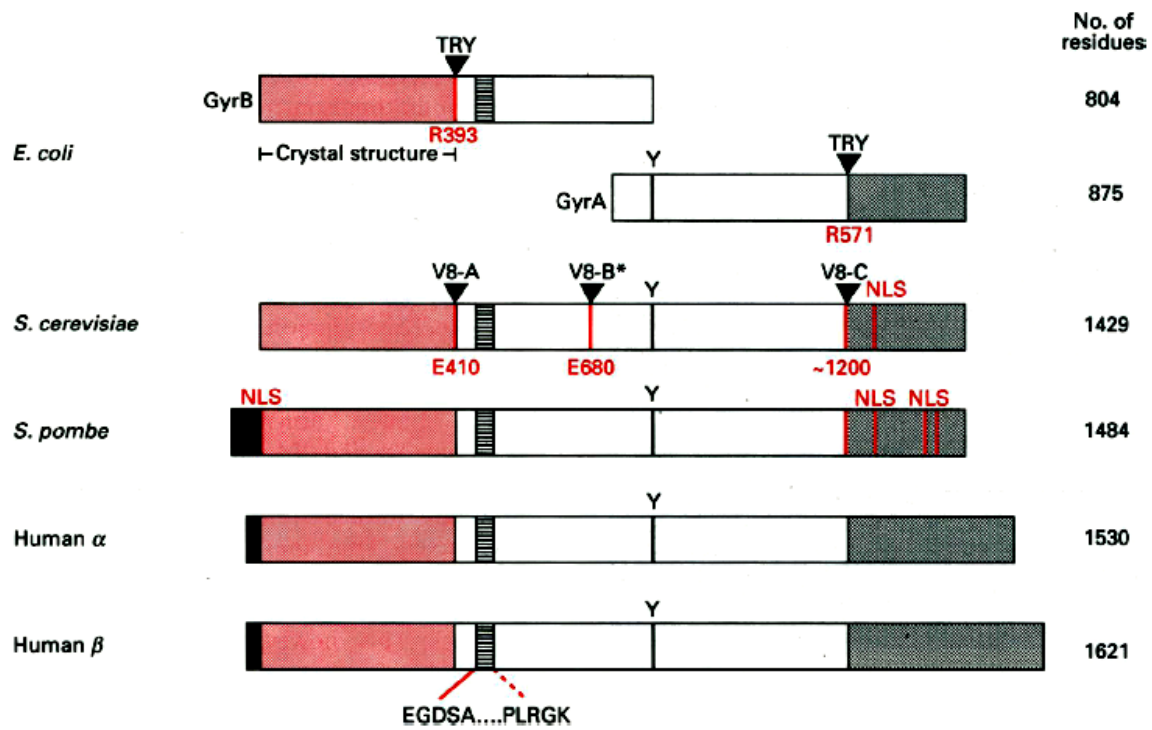
Catalytic cycle of topoisomerase II

As a result of its double-stranded DNA passage mechanism, topoisomerase II is able to remove negative or positive super helical twists (i.e., under- or overwinds) from the genetic material and resolve intramolecular DNA knots as well as intermolecular tangles (61-63). The ability to analyze specific steps of the topoisomerase II catalytic cycle has contributed greatly to our understanding of enzyme function and the interaction of topoisomerase II with anticancer drugs. A description of each step is as follows.

Step 1: DNA binding

Topoisomerase II catalytic cycle initiated by binding to its DNA substrate. This interaction requires no cofactor, Topoisomerase II-DNA interactions are governed by two properties of the double helix: nucleotide sequence and topological structure. Topoisomerase II can discern topological structures and interacts preferentially (as determined by levels of DNA binding and cleavage) with negatively or positively supercoiled nucleic acids over relaxed molecules (64-66). This differential recognition of DNA topology provides a straight forward mechanism by which the enzyme can interact strongly with its supercoiled DNA substrate, while releasing the relaxed DNA product. The ability of topoisomerase II to distinguish DNA topology probably stems from its recognition of points of helix-helix juxtaposition. However, it appears that the enzyme probably binds the two DNA segments in sequential order and that the first molecule bound is the segment that is cleaved (67- 68). Preferential binding to under- or overwound DNA by recognition of crossovers appears to be a common motif among eukaryotic topoisomerases and is shared with the type I enzyme (66, 69). Finally, the recognition of DNA topology appears to be modulated by the phosphorylation state of topoisomerase II. While binding to supercoiled DNA is unaffected by phosphorylation (70, 71), binding to relaxed (or linear) molecules is stimulated 2-3-fold following modification of the enzyme by casein kinase II (71).

Step 2: Pre-strand passage DNA cleavage/relegation

In the presence of a divalent cation, topoisomerase II establishes a DNA cleavage/religation equilibrium (72-75). Magnesium is thought to be the physiological cation, although such as Ca^{+2} and Mn^{+2} can substitute *in vitro*. This equilibrium is referred to as pre-strand passage to distinguish it from the cleavage/religation equilibrium that is established post-the strand-passage event. Under normal conditions this equilibrium lies towards the religated species of the reaction. The DNA scission event results from a transesterification reaction, in which the enzyme generates a protein-linked double-stranded break in one of the DNA segments. During this reaction, two active-site tyrosyl residues (one per protomer) bound to phosphoryl groups on both the strands of the DNA backbone (76-77). As a result of this reaction, the enzyme becomes covalently attached to the 5'-termini of the cleaved DNA via phospho-tyrosyl bonds. (Figure 1.3) These bonds are formed at the newly formed 5'-termini at four bases apart and in opposite strands, yielding a DNA molecule with two 4-base 5'- overhangs. This covalent complex is known as the cleavage complex, and is of critical and physiologically important. The 3'-termini, although are not covalently attached to the enzyme, are held in place by non-covalent interactions with topoisomerase II (78). By remaining covalently attached to the DNA ends, this intermediate protects the genomic integrity of the cell.
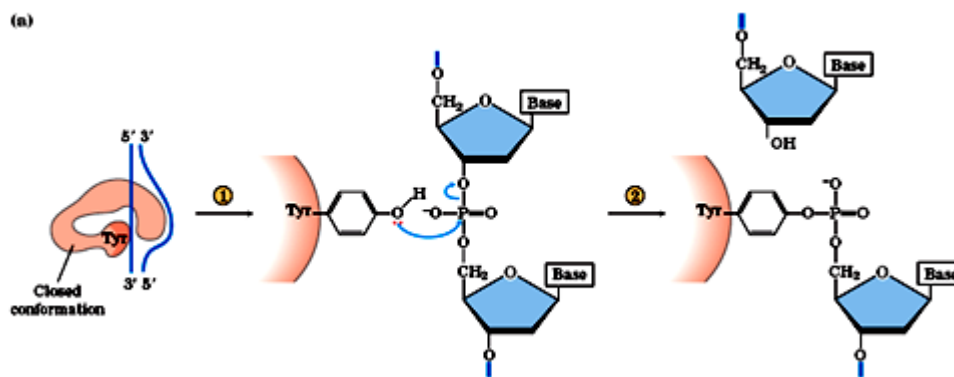
Fig 1.3:Transesterfication reaction:- Tyrosyl residue bound to phosphoryl groups on both the strands of the DNA backbone. and, the enzyme becomes covalently attached to the 5'-termini of the cleaved DNA via phospho-tyrosyl bonds.

Step 3:

DNA strand passage Upon binding of ATP, topoisomerase II undergoes a conformational change that triggers the passage of a second double helix through double-stranded DNA break previously generated (79,64) Concomitant with this structural reorientation, topoisomerase II becomes topologically linked to its nucleic acid substrate then enzyme acts as a protein clamp prior to recycling (80). The triphosphate portion of the high energy cofactor also is necessary to induce strand passage (64).

Step 4:Post-strand passage (i.e., ATP-bound)

Following the DNA translocation event, topoisomerase II once again establishes DNA cleavage/religation equilibrium (Figure 1.5) (65), the cleavage complex formed in the presence of ATP is intrinsically 2-4fold more stable than that generated prior to ATP binding (65,82).

Fig. 1.4:

Catalytic cycle of topoisomerase II (adapted from Burden and Osheroff, 1998 (81)). Enzyme catalysis is depicted as a series of five steps. Step 1, topoisomerase II DNA recognition and binding; step 2, pre-strand passage DNA cleavage/religation; step 3, ATP binding and DNA strand passage; step 4, post-strand passage DNA cleavage/religation; step 5, ATP hydrolysis and release of DNA and enzyme recycling.

Figure 1.4

Catalytic cycle of Topoisomerase II
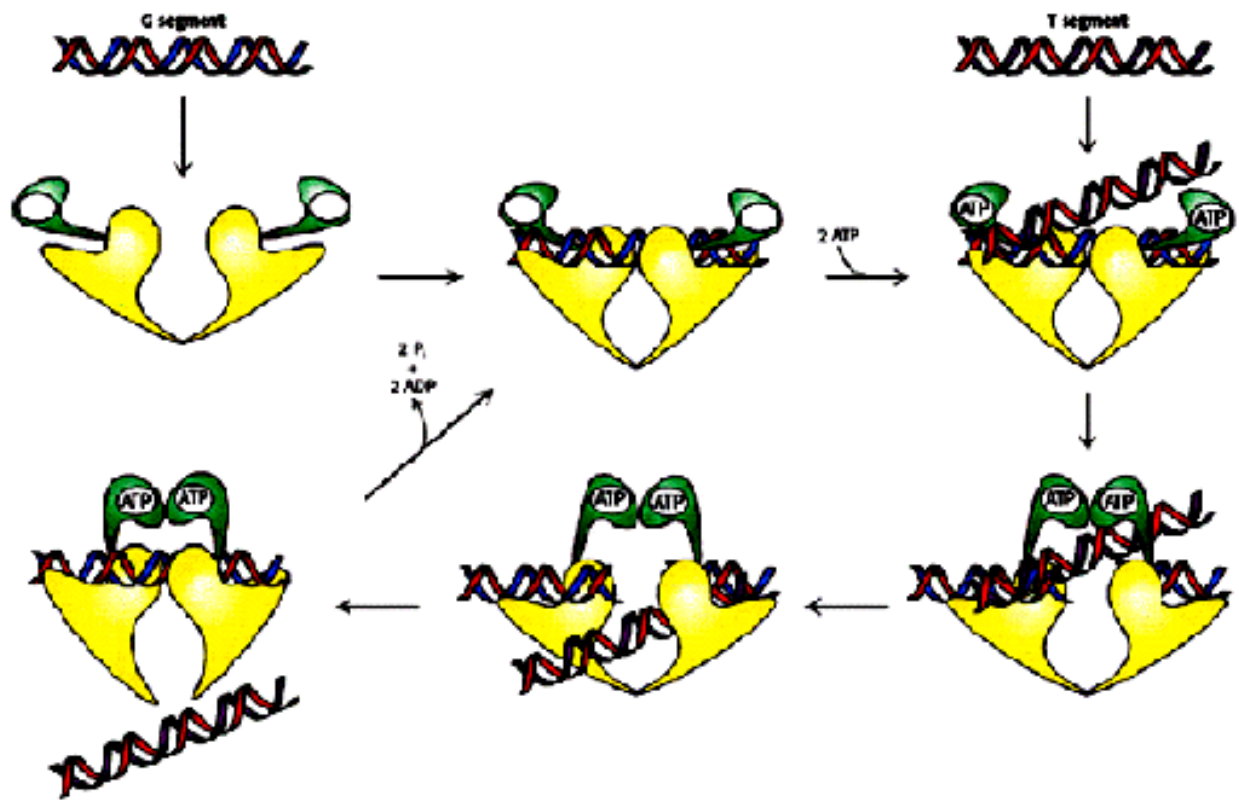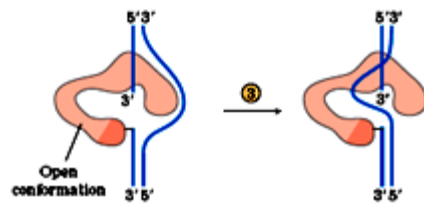
Figure 1.5 : DNA cleavage/religation equilibrium:cleave complexe formed in presence of ATP

Step 5: Hydrolysis of ATP

Topoisomerase II hydrolyzes ATP, which triggers the opening of the protein clamp and facilitates the release nucleic acid products (64,83,65,84).

Finally, phosphorylation of topoisomerase II (Figure 1.6) stimulates the rate of ATP hydrolysis by 2-3 folds. This appears to be the primary mechanistic basis for the enhancement of overall catalytic activity of topoisomerase II from lower eukaryotes following phosphorylation by either casein kinase II or protein kinase C (70, 85).

Fig 1.6
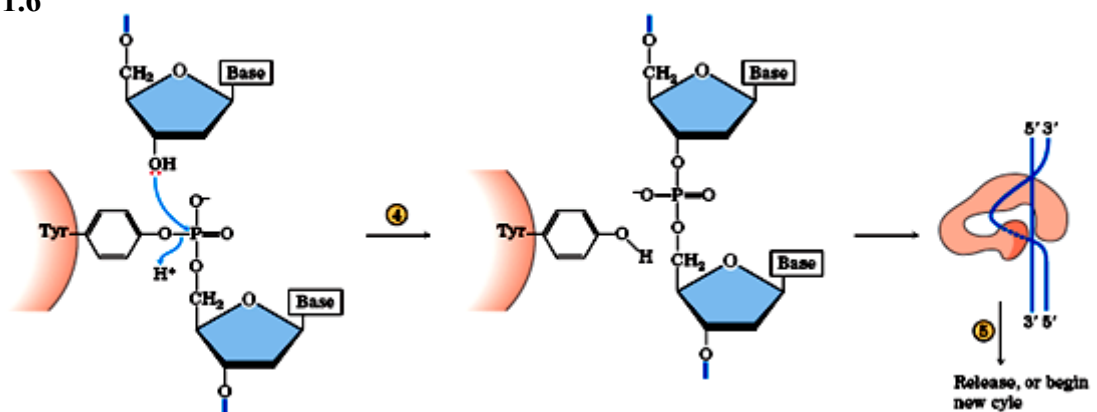
Topoisomerase II-DNA Cleavage Complexes

Topoisomerase II-DNA cleavage complexes are transient in nature and their cellular concentration is tightly regulated (Figure 1.7). Cleavage complex formation is essential for topoisomerase II to perform various cellular functions (5, 20, 21)

If the level of topoisomerase II-DNA cleavage complexes falls too low (i.e. enzyme activity is lowered), cells are unable to undergo chromosome segregation (68, 69, 91, 100-102). This loss of enzyme activity results in slow growth rates and ultimately cell death due to mitotic failure.

While formation of the cleavage complex is essential to enzyme activity, it is potentially deleterious to the cell. Transient, covalently linked topoisomerase II-DNA strand breaks are converted to permanent DNA strand breaks when nucleic acid tracking systems, such as replication or transcription complexes, attempt to traverse these topoisomerase-DNA roadblocks in the genetic material (20, 21, 87-89). The resulting strand breaks, as well as the inhibition of essential DNA processes, initiate multiple recombination/repair pathways (20, 21, 69-71). Accumulation of DNA breaks can lead to chromosome breakage, DNA translocations, and cancer (Figure 1.7) (65, 69, 71). If the accumulation of breaks becomes overwhelming, they trigger cell death pathways (70). There are several different classes of topoisomerase II-targeting compounds that either stimulate or inhibit cleavage complex formation in cells.

Figure 1.7:

Effects of topoisomerase II-cleavage complexes in the cell. (Illustrated from osheroff 2007 (86))

Topoisomerase II-DNA cleavage complexes are transient in nature, and their cellular concentration is tightly regulated. Cleavage complex formation is essential for topoisomerase II to perform its cellular functions. If the level of topoisomerase II-DNA cleavage complexes falls too low, cells are unable to undergo chromosome segregation, resulting in slow growth rates and ultimately cell death due to mitotic failure. Alternatively, if levels of cleavage complexes are too high, they can be converted to permanent strand breaks. The resulting strand breaks, as well as the inhibition of essential DNA processes, initiate multiple recombination/repair pathways. Accumulation of DNA breaks can lead to chromosome breakage and translocations. If the accumulation of breaks becomes overwhelming, they trigger cell death pathways.

Figure 1.7

Effects of Topoisomerase II-cleavage complexes in the cell
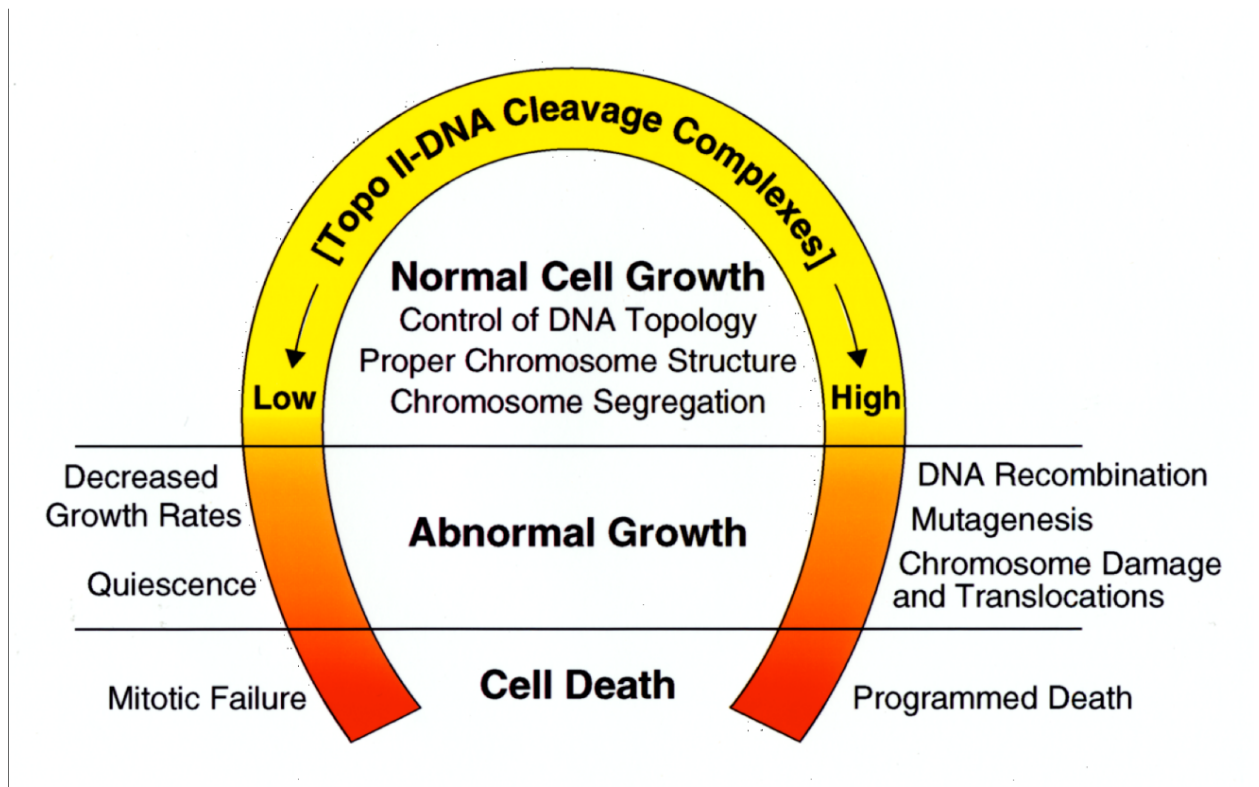
Fig 1.8

Routes of topoisomerase II-drug-DNA complex formation.

There are three possible routes by which this topoisomerase II-drug-DNA complex (ternary complex) can be formed (Fig. 1.5) (84): (1) drugs may become part of the ternary complex predominantly by interacting with DNA (route 1); (2) drugs may bind specifically to the topoisomerase-DNA binary complex and have minimal independent interactions with either the enzyme or the DNA (route 2); or (3) drugs may enter the ternary complex primarily via association with the enzyme (route 3). . Brackets are used to denote the transient nature of the cleavage complex..

Fig 1.8

Routes of topoisomerase II-drug-DNA complex formation.
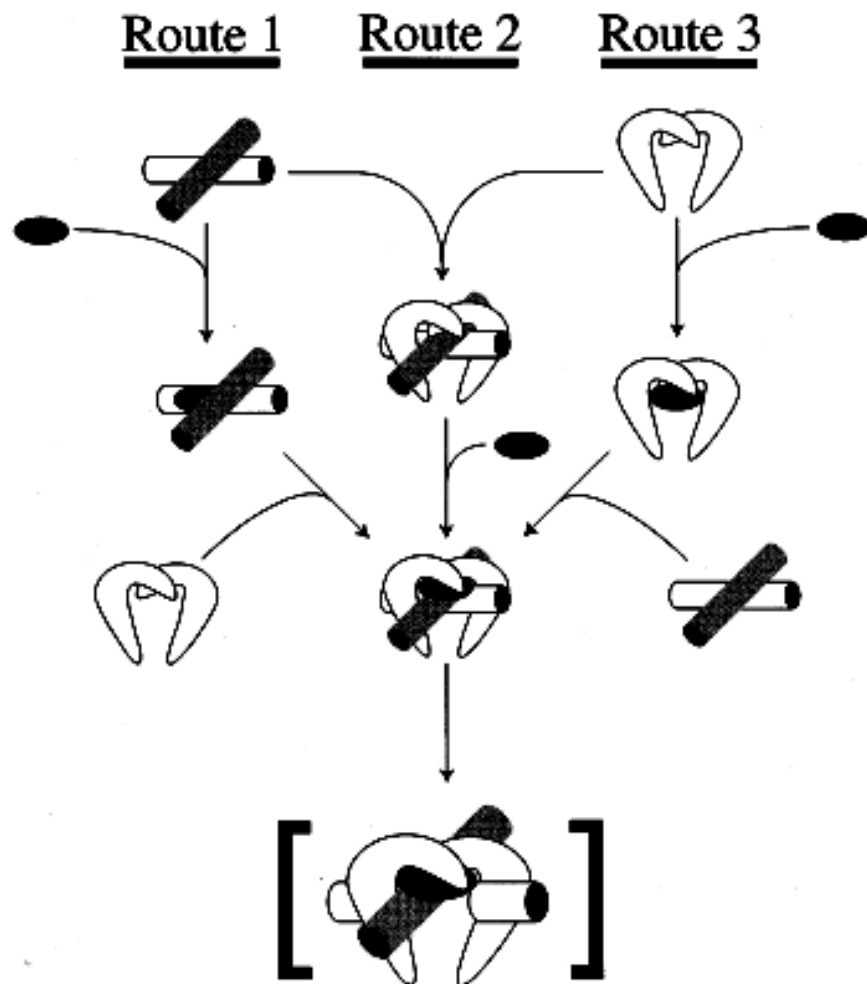
Cellular Function at activities of topoisomerase II

Resolving the need for a molecular swivel:

The local unwinding of the DNA helix during DNA replication and transcription leads to positive supercoiling ahead of the advancing fork and negative supercoiling in the region behind the fork (90,91). This causes torsional stress on the DNA, which is removed either by Topoisomerase I or II by relaxing the positive and negative super helices (92)

Decatenation of replicated chromatids and segregation:

DNA replication in the dense chromatin results in catenation of the newly replicated daughter chromatids. The separation of these interwined daughter strands requires decatenation, which is performed by topoisomerase II in the G2 phase of the cell cycle (93). This helps in segregation of the newly replicated daughter strands at mitosis and meiosis. Cells lacking topoisomerase II accumulate multiply-interwined, catenated dimers (94,95). The failure to segregate interwined DNA molecules eventually leads to cell death as the cells attempt to divide (96).

Maintaining genome stability:

Both the type I and type II topoisomerases, through relaxation of supercoils and unlinking of inappropriately paired interwined DNA strands, greatly reduce recombination frequency, especially in the rDNA clusters and help in maintenance of genome stability (97). Topoisomerase II plays an important role in suppression of recombination during meiosis (115). Absence of any these enzyme inadvertently results in a hyper-recombination phenotype, in which the rDNA gene clusters tend to get excised as extra chromosomal DNA rings (98)

Chromosome structure:

Topoisomerase II is associated with interphase chromatin as well as the cell division stage chromosomes (99, 100). In fact, topoisomerase II is the major component of the chromosome scaffold and is concentrated at the base of the chromosomal loops, called the scaffold attachment regions (101), it has been proposed that topoisomerase II gives structural alignment to chromosomes prior to mitosis but is not required for maintaining the chromosomal scaffold hrough mitosis (102).

Chromosome condensation/ decondensation:

Topoisomerase II is required for chromosome assembly and condensation prior to cell death (103,104). The enzyme is believed to interact with other proteins of the chromosome condensation (105,106). Removal of topoisomerase II activity either through immuno-depletion or antibody blocking completely inhibits chromosome assembly and condensation (102). Similarly, the enzyme is also required for chromosome decondensation after cell division.

Regulation of Topoisomerase II activity:

Topoisomerase II expression and activity is tightly regulated in cells. In G1 and S phases of the cell cycle, topoisomerase II activity is largely confined to the relaxation of supercoils generated during the processes of transcription and replication (107). This requires low expression levels and the enzyme activity is also very low, which is regulated through phosphorylation. As the cell passes on to the G2 and M phases, the phosphorylation status of enzyme is very high, consistent with its high activity (107). The functions of topoisomerase II and its regulation in the cell cycle are schematically shown Figure 1.9.

Rapidly growing cancer cells, unlike the normal cells show very high expression of topoisomerase II in all the phases of the cell cycle (108). The enzyme is also highly

phosphorylated in these fast dividing cells, without which the cells cannot accomplish their high turnover.

Depending on the requirement, phosphorylation of the enzyme can lead to increase in its activity by 2-15 folds (108-111). Casein kinase II and protein kinase C are the major enzymes that phosphorylate topoisomerase II (112-114). In addition other 'Mitotic Kinases' like the mitogen activated protein kinase (MAP Kinase) phosphorylate the enzyme during the G2 and M phases (115). The phosphorylation of topoisomerase II by these kinases may be regulated by the master controller of mitotic events, the p34 kinase (116)

Topoisomerase II is an anticancer drug target

The strand passage event in the catalytic cycle of topoisomerases comes with a heavy price, which is, generation of double stranded breaks in the DNA. Under normal circumstances, these DNA breaks are transient intermediates between the DNA cleavage and religation action of the enzymes (117-118). However, conditions that significantly increase the lifetime and physiological concentrations of these DNA breaks unleash a myriad of deleterious effects on the genetic material (119-121)

In the early 1980's researchers had shown that some of the well known anticancer drugs like etopside and amsacrine (m-AMSA) act on this aspect of the enzyme activity (122-123). These drugs, which allow DNA cleavage by the enzyme but block the DNA religation event, hence these are known as ` topoisomerase II poisons` unlike the topoisomerase II inhibitors which basically interfere with enzyme turnover (124). Typically, these poisons interact bi-directionally with the enzyme and DNA or with the enzyme alone (when the enzyme is bound to DNA). The drug bound topoisomerase II, as per its normal catalytic cycle, cleaves the DNA. At this point, the transient intermediate of the covalently linked enzyme–cleaved DNA complex` is frozen by the drug. This ternary complex consisting of

enzyme–drug-DNA is called the Cleavage Complex (125-126). Formation of this complex disturbs the DNA cleavage /relegation equilibrium, which shifts towards DNA cleavage and the enzyme is no longer capable of resealing the breaks (127-128).

Cancer cells generally over express topoisomerase II (108,129), and these cells when treated with Topoisomerase II poisons, tend to harbour numerous topoisomerase II induced DNA cleavage complexes (130,131). Traversal by replication or transcriptional complexes in the region of the breaks will apparently split up these cleavage complexes, which will expose the DNA breaks. Once exposed, these breaks will become targets for repair and recombination pathways. This in turn stimulates sister chromatid exchange, large insertions/ deletions, translocations and large chromosomal aberrations (119-121). When these genetic aberrations accumulate at high concentrations, they trigger a series of events which will ultimately lead to cell death through apoptosis or necrosis (132-133). The impact of topoisomerase II poisons on enzyme activity and the subsequent effects are depicted schematically (Fig 1.9).

Topoisomerase II-Targeting Agents

Beyond the critical physiological functions of type II topoisomerases; these enzymes are targets for some of the most important anticancer drugs currently used for treating human malignancies (20-22,134, 87,135,138). One of these drugs, etoposide, has been used in the clinic since the 1960's (135,136,138). It is prescribed as treatment for a wide spectrum of leukemias, lymphomas, and solid tumors. The relative contributions of topoisomerase IIα and β to therapeutic outcomes are not clear at the present time. Because topoisomerase IIα is upregulated in many cancer cells and is the isoform believed to be involved in DNA replication, it has been assumed to be an important drug target. In addition, drug interactions

Figure 1.9

Conversion of transient Topoisomerase II cleavage complexes to permanent double stranded DNA breaks.

Transient, covalently linked topoisomerase II-DNA strand breaks are converted to permanent DNA strand breaks when DNA tracking systems, such as replication or transcription complexes, attempt to traverse these topoisomerase-DNA roadblocks in the genetic material. The resulting strand breaks initiate multiple recombination/repair pathways Accumulation of DNA breaks can lead to chromosome breakage, DNA translocations and cancer, and ultimately trigger cell death pathways.
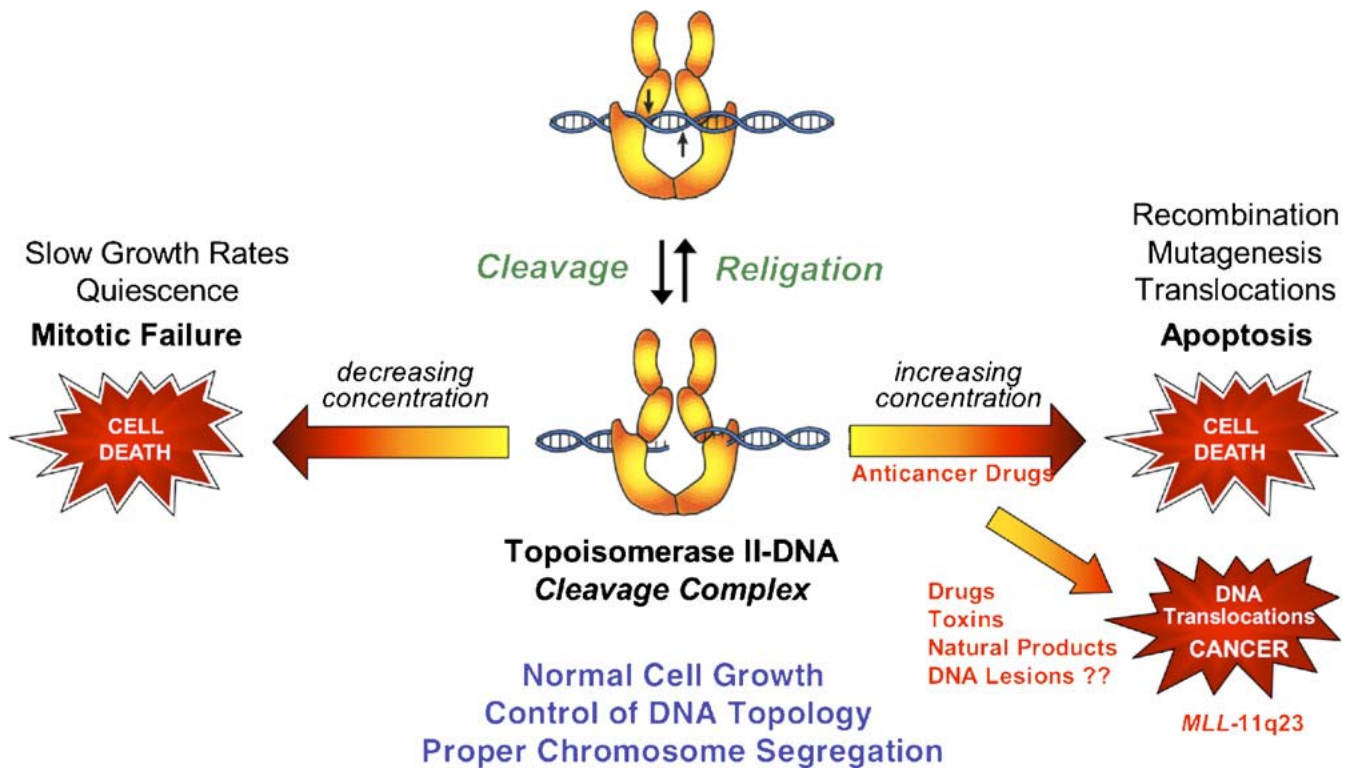
Figure 1.9.

Conversion of transient topoisomerase II cleavage complexes to permanent double stranded DNA breaks.

with topoisomerase IIβ in differentiated tissues, such as heart, are believed to contribute to the dose-limiting toxicity of some agents (140-141).

<div align="center">**Topoisomerase II Poisons**</div>

Topoisomerase II-targeting agents represent a structurally diverse group of natural and synthetic compounds. Some of these compounds are depicted in Figure 9. Etoposide is a non-intercalative drug that was among the earliest anticancer agents identified as targeting topoisomerase II (20, 21,135,136,138,142). TOP-53 is a non-intercalative drug that is a more potent derivative of etoposide (143,144). Genistein and CP-115,953 are non-intercalative compounds that share a similar core ring structure. Genistein is a naturally occurring bioflavonoid that is believed to possess chemo preventative properties (145-146). CP-115,953 belongs to the quinolone family (20,85,147-149), a drug class that includes a number of widely used antibacterials that target prokaryotic type II topoisomerases. TAS-103 displays strong interactions with DNA and is both an outside binder and an intercalating agent (150,151). Finally, amsacrine is an intercalative compound that is in clinical use (20,152,153). Although topoisomerase-targeted anticancer drugs come from several different structural classes, they all act by increasing levels of covalent topoisomerase-cleaved DNA complexes (i.e., cleavage complexes) that are essential intermediates in the catalytic cycle of topo II (20,21,87-89). When DNA tracking systems, such as replication forks, collide with these complexes, transient enzyme-associated DNA breaks are converted to permanent breaks in the genome (16,20,29,87,89,154). As a result, anticancer agents convert topoisomerases from essential enzymes to potent cellular toxins, and are thus called topoisomerase II "poisons."

Topoisomerase II poisons increase levels of enzyme-DNA cleavage complexes by two non-mutually exclusive mechanisms. Some drugs, such as etoposide, genistein, TOP-53,

16

Figure 1.10

Topoisomerase II-targeting poisons

The structures of four topoisomerase II poisons, etoposide, CP-115,953, genistein and amsacrine, are shown (top). These drugs induce topoisomerase II mediated DNA cleavage complexes. The structures of two topoisomerase II catalytic inhibitors also are shown (bottom). These drugs function by blocking specific steps in the catalytic cycle of topoisomerase II.

Figure 1.10.

Topoisomerase II-targeting poisons:

Etoposide

CP-115,953

Amsacrine

Genistein

Topoisomerase II Catalytic Inhibitors

Merbarone

Novobiocin
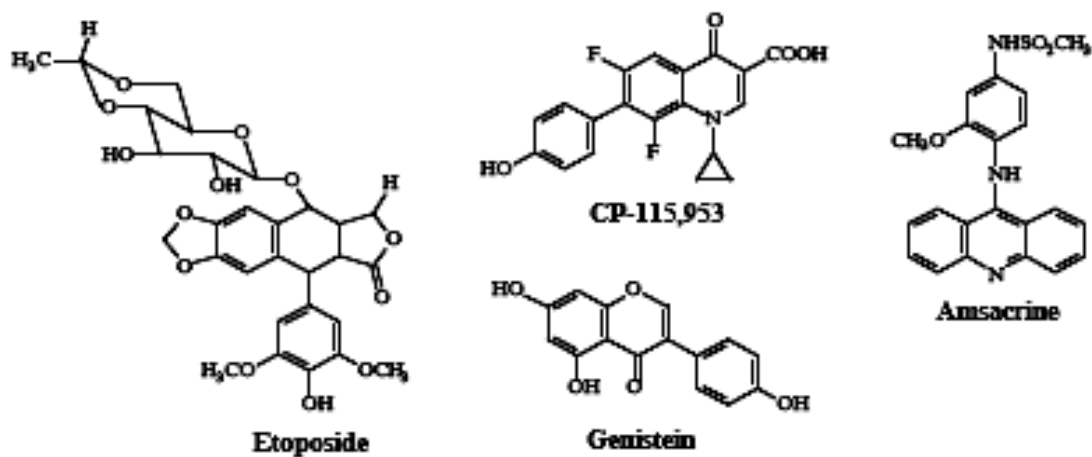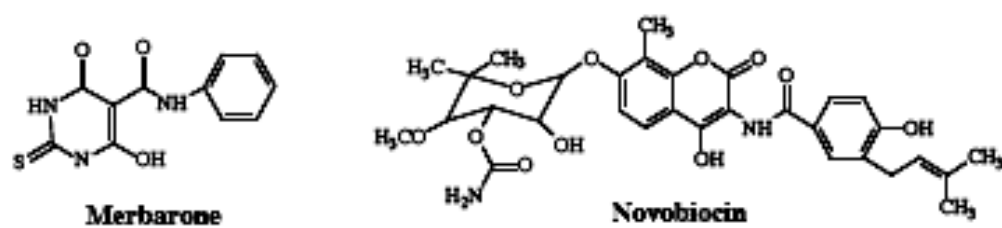
amsacrine and TAS-103, act by inhibiting the ability of topoisomerase II to ligate the cleaved substrate (20,21,138,155,156). These drugs not only increase the level of cleavage complexes, but also increase the lifetime of these complexes. Other drugs, such as CP-115,953, have little effect on the rate of enzyme-mediated ligation and are believed to act primarily by enhancing the forward rate of cleavage complex formation (157-159). The exact mechanism by which this second group of drugs increases levels of DNA cleavage is unknown. They may specifically act to enhance the forward rate of DNA scission. Alternatively, they may have some effect on the DNA binding/dissociation equilibrium, as the level of topoisomerase II-mediated DNA cleavage is proportional to the amount of enzyme bound (159-160).

Drugs that target topoisomerases are believed to work at the enzyme-nucleic acid interface (20, 21, 161-166). However, intercalative agents, such as amsacrine and TAS-103, have two additional effects on DNA that could impact levels of topoisomerase-mediated scission in a geometry-specific manner. First, since these compounds locally underwind DNA, they induce positive super helical twists in distal regions of covalently closed circular molecules (167,168). Hence, as the concentration of an intercalating agent increases, a plasmid that is topologically negatively supercoiled would appear to contain positive super helical twists. Second, the accumulation of drugs in the double helix has the potential to inhibit enzyme binding or activity. Because the generation of positive super helical twists by DNA intercalation induces torsional stress in the double helix, the ability of covalently closed molecules to absorb these compounds is limited. Since overwound plasmids are under positive torsional stress even in the absence of drugs, they cannot bind as many intercalative molecules as underwound DNA.

Topoisomerase II Catalytic Inhibitors

Catalytic inhibitors are another class of topoisomerase II targeting agents. These drugs do not increase the level of enzyme-mediated DNA cleavage complexes. Instead, they block specific steps in the catalytic cycle of topoisomerase II (169-171). For example, agents such as novobiocin inhibit ATP binding (172-173). Merbarone, on the other hand, has been shown to block DNA cleavage mediated by topoisomerase II (170-175). These two catalytic inhibitors are depicted in Figure 9.

Catalytic inhibitors kill cells by depriving them of essential activity of topoisomerase II while topoisomerase II poisons kill cells by fragmenting the genome. Cells treated with catalytic inhibitors result in elongated and entangled chromosomes and ultimately die from mitotic failure (176-178). While topoisomerase II poisons are used as chemotherapeutic agents, catalytic inhibitors have been used as modulators to increase the activity of other drugs (5,171,176). Additionally, some catalytic inhibitors have displayed potential anticancer activity in model organisms and currently are being tested in clinical trials (170,169,176,178).

Table 1.2:

A selection of the most extensively characterized Type I and Type II Topoisomerases from different organisms (179)

Drug	Class	Applications
Topoisomerase-II α poisons		
Epirubicin	Anthracycline	Adjuvant breast cancer
Doxorubicin	Anthracycline	Non-Hodgkin lymphoma, chronic lymphocytic leukaemia, Hodgkin's disease, multiple myeloma,acute leukaemia, small-cell lung cancer, breast, ovarian, and bladder cancers, sarcomas
Idarubicin	Anthracycline	Acute leukaemia
Daunorubicin	Anthracycline	Acute leukaemia
Mitoxantrone	Antracendione	Acute leukaemia, breast, ovarian, and bladder cancers
Amsacrine	Ansidide	Acute leukaemia
Etoposide	Epipodophyllotoxin	Small-cell lung cancer, testicular cancer, ovarian tumors, acute myeloid leukaemia, non-Hodgkin lymphoma
Teniposide	Epipodophyllotoxin	Small-cell lung cancer
Topoisomerase-II β catalytic inhibitors		
Aclarubicin	Anthracycline	Acute myeloid leukaemia
Sobuzoxane	Bisdioxopiperazine	T-cell lymphomas and leukaemia
Dexrazoxane	Bisdioxopiperazine	Central nervous system metastases, anthracycline extravasation

Structure of ferrocene:

In 1951, a new compound containing iron and two cyclopentadienide ligands was reported (180,181). Although, even the first report noted its high and unexpected stability, the correct structure was only soon afterward suggested independently by Wilkinson (182) and Fischer.(183) Owing to the resemblance of its reactivity to that of benzene, the name ferrocene (180) was coined for the new compound by Woodward (184). The term "sandwich compound" for this compound is today universally accepted for a much wider class of compounds. The discovery of ferrocene and elucidation of its remarkable structure is arguably the starting point for modern organometallic chemistry. In recent years, bioorganometallic chemistry has developed as a rapidly growing and maturing area which links classical organometallic chemistry to biology, medicine, and molecular biotechnology (185-187).

The stability of the ferrocenyl group in aqueous, aerobic media, the accessibility of a large variety of derivatives, and its favorable electrochemical properties have made ferrocene and its derivatives very popular molecules for biological applications and for conjugation with biomolecules.

Molecular Modeling and Rational drug design

Molecular modeling would appear to be concerned with ways to mimic the behavior of molecular systems. Molecular modeling is invariably associated with computer modeling but it is quite feasible to perform some simple molecular modeling studies using mechanical models or pencil, paper & hand calculator. Computational techniques have revolutionized molecular modeling (188) to the extent that most calculations could not be performed without the use of computer.

Molecular modeling places on the representation and manipulation of the structure of molecules and properties that are dependent upon those three-dimension structures.

The concepts used in rational drug design are quite simple. New molecules are conceived either on the basis of similarities with known reference structure or on the basis of their complementarily with the 3D structure on known active sites. Molecular modeling is a discipline that contributes to the understanding of these processes in a qualitative & sometimes quantitative way. It also provides the necessary tools for predicting the potential possibilities of prototype candidate molecules. Rational drug design (189) can be simply considered as a range of computerized techniques based on theoretical chemistry methods & experimental data that can be used either to analyze molecules & molecular system or to predict molecular & biological properties.

The techniques currently available provide extensive insight into the precise molecular features that are responsible for the regulation of the biological processes. Molecular geometries, atomic & molecular electronic aspects, and hydrophobic forces (190). All these structural characteristics are of primary importance in the understanding of structure activity relationships and in rational drug design.

Molecular modeling has widened the horizons of pharmaceuticals research by providing tools for finding new leads. The fields (191) currently covered by this discipline include,

1) **Direct drug design:** The three dimensional features of the receptor site (i.e., known X-ray structure or 3D model of a receptor) are directly considered for the design of lead structures.

2) **Indirect drug design:** The analysis is based on the comparison of the steriochemical and physiochemical features of a set of known active/inactive molecules; lead structures are designed on the basis of pharmacophore model obtained by such analysis.

3) **Database searches:** Lead compounds are identified from searches using databases defined with in 3D structure data. The input query describes the pharmacophore; it consists of a set of molecular fragments together with their relative location in 3D and additional structural constraints (geometrical or chemical).

4) **Three dimensional automated drug designs:** new lead compounds are generated by the computer on the basis of "growing" procedures inside the active site of a protein whose three dimensions structure is known or by a computerized treatment by assembling a set of pharmacophoric fragments defined in three dimensional space.

5) **Molecular mimicry:** lead molecules are conceived as mimics of a known reference compound as, for example, the design of selected peptide ligands.

In order to accelerate the drug discovery process, new technologies such as combinatorial chemistry and structure-based drug design have created the need to improve predictive experimental design and manage large amounts of experimental data.

QSAR as a method of rational drug design

Quantitative structure-activity relationship (QSAR) is the process by which chemical structure is quantitatively correlated with a well defined process, such as biological activity or chemical reactivity.

QSAR's most general mathematical form is:

Activity = f(physiochemical properties and/or structural properties)

Quantitative structure activity relationship (QSAR) is an indirect method of drug design, the idea of QSAR was introduced by Hansch et al. in 1963 (192) and first applied to analyze the importance of lipophilicity for biological potency. QSAR is a data exploration and productivity tool that can provide insight into structure-activity relationships. QSAR is a multivariate, mathematical relationship between a set of 2D and 3D physicochemical properties (descriptors) (193) and a biological activity. The QSAR relationship is expressed as a mathematical equation. Analysis of the statistical relationships between molecular structure and various properties provided by QSAR facilitates an understanding of how chemical structure and biological activity relate.

QSAR includes all statistical methods, by which biological activities (most often expressed by logarithms of equipotent molar activities) are related with structural elements (Free Wilson analysis), physicochemical properties (Hansch analysis), or fields (3D QSAR). QSAR has been useful for rationalizing compound activity and for rational design of new compounds.

Statistical methods involved in QSAR

Statistical methods (194) are an essential component of QSAR work. They help to build models, estimate a model's predictive abilities, and find relationships and correlations among variables and activities. Data analysis methods are used to recombine data into

different forms, and group observations into hierarchies. Regression methods are used to build a model in the form of an equation that gives one or more dependent variables (usually activity) in terms of independent variables (descriptors). The model can then be used to predict activities for new molecules, perhaps prioritizing or screening a large group of molecules whose activities are not known.

A model's ability to provide insight into the system is as important as its predictive ability. Possibly more valuable than being able to predict an activity or property is to know that it increases when a particular descriptor increases.

Regression methods

An important tool in model building is regression analysis (195). An equation sometimes more than one is produced that relates activity (or other properties) to descriptors. There are two main goals: prediction and experimental design. It is useful to have a model that is predictive (even if imperfect) because it can be used for screening a large set of molecules or proposed molecules for promising candidates. A regression model might be even more useful if it suggests a previously unrecognized correlation between some property (or combination of properties) and activity. This is especially true if we know how to adjust that property by changing some substituent. This can lead to new experiments designed to increase understanding of the system under study.

There is no single method that works best for all problems and that has the perfect balance of predictiveness, interpretability, and computational efficiency.

1. Simple and multiple linear regression (196) are very quick and easy to interpret, but do not work when the number of independent variables is larger than (or even comparable to) the number of molecules.

2. Stepwise multiple linear regression (196) and GFA work with any number of variables but do not perform well if important information is spread over more of them than can be included in the model. This often occurs for 3D QSAR.

3. Partial least squares (196) can handle any number of independent variables, but creates only linear relationships. Genetic partial least squares offer automatic creation of nonlinear terms.

To generate a QSAR equation several regression methods are available in cerius^2 QSAR module. These includes multiple linear regression, partial least squares (PLS) (197), simple linear regression, stepwise multiple linear regression, principal components regression (PCR) (198), genetic function approximation (GFA) (199), and G/PLS (200).

Simple linear regression (simple)

A linear one-term equation (196) is produced separately for each independent variable. This is useful for discovering some of the most important descriptors. However, it ignores the interaction of multiple descriptors.

Multiple linear regression (linear)

A single multiple-term linear equation (196) is produced. This method requires at least as many molecules as independent variables. To produce reliable results, we typically need 5 times as many molecules as independent variables.

Stepwise multiple linear regression (stepwise)

A multiple-term linear equation (196) is produced, but not all independent variables are used. Each variable is added to the equation in turn. A new regression is performed. The new term is retained only if the equation passes a test for significance.

Principal components regression (PCR)

A multiple-term linear equation is created based on a principal components analysis (198) transformation of the independent variables. The components are chosen so that they retain the largest amount of variance of the independent variables if some of the components are discarded. In effect, this method titrates the size of the model to the amount of data available. However, this method does not work well if some of the variables contain a lot of variance but do not correlate with activity (e.g., fingerprint-like descriptors). These variables are given a high loading in the components, pushing out others that are more relevant to activity. This means that, unless your independent variables are pre-screened for relevance, you should probably consider PLS instead.

Partial least squares (PLS)

Partial least squares (PLS) analysis (197) calculates equations describing the relationship between one or more dependent variables and a group of explanatory variables. Problems with PLS analysis: Sometimes, PLS analysis using the default number of steps fails with the error message.

Genetic function approximation (GFA)

In this method (199), models are collected that have a randomly chosen proper subset of the independent variables, and then the collected models are "evolved". A *generation* is the set of models resulting from performing multiple linear regressions on each model; a selection of the best ones becomes the next generation. Crossover operations are performed on these, which take some variables from each of two models to produce an offspring. In addition, the best model from the previous generation is retained. Besides linear terms there can also be spline, quadratic, and quadratic spline terms. These are added or deleted by mutation operations. A major advantage of this approach is that a collection of diverse small

models is generated that all have roughly the same high predictability. Each of these might provide a different insight into the system. Loading spread does not occur because at most one of the sets of collinear variable is retained in each model. This can make interpretation much easier than with PLS. A disadvantage is that it takes too long to perform cross validation on each generation and, thus, we need to have a reasonable idea of how many terms to keep before we start. Another disadvantage, compared to PLS, is that if the information in the system is highly diffuse, we may need to retain more terms in each model than can be determined by the number of molecules. This happens sometimes with 3D QSAR data.

Genetic partial least squares (G/PLS)

This method combines the best features of GFA and PLS (200). Each generation has PLS applied to it instead of multiple linear regressions, and so each model can have more terms in it without danger of over-fitting. G/PLS retains the ease of interpretation of GFA by back transforming the PLS components to the original variables.

These are the Cerius^2 software modules specific to activity prediction:

© **Molecular Field Analysis (MFA):** (201), which quantifies the interaction energy between a probe molecule and a set of aligned target molecules in a QSAR. Interaction energies measured and analyzed for a set of 3D structures can be useful in establishing QSARs.

© **Genetic Function Approximation (GFA):** (199), which is a statistical analysis method that generates multiple QSAR models. Usually, this population of models contains many models comparable or superior to the single model generated with standard regression analysis. The multiple models are created by evolving random initial models using a genetic algorithm. The default is to build linear models, but other options, including higher order

polynomials, splines, or other non-linear functions, also can be built. A method that combines genetic function approximation and partial least squares, G/PLS, is also available.

© **Molecular Shape Analysis (MSA):**(202) which extends QSAR operations for performing 3D QSAR studies. This technique generates quantitative measurements of molecular shape properties as part of QSAR analysis.

© **Alignment:** which provides tools to superimpose molecules (203) to satisfy various alignment conditions. These tools permit alignment of molecules using least square fitting with atom equivalencies specified either by automatic atom matching algorithms or by manual atom matching. In addition to rigid body superpositioning, the module provides tools for flexibly aligning one molecule over another using a fit optimizer algorithm.

© **Receptor**, which provides a 3D visual environment for receptor hypothesis exploration (204). The module creates receptor surface models using information generated from the overlay of active compounds. The receptor models can be used to evaluate new compounds and evaluate conformations and constraints on compounds in the receptor site.

Variables

Descriptors (Independent)

A descriptor (205) is a molecular property that QSAR can calculate. QSAR provides a wide variety of descriptors that one can use in determining new QSAR relationships. A *descriptor* is any one of a number of molecular properties that QSAR can calculate and use in determining new QSAR relationships. Examples Spatial, Electronic, Thermodynamic, Conformational, Topological, Information-content, Quantum mechanical, Structural, Descriptors based on fragment constants, Descriptors based on receptor surface models,

Descriptors based on molecular field analysis (MFA), Descriptors based on molecular shape analysis (MSA)

Biological activity (Dependent)

The experimentally determined activity is generally considered as the dependent variable (205).

Correlation coefficient

If X (independent) and Y (dependent) variables are highly correlated, X and Y contain much redundant information. The degree of correlation is measured by the correlation coefficient (206). We should also know the degree of correlation between independent variables because, in many calculations, it is assumed that they are uncorrelated.

The correlation coefficient is understood most easily using vector notation. If two vectors of the same length are correlated, the angle between them approaches zero and the cosine approaches one.
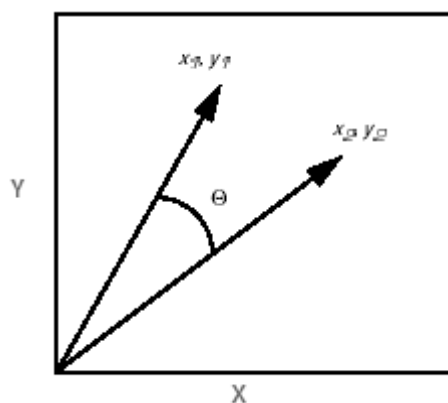

Figure 1.12. Correlation of two vectors

Using the notation from Figure 1 the normalized correlation coefficient between two variables (or vectors) X and Y is computed as:

$$\cos\theta = r = \frac{x'y}{(x'x)^{1/2}(y'y)^{1/2}}$$

The correlation coefficient has direction. Variables that are positively correlated have $0 > r > 1$, and those that are negatively correlated have $-1 < r < 0$.

Correlation coefficients for the variables in a dataset are compiled in a correlation matrix. This matrix is a symmetric matrix in which the diagonal elements are one and the off-diagonal elements are the correlation coefficients for the appropriate variable pairs. Variables that are not correlated are said to be orthogonal, and their correlation coefficients are zero. It is assumed that independent variables are orthogonal. If they are not, an unstable regression model can result.

Square of the correlation coefficient

The most commonly quoted statistic used to describe the goodness of fit of data for a regression model is the square of the correlation coefficient, r^2 (207).This statistic is defined as:

$$r^2 = \frac{\sum(Y_i - \bar{Y})^2 - \sum(Y_i - \hat{Y}_i)^2}{\sum(Y_i - \bar{Y})^2} = 1 - \frac{\sum(Y_i - \hat{Y}_i)^2}{\sum(Y_i - \bar{Y})^2}$$

As the residual sum of the squares goes to zero, $r2$ goes to one, and the model gives good predictions. $R2$ can be computed using cross validation methods (CV $r2$) or bootstrap methods (BS $r2$). It is also the fraction of the variance explained by the model.

Molecular field analysis (MFA)

This method for quantifying the interaction energy between a probe molecule (201) and a set of aligned target molecules in QSAR. Interaction energies measured and analyzed for a set of

3D structures can be useful in establishing structure- activity relationships. To generate an energy field (also known as a probe map), a probe molecule is placed at a random location, then moved about a target molecule within a defined 3D grid. At each defined point in the grid, an energy calculation is performed, measuring the interaction energy between the probe and the target molecule. Atoms in the target molecule are fixed, so that intramolecular energy in the target is ignored. When a complete probe map is calculated for each molecule in the target set, energy values for each point in the grid can be reported in columns added to the study table. For a set of structures for which energy fields are generated, some or all the grid data points can be used as descriptors in generating QSARs and analyzing structure–activity relationships. This chapter describes the procedures in MFA for generating energy fields and for incorporating field data into QSARs.

Creating a field

The process of generating energy fields (208) around a set of study molecules involves selecting the molecules to use as a target, selecting one or more probes, then running the calculation. As part of the calculation, the 3D region in which the probe moves and the points at which calculations are performed are defined. Calculations are performed at each point in the grid for the interaction energy between each probe and each structure in the study set.

For each model, two fields are generated, one with a proton probe and one with an uncharged methyl probe. Each calculation uses a cubic grid with 2-A^O spacing. Energy calculations are made between –30 and +30 kcal. For each map, point values are added to the study table, one value per column. Each column is labeled using the probe name and point number. A typical map contains several hundred points. Each new column is labeled an independent (X) variable.

Validation methods

Finally, validation methods (209) are needed to establish the predictiveness of a model on unseen data and to help determine the complexity of an equation that the amount of data justifies. Once a regression equation is obtained, it is important to determine its reliability and significance. Several procedures are available to assist in this. These can be used to check that the size of the model is appropriate for the quantity of data available, as well as provide some estimate of how well the model can predict activity for new molecules.

Internal and external Validation methods

Internal validation (210) uses the dataset from which the model is derived and checks for internal consistency. The procedure derives a new model using a reduced set of structural data. The new model is used to predict the activities of the molecules that were not included in the new-model set. This is repeated until all compounds have been deleted and predicted once. Internal validation is less rigorous than external validation.

External validation evaluates how well the equation generalizes. The original data are divided into two groups, the training set and the test set. The training set is used to derive a model, and the model is used to predict the activities of the test set members.

• Information about outliers (that is, data that is not modeled well by the equation). Outlier rows are also highlighted in the study table for quick identification.

• The sum of squared deviations.

• The predicted sum of squares (PRESS).

• The crossvalidated r^2, which is a measure of the predictive power of the equation.

Advantages of QSAR

Quantifying the relationship between structure and activity provides an understanding of the effect of structure on activity, which may not be straightforward when large amounts of data are generated.

- There is also the potential to make predictions leading to the synthesis of novel analogues (211). Interpolation is readily justified, but great care must be taken not to use extrapolation outside the range of the data set.

- The results can be used to help understand interactions between functional groups in the molecules of greatest activity, with those of their target. To do this it is important to interpret any derived QSAR in terms of the fundamental chemistry of the set of analogues, including any outliers.

Hence QSAR is employed in the thesis to find the structural descriptors contributing to biological activity of the molecule in chapter three

Drug delivery and targeting

Efficient drug delivery systems extend into all therapeutic classes of pharmaceuticals, the development of effective treatment modalities for the respiratory (212), central nervous system (213) and cardiovascular disorders (214) remains a therapeutically significant need. Many therapeutic agents have not been successful because of their limited ability to reach to the target tissue. In addition, the faster growth opportunities are expected in developing delivery systems for anti-cancer agents, hormones and vaccines because of safety and efficacy shortcomings in their conventional administration modalities.

For example, in cancer chemotherapy, cytostatic drugs damage both malignant and normal cells alike. Thus, a drug delivery strategy that selectively targets the malignant tumor is very much needed (215). Additional problems include drug instability in the biological milieu and premature drug loss through rapid clearance and metabolism. Similarly, high protein binding of certain drugs such as protease inhibitors (216) limits their diffusion to the brain and other organs.

Nanotechnology,

The term derived from the Greek word nano, meaning dwarf, applies the principles of engineering, electronics, physical and material science, and manufacturing at a molecular or submicron level (217). The materials at nanoscale could be a device or a system or these could be supramolecular structures, complexes or composites. An early promoter of nanotechnology, Albert Franks, defined it as 'that area of science and technology where dimensions and tolerances are in the range of 0.1 nm to 100 nm (218). In addition to the developments in other scientific disciplines such as in electronics and robotics, nanotechnology is expected to make significant advances in mainstream biomedical

applications, including in the areas of gene therapy, drug delivery, imaging, and novel drug discovery techniques (219,220).

Current nanoparticles as drug delivery agents and imaging:

Over the past few decades, there has been considerable interest in developing biodegradable nanoparticles as effective drug delivery devices (221-223). Nanoparticles are solid, colloidal particles consisting of macromolecular substances that vary in size from 10 nm to 1000 nm (224). The drug of interest is either dissolved, entrapped, adsorbed, attached or encapsulated into the nanoparticle matrix. Depending on the method of preparation, nanoparticles, nanospheres or nanocapsules can be obtained with different properties and release the encapsulated therapeutic agent. Nanocapsules are vesicular systems in which the drug is confined to a cavity surrounded by a unique polymer membrane, whereas nanospheres are matrix systems in which the drug is physically and uniformly dispersed. The advantages of using nanoparticles for drug due to, (1) nanoparticles, because of their small size, can penetrate through smaller capillaries and are taken up by cells, which allow efficient drug accumulation at the target sites (225-227), (2) the use of biodegradable materials for nanoparticle preparation allows sustained drug release within the target site over a period of days or even weeks, (3) Due to their size they can escape from the recognition by the immune system.

Targeted delivery can be achieved by either active or passive targeting. Active targeting of a therapeutic agent is achieved by conjugating the therapeutic agent or the carrier system to a tissue or cell-specific ligand (223, 229). Passive targeting is achieved by coupling the therapeutic agent to a macromolecule that passively reaches the target organ (230). Drugs encapsulated in nanoparticles or drugs coupled to macromolecules such as high molecular weight polymers passively target the tumor tissue through the enhanced

permeation and retention (EPR) effect (231,232). The alternative approach involves the infusion of nanoparticle suspension to the accessible target organ or tissue using infusion catheters. Localized delivery of nanoparticles in restenosis may be a useful strategy as it may provide sustained drug effect in the target artery (233,234).

Nanoparticles are also useful for the delivery of pharmaceutical agents after binding to target cellular epitopes by a mechanism called 'contact facilitated drug delivery'. Binding and close opposition to the targeted cell membrane permits enhanced lipid–lipid exchange with the lipid monolayer of the nanoparticle, which accelerates convective flux of lipophilic drugs (e.g. paclitaxel) dissolved in the outer lipid membrane of the nanoparticles into the targeted cells (235). Such nanosystems can serve as drug depots exhibiting prolonged release kinetics and long persistence at the site. Another characteristic function of nanoparticles is their ability to deliver drugs across several biological barriers to the target site (236,237). The brain delivery of a wide variety of drugs, such as antineoplastics and anti-HIV drugs, is markedly hindered because they have great difficulty in crossing the blood–brain barrier (BBB) (238,239). The application of nanoparticles to brain delivery is a promising way of overcoming this barrier. Recently, it has been demonstrated that poly-(butylcyanoacrylate) nanoparticles coated with polysorbate 80, are effective in transporting the hexapeptide dalargin and other agents into the brain (240).

Ceramic nanoparticles:

Ceramic nanoparticles have potential application in drug delivery. (241-243). Ceramic nanoparticles have several advantages easy to prepare, require ambient temperature condition, and can be easily prepared with the desired size, shape and porosity. Their ultra-low size (less than 50 nm) can help them evade by the reticulo-endothelial system (RES) of the body. In addition, there are no swelling or porosity changes with change in pH. These

particles effectively protect doped molecules (enzymes, drugs, etc) against denaturation induced by external pH and temperature (242). Such particles, including silica, alumina, titania, etc are known for their compatibility with biological systems (242, 244). In addition, their surfaces can be easily modified with different functional groups (244, 245). Therefore, they can be conjugated to a variety of monoclonal antibodies or ligands to target them to desired sites *in vivo*.

Polymeric micelles:

Polymeric micelles have been extensively studied as drug carriers (246-248). Polymeric micelles have several advantages like better thermodynamic stability in physiological solution, as indicated by their low critical micellar concentration, which makes polymeric micelles stable and prevents their rapid dissociation *in vivo* , avoid renal exclusion and the RES (249-250) , provides them with enhanced endothelial cell permeability in the vicinity of solid tumors by passive diffusion, prolonged systemic circulation time (246-251).

Micellar systems are useful for the systemic delivery of water-insoluble drugs. Drugs can be partitioned in the hydrophobic core of micelles and the outer hydrophilic layer forms a stable dispersion in aqueous media, which can then be administered intravenously. Accumulation of polymeric micelles in malignant tissue is because of increased vascular permeability and impaired lymphatic drainage (252, 253). As with other carriers, the drug delivery potential of polymeric micelles may be enhanced by conjugating targeting ligands including antibodies to the micelle surface. Thus, polymeric micelles can be a versatile system for the effective delivery of different classes of therapeutic agents.

Liposomes:

Liposomes are small artificial vesicles of spherical shape that can be produced from natural non-toxic phospholipids and cholesterol. Because of their size, hydrophobic and

hydrophilic character, as well as biocompatibility, liposomes are promising systems for drug delivery. The first suggested use of liposomes came from the research group of Weismann in 1969 (254). Since then liposomes have been used as a versatile tool in biology, biochemistry and medicine (255).

Liposome properties vary substantially with lipid composition, size, surface charge and the method of preparation. They are therefore classified into three classes based on their size and number of bilayers. Small unilamellar vesicles (SUV), large unilamellar vesicles (LUV). Multilamellar vesicles (MLV). The introduction of positively or negatively charged lipids provides the liposomes a surface charge. Drugs associated with liposomes have markedly altered pharmacokinetic properties compared to drugs in solution. They are also effective in reducing systemic toxicity and preventing early degradation of the encapsulated drug after introduction to the target organism (256,257). Liposome surfaces can be readily modified by attaching polyethylene glycol (PEG)-units (258), antibodies or ligands to enhance target-specific drug therapy.

Dendrimers:

Dendrimer molecules are monodisperse symmetric macromolecules built around a small molecule or in a linear polymer core using connectors and branching units. Dendrimers are attractive systems for drug delivery because of their nanometer size range, ease of preparation and functionalization, and their ability to display multiple copies of surface groups for biological reorganization processes (259, 260).

By modifying their termini, the interior of a dendrimer may be made hydrophilic while its exterior surface is hydrophobic, or vice versa. Dendrimers can be synthesized starting from the central core and working out toward the periphery (divergent synthesis) or in a top-down approach starting from the outermost residues (convergent synthesis)

(260,261). Drug molecules can be loaded both in the interior of the dendrimers as well as attached to surface groups.

Ex: 5-Fluorouracil (5FU) is known to have remarkable anti-tumor activity, but is highly toxic due to side effects. PAMAM dendrimers after acetylation can form dendrimer-5FU conjugates which upon hydrolysis releases free 5FU, thus minimizing toxicity (262).

Nanocrystals for drug delivery and imaging

Nanocrystals (also called quantum dots (QDs;Qdots) or nanodots) are crystalline clumps of a few hundred atoms, coated with an insulating outer shell of a different material (263).

Although fluorescent markers are routinely used in basic research and clinical diagnostic applications, there are several inherent disadvantages with current techniques, including the requirement of color-matched lasers, the fluorescence bleaching, and the lack of discriminatory capacity of multiple dyes. Fluorescent nanocrystals potentially overcome these issues.

The QDs absorb light at a wide range of wavelengths, but emit almost monochromatic light of a wavelength that depends on the size of the crystals (264). Quantum Dot Corp. (http://www.qdots.com) is commercially developing Qdot technology. Qdots can be attached to biological materials, such as cells, proteins and nucleic acids. Qdots can be designed to emit light at any wavelength from infrared to ultraviolet.

A related technology called Probes Encapsulated by Biologically Localized Embedding (PEBBLES) allows dye-tagged nanoparticles to be inserted into living cells to monitor metabolism or disease conditions (265, 266). The system was highly sensitive, had a rapid response time and used a reversible and photo stable nanosensor that was insensitive to interference from intracellular or extracellular proteins.

Magnetic nanoparticles

Magnetic nanoparticles are a powerful and versatile diagnostic tool in biology and medicine (267, 268). Bound to a suitable antibody, they are used to label specific molecules, cell populations, structures or microorganisms. Magnetic immunoassay techniques have been developed in which the magnetic field generated by the magnetically labeled targets is detected directly with a sensitive magnetometer. Binding of antibody to target molecules or disease-causing organism is the basis of several tests. Super paramagnetic nanoparticles are used as contrast agents in magnetic resonance imaging. They consist of an inorganic core of iron oxide (magnetite Fe_2O_3, maghemite or other insoluble ferrites) coated with polymer such as dextran. Ex: Lumiren and Endorem. These nanoparticulate contrast agents are being used for imaging of tissue for diagnostic applications.

Superconducting quantum interference device (SQUID) is a technique for specific, sensitive, quantitative and rapid detection of biological targets by using supermagnetic nanoparticles and a microscope based on a high transition temperature (269).

Ferrofluids

Ferrofluids are colloidal solutions of iron oxide magnetic nanoparticles surrounded by a polymeric layer coated with affinity molecules, such as antibodies, for capturing cells and other biological targets from blood or other fluid and tissue samples (270, 271). Ferrofluid particles are so small (25–100 nm in radius) that they behave in liquids as a solution rather than suspension. When the coated ferrofluid particles are mixed with a sample containing cells or other analytes, they interact intimately and completely. These properties enable the development of specialized reagents and systems with extremely high sensitivity and efficiency and capture (272, 273).

Table 1.3

Some principle Advantages and Disadvantages of Soft Drug Delivery systems (274)

	Advantage	**Disadvantage**
Micelles	Ease of preparation Good stability Many administration routes available	Risk of disintegration after administration
Liposomes	Many administration routes possible Inclusion of hydrophilic drugs, e.g., proteins possible	Complex preparation, limited stability
Cubosomes	Many administration routes possible Inclusion of both hydrophilic and hydrophobic drugs possible	Complex preparation, limited stability
Liquid crystalline phases	High viscosity →A interesting for depot formulation Possibilities for triggering between structures, e.g., following administration High solubilization capacity of both hydrophilic and hydrophobic drugs	Difficult preparation due to high viscosity Administration route limitations due to high viscosity Toxicity related to high surfactant concentration
Polymer (micro) gel	Highly responsive →A possibilities for triggering, e.g., at specific regions, tissues or cell types High water content →A good for sensitive protein drugs Many administration routes possible	(Molecular) solubilization capacity low for hydrophobic drugs Preparation and drug loading complex
Polymer microcapsules	Highly responsive →A possibilities for triggering, e.g., at specific regions, tissues or cell types High water content →A good for sensitive protein drugs	(Molecular) solubilization capacity low for hydrophobic drugs Preparation and drug loading complex Administration route limitations due to capsule size Preparation and drug loading complex
Nano tubes	Loading with both hydrophilic and hydrophobic drugs possible Possible biological adjuvant effects	Biological response largely unknown Administration route limitation due to tube length

Natural protein, Transferrin based delivery system:-

Cells demanding high iron metabolic activity such as rapidly proliferating malignant cells (275), high metabolic active brain cells (276) express higher number of transferrin receptors to facilitate higher iron transport. The use of apotransferrin, transferrin and transferrin receptor antibodies (OX-26) as carriers of drug for targeted delivery to transferrin receptor expressed cells is extensively studied (277).

Potential therapies–using Tf to sequester free iron, to deliver drugs to transferrin receptor expressed highly metabolically active cells rapidly growing cells. Since, Tf being an abundant plasma protein is an ideal candidate for purification from plasma (278). In this way, delivery systems could be tailored for specific delivery of drugs to rapidly dividing cells.

Transferrin structure:

The transferrin (Tf) protein contains 679 amino acid residues and has a molecular weight of ~79 kD (279). The molecule is stabilized by 19 intra-chain disulfide bonds and is protected by three carbohydrate side chains of which two are N-linked (Asn-413 and Asn-611) and the third is O-linked (Ser-32) (Swiss-Prot P02787, http://us.expasy.org/sprot/). The Tf molecule is divided into two evolutionary related lobes, designated the N-lobe (336 amino acids) and C-lobe (343 amino acids), which are linked by a short spacer sequence. Each lobe contains two domains comprising a series of α-helices, which overlay a central β-sheet backbone (Figure 1). The domains interact to form a deep, hydrophilic metal ion-binding site. The binding site in both the N- and C-terminal lobes has four conserved amino acids including two tyrosines, one aspartic acid and one histidine (N-terminal lobe – Asp-63, Tyr-95, Tyr-188 and His-249). These residues are arranged in a distorted octahedral arrangement (280). In addition, the binding site requires two further oxygen molecules donated by a
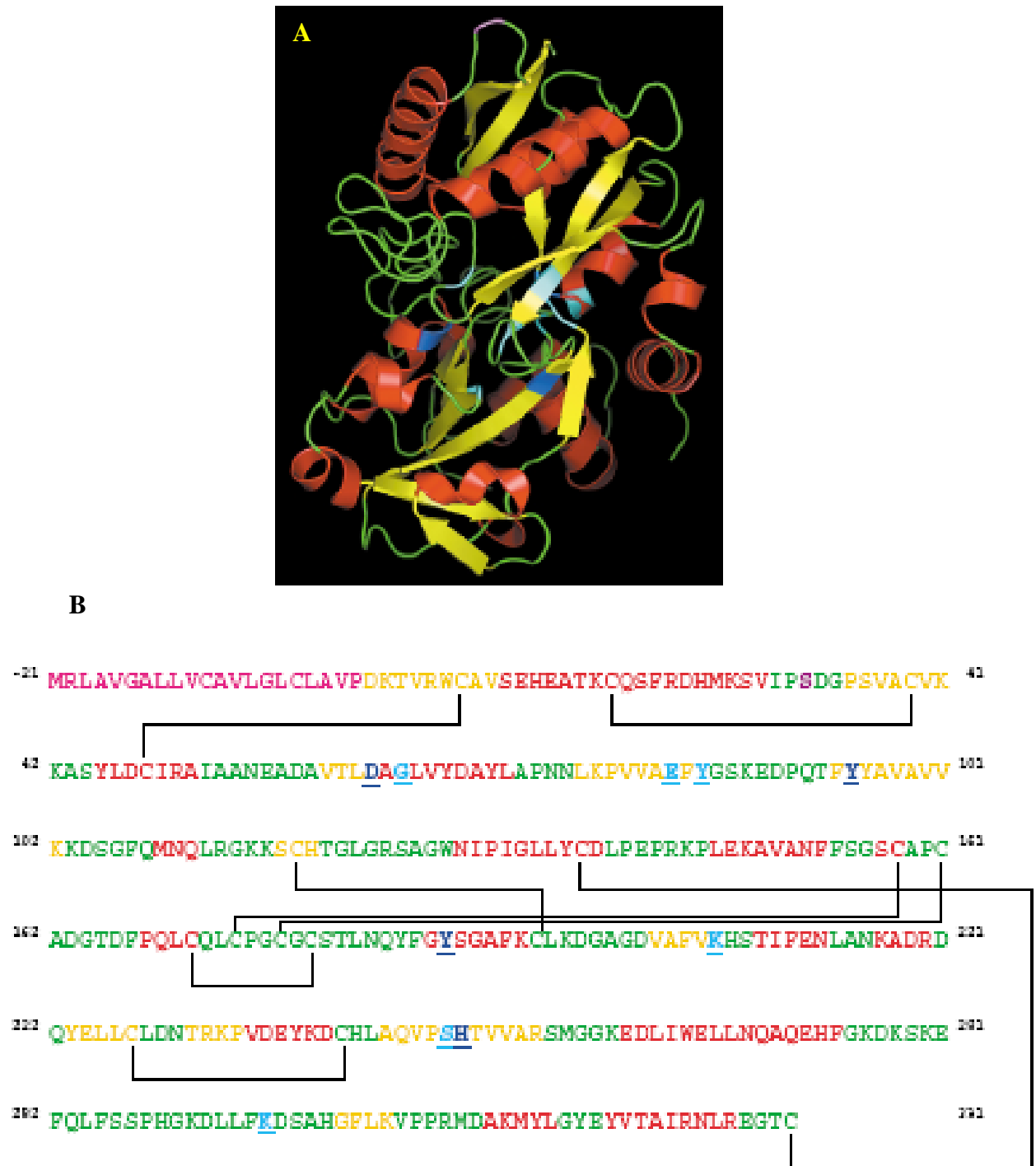
Figure 1.11

The Structure and Sequence of Transferrin.

(a) X-ray crystal structure of transferrin (Protein Data Bank–1a8e (http://www.rcsb.org/pdb/)).The yellow arrows indicate the ß-sheets. (b) Amino acid sequence of the N-terminal lobe of transferrin.

The iron-binding site residues are underlined and highlighted in dark blue, and the amino acids involved in stabilizing the metal-binding site are underlined and highlighted in light blue.Key: pink, leader sequence; yellow, β-sheet; red, α-helix; green, random coil; violet, O-linked carbohydrate attachment at Ser-32.The disulfide bonds linkages are marked in solid black lines.

Figure 1.11

The structure and sequence of Transferrin.

A

B

```
-21 MRLAVGALLVCAVLGLCLAVPDKTVRWCAVSEHEATKCQSFRDHMKSVIPSDGPSVACVK 41

 42 KASYLDCIRAIAANEADAVTLDAGLVYDAYLAPNNLKPVVAEPYGSKEDPQTFYYAVAVV 101

102 KKDSGFQMNQLRGKKSCHTGLGRSAGWNIPIGLLYCDLPEPRKPLEKAVANFFSGSCAPC 161

162 ADGTDFPQLCQLCPGCGCSTLNQYFGYSGAFKCLKDGAGDVAFVKHSTIPENLANKADRD 221

222 QYELLCLDNTRKPVDEYKDCHLAQVPSHTVVARSMGGKEDLIWELLNQAQEHFGKDKSKE 281

282 FQLFSSPHGKDLLFKDSAHGFLKVPPRMDAKMYLGYEYVTAIRNLREGTC 331
```

carbonate molecule to stabilize the iron atom (281). The surrounding amino acid residues (Gly-65, Glu-83, Tyr-85, Arg-124, Lys-206, Ser-248 and Lys-296 on the N-terminal lobe) are thought to further stabilize the metal-binding site, and they have crucial roles in iron release (280). For example, it has been demonstrated that Lys-206 and Lys-296, which are located on opposite domains of the N-terminal lobe, are hydrogen bonded to one another in the 'closed' iron-bound form. When the pH is reduced, this hydrogen bond is broken allowing the domains to rotate forming an 'open' conformation which promotes iron release (282).

Protein function

Iron plays a central role in DNA replication with one of the key enzymes, ribonucleotide reductase, requiring iron as a co-factor. Iron also acts as a co-factor for heme (283). However, free iron can be toxic, promoting free radical formation via the Fenton and Haber–Weiss reactions, thus resulting in oxidative damage to tissues (284). Free iron causes lipid peroxidation by converting hydro peroxides into reactive peroxyl and alkoxyl radicals (285). In addition, Tf promotes auto-oxidation reactions involving carbohydrate aldehyde groups and protein amino groups, which results in the formation of glycated products (286). For these reasons, it is vital that iron is transported in a redox-inactive form. The primary role of Tf is therefore to transport iron safely around the body to supply growing cells. The binding and release of iron by Tf involves several factors, for example, pH, temperature, chelator and ionic concentrations (287).

Protein distribution

Tf is synthesized predominantly by hepatocytes (288). Other tissues expressing Tf include Sertoli (289,290), ependymal (291), oligodendroglial (192), metastatic melanoma cell lines (293) and human breast cancer cell lines (294). Tf has been detected in various

body fluids including plasma, bile, amniotic, cerebrospinal, lymph and breast milk (295). Plasma concentration of Tf is stable from birth, ranging from 2 g l-1 to 3 g l-1, and the in vivo half-life of this protein is eight days (284). The level of Tf is important for healthy growth with levels below 0.1 g l-1 associated with an increased incidence of infection, growth retardation and anemia (296).

Transferrin–Transferrin Receptor system

Iron-loaded Tf binds transferrin receptors (TfR) on the surface of actively dividing cells (297). Subsequently, the Tf–TfR complex is internalized and transported to endosomes. ATP-dependent proton pumps then force H+ ions into the endosomes reducing the pH to 5.5, thus promoting iron release (298). Under low pH conditions, the TfR alters conformation to enable apotransferrin (apo-Tf) to remain bound. The binding characteristics of the apo-Tf–TfR complex are such that the apo-Tf is released only once the complex reaches the cell surface (297). The Tf molecule then circulates until it again comes in contact with free iron at intestinal sites and hemoglobin breakdown (e.g. macrophages) sites, and the cycle of Tf-mediated iron redistribution is continued. It has been estimated that one Tf molecule could participate in this transport cycle as many as 100 times (299)

Tf binds to at least two distinct types of TfRs, designated TfR1 and TfR2 (228). TfR1 is expressed on a range of cells, including red blood cells, erythroid cells, hepatocytes, monocytes and the blood–brain barrier. TfR2 is expressed as two transcripts (α-TfR2 and β-TfR2), with α-TfR2 expressed predominantly on liver cells and β-TfR2 expressed at low levels on a variety of cell types (300). The level of TfR expression varies depending on the cell type. Non-dividing cells can have extremely low levels of TfR expression, whereas rapidly proliferating cells (e.g. carcinoma cell lines) can express up to 100 000 TfRs per cell (294). The report in literature unequivocally showed overexpression of transferrin receptors

in cancer cells. If its ligand apotransferrin is used as carrier for this drug, it can localize

higher amount of drug in cancer cells leading to action of the drug. The chapter V of the

thesis presents results of apotransferrin mediated delivery of drug to cancer cells.

Table 1.4

Potential Therapeutic applications of Transferrin

Pathophysiological condition	Therapeutic application	Mode of action	Refs
Free iron and/or iron overload	Atransferrinemia	Transferrin replacement	288,296
	Ischemia reperfusion injury	Anti-oxidative	301
	Cardiovascular disease	Anti-oxidative	284
	Radiotherapy	Iron sequestering	302
	Bone marrow transplantation	Antimicrobial	303,304
Tumor or cancer	Targeted drug delivery	Delivery of therapeutic metals, proteins, drugs and genes via transferrin–transferrin receptor pathway	283, 294
Growth and differentiation	Cancer therapy	Promote cytotoxicity and proliferation of lymphokine-activated killer and natural killer cells	305

Table 1.5:

Various Cancers over expressing Transferrin Receptors showing the enhanced possibility of Transferrin ligand based therapy

Breast Cancer	•Sadava et al Cancer Lett. 2002 May 28;179(2):151-6. •Cavanaugh et al. Breast CancerResTreat. 1999 Aug;56(3):203-17. •Yang et al Anticancer Res. 2001 Jan-Feb;21(1B):541-9. •Walker RA, Day SJ. J Pa thol. 1986 Mar;148(3):217-24.	306-309
Squamous cell lung carcinoma	Rácz et al EurJ Cancer. 1999 Apr;35(4):641-6.	310
Nonsmall cell lung cancer	•Whitney et al Cancer. 1995 Jul 1;76(1):20-5.	311
Lung carcinoma	Kayser K, Ernst M, Bubenzer J. Exp Pathol. 1991;41(1):37-43. Lung carcinoma	312
Adenocarcinoma of the lung	•Kondo et al. Ches t. 1990 Jun;97(6):1367-71.	313
Colon cancer	Drewinko et al Anticancer Res. 1987 Mar-Apr;7(2):139-41.	314
Ovarian Cancer	•Calzolariet al. Blood Cells Mol Dis. 2007 Jul-Aug;39(1):82-91. Epub2007 Apr 10	315
Brain tumor	Wen et al Neurosurgery. 1995 Jun;36(6):1158-63; discussion 1163-4. •Prior et al Virchows Arch A PatholAnatHistopathol.990;416(6):491-6.	316,317
MDR cancers	•Kobayashi et al Int J Pharm. 2007 Feb 1;329(1-2):94-102. Epub2006 Sep 1. •Fritzer et al. BiochemPharmacol. 1996 Feb 23;51(4):489-93. •Wang et al Anticancer Re s. 2000 Mar-Apr;20(2A):799-808.	318-320

Earlier studies by Vashist Gopal et al (2001) showed that a non DNA binding and topo II non-interacting molecules, ferrocene acquires an affinity to topo II upon substitution at 2' position. Among the substitutions at 2' position acetyl substituted ferrocene showed significant inhibition of the catalytic activity of topo II. The present study aim at characterization of substituted ferrocene derivatives for isoform specific activity. A structural analysis was carried out to examine the physic chemical features that determine Topo II poisoning activity.

Mostly the organometallic compound due to their charge show lower cellular uptake and exhibit toxic side effects *in vivo.* Here a target directed nanoparticle based method is presented for cellular localization of the drug.

Potent ferrocene derivatives are tested in rat hepatocellular carcinoma model, these results are present in following objectives:

1) Design, synthesis and characterization of ferrocene derivatives with Topoisomerase II beta inhibitory activity.

2) Development of drug delivery system for target specific localization of ferrocene derivatives in cancer cells.

3) Evaluation of efficacy of potent molecules in rat ascetic hepatocellular carcinoma.

CHAPTER II

EXPERIMENTAL PROCEDURES

Materials:

The negatively supercoiled plasmid DNA pBR322 and pRYG were purified as described in (321). Mouse anti-human topoisomerase II alpha and topoisomerase II beta monoclonal antibodies, Mouse anti-human transferrin, Mouse anti-human Alpha feto protein antibodies were obtained from BD Bioscience USA, and γP^{32} were obtained from JONAKI, BRIT, India. Other chemicals and biochemicals were of analytical grade.

Apotransferrin was purified from human blood following the method of Cohn *et al.* (322). Doxorubicin was a pharmaceutical preparation of Biochem pharmaceutical industries, Pune. India. SUP-T1 were from NIH-AIDS reference and reagents programme, USA. SK-N-SH cells, COLO-205 was from NCCS Pune. All other reagents and biochemicals were of analytical and molecular biological grade.

Olive oil of superior grade purchased from local shop, ZH5 cells were obtained from CCMB. LDH, Alkaline phosphatase, Creatinine, Urea diagnostic kits are obtained from Qualigens-Sigma, India

2.1: Topoisomerase II enzyme source:

Rat brain cerebellum was used as enzyme source. Topoisomerase II alpha and beta were isolated using two sequential steps, First by MONO S and then by MONO Q ion exchange chromatography. The bound protein was eluted at 0.25 M NaCl. The alpha and beta isoforms present in the preparation were further affinity purified using corresponding antibody coupled agarose matrix. Mouse anti-human topoisomerase IIα and topoisomerase IIβ monoclonal antibodies were used. The antibody bound protein was eluted using buffer containing 20mM Tris-HCl (pH 8.0), 1M KCl, 0.5 mM EDTA,10 mM mercaptethanol,10% glycerol, followed by dialysis using the same buffer containing 100 mM KCl . The purity of protein was confirmed by Western blot analysis. The protein was estimated using the Bradford's method (323). The catalytic activity was assayed using supercoiled pRYG DNA (321). Alternatively topo II alpha and beta immunoprecipitates were also used directly to assay the isoform specific activity and topo II poisoning activity.

Synthesis of ferrocene derivatives

2.2: Ferrocene carboxyaldehyde: (324)

N-methyl formanilide method: N-methyl formanilide (4.4 gm, 0.032 mole) and phosphorous oxychloride (5 gm; 0.032 mole) were mixed and left at room temperature for 1 hour, ferrocene (2.99 gm, 0.016 mole) was then added in small portions with vigorous shaking during approximately 30 minutes, the mixture being kept cool throughout . It is then left in a stoppered flask for 72 hours. After addition of ice-water, the mixture was extracted with chloroform and solution dried (Na_2SO_4) and evaporated, A benzene solution of the residue was chromatographed on alumina to separate the product from unchanged ferrocene (0.125 gm, 4.2%) and N-Methyl formanilide, the main red band was eluted with benzene, evaporated and crystallized from 25% aqueous ethanol to yield ferrocene carboxyaldehyde.

2.3: Acetyl ferrocene :- (325)

A mixture of 93 gm of ferrocene 250 ml of acetic anhydride and 20 ml of 85% phosphoric acid was heated at $100^{\circ}C$ for 10 minutes the reaction mixture was cooled slightly and poured onto ice after standing overnight the mixture was neutralized with 200 gm of sodium carbonate in 200 ml of water the resulting brown pasty mass was cooled in ice bath and filtered the tan product was washed four times with 100 ml portions of water and filtered the granular product was dried in a vacuum dessicator over phosphoric anhydride sublimation of the crude product at $100^{0}C$ gave orange crystalline product.

2.4: Thiomorpholide amido methyl ferrocene (325)

A mixture of 9.5 gm of monoacetyle derivative and 1.9 gm of sulphur and 5.2 ml of morpholine was heated at $130^{\circ}C$ for 2.5 hours the viscous black reaction mixture was extracted with hot methanol and the extracts were diluted with water to give a dark brown precipitate of Thiomorpholide amido methyl ferrocene. Successive recrystallization from benzene hexane and water methanol mixture gave orange needles.

2.5: Azalactone ferrocene (326)

Ferrocene carboxyaldehyde (1gm) hippuric acid (1gm) and anhydrous sodium acetate were dissolved in acetic anhydride by refluxing for 5 minutes in a stream of nitrogen. The solution was then heated for 1.5 hours on a steam bath, cooled diluted with methanol (6 ml) and refrigerated overnight. Filteration followed by recrystallization from benzene afforded the azalactone ferrocene as deep purple crystals.

2.6: Ferrocene methanol (324)

Addition of $NaBH_4$ (0.061 gm) to a solution of ferrocene carboxyaldehyde (0.26 gm) in methanol (5 ml) cause immediate reduction as indicated by the change in colour from red to

yellow. Evaporation of the solvent and recrystallisation from water afforded ferrocenyl methanol (Hydroxy methyl ferrocene) (0.216 gm; 85%) mp 76^{0}C.

2.7: Methyl ferrocene (327)

Ferrocene carboxaldehyde (1gm) in glacial acetic acid (20 ml) was added to amalgamated zinc needles (7 gm) and concentrated hydrochloride acid (20 ml) under nitrogen. The mixture was heated on a steam bath for 15 minutes, cooled, and poured into water; the mixture was filtered and the solid material washed with benzene. The two layers in the filterate were separated, the aqueous layer was extracted three times with benzene, and the combined benzene solutions were washed with water, aqueous sodium hydrogen carbonate, and water and dried (Na$_2$SO$_4$). Removal of benzene under reduced pressure left yellow oil (0.8 g) slightly volatile with benzene. Distillation of this oil at 86/0.4 mm afforded methyl ferrocene (0.6 gm., 66%) which, crystallised from ligroin, had m.p 36 ^{0}C .

2.8: Ferrocene acrylic acid preparation (324)

The ferrocene carboxy aldehyde (0.5 gm), malonic acid (0.5 gm) and piperidine (10 drops) were dissolved in pyridine (12 ml) and heated under N$_2$ on a boiling water bath for 2 hours. The cooled solution was diluted with water and extracted with chloroform. The chloroform extracts was washed with diluted HCl and water and then extracted with 2N NaOH. Acidification of the aqueous layer precipitated the brick red–beta ferrocenyl acrylic acid (0.4 gm 68%). Recrystallisation from benzene afforded deep red prisms m.p 186-187^{0}C.

2.9: 11' di(hydoxy) methyl ferrocene (328)

A solution of dimethiodide (1.0gm 1.6 mM) in NaOH solution (5 N, 100 ml) was heated under reflux for 6 hours and then extracted with ether, the extracts were washed with water, dried over Na_2SO_4 and evaporated and the residue was dissolved in benzene and chromatographed, benzene, ether (1:1) eluted the sole product 1,1' di(hydroxyl) methyl ferrocene (0.36 gm, 87%).

2.10: Monosulfonic Acid of Dicyclopentadienyl iron (329)

Sulfuric acid (100%, 4.9gm.) was added at 25-33^{0}C to slurry of dicyclopentadienyl iron (37 g.) in acetic anhydride (200 ml.). The reaction mass was agitated overnight. The undissolved solids were filtered and identified by mixed melting points as unreacted dicyclopentadienyl iron (15.8 g.). The acetic anhydride filtrate was poured into water (1,000 cc.) and heated to 80^{0}C. An additional amount of dicyclopentadienyl iron (10 g.) thus was separated. The dilute acetic acid solution was evaporated on a steam-bath. The residue was slurried in an excess of aqueous ammonia, clarified by filtration and evaporated to dryness. The residue (12 g) was dissolved in absolute methanol. The solution was clarified by filtration and again evaporated. An ammonium salt of a monosulfonic acid of dicyclopentadienyl iron (11 g.), was obtained. Anal. Calcd. for $C_{10}H_{13}FeO_8NS$.

2.11: Ferrocene thiol synthesis

It is prepared from ferrocene sulphonyl chloride which is converted to ferrocene thiol

Ferrocene sulphonyl chloride (330)

Crude ferrocene sulphonic acid(62 gm, 0.2 mole) was added in portions to phosphorous trichloride (210 ml, 2.4 mM), preheated to 50^{0}C , at such rate as to maintain gentle refluxing the mixture was then heated on a water bath until evolution of hydrogen chloride ceased (appro 6 hrs), diluted with boiling ligroin (50 ml) and filtered. The orange filterate was

evaporated under reduced pressure and the residual solid (50 gm) crystallised from ligroin, giving ferrocenyl sulphonyl chloride (48.1 gm , 82%) as crimson needles, mp 100^{0}C which darkened rapidly in moist air (Found C 42.6 , H, 3.4 C$_{10}$H$_9$SClFe requires C , 42.2 H 3.2%)

Ferrocene thiol (331)

A stirred solution of lithium aluminium hydride (3.8 gm , 0.1 mole) in ether (150 ml) under nitrogen, the sulphonyl chloride (7.11 gm, 0.025 mole) in the same solvent (100 ml) was added during 35 minutes. After 18 hours refluxing, ethyl acetate (5 ml) was added drop wise, following by wet ether (50 ml) and then 3.5 N sulphuric acid (300 ml). The ethereal layer was separated, dried and evaporated, yielding ferrocenthiol as afoul smelling oil, b.p which crystallise at -70^{0}C formed orange crystals.

2.12: Ferrocene carboxylic acid (332)

It is prepared by the procedure, a mixture of 1.0 g. of acetyl ferrocene, 2 ml. of pyridine and 1.1 g. of iodine was agitated for 12 hr. at room temperature, then for 90 min. in a boiling water-bath. The mixture was diluted with aqueous 0.6 N sodium hydroxide and stirred for 24 hrs. at room temperature. Which was recrystallized from chloroform to give crystals which decomposed at 208.5 ^{0}C.

2.13: Preparation of ferrocene thiocarboxylic acid: (333)

To a suspension of ferrocene carboxylic acid (460 mg , 2.0 mM) in petroleum ether (b.p 40-45 ^{0}C) (20 ml) was added drop wise an excess of thionyl chloride (2.Gm, 16 mM) at room temperature. The resulting mixture was stirred for 2 hours at 50^{0}C. The solvents were evaporated at reduce pressure, and the residue was extracted several times with petroleum ether. Evaporation of the petroleum ether was followed by washing of the residual solid with a small portion of petroleum ether to give ferrocene carboxylic acid chloride (I) (320 gm, 64% m.p 48-49^{0}C).

Preparation of piperidinium ferrocenyl thiocarboxylate (II)

Two molar equivalents of freshly prepared sodium hydrogen sulphide in dry ethanol (30 ml) was added gradually to a solution of I prepared from I(460 mg, 2.0 mmole) in petroleum ether (20 ml) under cooling with ice water. The resulting solution was stirred for 1 hour. The reaction mixture was concentrated to about 1 ml and poured into 50 ml of ether. The ethereal layer was separated and extracted with 50 ml of 10% KOH solution. The resulting dark red aqueous layer was acidified with 50 ml of 10% HCl and then extracted with 50 ml of ether at 5^0C, the ether extracts were washed with water dried over anhydrous $MgSO_4$ and treated with 1.8 mmole of piperidine at 5^0C. filteration of the resulting residue and recrystallisation from n-Hexane /CH_2Cl_2 gave orange needles crystals of piperidinium ferrocenthiocarboxylate (II) (410 mg, 62%)

Preparation of ferrocene thiocarboxylic acid (III)

Concentrated HCl (20 ml) was added to a suspension of salt II (330 mg, 1.0 mM) in ether (100 ml) and the mixture was shaken vigorously. The ether layer was separated , washed with water and dried over anhydrous $MgSO_4$, removal of the solvent in vacuo gave dark purple crystals of pure ferrocene thiocarboxylic acid (III) (230 mg, 94%)

2.14: Condensation of acetyl ferrocene with ethyl carbonate to form beta keto ester (325)

To a stirred solution of 0.4 mole of potassium amide in 500 ml of liquid ammonia was added 45.6 g (0.2 M) of acetyl ferrocene followed, after 10 min by a solution of 47.2 gm (0.4 M) of redistilled ethyle carbonate in 100 ml of dry ether (added drop wise). The liquid ammonia was removed as more dry ether was added and the resulting ether suspension refluxed 30 min. The solid was collected on a funnel washed well with dry ether, dissolved in water, and acidified with cold acetic acid. The oil was taken up in ether washed with

saturated sodium bicarbonate solution dried over $MgSO_4$, filtered and the solvent removed. The oily residue slowly crystallize ester. M.p 55-57 ^{0}C. Recrystallisation from 9:1 hexane benzene raised the mp to 57.5^{0}C to 58.5^{0}C.

2.15: Preparation of Ferrocenyl acetic Acid (334)

A mixture of 20 g of acetyl ferrocene, 7 g. of sulfur, 50 ml. of dioxane and 150 ml of morpholine was heated at reflux for 18 hr. under nitrogen. The reaction mixture was filtered and evaporated to small volume under reduced pressure, then transferred to an alumina column and eluted in two fractions with benzene. From the first fraction was obtained 10.2 g. (35%) of ferrocenylacetothiomorpholide, m.p. 126-128°C, and from the second fraction 1.0 g. (5%) of recovered acetylferrocene.

Ferrocenylacetothiomorpholide, recrystallized from ether, had m.p. 130-131°. The crude thiomorpholide was heated under reflux for 4 hr. with 2 N aqueous sodium hydroxide, then filtered, washed with ether and acidified with hydrochloric acid. The precipitated acid was extracted into ether, and the ether extracts were washed with water, dried and evaporated to small volume. Addition of pentane gave 5.5 g. (73% from the thiomorpholide) of precipitated ferrocenylacetic acid. The yellow acid, recrystallized from ether-pentane, darkened 125-135 ^{o}C

2.16: β-Ferrocenyl ethyl alcohol (325)

It is prepared in quantitative yield from ferrocenyl acetic acid by reduction at room temperature with lithium aluminum hydride. The yellow alcohol was recrystallized from ether-pentane and had m.p 49-50^{0}C.

2.17: Ferrocene methyl chloride (331)

To a suspension of hydroxy methyl ferrocene (I) (460 mg, 2.0 mM) in petroleum ether (b.p 40-45^{0}C) (20 ml) was added drop wise an excess of thionyl chloride (2. Gm, 16 mM) at room temperature. The resulting mixture was stirred for 2 hours at 50^{0}C. The solvents were evaporated at reduce pressure, and the residue was extracted several times with petroleum ether. Evaporation of the petroleum ether was followed by washing of the residual solid with a small portion of petroleum ether to give ferrocene methyl chloride.

2.18: Preparation of ferrocenyl acetaldehyde (335)

A solution of methylsulfinyl carbanion (0.035 mol) in 1:1 DMSO-THF (50 ml) was cooled to -15 ^{0}C under a nitrogen atmosphere. To this solution was added, drop wise over 3 min, 7.0 g (0.035 mol) of trimethylsulfonium iodide dissolved in 30 ml of DMSO. After stirring for 1 min a solution of ferrocene carboxaldehyde (1.5 g, 0.0069 M) in THF (20 ml) was added drop wise to this ylide solution over a period of 2-3 min. The mixture was stirred at -15 ^{o} C for 5 min, and then allowed to warm to room temperature over 0.5 hr and poured into 300 ml of water. The resulting solution was extracted three times with 50 ml portions of diethyl ether; the combined ether portions were washed with water and dried (MgS0$_4$). Removal of the solvent gave the crude product, the components of which were separated by chromatography on silica gel with benzene as eluent. The major product was ferrocenylacetaldehyde, formed in 64% yield.

2.19: Ferrocenyl methyl Sulfide (336)

Hydroxy methyl ferrocene (10.0 g, 0.046 mol), mercaptoacetic acid (100 ml), and water (100 ml) were heated at the reflux temperature for 2 hr. The reaction mixture was cooled to room temperature and poured into 800 ml of water. The precipitate was washed with water, taken up in ether, and extracted into 5% aqueous sodium hydroxide. Ferrocenyl methyl

carboxymethyl sulfide (9.8 g, 74%) was isolated by neutralization (acetic acid), filtration, washing of the precipitate with water, and drying in vacuo (mp 125-126 ^{0}C). An authentic sample of ferrocenyl methyl sulfide was prepared as reported in the literature (m.p. 126-127 ^{0}C).

2.20: Mono ethyl ferrocene preparation: (337)

Mono acetylferrocene (4.5 g., 0.02 mole), dissolved in 30 cc. of glacial acetic acid, was added to a suspension of 300 mg. of reduced platinum oxide catalyst in 20 cc. of the same solvent. The mixture was stirred in an atmosphere of hydrogen, at room temperature, for a period of 70 hours, at the end of which time 994 cc. Of hydrogen had been taken up (100% based on a theoretical uptake of 2 moles of hydrogen per mole of ketone). The deep amber solution was filtered by suction, in an atmosphere of nitrogen, directly into 300 cc. of water containing sufficient sodium carbonate to neutralize the acetic acid. The aqueous solution was then extracted twice with 100ml. Portions of ether, and these were combined, washed to neutrality and dried. Removal of solvent left 4.3 g. of mobile, amber colored oil, possessing a mild camphoraceous odor. An infrared spectrum of this product revealed the presence of small amounts of partially reduced and unreduced material. Purification was effected by dissolving the crude product in a small volume of petroleum ether and chromatographing on 200 g. of alumina. On elution with petroleum ether, monoethyl ferrocene separated easily from alcoholic and ketonic contaminants. The product was distilled at 121-123 ^{o} C (10 mm.), (Yield 3.28 g. (77%)).

2.21: Ferrocene dicarboxylic acid preparation: (338)

To an ice-cold, stirred solution of 162 g. (2 M) of 37% aqueous formaldehyde was added 722 g. (4 M) of 25% aqueous dimethylamine solution maintaining the temperature below 15^{0}C. After stirring 0.5 hr. longer, solid potassium hydroxide was added until two

layers separated. The upper layer was removed and dried over solid potassium hydroxide. After filtering, the product was distilled to give 178 g. (8770) of N,N,N',N'-tetramethyldiaminomethane, b p. 82-84^{0}C.

Aminomethylatim of ferrocene to form tertiary amine III. (338)

A mixture of 25.5 g. (0.25 mole) of N,N,N',N'-tetramethyldiaminomethane, 7.9 g. (0.25 M) of paraformaldehyde and 200 g (3.3 M) of glacial acetic acid was heated for a few minutes until solution occurred, and 93 g (0.5 M) of ferrocene was then added with stirring. The mixture was stirred and refluxed for 5 hr. All of the ferrocene dissolved within about 1 hr. The solution was cooled slightly, and 500 ml. of water was added with stirring. The resulting mixture as filtered and the solid was washed with dilute acetic acid, followed by water.

This solid consisted largely of unreacted ferrocene which was reemployed in the aminomethylation reaction. The clear filtrate (and washings) was chilled in an ice bath, and made strongly alkaline with 50% sodium hydroxide solution. The resulting mixture was extracted three times with ether, and the combined extract was washed with water. The ethereal solution was dried over magnesium sulfate and, after filtering, the solvent was removed. The residue was distilled in vacuo to give 62.2 g. of N,N-dimethylaminomethylferrocene (III) (clear amber).

Alkylation of malonic ester with quaternary ion III. Dicarboxylic acid

The methiodide of N,N-dimethylaminomethylferrocene (III) was prepared as described previously by the aminomethylation of ferrocene (dicyclopentadienyl iron) with formaldehyde and dimethylamine, followed by the methylation of the resulting tertiary amine with methyl iodide. A solution of sodium ethoxide was prepared under nitrogen from 2.3 g. (0.1 M) of freshly cut sodium and 100 ml. of absolute ethanol, and a solution of 16.0 g. (0.1 M) of redistilled diethyl malonate in 20 ml. of absolute ethanol was added.

To the resulting sodio malonic ester (0.1 M) was added, with stirring, 38.5 g. (0.1 M) of the solid methiodide (III), and the solution stirred and refluxed for 43 hr. The odor of trimethylamine was detected at the top of the condenser. After cooling, the reaction mixture was poured onto crushed ice, acidified carefully with 1N hydrochloric acid, and extracted three times with ether. The combined ethereal extract was washed with saturated sodium bicarbonate solution and dried over magnesium sulfate. After filtering, the solvent was removed to leave 34 g. of the alkylation product as clear amber oil which crystallized slowly.

To 30.0 g. of this crude alkylation product was added 10 ml of 95% ethanol and 50 ml. of 30%, potassium hydroxide solution, and the resulting mixture was refluxed for 8 hr. After cooling, diluting with four volumes of water, and extracting with ether, the alkaline solution was acidified carefully with 6N hydrochloric acid to precipitate dicarboxylic acid which was collected on a funnel, washed with water, and dried. This acid (18 g., 67%) melted at 130-133 ^{o}C. A sample of the solid acid was boiled with water, and the resulting emulsion was filtered and cooled rapidly to produce fine golden plates m.p. 133-134 ^{o}C (sample immersed in the melting point bath at 120 ^{o}C).

2.22: Condensation with acetophenone to form alpha, beta unsaturated ketone (339)

To a stirred solution of 2.56 gm (0.064 M) of NaOH in 20 ml water (cooled to 15 ^{o}C) was added successively, solutions of 6 gm (0.05 M) of acetophenone in 10 ml of 95% ethanol and 10.8 gm (0.05 M) of ferrocene carboxyaldehyde in 30 ml of 95% ethanol, the mixture was stirred over night, the thick purple suspension was filtered and the solid washed thoroughly with water, followed by a small portion of ice cold 95% ethanol , after drying, there obtained 14.5 gm (92%) of α, β unsaturated ketone (purple solid) mp 126-128^{0}C.

2.23: Beta-Ferrocenyl propionic acid (340)

7.4 g. of ferrocene, 2.0 g. of succinic anhydride and 5.8 g. of aluminum chloride. The crude acid was extracted from methylene chloride with sodium carbonate filtered through Celite and re-precipitated with dilute hydrochloric acid; yield 5.0 g. (87%). A sample of orange β-ferrocenoyl propionic acid, recrystallized from methanolbenzene, had m.p. 166.5-167.5 °C.Anal. Calcd. for $C_{l4}H_{14}FeO_3$.

2.24: Isobuytric acid Ferrocene : (341)

To a mixture of 26 g of aluminum chloride and 300 ml. Of methylene chloride was added a solution of 44.3 g. of ferrocene and 10 g. of glutaric anhydride in 300 ml. of methylene chloride. The mixture was stirred for 2 hr. at room temperature, then decanted over ice and worked up in the usual manner. The methylene chloride solution was concentrated and the residue dissolved in benzene and transferred to an alumina column, which was eluted with benzene. The first of two bands gave 21.4 g. (48%) of recovered ferrocene, while the second band yielded 16.3 g. (53%) of isobuytric acid ferrocene as a red oil, which crystallized from pentane at Dry Ice temperature, Highly unstable in aqueous media.

2.25: Alpha Propionyl ferrocene (340)

It is prepared by the Friedel-Crafts acylation of ferrocene with propionic anhydride. To a mixture of 34.5 g. of aluminum chloride and 300 ml. Of methylene chloride was added a solution of 44.3 g. of ferrocene and l5.6 g. of propionic anhydride in 300 ml. of methylene chloride. The mixture was stirred for 2 hr. at room temperature, then decanted over ice and worked up in the usual manner. The methylene chloride solution was concentrated and the residue dissolved in benzene and transferred to an alumina column, which was eluted with benzene. The first of two bands gave 21.4 g. (48%) of recovered ferrocene, while the second

band yielded 16.3 g. (53%) of propionyl ferrocene as a red oil, which crystallized from pentane at Dry Ice temperature, m.p. 38-39 ^{0}C.

2.26: Ferrocenyl pyridine (342)

A solution of pyridine was prepared from 34 gm of pyridine, 20 gm of sodium nitirite and 8.3 ml of concentrated H_2SO_4 in 150 ml of water. This was added rapidly to a solution of 10 gm of ferrocene in 350 ml of acetic acid. The resulting dark solution was allowed to stir overnight at 10-15 ^{o}C. and was then poured to 1 litre of water containing sodium bisulfate. Chloroform, the extracts were combined, washed with Na_2CO_3. And water to neutrality and dried over $MgSO_4$. The drying reagent was filtered off and solvent removed leaving a deep orange solid

2.27: QSAR equation generation

Understanding the QSAR generation process

This section describes the general procedure for generating a QSAR, which consists of the following 11 steps: (343)

1. Identify the training set

First step, the molecular structures are chosen as the training set. QSAR provides tools that enable to build new structures, create a congeneric series of 3D structures, and import chemical structure files in a wide variety of formats.

2. Enter biological activity data

For each of the molecules in the training set observed biological activity is provided

3. Generate conformations

For a 3D QSAR analysis, conformational information is provided, which is usually obtained by performing a conformational search in G/PLS method.

4. Calculate descriptors

QSAR calculates a wide variety of spatial, electronic, topological, information-content, thermodynamic, conformational, quantum mechanical, and shape descriptors. QSAR gives you the ability to modify existing descriptors and the combination of descriptors in a descriptor set. You can create or import new descriptors from other Cerius^2 modules such as Molecular Field Analysis (MFA) and Receptor to meet your specific requirements.

5. Explore the data

Graphs are to depict structural descriptor distribution. If holes exist in descriptor sets, new compounds to fill the holes. You can also display correlation matrices to assist you in identifying descriptors that are highly correlated and histograms and rune plots to help you examine the uniformity of your data. Descriptive statistics are available to further characterize descriptors. Additionally, you can transform and normalize descriptors, as

appropriate. You can also carry out principal components analysis (PCA) and cluster analysis to further characterize your data.

6. Generate a QSAR equation

After you identify the appropriate dependent and independent variables, you can choose from several statistical methods for generating a QSAR equation. These include multiple linear regression, partial least squares (PLS), simple linear regression, stepwise multiple linear regression, and principal components regression (PCR). Additionally, if the genetic function approximation (GFA) functionality is installed, you can also perform a genetic analysis, either GFA or G/PLS, to create a QSAR equation.

7. Validate the equation

Apply validation techniques to identify outliers and leverage points. analyses and crossvalidation to characterize the robustness of the QSAR.

8. Analyze the equation

Graphical tools to plot observed vs. predicted activities and to identify outliers. You can also generate 3D plots to visualize the positions of important 3D-QSAR descriptors from Molecular Field Analysis (MFA) or Receptor Surface Analysis (RSA) in relation to the molecules.

9. Save the QSAR equation

You can save calculated QSAR equations.

10. Predict activity

QSAR, you can simply draw a candidate structure, add it to your study, apply your calculated QSAR equation, and immediately view the predicted activity.

11. Save the study When you are finished with your study, you can save the entire QSAR analysis, including all its component structures and conformations, for later review and use.

QSAR equation was generated as described in Accelrys Cerius^2 tutorials (349). Ferrocene models were sketched using 3D sketchers and models were minimized by smart minimizations in offset methods, while atomic charges were calculated by offset up method. The models were superimposed using the iron axis and the upper cyclopentadiene ring as the basic skeleton. These models were entered into QSAR study table, with the negative log value of the IC_{50} entered into study table, while the descriptors were added in default mode, the probing was done using H^+ and CH_3^+ probes and the grid was developed; The QSAR equation was generated using G/PLS (350). The above equation is further tuned to get a better QSAR equation by selecting appropriate training and test set. 3D points were generated by default. The models were used in receptor module of Cerius^2 and the interactions computed.

QSAR Validation methods:

R – Squared (r^2): the square of the correlation coefficient (344). This statistic is used to describe the goodness of fit of the data in the study in table to the QSAR model.

Cross validated r^2: A cross validated r2 is usually smaller than the overall r2 for a QSAR equation. It is used as a diagnostic tool to evaluate the predictive power of an equation generated using the multiple linear regression of PLS methods.

Dep SD: The sum of squared deviations of the dependent variable (346) values from their mean.

PRESS (Predicted sum of squares): the sum , over all compounds , of the squared differences between the actual and the predicted values of the independent variables(347).The values reported in the table is computed during a validation procedure and can be computed for the entire training set. The larger the value, the more reliable is the equation.

Outliners: - An outliner (348) is defined as a structure with a residual greater than two times the standard deviation of the residuals generated in the validation procedure.

2.28: Purification of pRYG negatively supercoiled plasmid DNA:

The negatively supercoiled pRYG plasmid DNA was purified from the E.coli HB101 strain containing the plasmid, using the alkaline lysis procedure. The procedure described in 1 litre culture which can be scaled upto 4 liters. An overnight culture of the plasmid containing bacteria (grown in the presence of 100 µg/ml ampicillin) was used for purification of the plasmid.

Bacterial cell growth and harvesting: 25 ml of LB broth was inoculated with a single bacterial colony containing the plasmid. The culture was grown in a shaking incubator for 8 hours at 37^0C. This culture was used for inoculating 1 liter of LB broth. The one liter culture was grown overnight (12-14 hours) at 37^0C in a shaker incubator. The purification procedure was carried out at 4^0C. Cells were harvested by centrifugation at 5000 rpm for 10 minutes. The cells were lysed with 40 ml of lysis buffer by constant stirring over a period of 15 min.

Alkanline lysis: 80 ml of freshly prepared alkaline solution was added and the constituents were mixed by swirling in a bottle. The mixture was placed in ice for 10 min. 50 ml of freshly prepared saturated ammonium acetate solution was added gently against the walls of the bottle. The bottle was placed on ice for 10 min. the precipitated proteins were removed by centrifugation at 12,000 rpm. The supernatant was clarified by filtrating it through glass wool. Ice cold isopropanol (0.7 volumes) was added to the supernatant and placed on ice for 20 min.

Phenol chloroform extraction of DNA: the precipitated DNA was pelleted at 12,000 rpm. The supernatant was removed and the pellet allowed for drying. This pellet was dissolved in 40 ml of sodium acetate buffer. After 5 min on ice, an equal volume of Tris saturated phenol and chloroform was added and vortex mixed for 2 min in 50 ml tubes. The tubes were

centrifuged at 12,000 rpm for 10 min. the aqueous phase was taken in an autoclaved conical flask and the phenol phase was removed.

Precipitation and dissolution of DNA: the aqueous phase containing the DNA was treated with 0.7 volume of ice cold-isopropanol and 0.1 volume of 3 M sodium acetate (pH 4.2) and placed on ice for 20 minutes. The DNA was pelleted and washed twice with ice cold ethanol (70%). The pellet was dissolved in a proper volume of Tris-EDTA buffer.

2.29: Relaxation assay

This assay was performed following the procedure of Osheroff et al (1983) (351). The reaction mixture contained of 0.6 μg of negatively supercoiled pRYG plasmid DNA with increasing concentrations of ferrocene drugs in relaxation buffer (50 mM Tris-HCl (p H 8.0), 120 m M KCl, 0.5 mM EDTA, 0.5 mM DTT, 10 mM $MgCl_2$, 30 μg/ml BSA, 1 m M ATP). The reaction was initiated by adding 2 units of topoisomerase II α or β and incubated at 37 ^{0}C for 30 min. The reaction was stopped by adding 2 μl of 10% SDS, and 3μl of loading dye (0.5 % bromo phenol blue, 0.5% xylenol cyanol, 30% glycerol in water) and the products were separated on a 1% agarose gel in TAE (20 mM Tris acetate, 0.5 mM EDTA) at 50 V for 10 hours. The gel was stained with ethidium bromide (1μg/ml), and was observed in photo dyne UV transilluminator and photographed.

2.30: Cleavage assay

The formation of cleavage complex was assayed following the procedure of Robinson and Osheroff (1990) (352). The reaction mixture contained 0.6 μg of negatively supercoiled pBR 322 DNA with increasing concentrations of ferrocene compounds in cleavage buffer (10 mM Tris-HCl (pH 7.9), 50 mM NaCl, 50 mM KCl, 0.1 mM EDTA, 2.5% glycerol, 5 m M $MgCl_2$). The reaction was initiated by adding 10 units of topoisomerase II and incubated at 37^{0}C for 15 min, then stopped with addition of 2 μl each

of 0.5 M EDTA, and 10% SDS. The DNA bound protein was proteolysed by incubating the reaction mixture with 2 μl of Proteinase K (2mg/ml) at 45^0C for 1 h. The products were separated on 1% agarose gel for 2 hours at 50 volts in TAE buffer, ethidium bromide (1μg/ml) stained and photographed under U.V.

2.31: ATPase assay

This assay was conducted as described in Jayaraju et al (1999) (353). The reaction mixture containing of 1ml reaction buffer (20 mM Tris-Hcl pH 7.5, 0.1 mg NADH, 100μM DTT, 1mM ATP, 2 mM Phosphoenol pyruvate, 4mM $MgCl_2$), 12.5 units of Pyruvate kinase and 12.5 units of Lactate dehydrogenase was incubated at 37^0C for 5 min. The incubation was continued further with addition of 0.3 μg of DNA with increasing concentrations of the ferrocene drugs and 4 units of topoisomerase II for 30 min and the absorbance was recorded at 340 nm. In control study, the reaction was also carried out without Topoisomerase II.

2.32: DNA thermal denaturation assay

Calf thymus DNA (sodium salt) was dissolved in 1 mM sodium phosphate buffer containing 1 mM sodium chloride and 1 mM EDTA. DNA concentration was adjusted to give an absorbance of 1.0 in 1 cm path length cuvette at 260 nm (354). The ferrocene drugs were added to DNA at concentrations, which gave drug to nucleotide ratio of 1:10, 1:5, 1:2, and 1:1 respectively. The samples were incubated in 1 cm path length cuvette for 2 min to allow drug-DNA binding. A JASCO 550 spectrophotometer was set to give a 1^0C rise in temperature per minute with ETC 505 T thermo programmer and temperature controller. Increase in absorbance at 260 nm was recorded from 40-90^0C.

2.33: Drug interaction assay

The interaction of drug with enzyme was done in 2 ways. In the first, the enzyme was immunoprecipitated using ProteinA agarose method as described in (321).

Immunoprecipitated enzyme was incubated with Azalactone ferrocene at 50 and 100μM, for 15 minutes. The unbound drug was removed by washing 3 times with TBS buffer containing 0.1% Tween20. The drug treated enzyme immunoprecipitate was mixed with super coiled DNA and the relaxation assay was conducted.

In the second approach, pRYG DNA was preincubated at 50, 100 μM of Azalactone ferrocene. The complex was incubated for 15 minutes at 37 ^{0}C. After incubation the drug was diluted by 10 fold to get drug concentrations of 5 and 10 μM. The reaction mixture containing diluted drug and DNA was added to immunoprecipitated topoisomerase II β isoform and the relaxation assay was conducted.

2.34: Apotransferrin purification

Blood sample collection and protein purification:

Transferrin protein was purified form plasma. Fresh and healthy human blood sample was collected and plasma is separated. Plasma is treated with a series of alcohol gradients and kept on ice for 10 minutes, protein is precipitated, and the sample was centrifuged at 10,000 rpm for 15 minutes. The supernatant and pellet is analysed (355) for the presence of transferrin. At 40% (v/v) was precipitated. It is solubilised in Tris buffer and further purified by gel filteration chromatrography.

2.35: Gel filtration chromatography

20 mg of 40% alcohol precipitated protein was loaded onto 100 ml sephacryl S-100 gel filterate. 1ml fractions are collected. The transferrin is converted to apotransferrin by dialyzing the protein in 10mM EDTA, 10mM sodium acetate (pH 5) for three hours thrice and then dialyzing the protein in TBS for overnight and this protein is used for all further experiments. Protein estimated by Broadfords method and analyzed by SDS-PAGE

2.36: Nanoparticle Preparation

For preparation of nanoparticles, procedure described in Kondapi (356) was adapted. 25 mg of apotransferrin in 100 µl of phosphate buffer saline (PBS) was slowly mixed with a 100 mM of Doxorubicin hydrochloride (3.46 mg)/ azalactone ferrocene (5.2 mg) in 100 µl DMSO (100mM) and the mixture was incubated on ice for 5 min. The mixture of apotransferrin and the drug was slowly added to 15 ml of olive oil at 4^0C with continuous dispersion by gentle manual vortexing. The sample was sonicated at 4^0C using a narrow short probe of MSE sonicator (PG43301, MSE Instruments, UK) with a 30 sec period pulse, having an amplitude of 5 microns (and a time period of 30 seconds) and this sonication step was repeated 15 times with a gap of 1 minute between successive steps. The resulting mixture was immediately frozen in liquid nitrogen for 10 min. and was then transferred to ice and incubated for 4 hours. The particles formed were pelleted by centrifugation at 6000 rpm for 10 minutes and the pellet was extensively washed with diethyl ether and dispersed in Phosphate buffered saline. The particles were estimated for protein using Biurett method and protein equivalent of nanoparticles were used for each experiment.

Microscopic analysis of nanoparticles

Structure and morphology of the nanoparticles were investigated using Scanning electron microscope (Philips FEI-XL 30 ESEM operated at 20 KV USA), Transmission electron microscope (JOEL JEM 1011 operated at 100 KV, USA), Atomic force microscope (SPA-400, USA); Manufacturer's instructions were followed for sample preparation, data collection and analysis of particles.

2.37: TEM procedure (357)

Place several drops of dispersed Nanoparticles on a clean piece of Parafilm. Pick up the grid with clean forceps and float the grid, carbon mess containing side down, on a drop

of Nanoparticles. Leave the grids on the sample for 5 to 10 min. Transfer the grid with clean forceps and float the grid, section side down, on a drop of uranyl acetate stain. Leave the grids on the stain for 5 to 10 min.

After 5 to 10 min in uranyl acetate, remove the grid from the uranyl acetate, dip the grid in the first beaker of warm, freshly boiled deionized water and swirl the grid around. Repeat the process in the three other beakers of warm, freshly boiled deionized water. Keep the grid wet. Dry the grid using filter paper points (cut triangles of filter paper) by placing the paper point between the points of the forceps.

Aqueous Uranyl Acetate

Prepare 2% (w/v) solution of uranyl acetate ($UO_2(CH_3COO)_2.2H_2O$) in 5 ml of freshly boiled warm deionised or distilled water. The pH of a freshly prepared 2% aqueous solution of uranyl acetate is approx 4. Filter the solution through Whatman #42 or #50 filter paper or equivalent. Store the filtered solution in a dark colored container or wrap the container with aluminum foil to exclude light since uranyl acetate is light sensitive. Filter an appropriate volume of stain through a 0.22-μm micro filter when ready to stain grids.

2.38: SEM protocol (358)

The surface morphology and particle size of the sample is determined by SEM FEI-XL 30 ESEM (Philips) operated at 20 KV. 0.5 mm x 0.5 mm clean square glass slide is cut and placed on the stub with Carbon double-sided sticky tapes. Stubs should be labeled on the bottom side using a permanent marker. Place 2 μl of the buffer dispersed sample and spread all over the glass slide with the pipette manually and air dry the sample. Air dry specimen in dust free environment at room temperature for one hour. And coat with gold in Sputter Coater,

Sputter Coater:

The sputter coater uses argon gas and a small electric field. The sample is placed in a small chamber which is at vacuum. Argon gas is then introduced and an electric field is used to cause an electron to be removed from the argon atoms to make the atoms ions with a positive charge. The Ar ions are then attracted to a negatively charged piece of gold foil. The Ar ions act like sand in a sandblaster, knocking gold atoms from the surface of the foil. These gold atoms now settle onto the surface of the sample, producing a gold coating. Store specimens in dry, dust free environment till the analysis. Images are recorded using appropriate resolution.

2.39: AFM protocol (359)

0.5 x 0.5 mm glass piece is taken to one side double sided tape is placed and on the other side a mica sheet is attached. The mica sheet is peeled by sticking the cellophane tape and remove it and repeat the step several times to get a smooth surface for the analysis.
On the smooth surface keep a 5 µl of the sample and uniformly dispersed in spin coater, the sample is dried in a dust free zone for 12 hours. The sample is kept in SPA-400 and manufacturer's instructions are followed. Images are recorded at different resolution and surface morphology is predicted.

2.40: Drug release kinetics (360)

10 mg protein equivalent doxorubicin encapsulated nanoparticles are taken in a 1N acid in phosphate buffer saline, absolute alcohol and 100% DMSO, and incubated for the 5 minutes and the samples are centrifused at 12,000 rpm for 10 minutes and the supernatant is analysed for the characteristic peak of doxorubicin at 555 nm by spectrofluorimeter and fluorescence is recorded.

2.41: Drug estimation in the nanoparticles

The drug from the drug encapsulated nanoparticles is released by the acid release method and characteristic peak is calculated by UV-VIS spectroscopy and the peak absorbance is calculated.

2.42: Dot blot analysis (361)

Drug loaded Nanoparticles, apotransferrin and BSA were loaded onto the dot blot and allowed to absorb for 5 minutes. The blot is blocked by 5% milk powder and probed by Mouse anti-human transferrin monoclonal antibody and goat anti mouse IgG conjugated with alkaline phosphatase (Fitzgerald, Germany). The blot was developed by the BCIP/NBT.

Blotto

5 gms of non-fat dry milk dissolved in 100 ml of TBS.

Stop solution

Tris-HCL (pH 2.9)   20mM
Calcium chloride   1mM

2.43: Competition of the Soluble Apotransferrin with the Apotransferrin-drug Nanoparticles (362)

Two million Cells were incubated in serum free media for 30 minutes in 12 well plate. Apotransferrin-drug nanoparticles (equivalent to 20 μg protein) in the presence of indicated concentrations of soluble apotransferrin at 0,80,160,240 μg and cells were incubated for 30 minutes. These were then washed thrice with PBS and were observed for the fluorescence emission by labeled cells in fluorescence activated cell sorter (FACS) analysis (Beckmann FACS STAR). Concurrent results of three independent studies reported.

2.44: Confocal microscopy analysis of Nanoparticle Localization Assay

Since cancer cells express higher number of transferrin receptors, SUP-T1 cells (T cell lymphoma) were used. The cells were incubated in the presence of 20 μg protein equivalent of apotransferrin-drug nanoparticles for a period of 30 min, 60 min, 90 min, 16 hours and the localization of particles was assessed through the use of Rhodamine Isothiocyante (RITC) labeled apotransferrin nanoparticles and using laser confocal microscopy (Leica). The reproducibility of the results was verified through three independent experiments.

2.45: FACS analysis of Nanoparticle recycling Assay (363)

Two million SUP-T1 cells were incubated for 30 minutes in serum free RPMI medium and nanoparticles were then added to these cells and the incubation was continued for 30 minutes. The cells were pelleted by centrifugation at 1200 rpm for 5 minutes. The pellet was extensively washed with PBS and transferred to a fresh 12 well plate in 10% serum containing media. The cells were dispersed in PBS and analysed for fluorescently labeled cells through FACS analysis. Studies of protein recycling were carried out using particles comprising RITC labeled apotransferrin, while drug recycling was monitored using particles comprising unlabelled apotransferrin and doxorubicin. Doxorubicin intrinsic fluorescence was monitored for drug localization in cells. Each of the above experiments was repeated three times independently to check the reproducibility.

2.46: MTT assay (364)

0.2 million SUP-T1/COLO-205/SK-N-SH cells per each well were seeded in 96 well plate and incubated at 37^0C for 4 hours in CO_2 incubator. These cells were treated with increasing concentrations of protein equivalent of nanoparticles, and incubated for 16 hours. The cells were pelleted at 1200 rpm for 10 minutes and medium was changed. To this, 20 μl

of 5 mg/ml (Sigma) MTT was added and incubated for 4 hours. The cells were pelleted at 1200 rpm for 20 minutes and the medium was removed and the precipitate was dissolved in DMSO and read in ELISA reader at 595 nm. Each experiment was repeated 3 times and the error is represented in terms of standard deviation.

2.47: Rat Hepatocellular carcinoma Model generation

A group of 6 rats was taken for each of the drug concentration and the experiments were done as approved by the Animal Ethics Committee, University of Hyderabad.

100 million ZH5 cells (Obtained from CCMB, Hyderabad) in 0.5 ml of peritoneal fluid was taken and injected into intra peritoneal cavity to the 2 months old Wister rat (120-140 gms). The Rat develops ascetic hepatocellular carcinoma symptoms within 4 days and by 7th day it will lose the activity and the animal will die during 7-8th day due to multiple metastasis and hepatocellular carcinoma (365).

Dosage schedule: One dose per day for 10 days with the drug administered through intra peritoneal route using 31 gauge insulin syringe (BD biosciences)

Effective dose: 500μg of protein equivalent-azalactone ferrocene/doxorubicin nanoparticles contain 125 microgram of azalactone ferrocene/doxorubicin nanoparticles. The particles were dispersed in 0.5 ml of PBS and were administered through *intra peritoneal* route to the 120-140 gm Wistar rat.

2.48: Liver sample collection

Treated and untreated rats were anaesthetized and sacrificed by standard cervical dislocation method, and blood sample was collected by heart puncture method and liver tissue was collected and immediately washed thrice with PBS and kept in 4% Para formaldehyde solution. These samples were embedded in paraffin wax and processed for Haematoxylin/eosin staining and the specimen was photographed and analysed.

2.49: Estimation of biochemical markers in serum

Estimation of Urea was done by Bertholet method (366), Creatinine by picrate method (367), Alkaline phosphatase by PNPP method (368) b, LDH (369) by the kits supplied by Qualigens Diagnostics manufactured by Sigma diagnostics (India)

2.50: Urea estimation by Bertholet method

Basic principle involves hydrolysis of urea following oxidation in the presence of salicylate. The product formed, indophenols, will be quantified at 600 nm.

$$\text{Urea} + H_2O \longrightarrow 2NH_3 + 2CO_2$$

$$NH_3 + 5NaOCl + 2 \text{ salicylate} \longrightarrow \text{Indophenol} + 5NaCl + 5H_2O$$
$$600 \text{ nm}$$
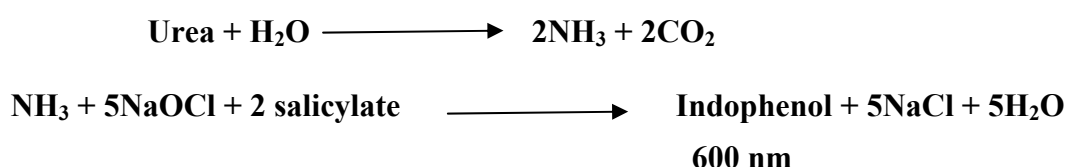
Urea estimation kit supplied by Qualigens Diagnostics manufactured by Sigma diagnostics (India) .1 ml of the working reagent I and 10 µl of the sample is taken and incubated for 5 minutes at $37^{o}C$ then 1 ml of the working reagent II is added and incubated for 5 minutes at $37^{o}C$ and to this 1 ml of the distilled water is added and absorbance is recorded at 600 nm against blank contain 10 µl of double distilled water.

2.51: LDH estimation

LDH in serum is estimated by kit supplied by Qualigens Diagnostics manufactured by Sigma diagnostics (India)

$$\text{Pyruvate} \xrightarrow{\text{LDH}} \text{Lactate}$$

NADH 340nm   NAD$^+$
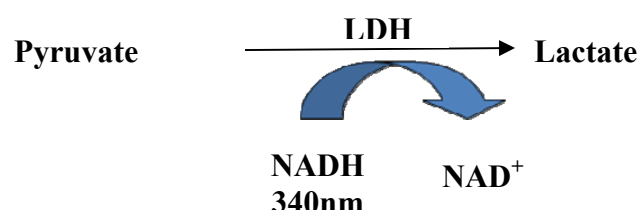
Pyruvate is converted to lactate in presence of LDH by utilizing NADH, the activity of LDH is quantified by measuring levels of NADH at 340 nm.

1 ml of the reagent I and 30 µl of the sample is taken and mixed gently and incubated for 1 minute at 37°Cand initial reading at 60 seconds and thereafter at intervals of 30 seconds (four readings). Determine the difference of absorbance per minute from the linear part of the assay.

2.52: Alkaline phosphatase estimation by PNPP method

Alkaline phosphatase in serum is estimated by kit supplied by Qualigens Diagnostics manufactured by Sigma diagnostics (India). PNPP is converted to PNP in presence of alkaline phosphatase, the product PNP is measured as a activity of alkaline phosphatase at 405 nm.

1 ml of the reagent I and 20 µl of the sample is mixed well and absorbance is recorded at 405 nm at 60, 90,120, and 150 seconds, determine the difference of absorbance per minute from the linear part of the assay.

$$\textbf{P-nitrophenyl phosphate} + \textbf{H}_2\textbf{O} \xrightarrow{\textbf{Alkaline phosphatase}} \textbf{P-nitro phenol} + \textbf{phosphate}$$
$$\textbf{405 nm}$$
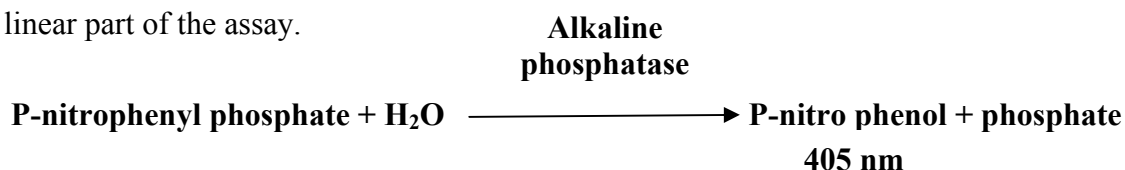
2.53: Creatinine estimation by alkaline picrate method

Creatinine in serum is estimated by creatinine estimation kit supplied by Qualigens Diagnostics manufactured by Sigma diagnostics (India). Creatinine in presence of alkaline picrate forms creatinine picrate complex which strongly show absorption intensity at 505 nm.

To the 1 ml of the working reagent add 100 µl of the sample mix and incubate at 30°C and absorbance is recorded at 0, 60, 120 seconds, determine the difference of absorbance during the linear part of the reaction.

$$\textbf{Creatinine} + \textbf{Alkaline picrate} \xrightarrow{\hspace{2cm}} \textbf{Creatinine picrate complex}$$
$$\textbf{505 nm}$$
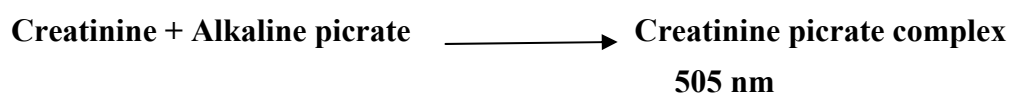
2.54: Statistical analysis of the markers

The above markers were estimated in six individual rats. The significance was analysed by ANOVA (370) to test whether the mean values among the groups were significantly different and HSD (371) significance test was carried out for pair wise comparison of mean values of each group. The data is presented in Table 5.1. Statistical values are presented in Appendix II.

2.55: Western blotting

Protein is solubilised in RIPA buffer (372). Lysates containing 75 μg of protein were resolved on 7.5% SDS PAGE mini gels and transferred to PVDF membrane, then immunoblotted with a 1:1000 dilution of mouse anti-human topoisomerase II α or β or actin or Transferrin antibodies and incubated with alkaline phosphatase–conjugated anti-mouse Ig-G antibody (1:2000 dilution in TBS) for 60 minutes at room temperature and then with TBS containing 0.15% Tween-20. The blots were developed using NBT-BCIP substrate in TBS and documented using an UVI-Tech gel documentation system.

2.56: RITC conjugation to protein (373)

2 mg/ml of protein was dissolved in 0.1 M sodium carbonate buffer pH 9. RITC in anhydrous DMSO at 1mg/ml (note: this should be prepared fresh for each labeling reaction. For each 1 ml of protein solution, add 50 μl of RITC solution very slowly in 5 μl aliquots very gently with continuous stirring the protein solution. After all the required amount of FITC solution has been added incubate the reaction in the reaction in the dark for 8 hours at 4 ^{o}C. Add NH$_4$Cl to a final concentration of 50 mM and incubate for 2 hours at 4 ^{o}C. xylene cyanol was added to 0.1% and glycerol to 5% gel filtration using the exclusion limit 20,000 to 50,000. The eluted conjugate is stored in light proof container.

2.57: Development and maintenance of hepatocellular carcinoma in rat model

Wistar rat (2 months old, 180 gm) is intra-peritoneal injected with 100 million ZH5 cell line (obtained from CCMB, hepatoma cell line). The rat develops hepatoma in 5-6 day which is clearly demarked by the increase of peritoneal fluid which contains the replicating ZH5 cell line. In 7-8 day rat looses all its metabolic activities and dies

At 5-6 day 0.5 ml of intra-peritoneal fluid of full blown hepatoma rat which contain 100 million cells in carefully injected into a healthy rat for the maintenance of hepatoma in rat model.

2.58: Paraformaldehyde fixation and paraffin wax embedding of tissues (374)

Sections prepared to examine cell and tissue morphology and in studies involving in situ hybridization, immuno-histochemistry, and enzyme histochemistry

Procedure:

Fixation of the tissue samples collected

Place dissected organs in labeled 20 ml glass vials. fill vials with freshly prepared 4 PFA fixative,4ºC, allowed fixation for 3 hours at 4ºC.After fixation 50% ethanol was added, rinse twice with 50% ethanol. Then the specimen incubated in 80% ethanol for 20 minutes, then replace 100% ethanol with xylene, two changes in ethanol xylenes were given, each time the tissues were incubated for 10 minutes. All steps were carried at room temperature.

Prepare samples for embedding in wax

Xylene decanted and add 5 ml fresh xylenes was added. An equal amount of molten wax was added using a hot glass pipette. Mix and leave samples at room temperature overnight. The wax/xylenes mixture will harden, but enough paraffin is dissolved in the xylenes to start impregnation of the samples. Samples were transferred to 60º C oven to melt wax/xylenes mixture. When the wax/xylenes mix is molten, transfer vials to heating block.

the wax/xylenes mixture from each vial into a waste bottle (be careful to retain the samples). fresh molten wax was immediately added to the vial with a hot glass pipette. The vial placed again in the heat block. The vials are incubated for 3 hrs at 60ºC oven.

Embed samples in wax and prepare blocks (375)

Samples were transferred to the wax- filled mold using hot forceps or a hot cut off Pasteur pipette. Place an embedding ring on the mold and filled with paraffin wax. the embedding ring was labeled to facilitate future identification of samples. Samples can be oriented within the mold using a hot drawn-out and sealed Pasteur pipette. The blocks were left at room temperature to harden completely. Cast blocks were resumed from embedding molds and stored in a dry place at room temperature. Paraffin blocks were cut into thin (8μm) tissue sections, which are mounted on subbed slides to be further, processed for *in situ* hybridization.

A wax block containing samples was cut into a trapezoidal shape using a razor blade. The extra wax was carefully shaved off. The trapezoid block (with the wide edge facing the knife) attached to the holding clamp of a microtome and begin sectioning. 8μm sections were taken. A drop of 0.2x gelatin subbing solution is placed on a gelatin–subbed glass slide. Transfer the ribbon of sections onto the drop on the subbed slide using fine brushes. The slides were transferred onto a slide warmer or heating plate set between 45ºC and 50ºC. After stretching is complete, remove slide from slide warmer and carefully remove the remaining subbing solution using the Pasteur pipette and slides are dried at room temperature. Then slides were incubated 24 hours at 42ºC to firmly attach sections to subbed slides. Stored sections in a slide box with desiccant at -20ºC for up to several weeks.

Staining of tissue sections with Hematoxylin (376)

The sections were placed in fresh Xylene (to deparaffinize the sections) for 5 min, these sections are placed in 100%, 95%, 70% and 50% of Ethanol for 15 sec each. This section is now placed in Mayer's Hematoxylin for 30 sec and rinse the sections twice in ddH$_2$O for 15 sec each time. The sections were placed in 70% Ethanol for 15 sec, Eosin Y Stain for 5 sec, 95% Ethanol for 15 sec twice, 100% Ethanol for 15 sec twice and finally in fresh Xylenes (to ensure dehydration of the section) for 1 min. the sections were air dried for 2 minutes, xylene was removed by air drying. The tissue is now ready for microscopic observation.

CHAPTER III

Design, synthesis and characterization of ferrocene derivatives with Topoisomerase II beta inhibitory activity
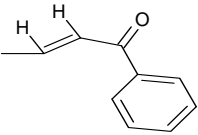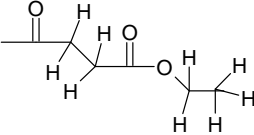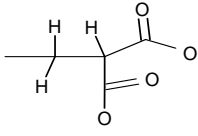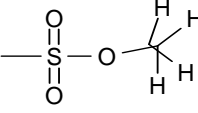
Topoisomerase II is present in two isoforms alpha and beta isoforms, which are differentially regulated in various cancers (377,380,382). It has been reported that alpha is up-regulated regulated in colon, breast cancers(386), while beta is unregulated in liver (377), brain cancer tissues (386). Thus suggesting the potential applications of alpha and beta specific-inhibitors in regressing these cancers. Among various Topoisomerase II poisons reported, organometallic compounds can serve as covalently interacting inhibitors that can permanently block the enzymatic activity. Ferrocene is a cyclopentadienyl caged iron compound that can provide an inert environment, the initial studies of activity of ferrocene against topoisomerase II show no significant activity, while the substitution at 2'- position could significantly enhance the topoisomerase II inhibitory activity of ferrocene (378) suggesting an importance of substitution in interfering the catalytic activity of enzyme. Since ferrocene being non DNA binding molecules with specific interaction to enzyme, they attract an attention for its potential application to cancer chemotherapy. But the initial studies were found using few substituted ferrocenes, at 200 micromolar concentration in terms of topoisomerase II antagonism, while the isoform specificity of these compounds is unknown. The present investigation aims studying isoform-specific topoisomerase II antagonism of a series of derivatives of ferrocenes with goal to identify a compound with IC_{50} 100 micromolar or below, which compares the known Topoisomerase II inhibitor Etoposide.

Synthesis of ferrocene derivatives:

Ferrocene derivatives containing substitution at 2' position as in Table 3.1 were synthesized as described in Chapter II. The functional groups substituted are given in the Figure 3.1. The structures of each compound was confirmed by their characteristic spectroscopic signal using IR/NMR as given in the column III of Table 3.1. These compounds were used for the analysis of biological activity.

Table 3.1

Ferrocene derivatives with corresponding IR/NMR spectra peaks

	Substitution R	IR/NMR spectra values of compounds
1	-CH$_3$	**IR** 2975(-CH$_3$) Ferrocene ring 1132, and 1002 cm^{-1}
2	-CHO	**IR** 1682 (aldehyde C=O), Ferrocene ring 1105, and 1033 cm^{-1} **NMR :** 2.42 ,9.9 PPM corresponding to the shifted hydrogens in the CHO substituted ring
3		**IR** 1660 (aldehyde C=O), phenyl absorption at 1446, 1575 and 1591 cm^{-1}, Ferrocene ring 1103 and 1012 cm^{-1} **NMR:** 7.7, 7.5, 4.6, 4.4, 1.5, 1.2, 1.02 PPM corresponding to the shifted hydrogens in the acetophenone substituted ring
4	-C$_2$H$_5$	**IR** 3005(-CH$_3$) Ferrocene ring 1115 and 995 cm^{-1}
5	-CH$_2$CH$_2$COOH	**IR:** 2932 cm^{-1} (OH) COOH, 1652 cm^{-1} (C=O) COOH, 1254 cm^{-1} (C-O) COOH.
6	-COCH$_3$	**IR** 1651 cm^{-1} (aldehyde C=O), 1101 and 960 cm^{-1} **NMR:** 4.4, 4.7 PPM corresponding to the shifted hydrogens in the acetyl substituted ring
7	-CH$_2$OH	**IR** of alcoholic –OH 3219 cm^{-1}. Ferrocene ring 1103 cm^{-1} and 1000 cm^{-1}
8	-CH$_2$Cl	**IR** Ferrocene ring 1095 and 1001 cm^{-1}
9		**IR :** 2964 and 2875 cm^{-1} (C-H) aliph,1736 cm^{-1} (C=O) -COOH, Ferrocene ring 1113 and 1037 cm^{-1}
10	-CH$_2$CHO	**IR** 1694 cm^{-1} (C=O), Ferrocene ring 1123 and 1002 cm^{-1}
11		**IR:** 2995 cm^{-1} (OH) COOH, 1641 cm^{-1} (C=O) COOH, 1249 cm^{-1} (CO) COOH.
12		**IR:** -S=0 absorption bands at 1022 and 814 cm-1. Ferrocene bands 3097, 1408, 1176, 1022 cm^{-1}, -NH 3439 cm^{-1}
13	-CH$_2$-SH	**IR:** Ferrocene bands 1178, 987 cm^{-1}. -SH absorption bands at 1034 and 838 cm^{-1}
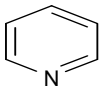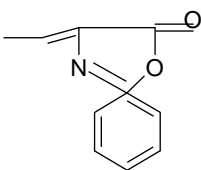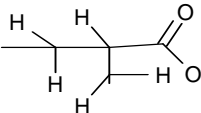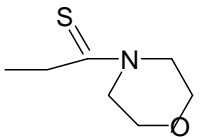
14	-CH$_2$COOH	**IR** : 2975 , 2859 cm^{-1} (C-H) aliphatic 1742 cm^{-1} (C=O) -COOH, Ferrocene ring 1100 and 995 cm-1
15	-CH$_2$(OH)$_2$	**IR** of alcoholic –OH 3264 cm^{-1},Ferrocene ring 1121 and 1005 cm-1
16	-COOH	**IR** : 2953, and 2874 cm^{-1} (C-H) aliph. 1795 cm^{-1} (C=O) -COOH, Ferrocene ring 1107 and 995 cm^{-1}
17	-CH$_2$(COOH)$_2$	**IR** : 2993 cm^{-1} (OH) COOH, 1655 cm^{-1} (C=O) COOH, Ferrocene ring 1108 and 1002 cm-1
18	-CH$_2$CH$_2$OH	**IR** of alcoholic –OH 3252 cm^{-1}, Ferrocene ring 1105 and 987 cm-1
19	-COSH	-SH absorption bands at 1037 and 863 cm^{-1} **IR** 1684 cm^{-1} (C=O), Ferrocene bands 1123, 997 cm^{-1}
20	-CHCHCOOH	**IR** 1724 cm^{-1} (C=O), Ferrocene bands 1142, 978 cm^{-1}
21	-SH	**IR**: -SH absorption bands at 1043 and 885 cm-1,Ferrocene bands 1105, 996 cm^{-1}
22		**IR**: Phenyl absorption at 1477, 1566 and 1597 cm^{-1}, NH 1651 cm^{-1} **NMR:** 7.3, 4.91, 4.63,1.3,1.2,1.02 PPM corresponding to the shifted hydrogens in the pyridine substituted ring
23		**IR**: -phenyl absorption at 1491,1645 cm^{-1}, (C=O) 1780 cm^{-1}, NH 3414 cm^{-1}, Ferrocene bands 1103, 975 cm^{-1} **NMR:** 4.68, 7.25 , 1.25,1.43 PPM corresponding to the shifted hydrogens in the azalactone substituted ring
24		**IR**: 2985 cm^{-1} (OH) COOH, 1645 cm^{-1} (C=O) COOH, 1234 cm^{-1} (C-O) COOH. Ferrocene bands 1105, 1001 cm^{-1}
25		**IR**: Thiomorpholide (–CSN=) IR : 1493 cm^{-1} -SH absorption bands at 1068 and 864 cm^{-1}, 1660 cm^{-1} (C=O) COOH, Ferrocene bands 1113, 997 cm^{-1}. **NMR:** 4.27, 4.29 ,7.25 , 1.25,1.43 PPM corresponding to the shifted hydrogens in the thiomorpholide amido methyl substituted ring

Figure 3.1

Structures of ferrocene derivatives
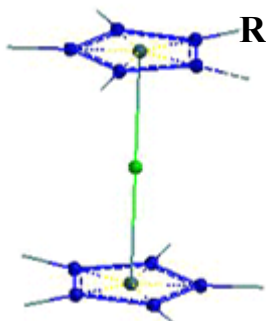
Ferrocene basic skeleton.
R is the substitution

1. Methyl ferrocene

CH_3

2. Ferrocene carboxyaldehyde

CHO
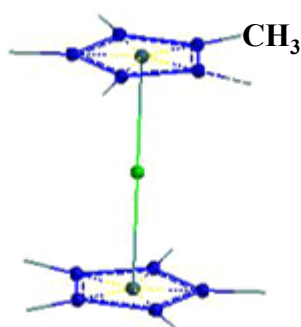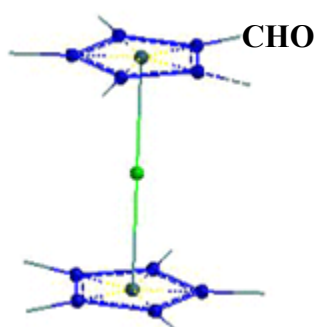
3. Acetophenyl ferrocene

CH=CH-C=O

4. Ethyl ferrocene

C_2H_5

5. Alpha ferrocenyl propionic acid

CH_2CH_2COOH
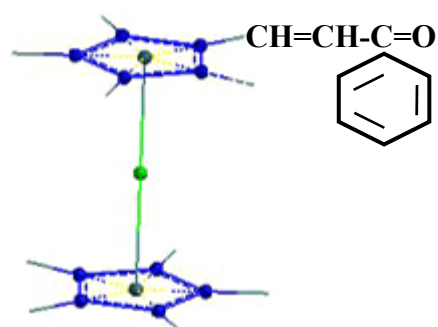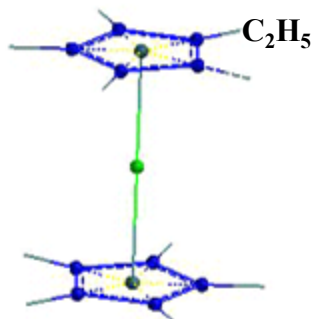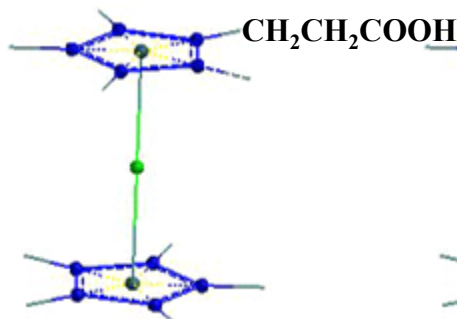
6. Acetyl ferrocene

$COCH_3$
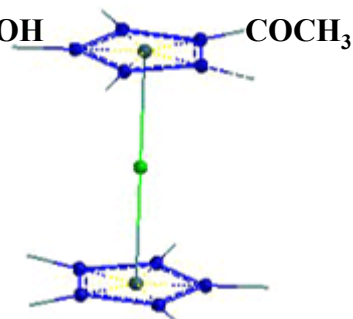
7. Hydroxy methyl ferrocene

CH_2OH
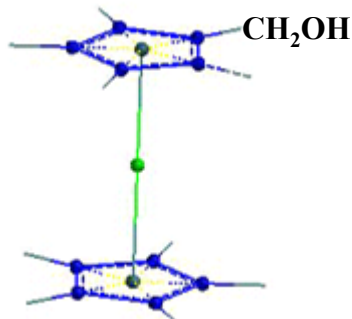
8. Chloro methyl ferrocene

CH_2Cl
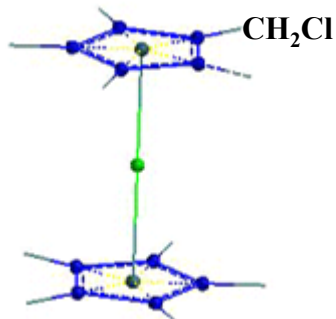
8. Acetyl Keto ester ferrocene

$\overset{O}{\overset{\|}{C}}CH_2CH_2\overset{O}{\overset{\|}{C}}C_2H_5$
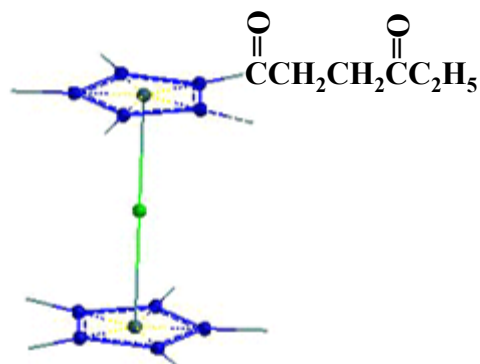
Figure 3.1 (contd)

Structures of ferrocene derivatives

10. Ferrocene acetaldehyde

CH$_2$CHO
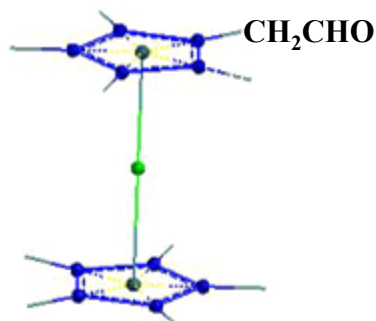
11. Ferrocenyl dicarboxylic acid

CH$_2$CH(COOH)$_2$
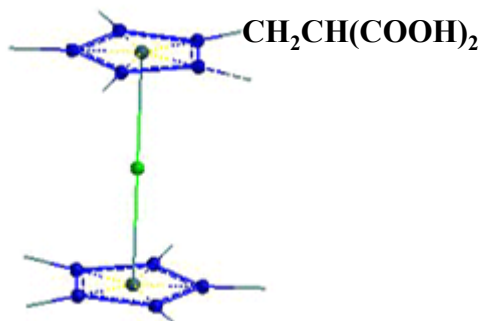
12. Ferrocenyl sulphonoamide

SO$_3^-$.NH$_4^+$
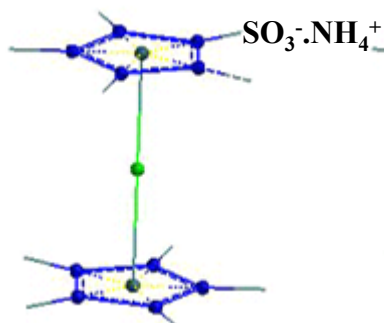
13. Ferrocenyl methyl sulphide

CH$_2$SH
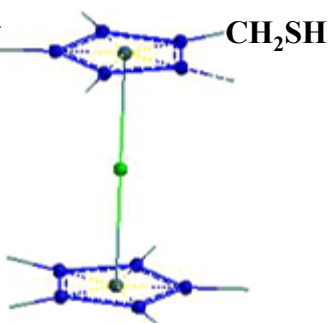
14. Ferrocenyl acetic acid

CH$_2$COOH
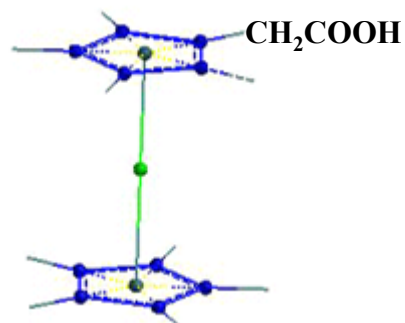
15. 1,1 (di hydroxy) methyl Ferrocene

CH$_2$(OH)$_2$
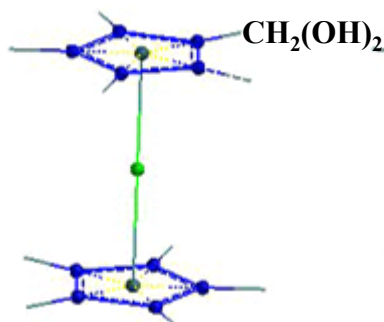
16. Ferrocene carboxylic acid

COOH
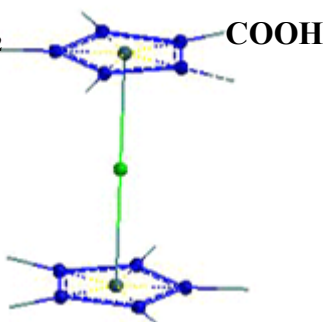
17. Ferroceneyl dicarboxyl proionic acid

CH(COOH)$_2$
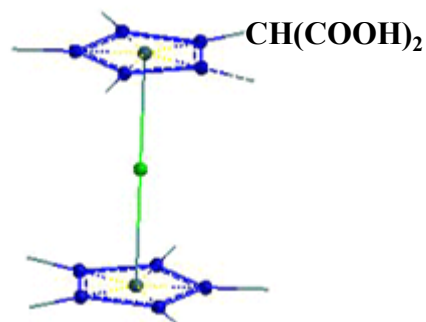
Figure 3.1 (contd)

Structures of ferrocene derivatives

18. Ferrocenyl ethyl alcohol — CH₂CH₂OH
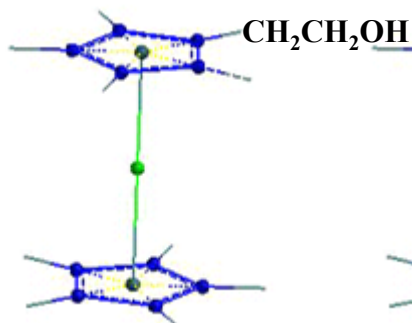
19. Ferrocene thio carboxylic acid — COSH
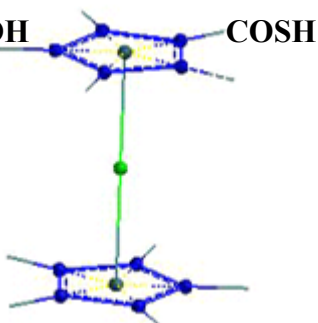
20. Ferrocenyl acrylic acid — CH=CHCOOH
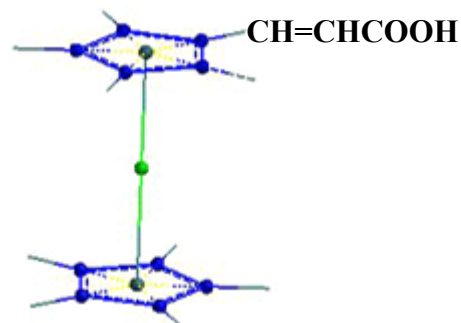
21. Ferrocene thiol — SH
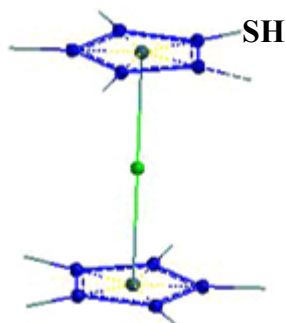
22. Pyridyl ferrocene — C_5H_5N

23. Azalactone ferrocene

- CH = C = O
N   O
   C
   (phenyl ring)
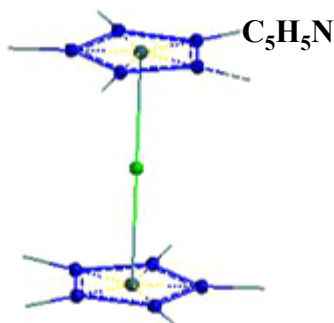
24. Ferrocenyl Isobutryic Acid — CH₂CHCOOH, CH₃
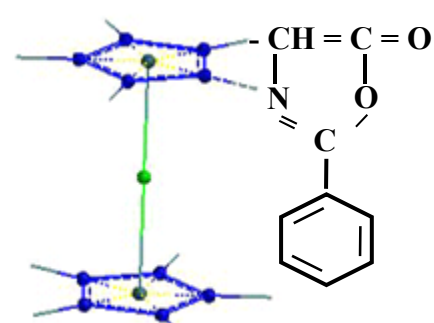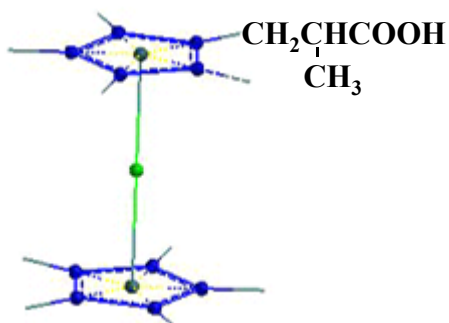
25. Thiomorpholide amido methyl ferrocene

S
‖
CH2 – C – N
CH₂ – CH₂
CH₂ – CH₂
O
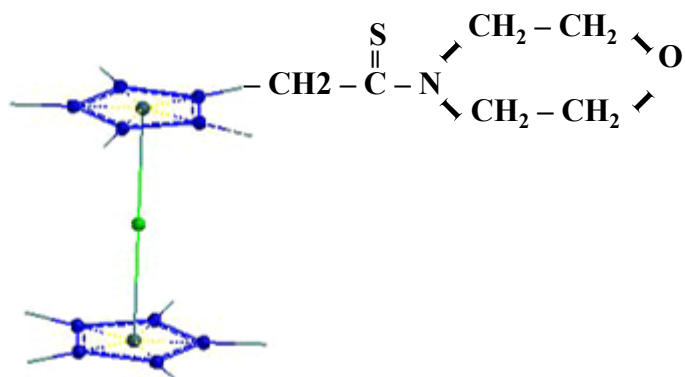
Biological activity of synthesized compounds:

The compounds synthesized are analysed for their action on the catalytic activity of topo II α and topo II β. The topo II α and topo II β catalysed relaxation of supercoiled DNA of was carried out in the presence of increasing concentrations of each compound. The results given in Fig 3.2 to 3.6, show significant differences in the inhibition of topo II β catalytic activity. The concentration of each compound required for 50% inhibition of the relaxation of supercoiled DNA was determined and given in Table 3.2. The results show a substitution dependant inhibition of catalytic activity of Topo II β, while these compounds show lower inhibitory activity against Topo II α. The structural features of the compounds involved in interaction at the active site of Topo II β was characterized by Receptor module in accelrys Cerius^2 using QSAR methodology (2.27).

Quantitative structure and activity analysis of Ferrocene derivatives:

The structures obtained were superimposed using Accelrys Cerius^2 pointing towards iron ferrocene axis (Figure 3.7). The overlaid structures were analyzed using Quantitative structure activity relationship (QSAR) methodology as per Accelrys. The Molecular Field Analysis (MFA) (20) yielded good fit of data, with cross validation square of correlation coefficient (r^2_{cv}) of 0.943, Square of correlation coefficient r^2 of 0.985, Predicted sum of squares (PRESS) of 0.083, outliers of 4.0. This model has been generated with the following linear regressed equation, (379).

Activity = $3.47383 - 0.005202 (H^+/373) + 0.005198(CH_3/216) + 0.00866 (H^+/455) - 0.0088 (CH_3/527) + 0.01219 (CH_3/226) - 0.00552(H+/215) + 0.011875(CH_3/375)$ -----(1) As the equation suggests, the steric CH_3 216, 226, 375 and electrostatic probes H^+ 455 have positive contributions to the activity (Fig 3.7).

Figure 3.2

Topoisomerase II Catalytic Assays.

Panel A: Purified Plasmid DNA as substrate

Lane 1:- DNA ladder

Lane 2:- pRYG plasmid (2,725 bps)

Lane 3:- pBR 322 plasmid (4,361 bps)

Panel B: Topoisomerase II beta relaxation assay

Lane 1:-Supercoiled pRYG plasmid DNA

Lane 2:-Plasmid DNA in presence of topoisomerase II beta and relaxation buffer (Reaction mixture beta)

Lane 3:- Reaction mixture beta in presence of 100 µm etoposide (Drug positive control)

Lane 4:- Reaction mixture beta in presence of 500 µm ferrocene (Drug negative control)

Panel C: Topoisomerase II alpha relaxation assay

Lane 1:-Supercoiled pRYG plasmid DNA

Lane 2:-Plasmid DNA in presence of topoisomerase II alpha and relaxation buffer (Reaction mixture alpha)

Lane 3:- Reaction mixture alpha in presence of 100 µm etoposide (Drug positive control)

Lane 4:- Reaction mixture alpha in presence of 500 µm ferrocene (Drug negative control)

Figure 3.2

Topoisomerase II Catalytic Assays.

Panel A

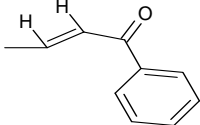

Panel B

Panel C
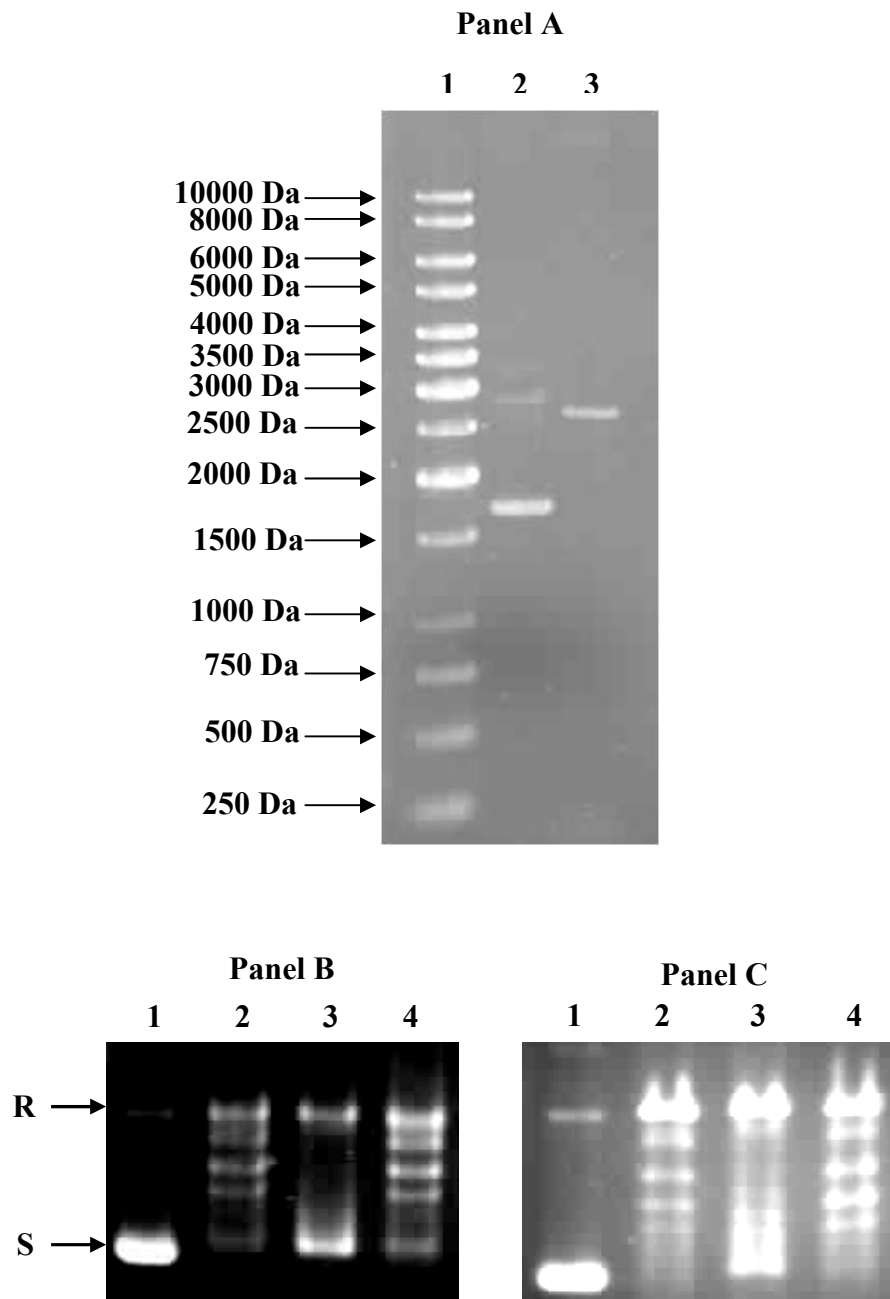
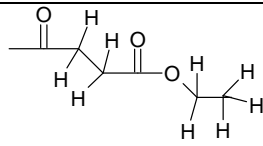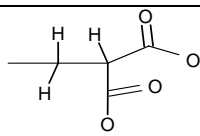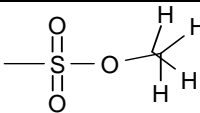**Table 3.2:** Structures and experimental and calculated inhibitory activities against enzyme-catalyzed relaxation of super coiled DNA, - (log IC$_{50}$), of the molecules used in the training set based on the molecular skeleton

	Substitution	Topo II	Topo II	Predicted Topo II
	R	Beta IC$_{50}$	alpha IC$_{50}$	Beta IC$_{50}$ activity from QSAR equation
1	CH$_3$	350 μM	1000 μM	281 μM
2	CHO	300 μM	1000 μM	243 μM
3		300 μM	1000 μM	303 μM
4	C$_2$H$_5$	300 μM	1000 μM	236 μM
5	CH$_2$CH$_2$COOH	300 μM	1000 μM	280 μM
6	COCH$_3$	250 μM	1000 μM	242 μM
7	CH$_2$OH	250 μM	1000 μM	244 μM
8	CH$_2$Cl	250 μM	1000 μM	178 μM
9		200 μM	1000 μM	202 μM
10	CH$_2$CHO	200 μM	1000 μM	186 μM
11		200 μM	1000 μM	192 μM
12		150 μM	500 μM	162 μM
13	CH$_2$-SH	150 μM	1000 μM	145 μM
14	CH$_2$COOH	150 μM	1000 μM	158 μM
15	CH$_2$(OH)$_2$	150 μM	1000 μM	144 μM
16	COOH	150 μM	1000 μM	181 μM
17	CH$_2$(COOH)$_2$	150 μM	1000 μM	130 μM
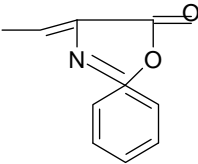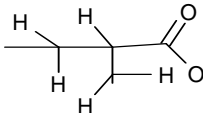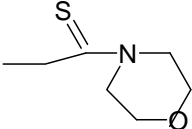
18	-CH$_2$CH$_2$OH	150 μM	1000 μM	131 μM
19	COSH	150 μM	1000 μM	132 μM
20	CHCHCOOH	150 μM	1000 μM	143 μM
21	SH	150 μM	1000 μM	353 μM
22		150 μM	1000 μM	136 μM
23		100 μM	300 μM	93 μM
24		80 μM	500 μM	76 μM
25		50 μM	200 μM	49 μM

Figure 3.3:

Action of Ferrocene derivatives on Catalytic action of Topoisomerase II β

DNA relaxation activity of Topoisomerase II β was studied in presence of indicated concentrations of ferrocene derivatives. The relaxing DNA intermediates were separated on agarose gel and stained with ethidium bromide and photographed. (S: Supercoiled form, R: Relaxed form).

C: supercoiled DNA and 5% DMSO

+ : DNA and topoisomerase II beta with relxation buffer incubated for 30

Minutes (relaxation mixture beta)

F: 500 µM Ferrocene (Negative control)

D: 100 µM Doxorubicin (Positive control)

1,2,3,4: 40,60,80, 100 µM of ferrocenyl beta propionic acid

5,6,7,8: 50,100, 150,200 µM of ferrocenyl methyl sulphide

9,10,11: 100, 200, 300 µM acetophenone ferrocene

12,13,14: 100, 200, 300 µM of ferrocene carboxy aldehyde

15,16,17: 100, 200, 300 µM of ferrocene monosulphonic acid

18,19,20: 100, 200, 300 µM of alpha propionic acid

21,22,23: 200, 300, 350 µM of methyl ferrocene

24,25,26,27: 25,50,100,150 µM of ferrocenyl acetic acid

28,29,30,31: 25,50,100,150 µM 1,1 dihydroxy methyl ferrocene

32,33,34,35: 50,100,150,200 µM dicarboxylic acid ferrocene

36,37,38 39: 50,100,150,200 µM acetaldehyde ferrocene

40,41,42,43: 100,150,200,250 µM keto ester ferrocene

Figure 3.3

Action of ferrocene derivatives on catalytic action of Topoisomerase II β
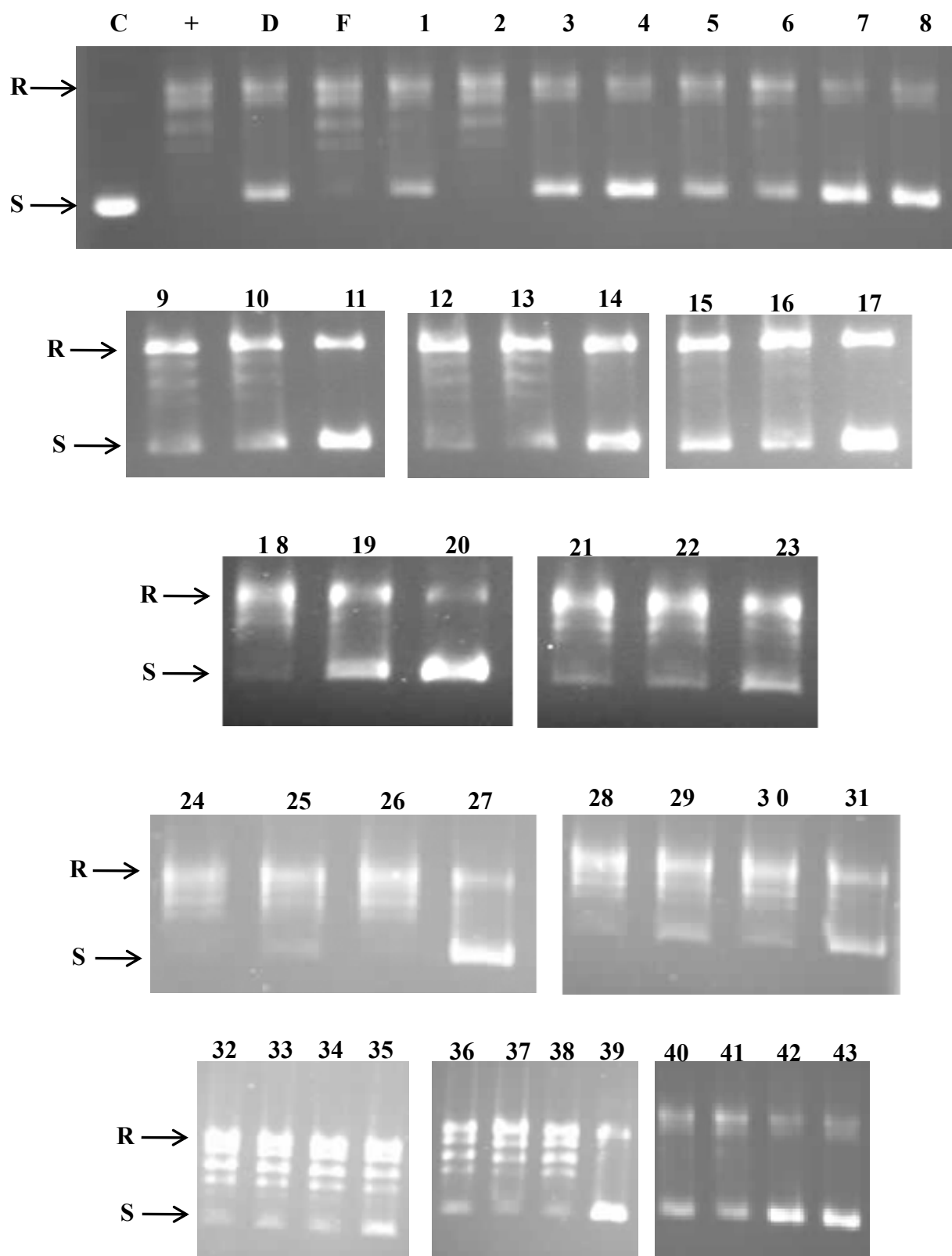
Figure 3.4:

Action of Ferrocene derivatives on Catalytic action of Topoisomerase II β

DNA relaxation activity of Topoisomerase II β was studied in presence of indicated concentrations of ferrocene derivatives. The relaxing DNA intermediates were separated on agarose gel and stained with ethidium bromide and photographed. (S: Supercoiled form, R: Relaxed form).

44,45,46,47: 25 50 100 150 µM of ferrocenyl carboxylic acid

48, 49, 50, 51: 25 50 100 150 µM ferroceneyl isobutyric acid

52, 53, 54, 55:- 25 50 100 150 µM ferrocene ethanol

56, 57, 58, 59: 25 50 100 150 µM carboxy sulphide ferrocene

60, 61, 62, 63: 25 50 100 150 µM sulphadryl ferrocene

64, 65, 66,67: 25 50 100 150 µM pyridyl ferrocene

68, 69, 70: 25 50 100 150 µM acrylic acid ferrocene

71, 72, 73, 74: 25 50 100 150 µM ethyl ferrocene

75, 76, 77, 78: 100 150 200 250 µM acetyl ferrocene

79, 80, 81: 200, 250, 300 µM methanol ferrocene

82, 83, 84, 85: 25 50 100 150 µM chloro methyl ferrocene

Figure 3.4

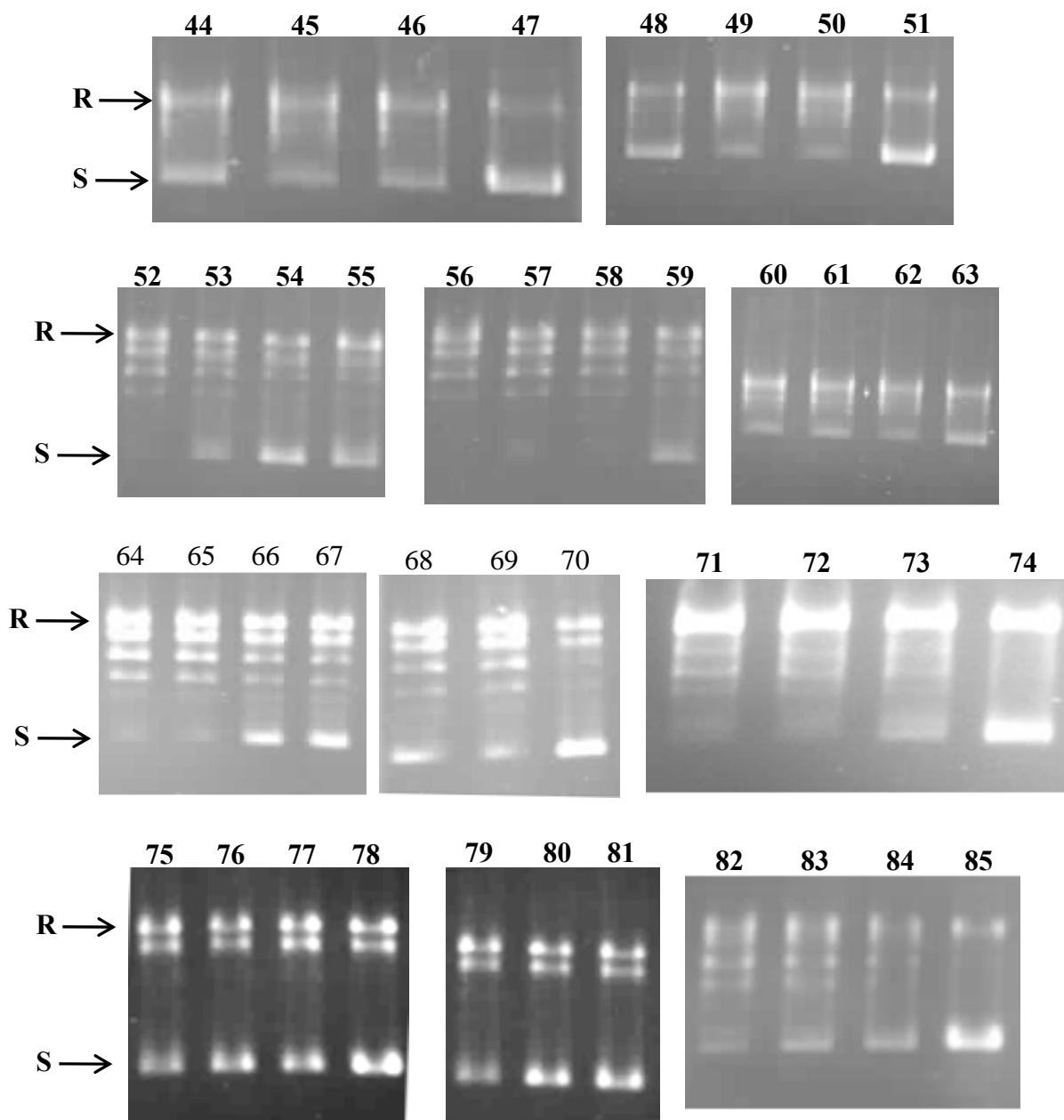## Action of ferrocene derivatives on catalytic action of Topoisomerase II β

Figure 3.5:

Action of Ferrocene derivatives on Catalytic action of Topoisomerase II α

DNA relaxation activity of Topoisomerase II α was studied in presence of indicated concentrations of ferrocene derivatives. The relaxing DNA intermediates were separated on agarose gel and stained with ethidium bromide and photographed. (S: Supercoiled form, R: Relaxed form).

C: supercoiled DNA and 5% DMSO

+: DNA and topoisomerase II alpha with relaxation buffer incubated for 30 Minutes

F: 500 µM Ferrocene (negative control for drug activity)

D: 100 µM Doxorubicin (positive control for drug activity)

1, 2, 3: 100,500,1000 µM ferrocenyl beta propionic acid

4, 5, 6: 100,500,1000 µM ferrocenyl methyl sulphide

7, 8, 9: 100,500,1000 µM acetophenone ferrocene

10, 11, 12: 100,500,1000 µM ferrocene carboxy aldehyde

13, 14, 15: 100,500,1000 µM ferrocene monosulphonic acid

16, 17, 18: 100,500,1000 µM alpha ferrocenyl propionic acid

19, 20, 21:- 100,500,1000 µM methyl ferrocene

22, 23, 24: 100,500,1000 µM ferrocenyl acetic acid

25, 26, 27: 100,500,1000 µM dihydroxy methyl ferrocene

28, 29, 30: 100,500,1000 µM dicarboxylic acid ferrocene

31, 32, 33: 100,500,1000 µM acetaldehyde ferrocene

34, 35, 36: 100,500,1000 µM keto ester ferrocene

Figure 3.5

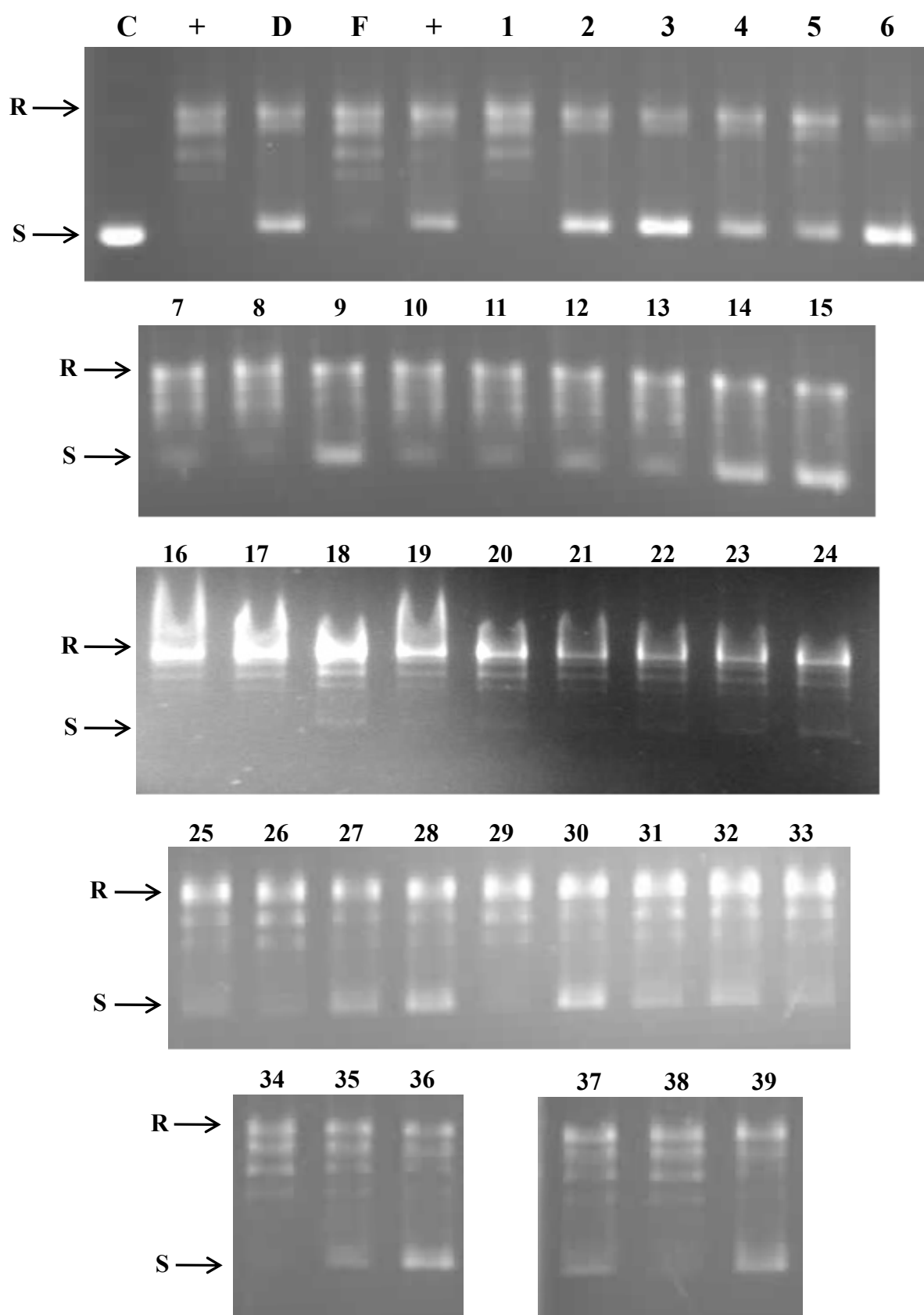## Action of ferrocene derivatives on catalytic action of Topoisomerase II α

Figure 3.6:

Action of Ferrocene derivatives on Catalytic action of Topoisomerase II α

DNA relaxation activity of Topoisomerase II α was studied in presence of indicated concentrations of ferrocene derivatives. The relaxing DNA intermediates were separated on agarose gel and stained with ethidium bromide and photographed. (S: Supercoiled form, R: Relaxed form).

37, 38, 39: 100,500,1000 μM ferrocenyl carboxylic acid

40, 41, 42: 100,500,1000 μM ferroceneyl isobutyric acid

43, 44, 45: 100,500,1000 μM ferrocene ethanol

46, 47, 48: 100,500,1000 μM carboxy sulphide ferrocene

49, 50, 51: 100,500,1000 μM sulphadryl ferrocene

52, 53, 54: 100,500,1000 μM pyridyl ferrocene

55, 56, 57: 100,500,1000 μM acrylic acid ferrocene

58, 59, 60: 100,500,1000 μM ethyl ferrocene

61, 62, 63: 100,500,1000 μM acetyl ferrocene

64, 65, 66: 100,500,1000 μM hydroxyl methyl ferrocene

67, 68, 69: 100,500,1000 μM chloro methyl ferrocene

Figure 3.6

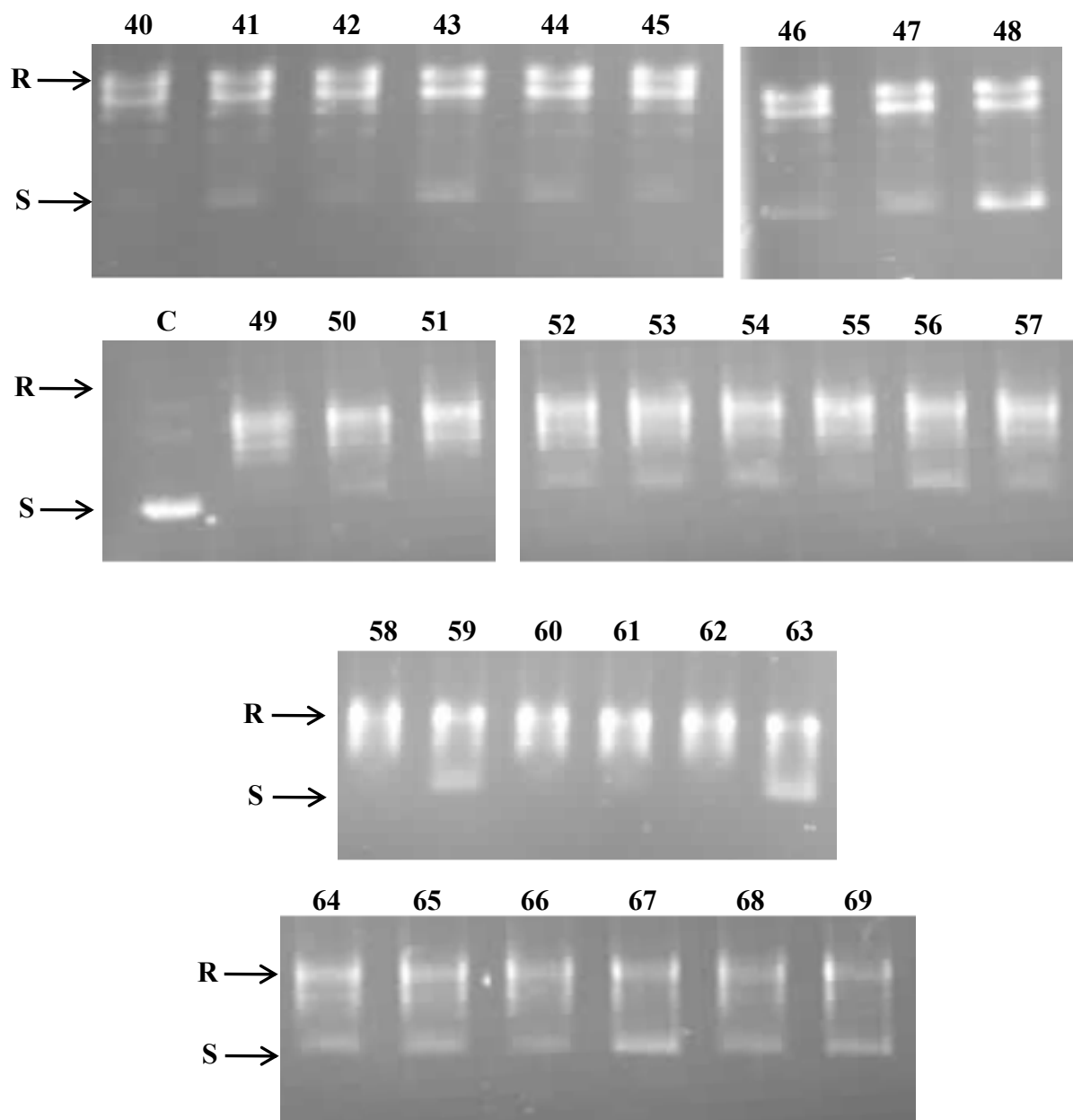## Action of ferrocene derivatives on catalytic action of Topoisomerase II α
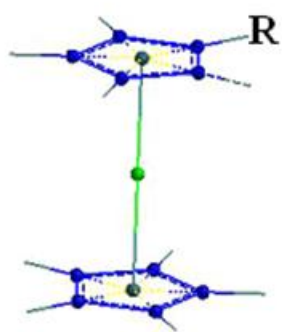
Figure 3.7:

Structure alignment of ferrocene derivatives

Structural alignment of structures towards iron cyclopentadiene ring axis using 3D alignment procedure of Cerius[2]. A view of the molecular rectangular field grid around the superposed molecular units was presented. Both steric (CH_3) and electrostatic (H^+) grid points in the final QSAR equation are depicted
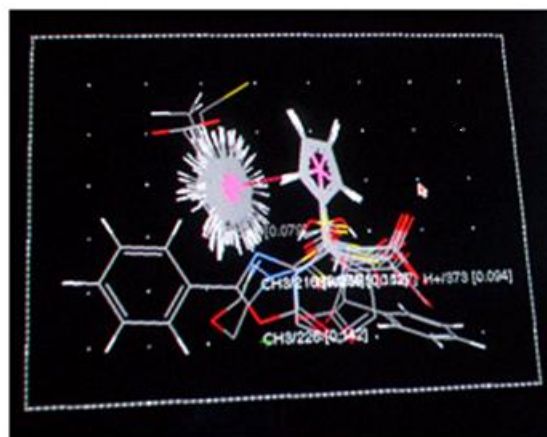
Figure 3.7

Structure alignment of ferrocene derivatives

Panel A   **Panel B**

Basic skeleton of ferrocene   Alignment of ferrocene derivatives

The QSAR analysis yielded a linear relation (Figure 3.8) between the predicted activities from equation (1) versus experimental activity as per Table 3.2 These results predicted several compounds that include two potent compounds azalactone ferrocene and thiomorpholide ferrocene containing active structural features. These two compounds were further characterized for their molecular activity on catalytic activity of Topoisomerase II α and Topoisomerase II β.

Azalactone ferrocene and Thiomorpholide amido methyl ferrocene exhibit enhanced inhibition of catalytic activity of topoisomerase IIβ

Topoisomerase IIα and β catalyzed relaxation activity was analyzed with increasing concentrations of azalactone ferrocene and thiomorpholide methyl ferrocene. The results show that azalactone ferrocene inhibits catalytic activity of topoisomerase II β at 100μM (Figure 3.9A) while it requires 300μM for inhibition of catalytic activity of topoisomerase IIα catalytic activity (Figure 3.9B). Thiomorpholide amido methyl ferrocene could inhibit catalytic activity of topoisomerase II beta at 50μM (Figure 3.10A), while 200μM was required for inhibition of topoisomerase II alpha (Figure 3.10B), These results suggest that azalactone ferrocene is 3 fold higher potent against topoisomerase II beta compared to alpha isoform, while thiomorpholide amido methyl exhibits 4 fold higher activity against topoisomerase II beta isoform compared to that of topoisomerase II alpha. Further, thiomorpholide amido methyl ferrocene shows a 2-fold higher activity against topoisomerase II beta compared to that observed for azalactone ferrocene.

Figure 3.8:

Comparison of Predicted vs Observed activity generated QSAR equation

Plot of theoretically predicted activity versus experimentally determined enzyme inhibition activity. The theoretical activity was determined using Molecular shape analysis followed by generated QSAR equation. The statistical parameters are given in text.

Figure 3.8

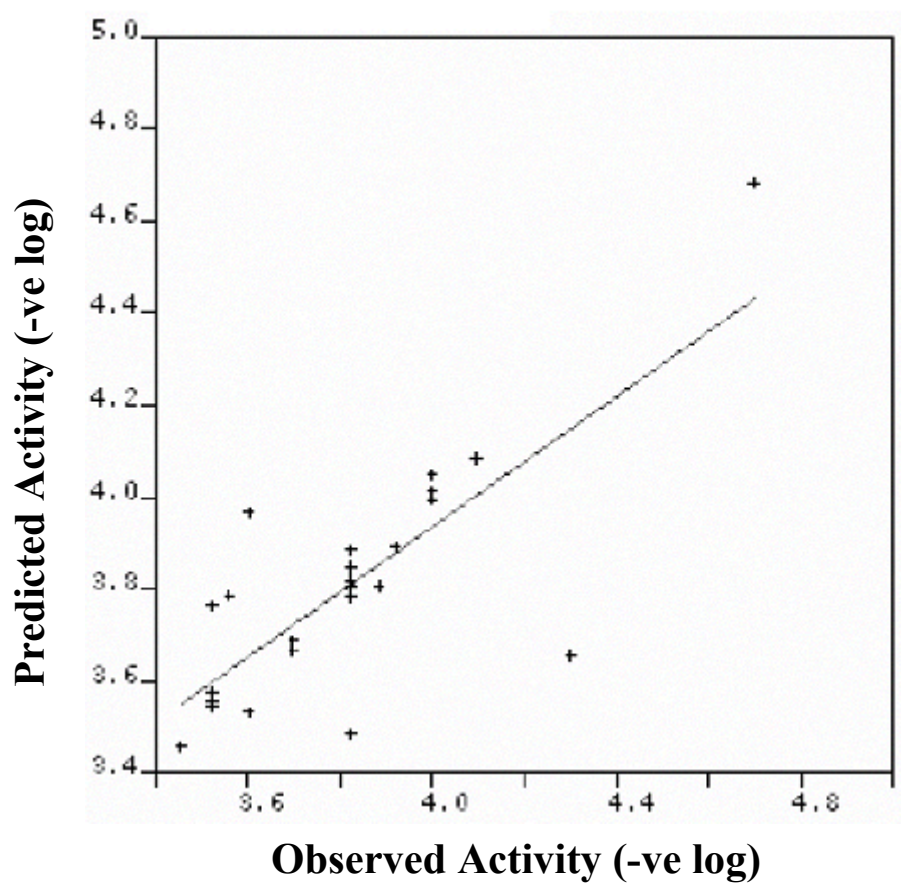**Comparison of predicted vs observed activity generated QSAR equation**

Figure 3.9

Action of Azalactone Ferrocene on the Catalytic activity of Topoisomerase II Alpha isoform and Beta isoform.

DNA relaxation activity of Topoisomerase II beta was studied in presence of indicated concentrations of ferrocene derivatives. The relaxing DNA intermediates were separated on agarose gel and stained with ethidium bromide and photographed. (S: Supercoiled form, R: Relaxed form).

Figure 3.9

Action of Azalactone Ferrocene on the Catalytic activity of Topoisomerase II Alpha isoform and Beta isoform
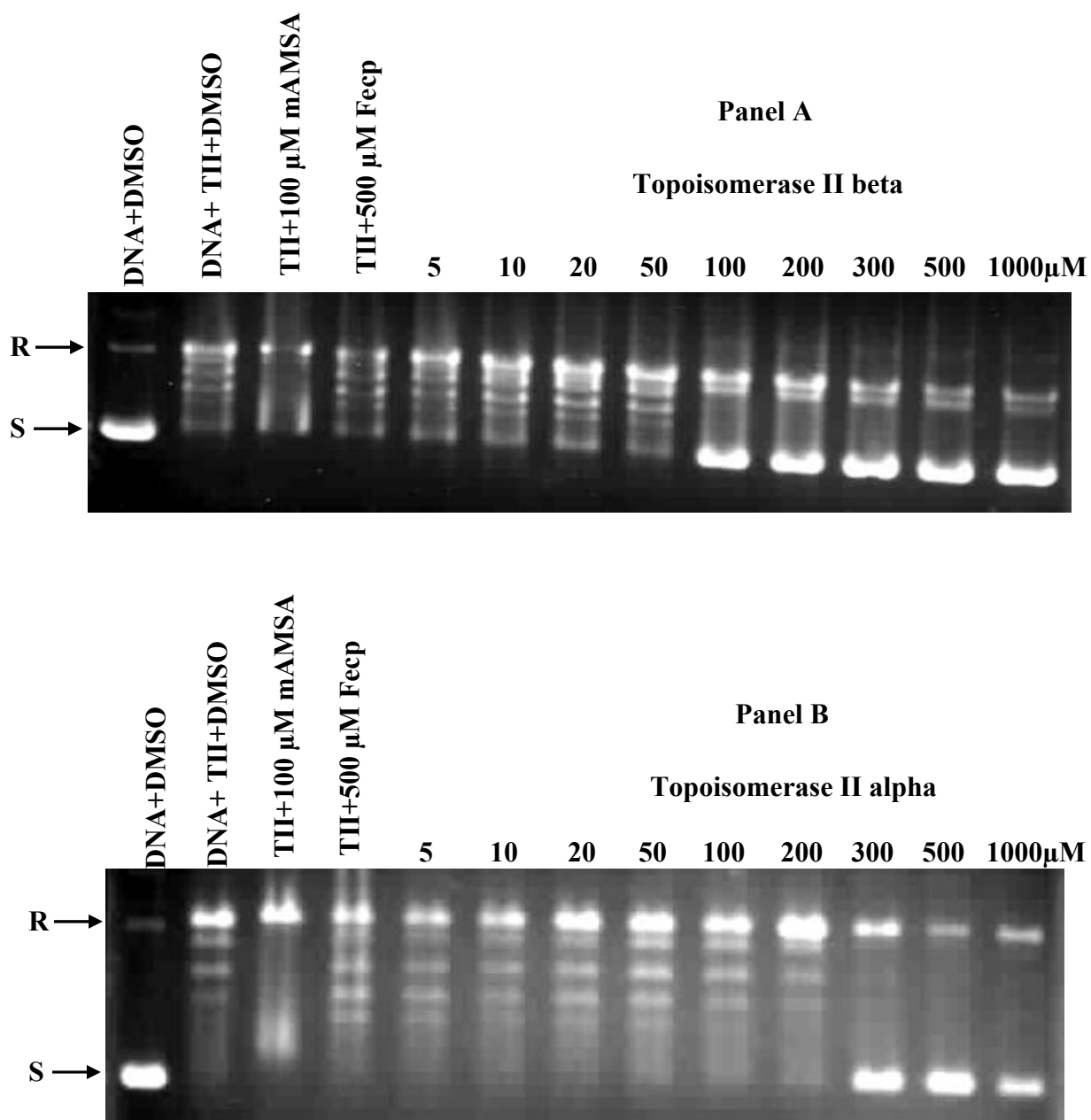
Figure 3.10:

Action of Thiomorpholide Amido Methyl Ferrocene on the Catalytic activity of Topoisomerase II Alpha isoform and Beta isoform

DNA relaxation activity of Topoisomerase II alpha was studied in presence of indicated concentrations of ferrocene derivatives. The relaxing DNA intermediates were separated on agarose gel and stained with ethidium bromide and photographed. (S: Supercoiled form, R: Relaxed form).

Figure 3.10

Action of Thiomorpholide Amido Methyl Ferrocene on the Catalytic activity of Topoisomerase II Alpha isoform and Beta isoform

Panel A

Topoisomerase II beta

Panel B

Topoisomerase II alpha
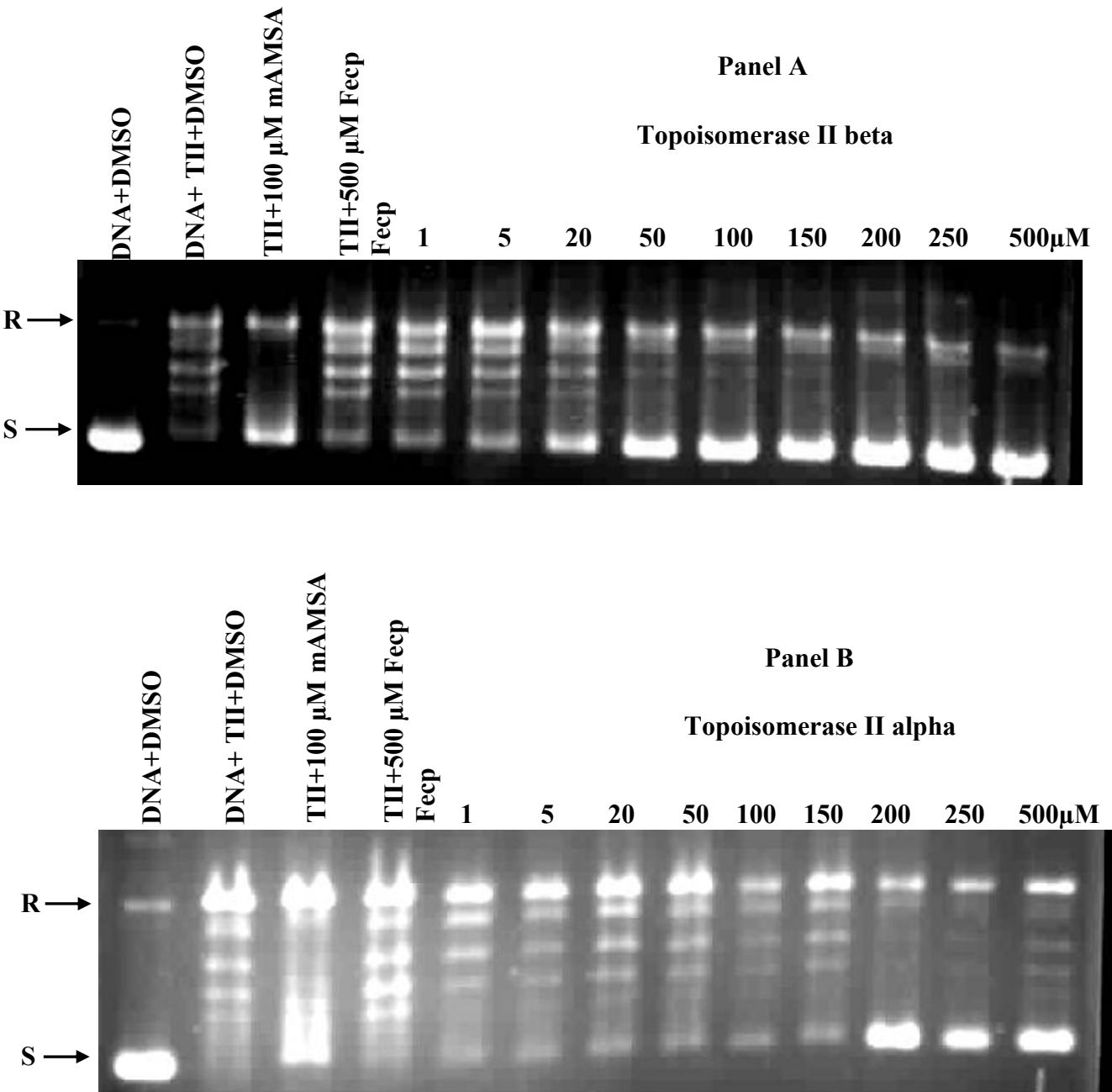
Thiomorpholide amido methyl ferrocene and Azalactone ferrocene show distinct mode of mechanism of action against topoisomerase II beta

To investigate the mechanism of action of the two compounds, thiomorpholide amido methyl ferrocene and azalactone ferrocene, we have carried out cleavage assay to monitor the ability of these two compounds in inducing the formation of enzyme-linked DNA complexes. The cleavage assay was conducted with increasing concentrations of drug and the cleavable complexes formed were analyzed through formation of linear DNA on agarose gel. The results presented in Figure 3.11 panel A show that azalactone ferrocene induces formation of linear double stranded DNA intermediates in a dose dependant manner. On the other hand the results of cleavage assay conducted in the presence of thiomorpholide ferrocene show that it cannot mediate formation of cleavable complex as intermediate (Fig.3.11 A). The experiments were repeated using topoisomerase II α (Figure 3.11 panel B), the results suggest that azalactone ferrocene also poisons topoisomerase II α through formation of cleavage complex, where as thiomorpholide amido methyl ferrocene cannot form cleavage complex and does not induce enzyme-linked cleavable complex. The concentration at which the cleavable complex formed by azalactone ferrocene with topoisomerase II α was ~2 fold lower compared to that of topoisomerase II β. These results thus suggest distinct different mode of mechanism for the two compounds. The highly potent thiomorpholide amido methyl ferrocene which does not induce formation of drug induced enzyme associated DNA double strand breaks, may be classified as a "catalytic inhibitor", while the azalactone ferrocene that induces formation of enzyme associated double strand breaks may be classified as "Topoisomerase II poison".
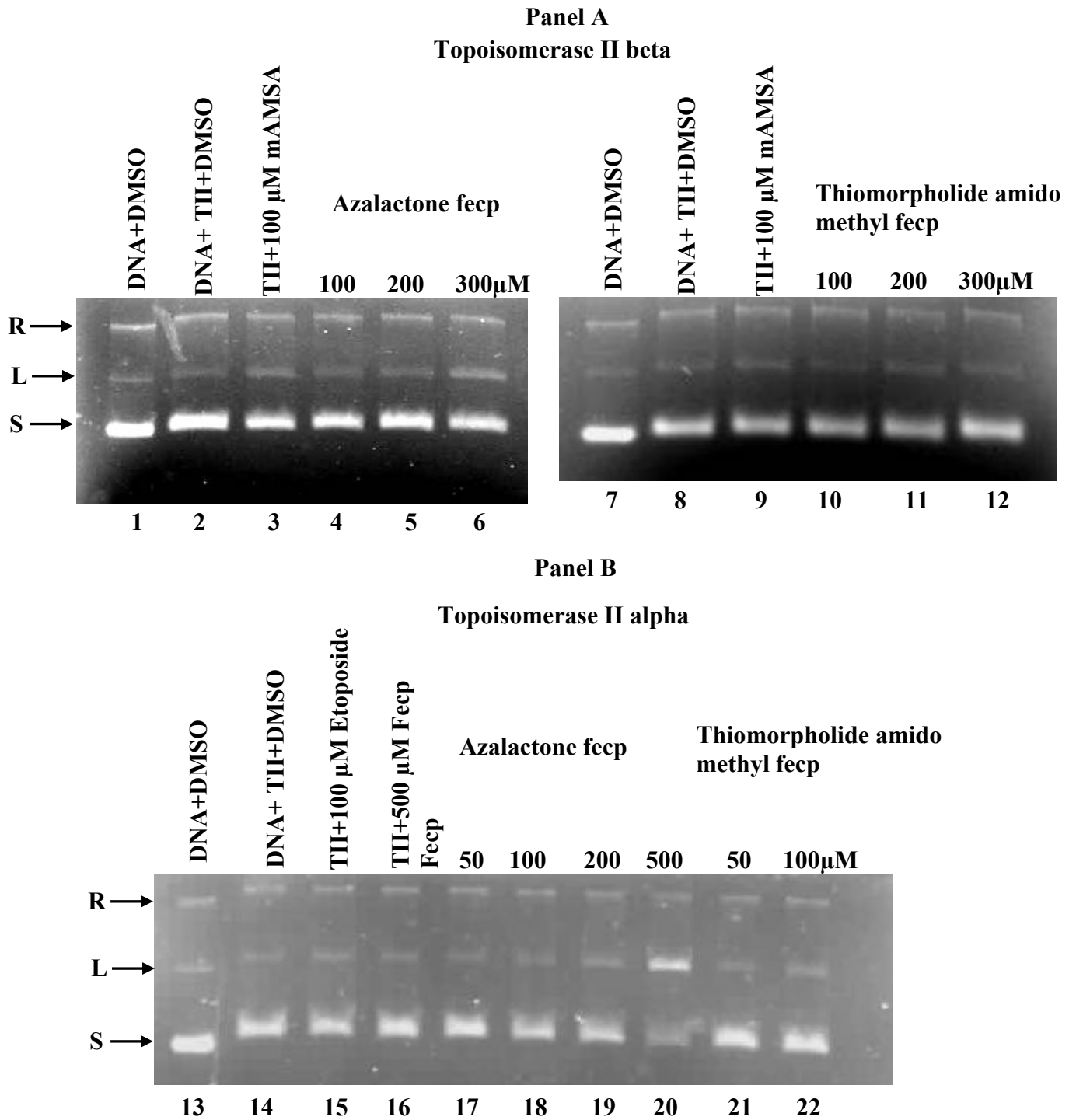
Figure 3.11:

Ability of Azalactone Ferrocene and Thiomorpholide Amido Methyl Ferrocene in formation of Cleavage complex

Azalactone ferrocene induces the formation of enzyme-linked cleavable complexes, while Thiomorpholide amido methyl ferrocene does not. Cleavage assay was carried out using Topoisomerase II beta isoform (Panel A) and alpha isoform (Panel B). The assay was done in the presence of indicated concentrations of azalactone ferrocene and thiomorpholide amido methyl ferrocene. The cleaved DNA intermediates were digested with proteinase K and separated on agarose gel and stained with ethidium bromide and photographed. (S: Supercoiled form, L: linear, R: Relaxed form)

Figure 3.11

Ability of Azalactone Ferrocene and Thiomorpholide Amido Methyl Ferrocene in formation of Cleavage complex

Panel A
Topoisomerase II beta

Panel B

Topoisomerase II alpha

Affinity of Azalactone ferrocene and Thiomorpholide amido methyl ferrocene to calf thymus DNA

The DNA melting experiment was carried out at drug to nucleotide ratios of 1:10, 1:5, 1:2, and 1:1. The results show that both the compounds do not protect melting of calf thymus DNA, and hence are classified as non-DNA binding molecules (Figure 3.12).

The mechanism of drug interaction with the enzyme:

Since both the drugs do not bind to DNA and azalactone ferrocene can only induce the formation of cleavable complexes, we have investigated whether azalactone ferrocene binding to enzyme alone is adequate to account for its activity.

We have conducted two sets of experiments. In one set, the enzyme incubated with drug, and then the enzyme was immunoprecipitated and washed 3 times with TBS. The activity of the immunoprecipitated enzyme was assayed in the presence of supercoiled DNA using relaxation assay. The results presented in Figure 3.13 at lane 5 and 6; show that pretreatment of enzyme with azalactone ferrocene is indeed adequate for inhibition of catalytic activity of topoisomerase II beta.

In the second set of experiments, the azalactone ferrocene was preincubated at 37^0C for 15 minutes and the drug concentration was reduced by diluting 10 times to bring below its inhibitory concentration. The diluted mixture containing DNA and drug was incubated with topoisomerase II beta and the relaxation assay was conducted. The results for lane 7 and 8 presented in Figure 3.13 show that the relaxation of DNA is not affected when DNA is pretreated with the drug. This suggests that the drug does not form complexes with DNA, confirming our earlier results of DNA melting studies. These findings clearly show that azalactone ferrocene interacts with the enzyme and induces the formation of enzyme-linked cleavable complexes. confirming our earlier results of DNA melting studies. These findings

85

Figure 3.12:

Analysis of DNA binding affinity of Azalactone Ferrocene and Thiomorpholide Methyl Ferrocene

The melting temperature curves indicate that, calf thymus DNA alone showed a Tm of 59^0C, while drug to DNA nucleotide ratio of 1:1 of azalactone and thiomorpholide Amido methyl ferrocene induce a small increase ~1^oC showed. The DNA intercalator m-AMSA induces a strong increase in Tm ~65^0C at a drug to nucleotide ratio of 1:5, suggesting that the compounds are essentially DNA non-binders.

Figure 3.12

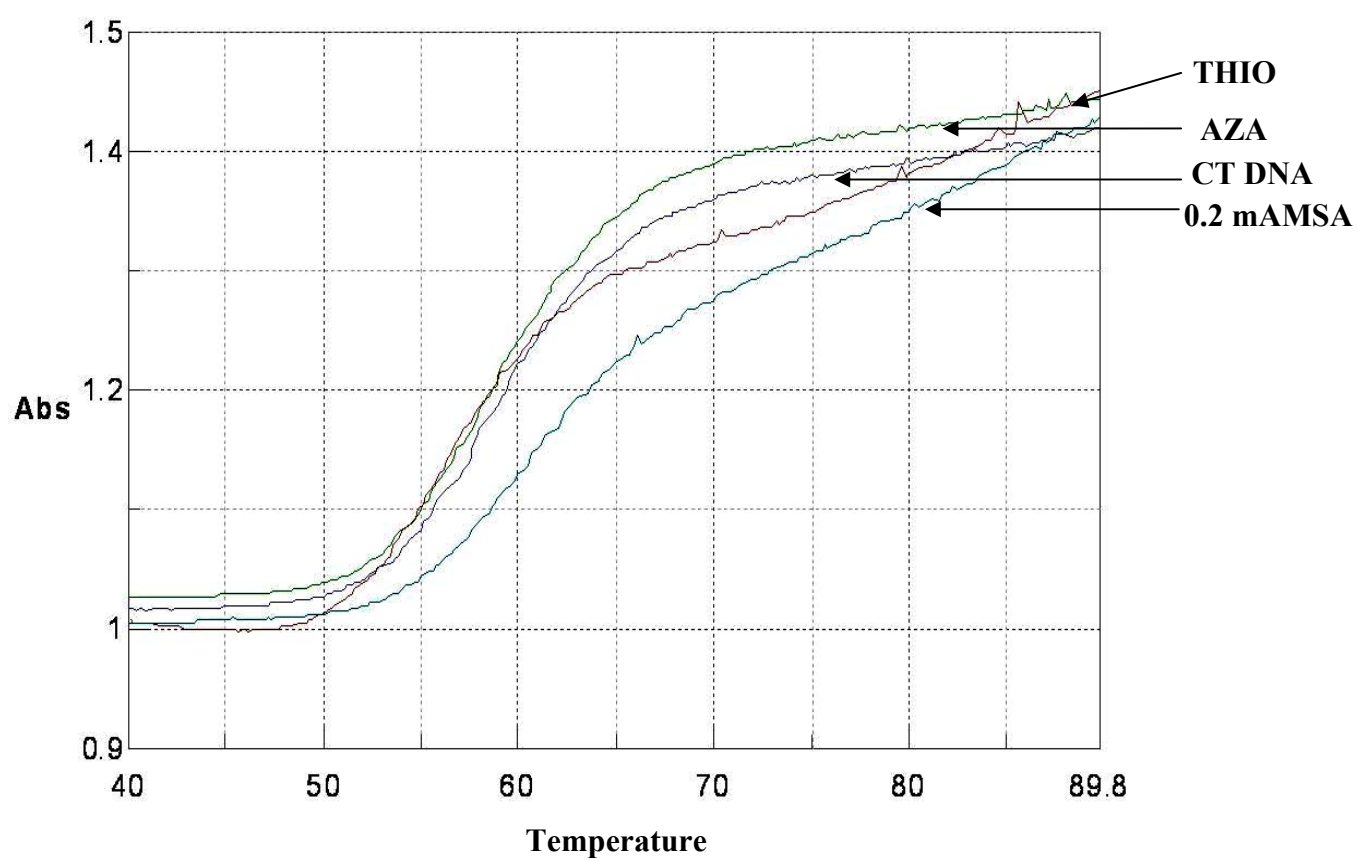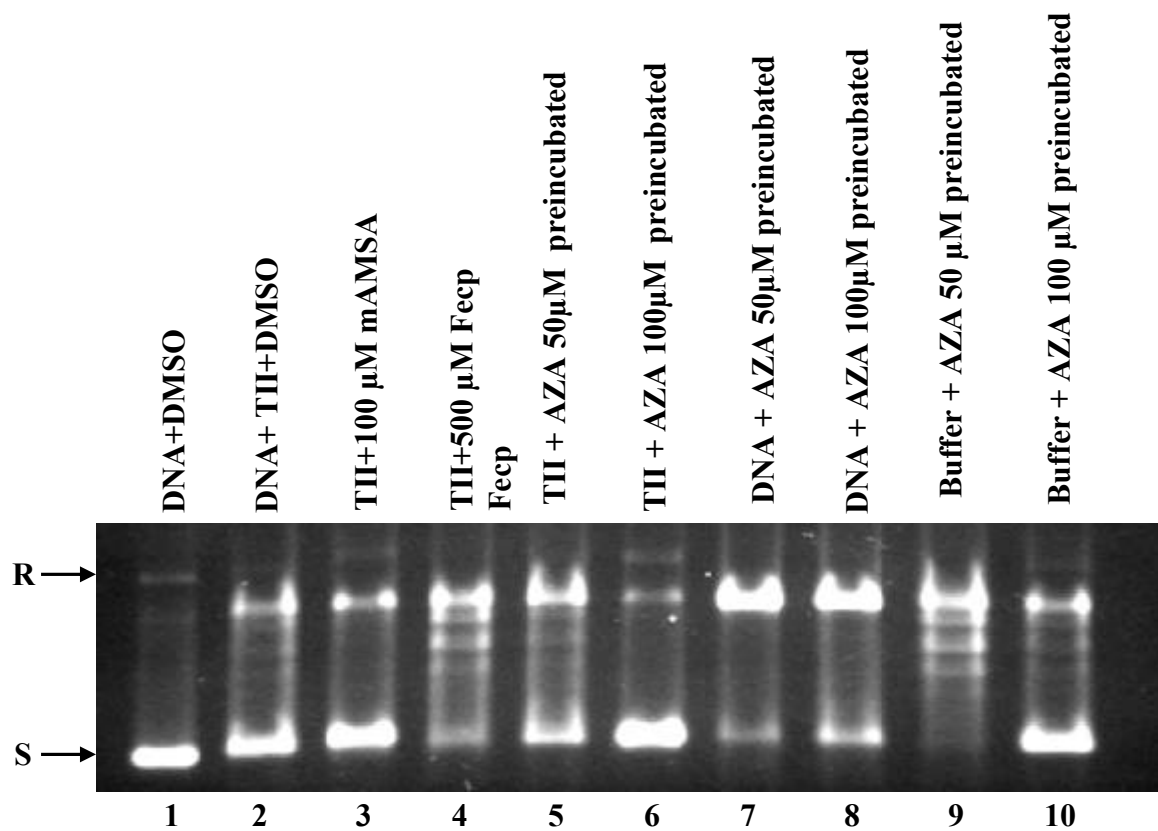**Tm studies in presence of Ferrocene Derivatives**

Figure 3.13:

Drug Interaction Assay

The assay was carried out at two concentration of azalactone Ferrocene 50 μM (non-inhibitory dose) and 100 μM (inhibitory dose). Azalactone Ferrocene interaction with Topoisomerase II beta (TII) was assessed by pre-incubation of drug with enzyme followed by immunoprecipitation of enzyme using Mouse anti-topoisomerase II beta monoclonal antibody and the free drug is washed off, the activity of immunoprecipitated enzyme was assayed in presence of DNA as shown at lane #5 (50 μM) and #6 (100 μM). While Azalactone Ferrocene interaction with DNA was assessed by pre-incubation of drug with enzyme followed by 10 fold dilution of drug (to bring down drug to inactive dose), then the DNA relaxation activity was studied with Topoisomerase II beta as shown at lane #7 (50 μM) and #8 (100 μM). The relaxing DNA intermediates were separated on agarose gel and stained with ethidium bromide and photographed (S: Supercoiled form, R: Relaxed form).

Figure 3.13

Drug Interaction Assay

Lanes (left to right):

1. DNA+DMSO
2. DNA+ TII+DMSO
3. TII+100 µM mAMSA
4. TII+500 µM Fecp Fecp
5. TII + AZA 50µM preincubated
6. TII + AZA 100µM preincubated
7. DNA + AZA 50µM preincubated
8. DNA + AZA 100µM preincubated
9. Buffer + AZA 50 µM preincubated
10. Buffer + AZA 100 µM preincubated

R →

S →

1   2   3   4   5   6   7   8   9   10

clearly show that azalactone ferrocene interacts with the enzyme and induces the formation of enzyme-linked cleavable complexes.

Action of Thiomorpholide amido methyl ferrocene and Azalactone ferrocene on DNA dependant ATPase activity of the enzyme

The DNA dependant ATPase activity of enzyme was monitored with increasing concentrations of thiomorpholide amido methyl ferrocene and Azalactone ferrocene using spectrophotometric assay. The results (Figure 3.14) show that both the compounds are potent inhibitors of DNA dependant ATPase activity of enzyme. To further investigate whether the inhibition of ATPase activity of enzyme is due to competitive inhibition of ATP binding to the enzyme or due to the drug associated inhibition of DNA passage activity, we have carried out ATP binding experiments using $\gamma^{32}P$ ATP (Figure 3.15). In this experiment, the enzyme was incubated with DNA and $\gamma^{32}P$ ATP at increasing concentrations of the drug. The enzyme was immunoprecipitated and washed 3 times, and the amount of ATP bound in terms of incorporated ^{32}P was monitored in immunoprecipitated topoisomerase II. The results of these experiments showed that the ATP binding in terms of ^{32}P incorporation increased in a dose dependant manner in the presence of increasing concentrations of azalactone ferrocene, while the thiomorpholide amido methyl ferrocene completely inhibited $^{32}\gamma P$ ATP incorporation into the enzyme. These results suggest that azalactone ferrocene binding do not competitively inhibit ATP and it will rather increase ATP binding in a concentration dependant manner (Figure 3.15). Thus azalactone ferrocene may block DNA passage activity of enzyme leading to the formation of enzyme linked cleavable complexes, while thiomorpholide amido methyl ferrocene inhibits catalytic activity of enzyme through blocking of ATP interaction with the enzyme.

Figure 3.14:

ATPase Assay

Inhibition of DNA-dependent ATPase activity of Topoisomerase II by Azalactone ferrocene and Thiomorpholide amido methyl ferrocene ATPase assay was conducted using spectrophotometer method. ATP hydrolysis in the absence of drug was taken as 100% and the ATP hydrolysis in the presence of increasing concentrations of the drug was calculated and presented. Each data value is an average of three experiments
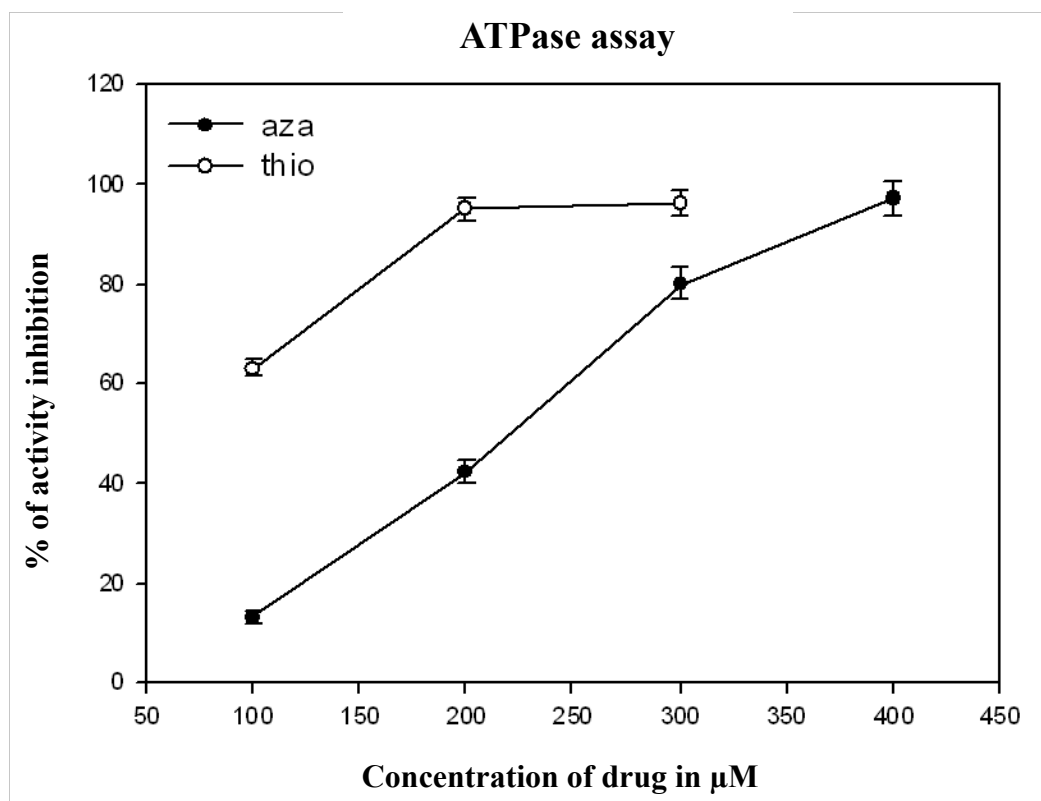
Figure 3.14

ATPase assay

Figure 3.15:

Analysis of ATP binding in the presence of drugs Topoisomerase II beta

Relaxation assay was carried out in the presence of increasing concentrations of drug using $\gamma^{32}P$ ATP. Drug bound enzyme was immunoprecipated by Mouse anti-topoisomerase II beta monoclonal antibody. The enzyme was TCA eluted and ^{32}P was estimated using scintillation counter. Experiments were done in triplicates and an average data is plotted.

Lane #1: Topo II with mAMSA; #2: Topo II with Ferrocene, Topo II with Azalactone concentrations 50 (#4), 100 (#5), 500 μM (# 6), Topo II with Thiomorpholide amido methyl ferrocene concentrations 50 (#7), 100 (#8), 200 (#9), 500 μM (#10).

Figure 3.15

Analysis of ATP binding in the presence of drugs
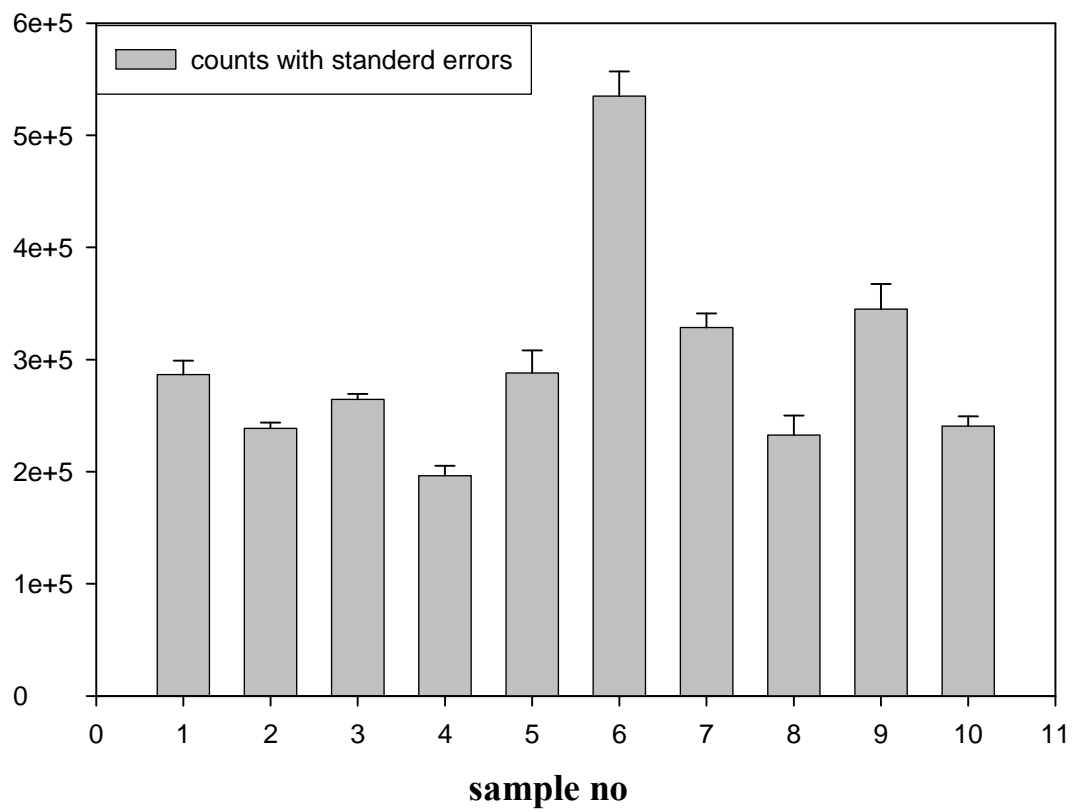
Receptor module ferrocene surface display analysis

Cerius^2 receptor module is used to calculate the hypothetical surface interaction between ferrocene derivatives and protein site of action. The models are generated as described in the methodology 2.27. Receptor module predict four different interactions namely hydrogen bonding, hydrophobic interactions , charge , electrostatic interactions. These interactions are represented by specific colour.

Hydrophobic interactions: The brown color areas are hydrophobic and areas that are not hydrophobic are white.

Hydrogen bonding: The area shown light blue are hydrogen bond acceptors and the surface shown purple are hydrogen bond donors, the surface showing white has no hydrogen bonding.

Charge: The surface shown red is positively charged, blue area is negatively charged and the area white is neutral.

Electrostatic interactions: The surface with red area is negatively electrostatic potential and the blue area is positively electrostatic potential and the white area is neutral potential

These interactions are calculated for Azalactone ferrocene (Fig 3.16), thiomorpholide amido methyl ferrocene (Fig 3.17) and over layed structure of XK469 and Aza fecp and Thio fecp (Fig 3.18) these ferrocene derivatives showed significant difference in electrostatic interaction (Fig 3.19) indicating that they play important role in the inhibitory activity.

Figure 3.16:

Azalactone Ferrocene showing various Receptor interactions:

Cerius^2 receptor module is used to calculate the hypothetical surface interaction between ferrocene derivatives and protein site of action. The models are generated as described in the Methodology (2.27). Receptor module predict four different interactions namely hydrogen bonding, hydrophobic interactions, charge, electrostatic interactions. These interactions are represented by specific colour.

In panel (a) the brown color area are hydrophobic and areas that are not hydrophobic are white.

In panel (b) the area shown light blue are hydrogen bond acceptors and the surface shown purple are hydrogen bond donors, the surface showing white has no hydrogen bonding.

In panel (c) the surface shown red is positively charged, blue area is negatively charged and the area white is neutral.

In panel (d) the surface with red area is negatively electrostatic potential and the blue area is positively electrostatic potential and the white area is neutral potential.
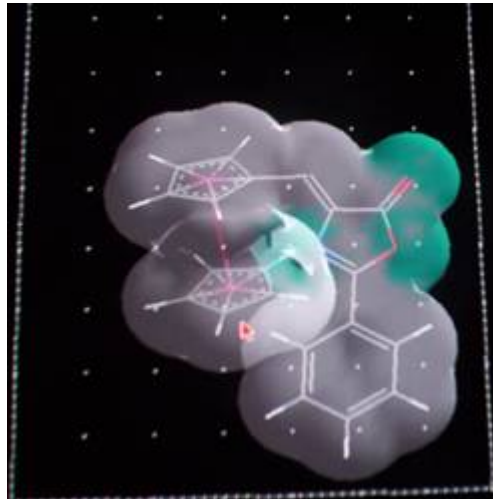
Figure 3.16

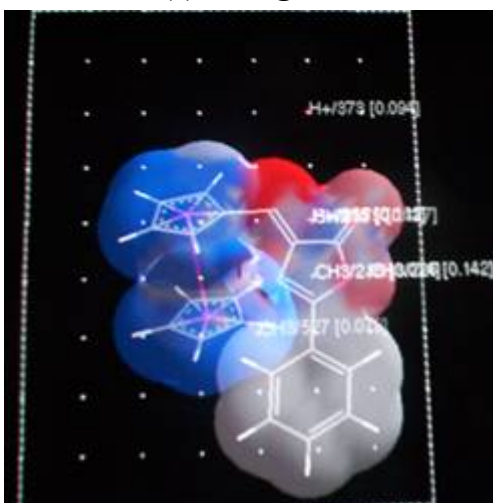**Azalactone Ferrocene showing various Receptor interactions.**

(a) Hydrophobic interactions
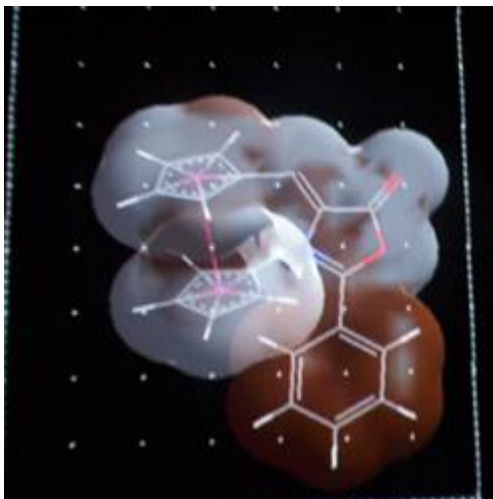
(b) Hydrogen bonding

(c) Charge
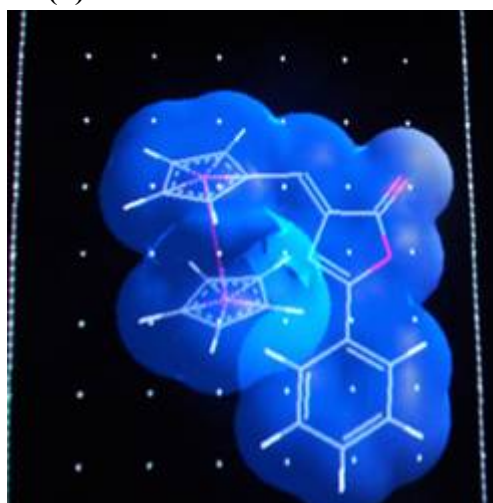
(d) Electrostatic interactions

Figure 3.17:

Thiomorpholide Amido Methyl Ferrocene showing various Receptor interactions

Cerius^2 receptor module is used to calculate the hypothetical surface interaction between ferrocene derivatives and protein site of action. The models are generated as described in the Methodology (2.27). Receptor module predict four different interactions namely hydrogen bonding, hydrophobic interactions, charge, electrostatic interactions. These interactions are represented by specific colour.

In panel (a) the brown color area are hydrophobic and areas that are not hydrophobic are white.

In panel (b) the area shown light blue are hydrogen bond acceptors and the surface shown purple are hydrogen bond donors, the surface showing white has no hydrogen bonding.

In panel (c) the surface shown red is positively charged, blue area is negatively charged and the area white is neutral.

In panel (d) the surface with red area is negatively electrostatic potential and the blue area is positively electrostatic potential and the white area is neutral potential.

Figure 3.17

Thiomorpholide Amido Methyl Ferrocene showing various Receptor interactions

(a) Hydrophobic interactions
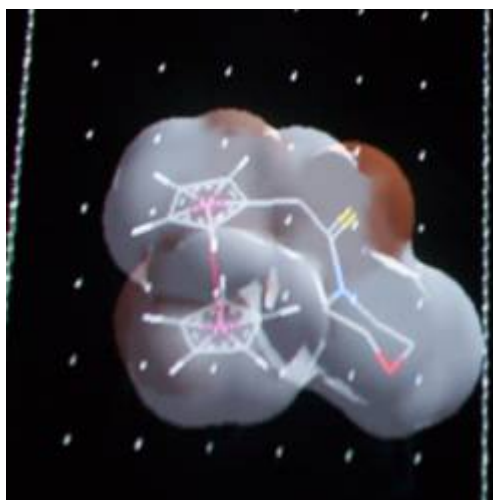
(b) Hydrogen bonding

(c) Charge

(d) Electrostatic interactions

Figure 3.18:

The closely overlaid structures of the Azalactone Ferrocene and Thiomorpholide Amido Methyl Ferrocene and XK469 (Topo II β inhibitor)

Cerius^2 receptor module is used to calculate the hypothetical surface interaction between ferrocene derivatives and protein site of action. The models are generated as described in the Methodology (2.27). Receptor module predict four different interactions namely hydrogen bonding, hydrophobic interactions, charge, electrostatic interactions. These interactions are represented by specific colour.

In panel (a) the brown color area are hydrophobic and areas that are not hydrophobic are white.

In panel (b) the area shown light blue are hydrogen bond acceptors and the surface shown purple are hydrogen bond donors, the surface showing white has no hydrogen bonding.

In panel (c) the surface shown red is positively charged, blue area is negatively charged and the area white is neutral.

In panel (d) the surface with red area is negatively electrostatic potential and the blue area is positively electrostatic potential and the white area is neutral potential.
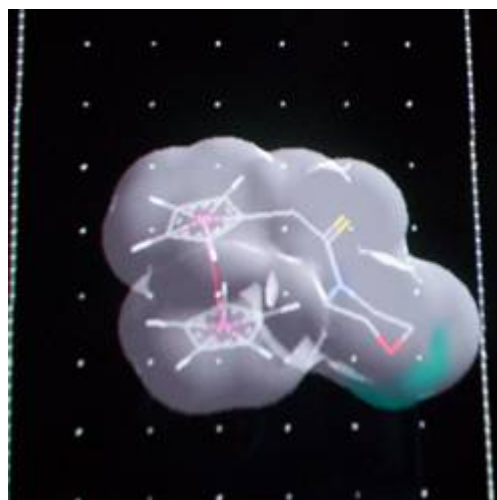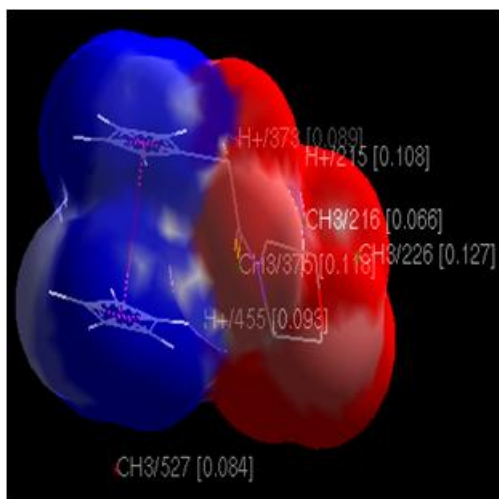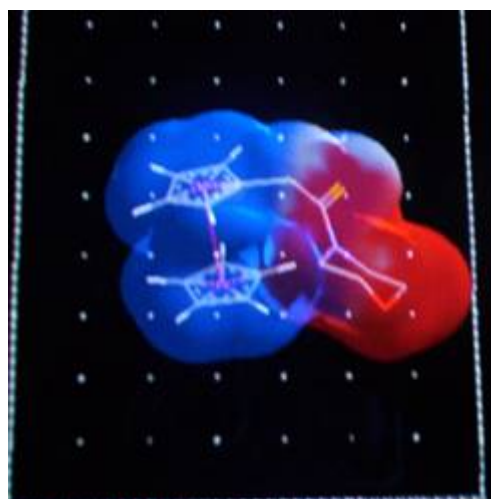
Figure 3.18

The closely overlaid structures of the Azalactone Ferrocene and Thiomorpholide Amido Methyl Ferrocene and XK469 (Topo II β inhibitor)

(a) Hydrophobic interactions
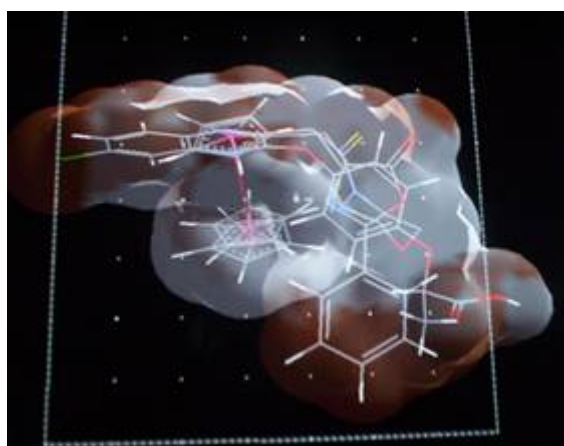
(b) Hydrogen bonding
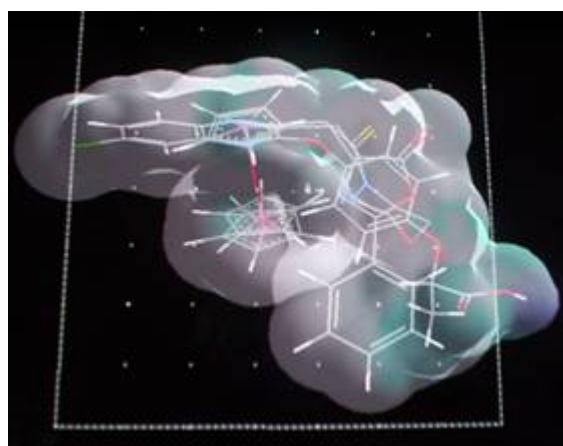
(c) Charge
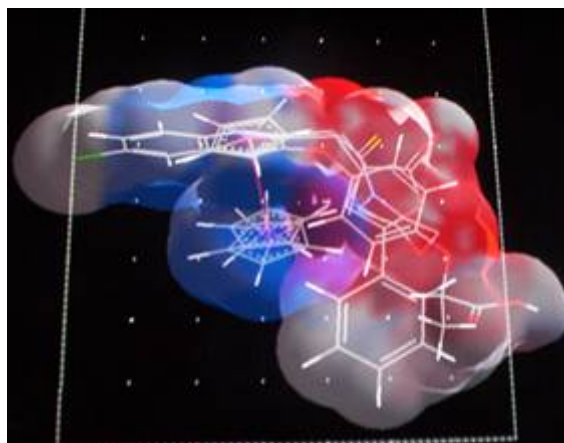
(d) Electrostatic interactions
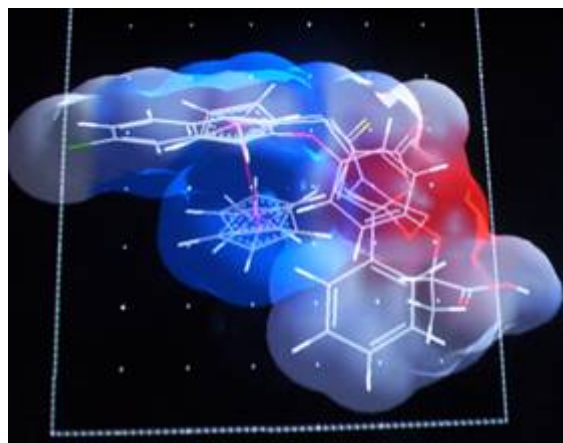
Figure 3.19:

Surface Electrostatic Interactions

Ferrocene derivatives showing various receptor interactions. The surface with red area is negatively electrostatic potential and the blue area is positively electrostatic potential and the white area is neutral potential.

➢ The +ve electrostatic potential (Fig A) side chain of azalactone ferrocene may be forming bonding with –ve electrostatic potential of the phosphate group exposed during catalytic assay and form cleavage complex

➢ The –ve electrostatic potential (Fig B) side chain of the thiomorpholide amido methyl ferrocene (similar to ATP phosphate group which also have –ve electrostatic potential group) may be forming linkage with the ATP binding site and inhibiting the reaction

Figure 3.19

Surface Electrostatic Interactions

Unique Features

Fig A
Azalactone ferrocene
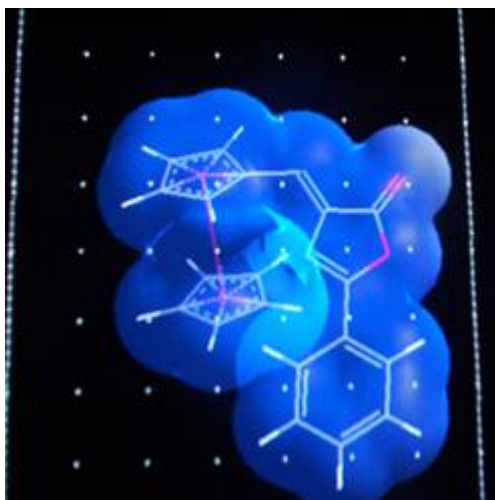
Fig B
Thiomorpholide amido methyl ferrocene
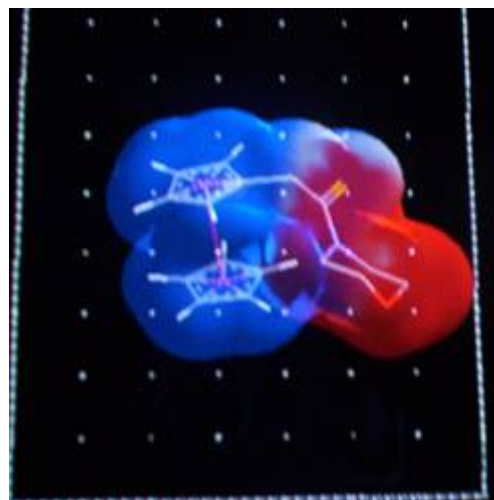
Common Features
Over laid image of aza, thio ferrocene and XK469

DISCUSSION

Topoisomerase II alpha and beta are known to be potential targets for the cancer chemotherapy (380-382). The levels of topoisomerase II alpha isoform were shown to be up-regulated in certain cancers, lung (383) ovarian (384), prostate (384), where as topoisomerase II beta levels are up-regulated in breast (385), and brain cancer (386). This differential expression of topoisomerase II isoforms in different cancers prompted efforts towards development of topoisomerase II isoform-specific poisons or inhibitors for targeting against cancer tissue of interest.

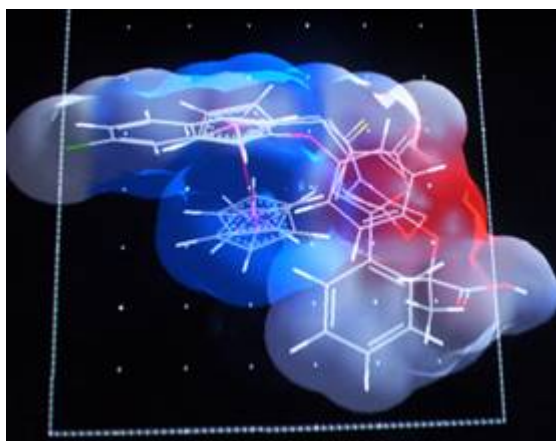XK469 was the first, topoisomerase II β-specific poison reported from screening of large library of various compounds (387), and it was found to poison the activity of Topoisomerase II beta. Other Topoisomerase II poisons namely etoposide (388), quinoline derivatives poison both the isoforms of the Topoisomerase II. In the present study, we used QSAR methodology in finding Topoisomerase II beta-specific poisons from derivatives of ferrocene. The two active ferrocene derivatives namely azalactone ferrocene and thiomorpholide methyl ferrocene do not possess affinity to DNA. This could be due to the absence of a planar ring system that has been shown to be involved in DNA binding in other topoisomerase II inhibitors. Also, the caged iron is not directly available for DNA interaction. But the positive electrostatic potential induced by iron through cyclopentadiene ring may provide weak interaction of the ferrocene with the negatively charged phosphate backbone, when the ferrocene derivative interacts with the enzyme (Figure 3.16- 3.19).

The inhibition of Topoisomerase II beta isoform by thiomorpholide amido methyl ferrocene is higher than Azalactone ferrocene. The action of thiomorpholide amido methyl ferrocene is found to be due to inhibition of ATP-enzyme interaction without forming cleavable complexes, whereas the azalactone ferrocene allows ATP binding to the enzyme

and induces the formation of cleavable complexes. Comparison of structure of XK469 with those of azalactone ferrocene and thiomorpholide methyl ferrocene shows that the later posses largely charged surfaces on the interacting face, as shown in Figure 3.18. This may be one of the structural features that these compounds possess which might be enhancing their ability in Topoisomerase II beta interaction. The higher molecular volume containing hydrophobic groups may allow azalactone ferrocene in freezing enzyme-DNA covalent intermediates.

The comparison of structural features of these two compounds show that the distance and orientation of the interacting atom of the substituent from iron cyclopentadiene ring may play a key role in modulating the activity of the drug (Fig 3.6). This analysis suggests that the orientation of interacting groups away from the ferrocene axis and above and below the plane of cyclopentadiene ring is important for affecting the activity of the enzyme. The difference between azalactone ferrocene and thiomorpholide amido methyl ferrocene in inducing cleavable complex could be due to the difference in orientation of the substituent, while the thiomorpholide ferrocene orients towards the iron axis and lies in the plane of the second cyclopentadiene ring (Figure 3.17), the azalactone ferrocene moves away from the iron axis and lies above the substituted cyclopentadiene ring (Fig 3.16). These findings indicate that the structural requirement of ferrocene drugs for inhibition of catalytic activity of topoisomerase II beta and substitutions away from iron axis may play a role in blocking the DNA passage activity of enzyme. In addition, substitution towards iron axis may be important in blocking ATP binding domain of the enzyme. Further analysis of a few more structurally distinct ferrocene derivatives may provide critical details of conformational molecular changes that ferrocene derivatives confer upon enzyme. In summary, both azalactone ferrocene and thiomorpholide amido methyl ferrocene are found to be potent

inhibitors of topoisomerase II with preferential action against beta isoform, and the two compounds show distinctly different modes of action against enzyme.

CHAPTER IV

Development of drug delivery system for target specific

localization of ferrocene derivatives in cancer cells

The drugs are absorbed by epithelial lining of specific tissues in reaching the circulatory system. The extent of drug absorption is dependent on the chemical and biological properties of the drug, which determine its side effects. Localized application of drug is known to be very effective with reduced side effects, but this is an invasive technique (223). To reduce the entry of drug into non target cells, several target specific technologies were developed during the last few years and some of them implemented. Majority of these technologies invoke the use of polymeric materials (PEG, PLGA) (225), proteins (chitins, albumin) (226). These materials though are excellent carriers of drug, they lack target specificity (226). Thus target specific ligands like transferrin, antibodies, carbohydrates, signal peptides are widely studied for guiding these delivery systems to specific cells and tissues (227). The present investigation, reports a target directed nanoparticle drug delivery system comprising of apotransferrin-drug nanoparticles.

Transferrin as drug delivery system

From a therapeutic perspective, this enables the one molecule to be used for various treatments. Binding of the proteins apotransferrin/transferrin with cells requires transferrin receptors. The amount of transferrin receptors present on the surface of the cells is regulated by two factors (I) the concentration of iron in the cell and (II) cell growth. These receptors are highly expressed by tissues having high metabolic activity such as brain as well as those which are in active growth such as in cancer cells. Hence, transferrin receptors are widely tested and accepted target for delivery of drugs to cancer, brain and other infectious and diseases demanding iron metabolism. The ligands that have been well tested as carriers of drug through transferrin receptor mediated endocytosis are soluble Transferrin, Apotransferrin, and Transferrin receptor antibody (OX-26). A Nanoparticle based drug delivery system is presented in this Chapter IV

Current transferrin drug delivery systems:-

1. Chemical conjugation (glutaraldehyde) apotransferrin with antitumour agents (388)

2. Binding of metal complexes to soluble apotransferrin (389), in this method the drug is immobilised under hydrophobic conditions to protein which also requires metal as iron /ruthenium for binding the drug to the active site of apotransferrin. The limitation of this process is that the drug can only be released in a pH dependant manner in lysosome (390). The drug is released in lysosome and thus the efficiency of drug release is low.

3. Coating of protein around the iron containing nanoparticles

   Iron nanoparticles core is layered by a primary synthetic layer of polymer and then by second layer of apotransferrin and a pharmaceutical adjuvant. The drawback of the process is that the polymer and the iron core will remain in the cell and form a source of toxicity which is not advisable (391)

4. TrR antibody (OX26) / transferrin / apotransferrin were conjugated directly or through biotin /avidin coupling to liposome/ polymer micro spheres composing PEG or carbohydrates (392, 393)

The conjugated TfR antibody/transferrin/apotransferrin can mediate the binding of liposome/ microspheres to transferrin receptor and intake occurs through receptor-mediated endocytosis TfR antibody (OX26)/transferrin/apotransferrin were conjugated directly or through biotin /avidin coupling to liposome/polymer micro spheres composing PEG or carbohydrates (394) The drug can be released into cytosol directly. The left over compounds of delivery system such as TfR antibody (OX26)/transferrin/apotransferrin conjugated liposome/micro spheres will remain in the cell and degradation is slow and they form potential cytotoxicity to the cells due to high metabolic stress on the cell for their degradation. The extent of drug release from such liposome may not also be efficient. Due to

irreversible binding of the conjugated antibody / transferrin / apotransferrin to liposome/ micro spheres, they compete out soluble transferrin binding, thus the iron transport is drastically inhibited, which would lead to iron depletion and anaemia. Apotransferrin nanoparticles drug delivery is developed in this chapter provide a natural mode of delivery of drug.

Protein purification and characterization:

Transferrin is purified from plasma as described in chapter II. This protein is solubilised in TBS and the protein in the sample were chromatographed and separated based on size on S-100 gel filteration chromatography. The eluted fractions were analyzed by SDS-PAGE. The homogenous protein fractions 11-17th (Figure 4.1) containing transferrin shown homogenous. The transferrin protein is converted to apotransferrin by dialysis in 10 mM EDTA and 10 mM sodium acetate pH 5. At the pH 5, the bound iron in the protein is released and the transferrin is converted to apotransferrin. The purity of the apotransferrin assessed using SDS PAGE (Figure 4.2) and native PAGE analysis (Figure 4.3) the results confirm that the purified apotransferrin is significantly homogenous. Purified apotransferrin was confirmed by western blotting (Figure 4.4) using monoclonal mouse anti-human transferrin antibody.

Characterization of particles by Scanning electron microscopy:

The particles were characterized by Scanning electron microscopy (SEM) in Figure 4.5 The results on determination of particle size by SEM show that the apotransferrin particles were of 20-45 nm dimension (Figure 4.5A), while the nanoparticles of apotransferrin-doxorubicin were of 60-70 nm (Figure 4.5 B) and apotransferrin-azalactone ferrocene nanoparticles were of 70-80 nm dimension (Figure 4.5 C). Thus suggesting that the method followed for preparation of particles could produce particles of nanometer

Figure 4.1

Purification of Transferrin by Gel exclusion Chromatography

Serum protein is separated based on molecular size by S-100 gel exclusion chromatography as described in Chapter II. The eluted collections were analysed by SDS–PAGE stained by comassie blue R-250.

 # 1-17:- 1-17th S-100 column elutes

Figure 4.1

Purification of Transferrin by Gel exclusion Chromatography

1 2 3 4 5 6 7 8 9 10 11 12 13 14 15 16 17
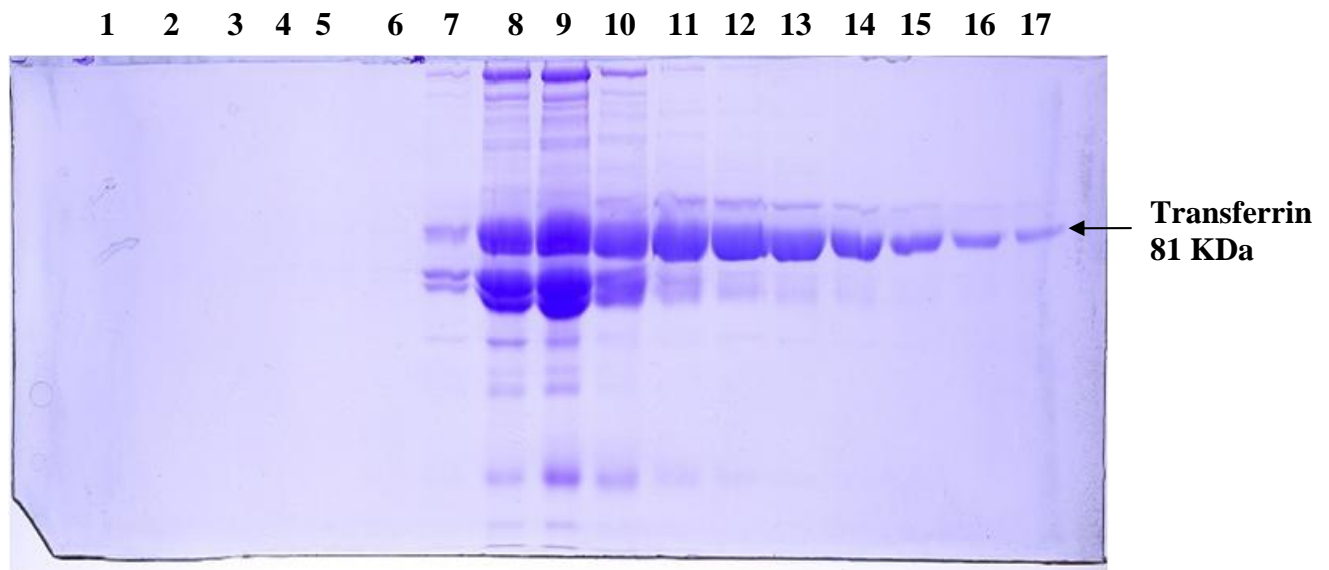
Transferrin
81 KDa

Figure 4.2:

Preparation of Apotransferrin

The protein elutes 8,10, and 12 in figure 4.1 were dialyzed with 10 mM EDTA and 10 mM sodium acetate pH 5.0. 20 µg of protein in dialyzed elute was separated on 8% SDS PAGE at 70 volts for 3 hours. The gel was stained with comassie blue R-250. The purified 12th fraction of the protein show single band of apotransferrin a 81 kDa protein. Molecular weight markers 26, 47, 85, 118 kDa band are shown in the gel

      # 1   Protein molecular weight marker

      # 2   Bovine transferrin (control)

      #3 8th dialysed elutes

      #4 10th dialysed elutes

      #5 12th dialysed elutes

Figure 4.2

Preparation of Apotransferrin
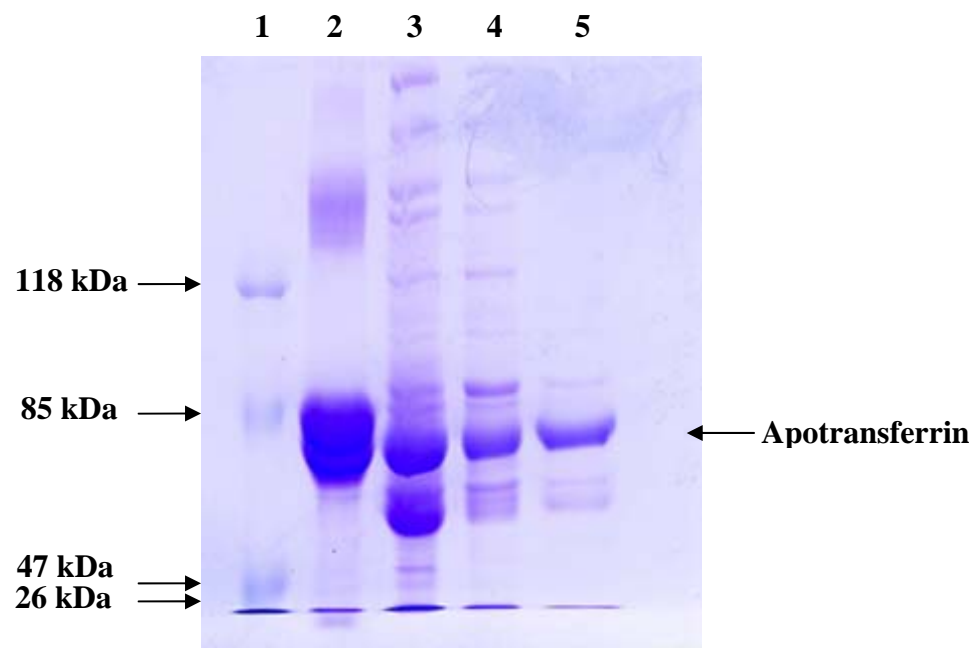
Figure 4.3:

Native PAGE analysis of purified Apotransferrin protein

The protein in 12th elutes Fig 4.2 were reanalyzed by Native PAGE. Apotransferrin purified

in Fig 4.2 (12th elute) was analyzed on Native-PAGE

Lane 1, 2 10, 20 µg protein of 12th elute analyzed in Native PAGE

Figure 4.3

Native PAGE analysis of purified Apotransferrin
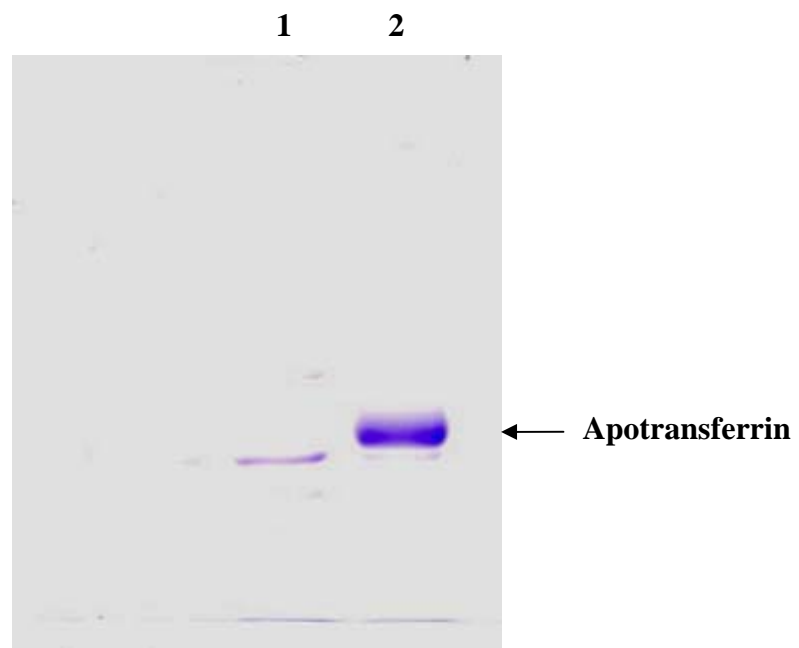
Figure 4.4:

 Immunoreactivity of Apotransferrin

The purified protein elutes were separated on SDS PAGE (8%). The protein is transferred to the Nitrocellulose membrane by standard western blotting procedure. Human transferrin, bovine transferrin and rat apotransferrin were used as control. Apotransferrin is detected by mouse anti-human transferrin monoclonal antibodies followed by detection using IgG goat antimouse IgG conjugated with alkaline phosphatase. The purple colored immunoprecipates formed were photographed.

> # 1: 10 µg Bovine apotransferrin
>
> # 2: 10 µg rat apotransferrin
>
> #3-5: 1,2,10 µg of purified human apotransferrin

Figure 4.4

Immunoreactivity of Apotransferrin
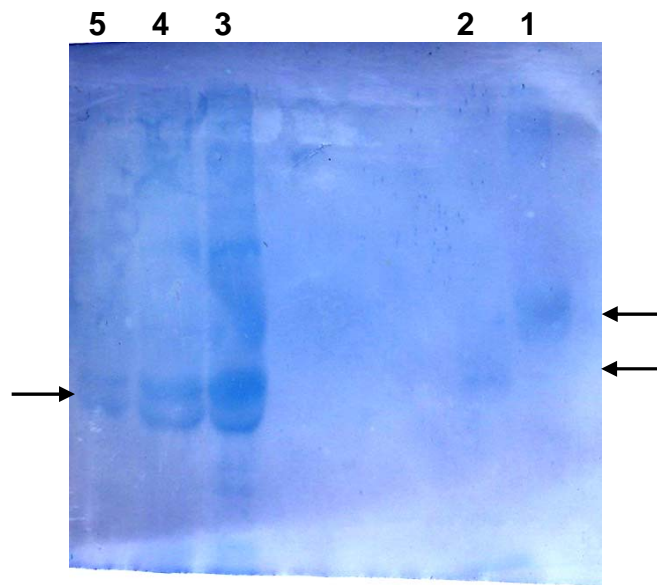
Figure 4.5:

Electron Microscopic analysis of Nanoparticles:

Apotransferrin nanoparticles were prepared as described in Methodology 2.34. The particles were analyzed by SEM, TEM. Electronically generated scale is represented in the SEM image and size of the nanoparticles are measured and indicated in the Figure. Scale in TEM figure was calculated based on the NEG magnification and the point magnification.

     Panel A: Apotransferrin protein nanoparticles

     Panel B: Doxorubicin - Apotransferrin nanoparticles

     Panel C: Azalactone ferrocene- Apotransferrin nanoparticles

Figure 4.5

Electron Microscopic analysis of Nanoparticles

SEM image **TEM image**

Panel A

Apotransferrin nanoparticles

SEM image **TEM image**

Panel B

Doxorubicin-Apotransferrin nanoparticles

SEM image

Panel C

Azalactone ferrocene-Apotransferrin nanoparticles
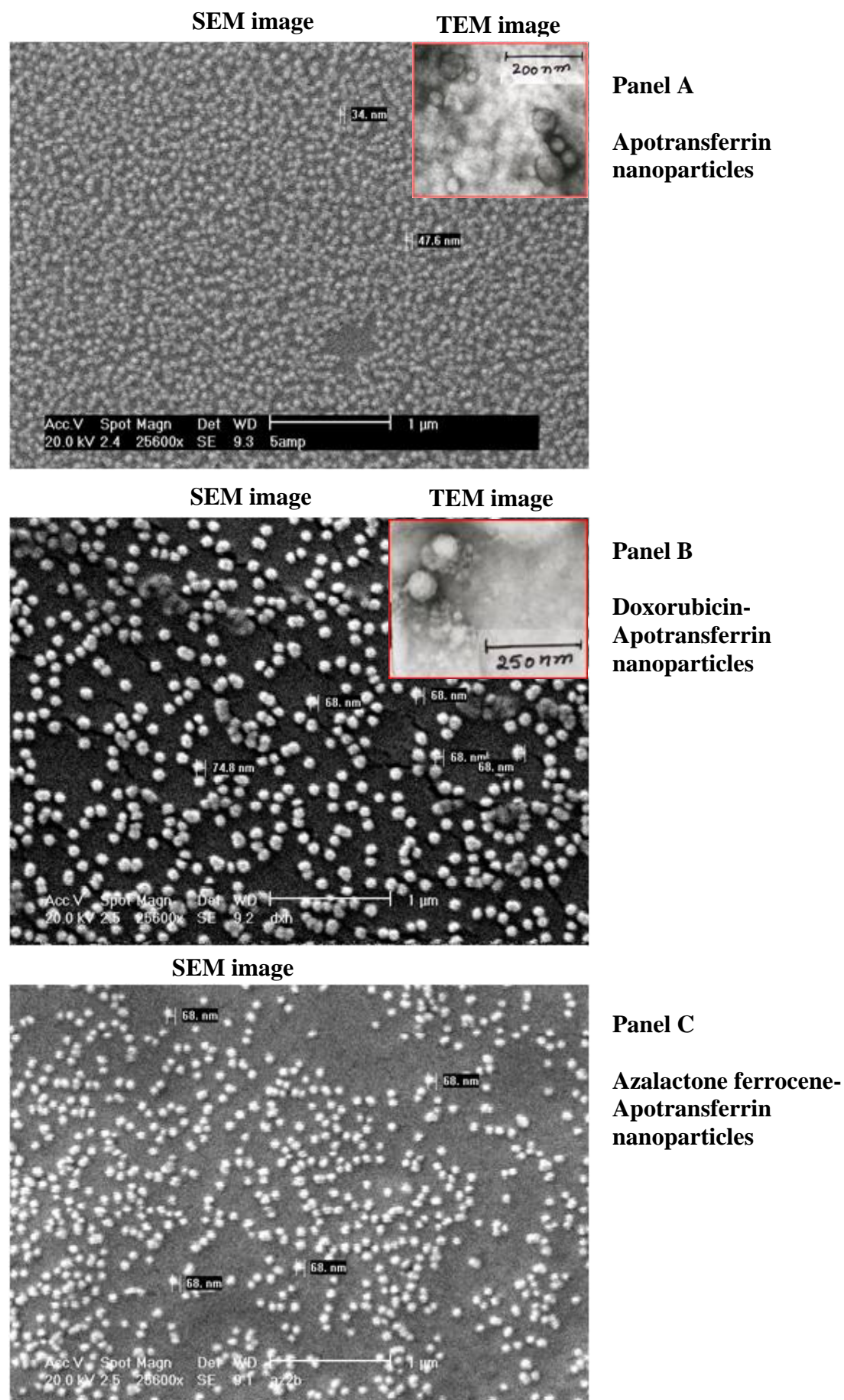
dimensions. The particle size increases when drug is encapsulated and such an increase is due to the enhanced molecular volume of protein in the presence of drug.

Characterization of particles by Atomic force microscopy:

To know the surface morphology of the particles, a high resolution analysis of surface properties of the particles has been carried out using the Atomic Force microscopy (AFM). The results (Figure 4.6) show that the surface morphology of particle follows a pattern characterized by distinct morphological separation in the range of a ~ 1 nm scale. Such surface structural features may play an important role in conferring molecular recognition and biological activity to the particles in terms of binding to the transferrin receptor. The particles due to high concentration of the protein in the particles. These results suggest that the optimum concentration for the formation of nanoparticles is 10 mg in 30 ml of olive oil.

Optimization of sonication conditions (Table 4.1)**:**

The sonication conditions were optimized based on amplititude of pulse, where there is optimum formation of the nanoparticles. Equal amount of the protein and the drug is added to the 15 ml of the olive oil and sonicated at various intensities of the pulse as indicated in the Table 4.2. The samples were processed as described in Methodology 2.36. The particles formed were analysed by the SEM imaging (Figure 4.7). At 0.5 and 1 amplitude there is no formation of the nanoparticles, while at the intensities 2-6 amplitude there is a formation of the nanoparticles. Based on the results shown SEM imaging, 5 micron amplitude of the pulse shown optimum condition for the formation of the nanoparticles.

Optimization of centrifugation speed (Table 4.2): The above method the experiment is repeated at different centrifugation speed to find optimum speed required for pelleting of particles.

Figure 4.6:

Atomic force Microscopic analysis of Nanoparticles

Surface morphology of apotransferrin-doxorubicin nanoparticles using AFM. D1 show 3D topographical image that was top projected in D2 and magnified in D3 and D4. One area in D2 was chosen and its surface is displayed in D5 (147 nm/ per 3 particles) and D6 depicts magnified single in 33 nm scale. Each experiment was repeated thrice to confirm these results.

The image is analyzed by the AFM Spiwin software, scale in the figure is generated electronically. The distance between two nanoparticles is measured by surface display analysis, In the panels D5, D6 two colored lines are displayed (red, yellow, blue, green, pink) These represents the diameter of corresponding nanoparticle as given in the appended table in D5, D6 image.

Figure D1: AFM 3D Topographic image (scale 500 x 500 nm)

Figure D2: AFM Topographic image (scale 500 x 500 nm)

Figure D3: AFM 3D Topographic image (scale 250 x 250 nm)

Figure D4: AFM Topographic image (scale 250 x 250 nm)

Figure D5: Surface display analysis (scale 147 nm)

Figure D6: Surface display analysis (scale 33 nm)

Figure 4.6

Atomic force Microscopic analysis of Nanoparticles
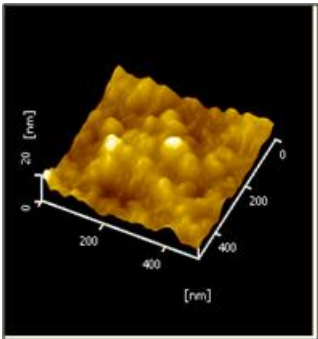
| **(D1) AFM 3D Topographic image** | **(D2) AFM Topographic image** | **(D3) AFM 3D Topographic image** | **(D4) AFM Topographic image** |
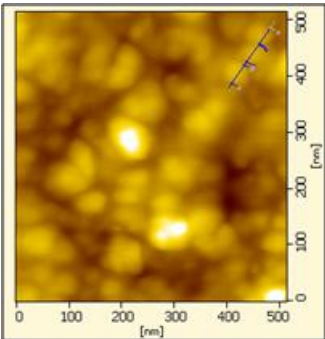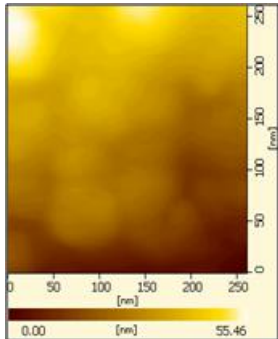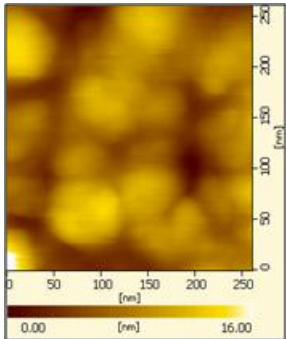
(D5) Surface Display Analysis

	Z1[nm]	Z2[nm]	ΔZ [nm]	Distance [nm]	Φ[°]
🟥	10.54556	11.11890	0.573344	41.45663	0.792348
🟨	10.86170	11.61917	0.757479	39.15348	1.108328
🟦	11.63139	9.089856	2.541538	35.69876	4.072246

(D6) Surface Display Analysis

	Z1[nm]	Z2[nm]	ΔZ [nm]	Distance [nm]	Φ[°]
🟥	5.770245	5.526882	0.243363	30.26564	0.460700
🟨	6.433148	6.399467	0.033681	1.768771	1.090891
🟦	5.788815	5.688483	0.100332	1.506731	3.809661
🟩	6.496534	6.440259	0.056275	1.703261	1.892352
🟪					
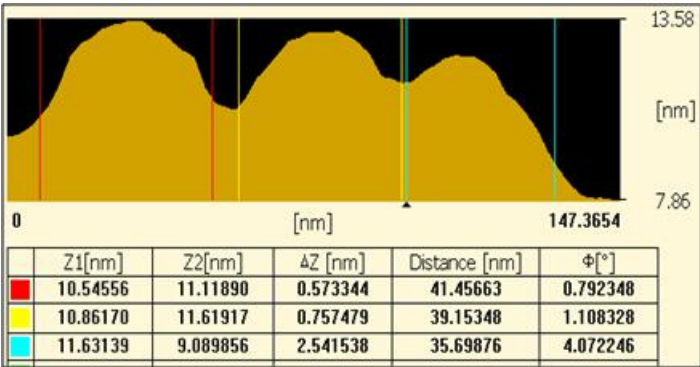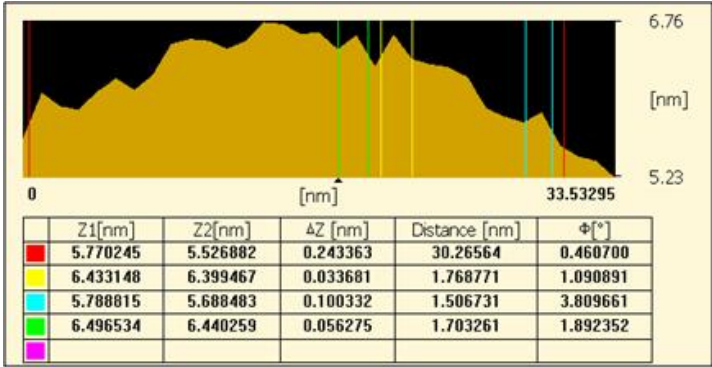
Table 4.1:

Optimization of Sonication condition

Nanoparticles are prepared as described in Methodology 2.36, the protein drug mixture was sonicated at indicated intensity of amplitude in microns and mixture is frozen and thawed, this is now centrifuged at 5000 rpm and the pellet is collected. The pellet is dispersed in PBS and particles are analyzed by the SEM. The dimensions of the particle formed as observed by the SEM images are given in the Figure 4.7. Based on the SEM analysis the optimum intensity of nanoparticle formation is 5 microns taken as standard.

Table 4.1

Optimization of Sonication condition

Condition	Particle formation	SEM analysis of the nanoparticles
0.5 microns	No particle formed	---
1 microns	No particle formed	---
2 microns	Yes	60 -70 nm
3 microns	Yes	60 -70 nm
4 microns	Yes	60 -70 nm
5 microns	Yes	60 -70 nm
6 microns	Yes	60 -70 nm

Figure 4.7:

Optimization of Sonication condition

SEM images of the nanoparticles prepared at the respective amplitude 1-6 microns

Nanoparticles are prepared as described in Methodology 2.36, the protein drug mixture was sonicated at indicated intensity of amplitude in microns and mixture is frozen and thawed, this is now centrifuged at 5000 rpm and the pellet is collected. The pellet is dispersed in PBS and particles are analyzed by the SEM. The dimensions of the particle formed as observed by the particle size are given in the Table 4.1. Based on the SEM analysis the optimum intensity of nanoparticle formation is 5 microns taken as standard

Figure 4.7

Optimization of Sonication condition

1 amplititude
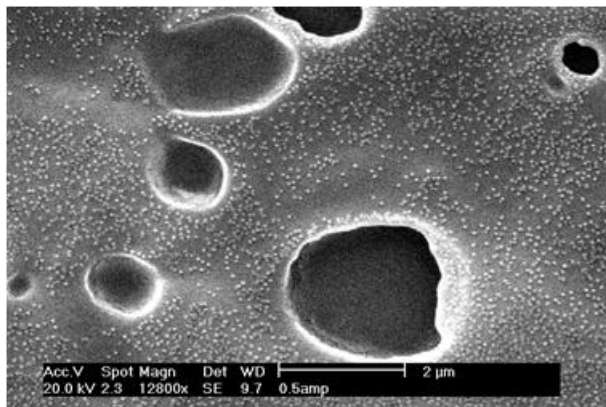
2 amplititude
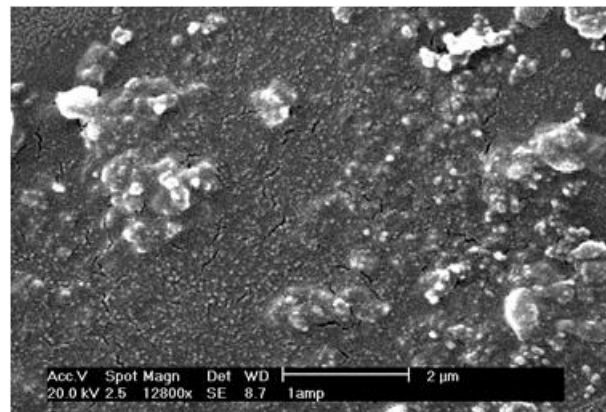
3 amplititude
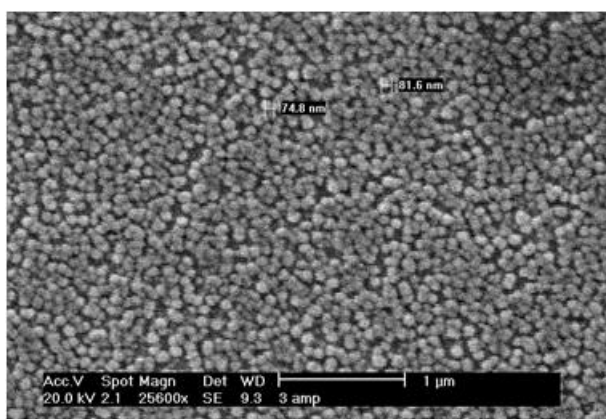
4 amplititude
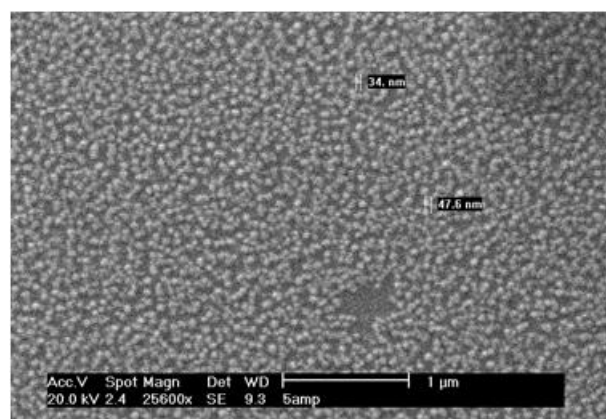
5 amplititude
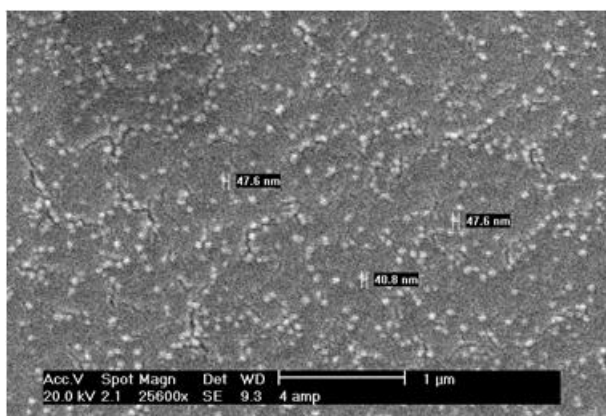
6 amplititude
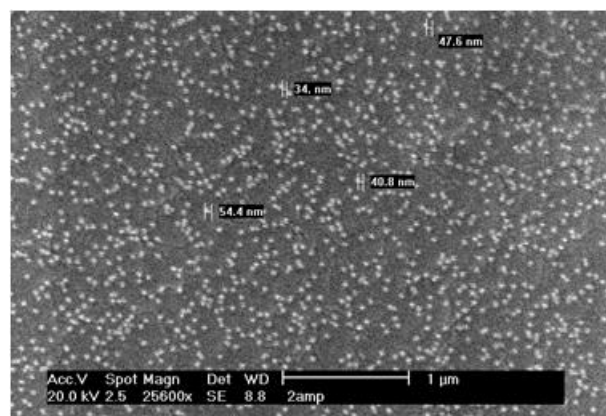
Table 4.2:

Optimization of Centrifugation Speed for Pelleting Nanoparticles:

Nanoparticles are prepared as per the Methodology 2.36 and sonicated mixture is frozen and thawed, this is now centrifuged at various speed as indicated and the pellet is collected. The pellet is dispersed in PBS and particles are analyzed by the SEM. The dimensions of the particle formed are given in the Figure 4.8. Based on the SEM analysis and the pellet dispersion the optimum centrifugation speed is characterized as 5000 rpm.

Table 4.2:

Optimization of Centrifugation Speed for Pelleting Nanoparticles

Condition	Particles formation	SEM image analysis of the particle Dimension formed
1000 rpm	Yes	60-70 nm (Nanoparticle pellet could not be clearly separated from oil. Loose pellet formed)
2000 rpm	Yes	60-70 nm (Loose pellet formed)
3000 rpm	Yes	60-70 nm (Loose pellet formed)
4000 rpm	Yes	60-70 nm (Loose pellet formed)
5000 rpm	Yes	60-70 nm
6000 rpm	Yes	60-70 nm
7000 rpm	Yes	60-70 nm (Difficult in dispersion of pellet)
8000 rpm	Yes	60-70 nm(Difficult in dispersion of pellet)

The sonicated mixture is frozen and samples are thawed and nanoparticles are analyzed at various centrifugation speeds. The centrifused samples are dispersed in PBS and analyzed by SEM imaging (Figure 4.8) for the formation and the size of the nanoparticles. The results of the SEM analysis show that the speeds below 2000 rpm the pellet did not settle well and could not be clearly separated from the olive oil, while at centrifugation speed above 5000 rpm the pellet tightly formed and could not be dispersed properly. Hence, the results suggest that speed of 5000 rpm is optimum for the pelleting of nanoparticles, easy dispersion of pellet formed and is stable.

Optimization of protein concentration for the formation of nanoparticles (Table 4.3)

The protein concentration minimum required for the formation of nanoparticles is studied. 1, 5, 10, 20, 40 mg of protein and 100 mM of drug are used for preparation of nanoparticles in 15 ml olive oil. At protein concentrations 1 mg and 5 mg, particles were not formed (Figure 4.9), while at the protein concentrations 5 mg and above there is a significant nanoparticle formation, but at the protein concentration 40 mg and above there is a formation of nanoparticles but the pellet is difficult to disperse this may be due to the strong aggregation of the particles due to high concentration of the protein in the particles. These results suggest that the optimum concentration for the formation of nanoparticles is 10 mg in 30 ml of olive oil.

Characterization of Apotransferrin-drug Nanoparticles:

Apotransferrin nanoparticles were prepared as described in the Methodology 2.36 Uniformly dispersed particles in PBS were characterized for chemical composition using biochemical methods. The results of assessment of particles for the presence of protein, oil and drug, show that particles were sensitive to low pH and resistant to organic solvents suggesting that the particles were composed of protein (Figure 4.10). The apotransferrin in

Figure 4.8:

Optimization of Centrifugation Speed for Pelleting Nanoparticles

SEM images of the nanoparticles pelleted at the respective centrifugation speeds 1000-6000 rpm.

Nanoparticles are prepared as per the Methodology 2.34 and sonicated mixture is frozen and thawed, this is now centrifuged at various speed as indicated in Table 4.1 and the pellet is collected. The pellet is dispersed in PBS and particles are analyzed by the SEM. The SEM images of particles are given in the Figure 4.7. Based on the SEM analysis and the pellet dispersion the optimum centrifugation speed is characterized as 5000 rpm.

Figure 4.8

Optimization of Centrifugation Speed for Pelleting Nanoparticles

1000 RPM
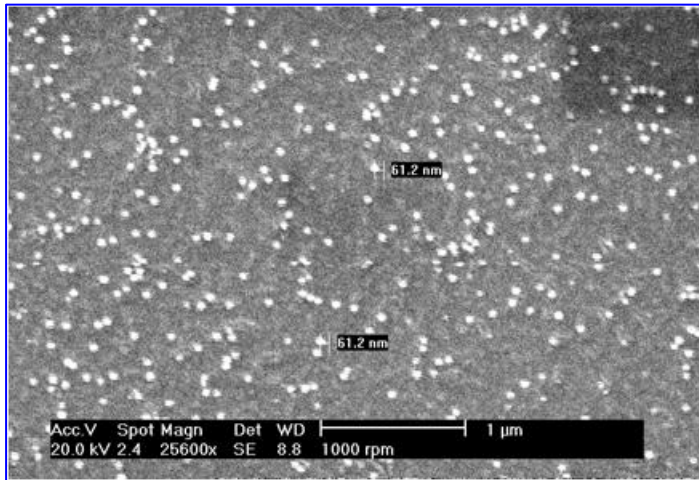
2000 RPM
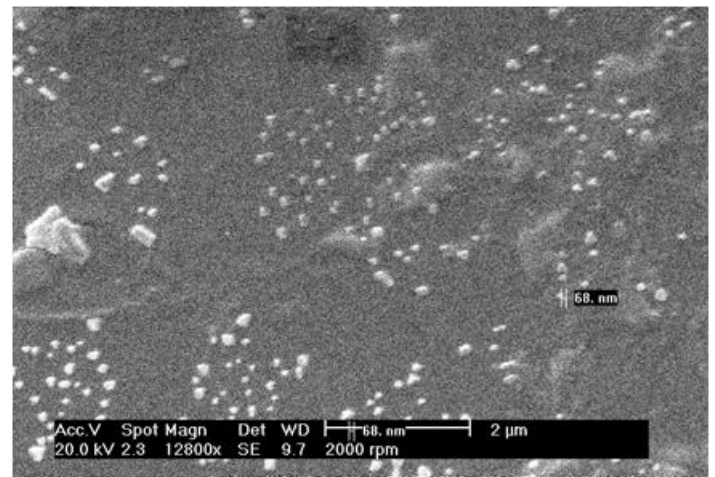
3000 RPM
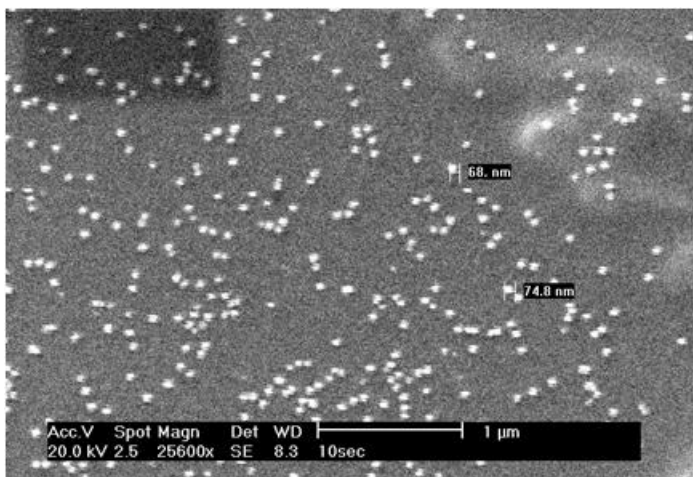
4000 RPM
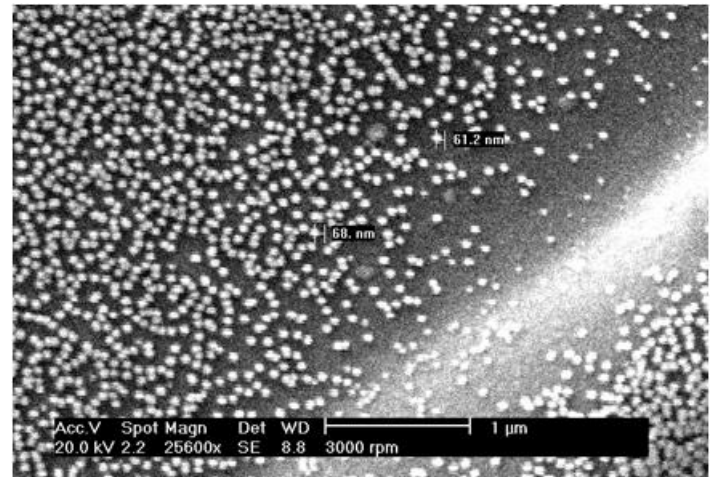
5000 RPM
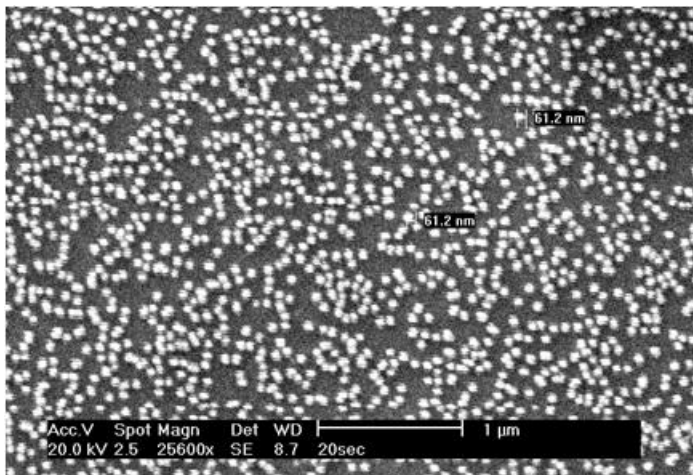
6000 RPM
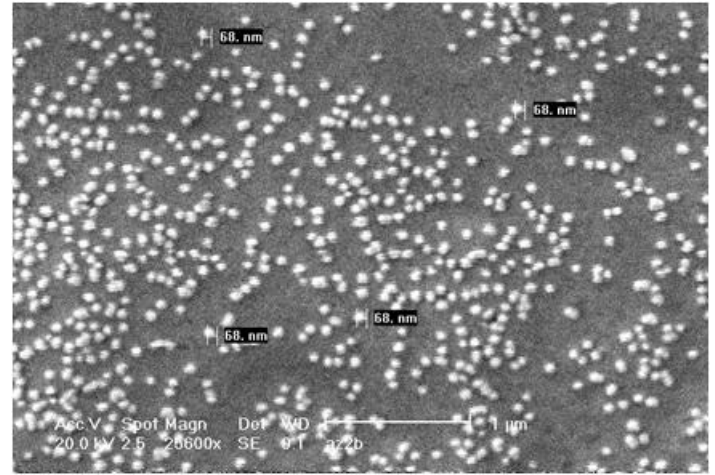
Table 4.3

Protein concentration for formation of nanoparticles:

Nanoparticles are prepared as described in Methodology 2.36. 100mM drug and the indicated protein concentrations are mixed and added in aliquots to the 15 ml olive oil and the mixture is sonicated at 5 amplitude and mixture is frozen and thawed, this is now centrifuged at 5000 rpm and the pellet is collected. The pellet is dispersed in PBS and particles were analyzed by the SEM (Method 2.38). The dimensions of the particle formed are given in the Table 4.3. Based on the SEM analysis (Figure 4.9) the optimum concentration required for the formation of the nanoparticles is 10 mg.

Table 4.3

Protein concentration for formation of Nanoparticles

Condition	Particle formation	Dimensions of the nanoparticles
1 mg	No particle formed	---
2.5 mg	No particle formed	---
5 mg	Yes	50 - 60 nm
10 mg	Yes	60 - 70 nm
15 mg	Yes	60 - 70 nm
20 mg	Yes	60 -70 nm
25 mg	Yes	60 - 70 nm
30 mg	Yes	60 - 70 nm
40 mg	Yes	200 - 400 nm

Figure 4.9:

 Protein concentration for formation of Nanoparticles

SEM images of the nanoparticles prepared at the respective protein concentrations 1-40 mg. Nanoparticles are prepared as described in the Methodology 2.36. 100mM drug and the indicated protein concentrations are mixed and added in aliquots to the 15 ml olive oil and the mixture is sonicated at 5 amplitude and mixture is frozen and thawed, this is now centrifuged at 5000 rpm and the pellet is collected. The pellet is dispersed in PBS and particles are analyzed by the SEM (Method 2.38). The dimensions of the particle formed are given in the Table 4.3. Based on the SEM analysis the optimum concentration required for the formation of the nanoparticles is 10 mg.

Figure 4.9
Protein concentration for formation of Nanoparticles

2.5 mg
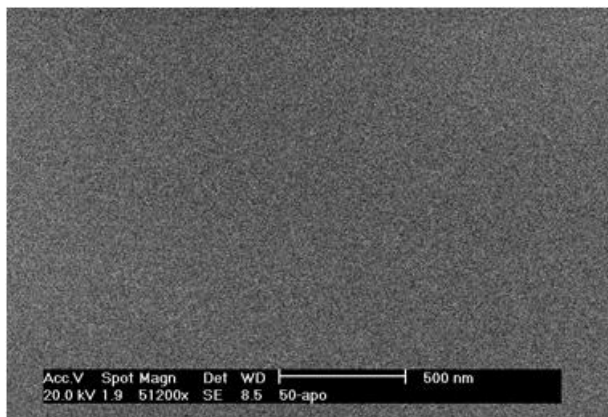
5 mg
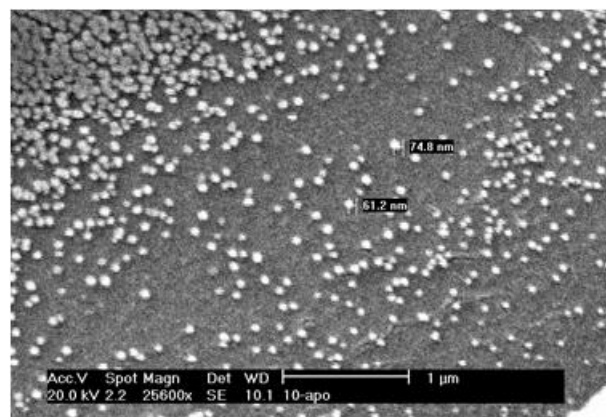
10 mg
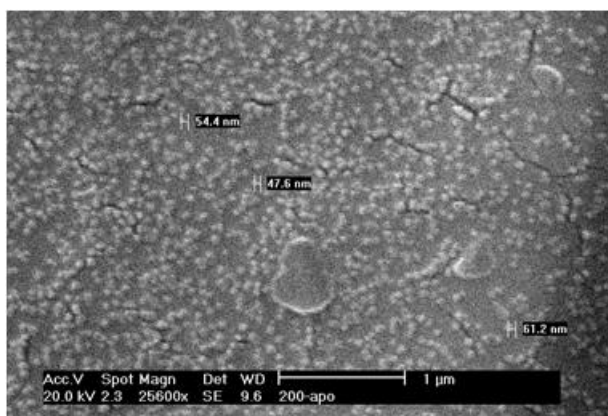
15 mg
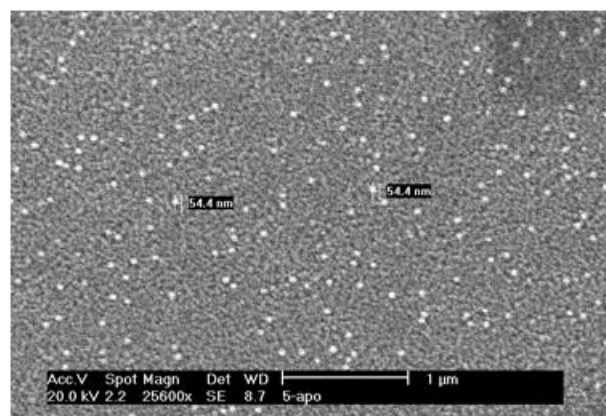
20 mg
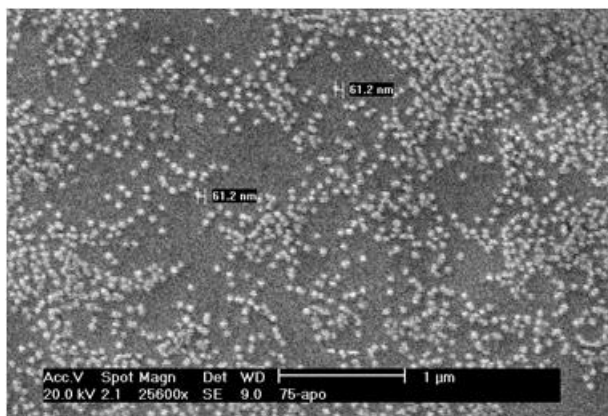
25 mg
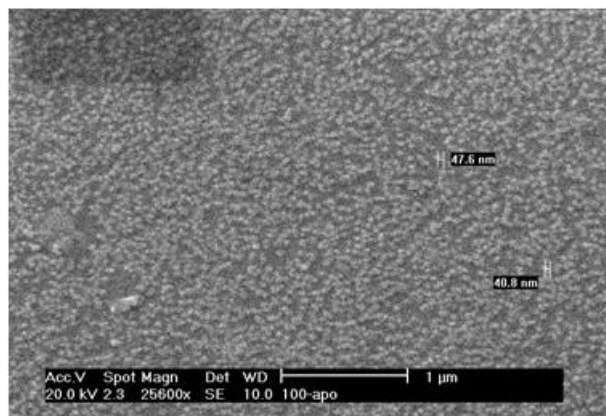
30 mg
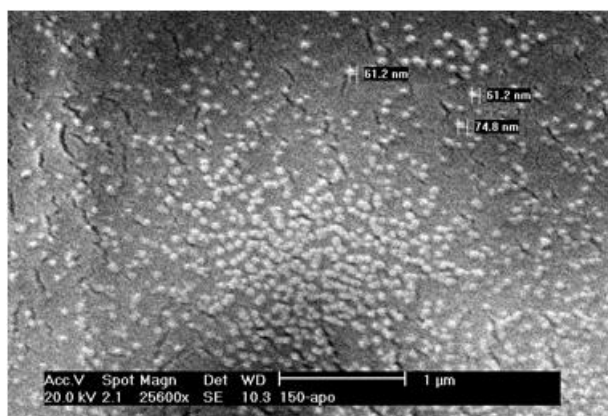
40 mg
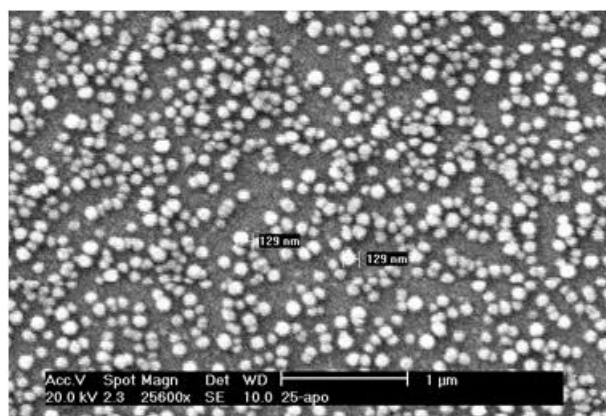
Figure 4.10

Chemical characteristics of Nanoparticles

20 mg doxorubicin loaded apotransferrin nanoparticles were treated with the indicated solvents/buffers and the amount of soluble drug release was quantified by measuring intrinsic fluorescence of doxorubicin at lambda emission 594 nm (lambda excitation 470 nm) by spectrofluorimeter (Fluoromax).

Bar 1: 100% alcohol, **Bar 2**: 100% DMSO, **Bar 3**: 1 N HCl in PBS, **Bar 4**: 1 N HNO_3 in PBS, **Bar 5**: 1 N H_2SO_4 in PBS, **Bar 6**: 1 N CH_3COOH in PBS, **Bar 7**: 1 N HCl in alcohol, **Bar 8**: 1 N CH_3COOH in alcohol.

Figure 4.10

Chemical characteristics of Nanoparticles
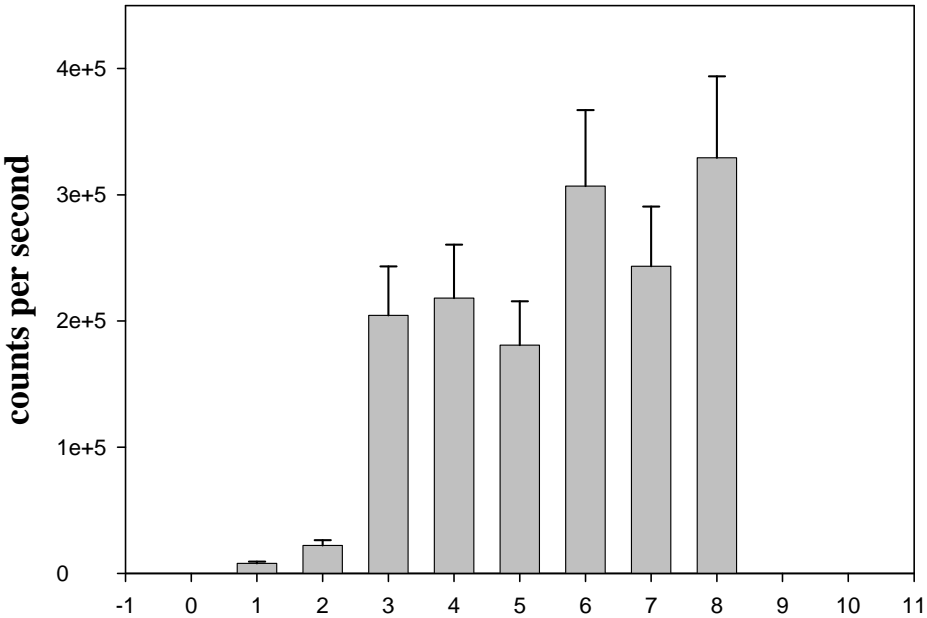
the particles was assessed by dot blot analysis. The results in Figure 4.11 show that the particles were immuno reactive to mouse anti human transferrin monoclonal antibody, suggesting that the apotransferrin retains its immunoreactive epitopes on the surface of the particle.

Stachiometry of protein and drug in the particles:-

Based on the spectroscopic estimation of drug and protein in the nanoparticles, It is estimated that 500 µg of doxorubicin is encapsulated per mg of apotransferrin.

A soluble doxorubicin (Fig 4.12) and azalactone ferrocene (Fig 4.13) show a characteristic absorbtion maxima at 490 nm for doxorubicin and 375 and 555 nm for azalactone ferrocene. When nanoparticles of these drugs were treated with acids, the spectrum of the drug shown in Fig 4.12 B and Fig 4.13B show similar absorption spectrum of soluble one showing that the drug remain unaltered upon nanoparticle preparation. Furthermore, the drug loaded in concentration dependant.

pH Dependent Drug Release, Spectrophotometric Analysis:

Apotransferrin nanoparticles were treated with a gradient of alcohol and DMSO in PBS/acidic buffers. The treated samples are centrifuged at 10,000 rpm for 15 minutes and the supernatant is analysed for the doxorubicin fluorescence, so that a very low levels of the doxorubicin can be monitored. The results (Figure 10) revealed that there is no significant increase in the fluorescence in presence of organic solvents indicating the particles do not have oil/liposomal nature and suggesting nanoparticles are made of protein, but when the particles are treated under low pH conditions, Where most of the protein denature under these conditions, the drug in the particles is leaked out, due to the change in the conformation of the protein in the particles. The drug released into the media was quantified by monitoring the fluorescence of media. The low pH buffer is prepared with four different acids, where the

Figure 4.11

Immuno reactivity of Apotransferrin in the Nanoparticles by Dot blot Assay

Apotransferrin nanoparticles and the soluble apotransferrin was spotted on nitrocellulose and dot blot was carried, soluble BSA protein and BSA loaded were used as negative controls

Panel A

1,2 : 40,80 µg of apotransferrin nanoparticles

3: Soluble 100 µg of apotransferrin (Positive control)

4: 100 µg of soluble serum protein (Positive control)

5: 100 µg soluble BSA protein (Negative control)

Panel B

1, 2: 80, 40 µg BSA nanoparticles

3, 4: 100 µg of apotransferrin soluble protein

5, 6, 7: 100, 50, 10 µg of soluble BSA protein alone (Negative control)

Figure 4.11

Immuno reactivity of Apotransferrin in the Nanoparticles by Dot blot Assay

Panel A
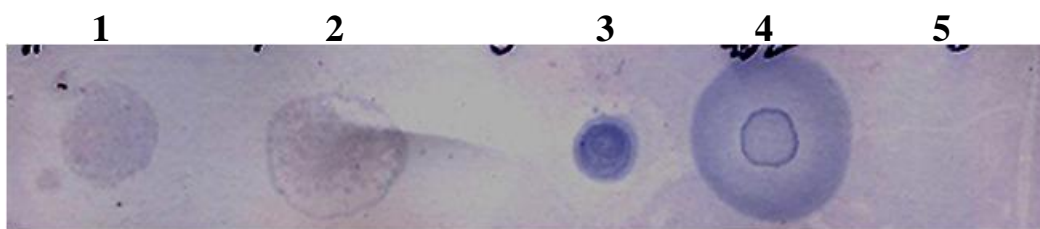
Panel B

drug release is observed in all conditions indicating the sensitivity to the change in the H$^+$ conditions.

5.12 Spectral analysis of drug when loaded into nanoparticles:

Azalactone ferrocene (375, 555 nm) / doxorubicin (490 nm) have a characteristic peak (Figure 4.12 A, 4.13 A). of visible spectra. When these molecules are loaded into nanoparticles and spectra is taken from 200-900 nm, under these conditions the nanoparticles containing doxorubicin show a characteristic spectrum with absorption maxima at (Figure 4.13 B, C, 4.14 B, C) at 280 nm indicating the presence of protein. Doxorubicin loaded nanoparticles 10, 100 mM drug show significant differences in intensities of the doxorubicin absorption peaks, with similar absorbance intensity at 280nm, of protein in the spectra indicate the equal loading of protein thus there is a 10 fold difference in drug loading in the nanoparticles. Hence the protein concentration remains constant for a protein condition to form nanoparticles, while amount of drug loaded dependant on its concentration.

Figure 4.12:

Differential loading of Doxorubicin (drug) in Apotransferrin Nanoparticles.

100 µl of 10/100 mM doxorubicin is added to 10 mg/ 100 µl of apotransferrin and mixed gently and nanoparticles are prepared as described in Chapter II . These nanoparticles are dispersed in dissolved in 5% HCl in ethanol and absorbance vs wavelength spectra is scanned from 200-900 nm. Soluble doxorubicin show four characteristic peaks 490,292,252,233 nm. Among these the peak, the visible range peak at 490 nm is taken as standard. The drug encapsulated nanoparticles are dispersed in PBS which show differential intensity of doxorubicin peaks are studied. While peak at 280 nm remain constant in intensity indicating the nanoparticles are differentially loaded with 10/100 mM doxorubicin. The blank line present at the bottom is the 5% HCl in ethanol blank

Panel A: Sample 1-5 soluble Doxorubicin in Tris buffer saline of concentration 10, 20, 30, 40, 50 µM respectively

Panel B: 100 mM doxorubicin loaded nanoparticles in presence of 5% HCl in ethanol,

Panel C: 10 mM doxorubicin loaded nanoparticles in presence of 5% HCl in ethanol

Figure 4.12

Differential loading of Doxorubicin (drug) in Apotransferrin Nanoparticles

Characteristic spectra of Doxorubicin

Panel A
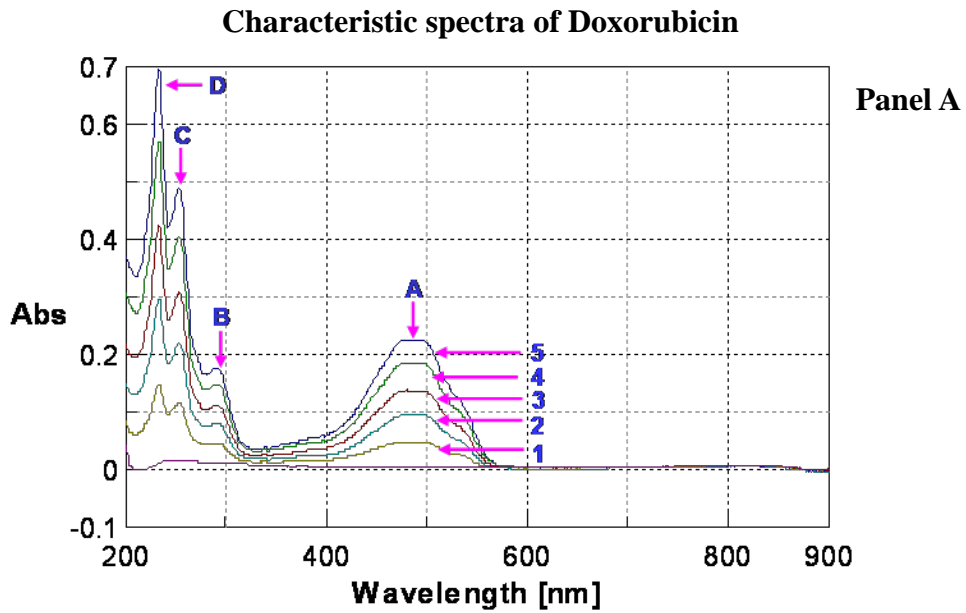
Doxorubicin 100 mM loaded Apotransferrin Nanoparticles

Panel B
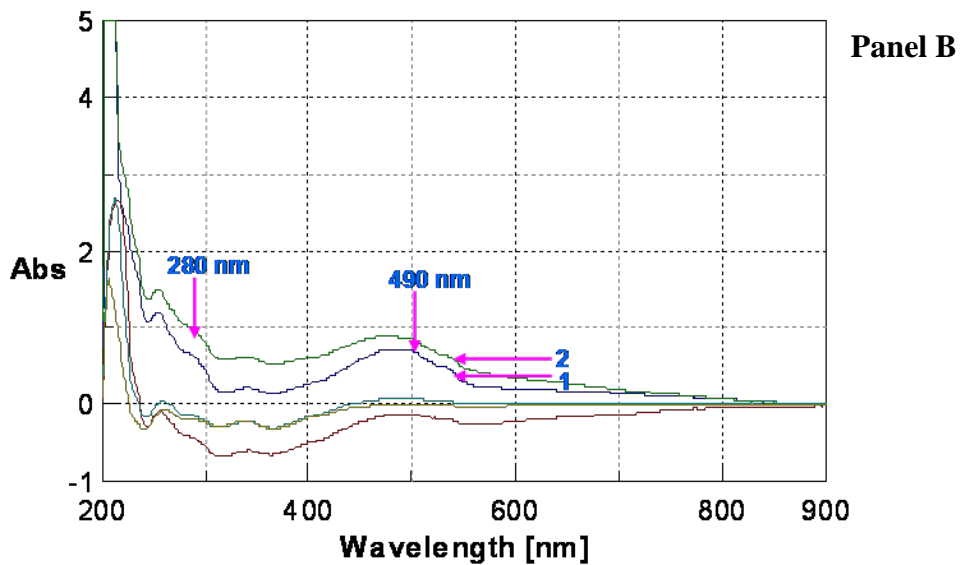
Doxorubicin 10 mM loaded Apotransferrin Nanoparticles

Panel C
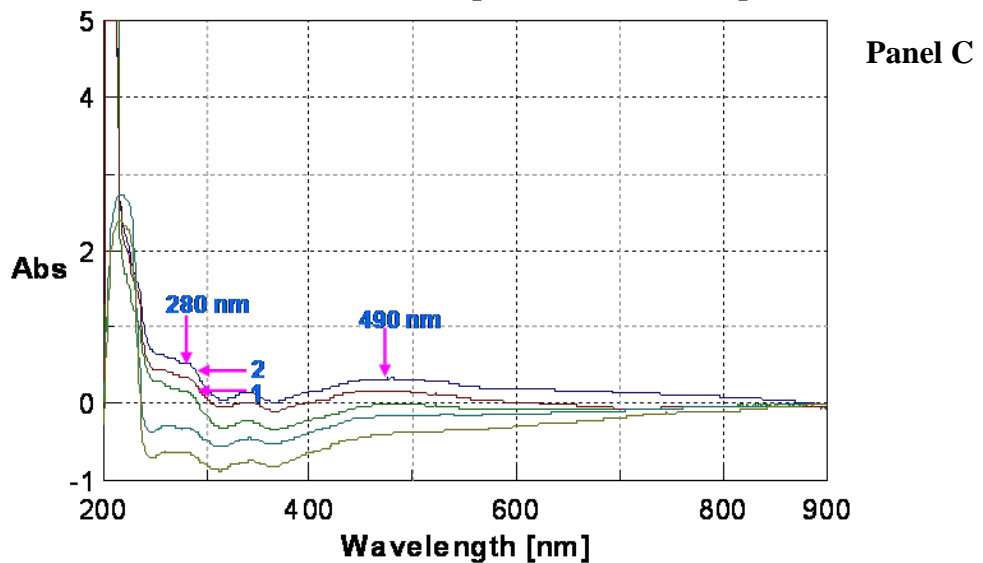
Figure 4.13:

Azalactone Ferrocene loading in the Apotransferrin Nanoparticles:

The characteristic peak of the azalactone ferrocene at 555 nm and 375 nm is taken as standard. Azalactone ferrocene is loaded in the apotransferrin nanoparticles is confirmed by the presence of peaks at 555 and 375 nm in 5% HCl in ethanol.

Legend:

Panel A: Azalactone ferrocene characteristic spectra in 5% HCl in ethanol, spectra is taken at concentrations1- 5; 20,40,60,80,100 μM concentration of soluble azalactone ferrocene.

Panel B: Azalactone ferrocene loaded apotransferrin nanoparticles spectra in presence of 5% HCl in ethanol.

Panel C: Enlarged spectra azalactone ferrocene loaded apotransferrin nanoparticles from 324 nm to 670 nm.

Figure 4.13

Azalactone ferrocene Loading in the Apotransferrin Nanoparticles

Panel A

Panel B

Panel C
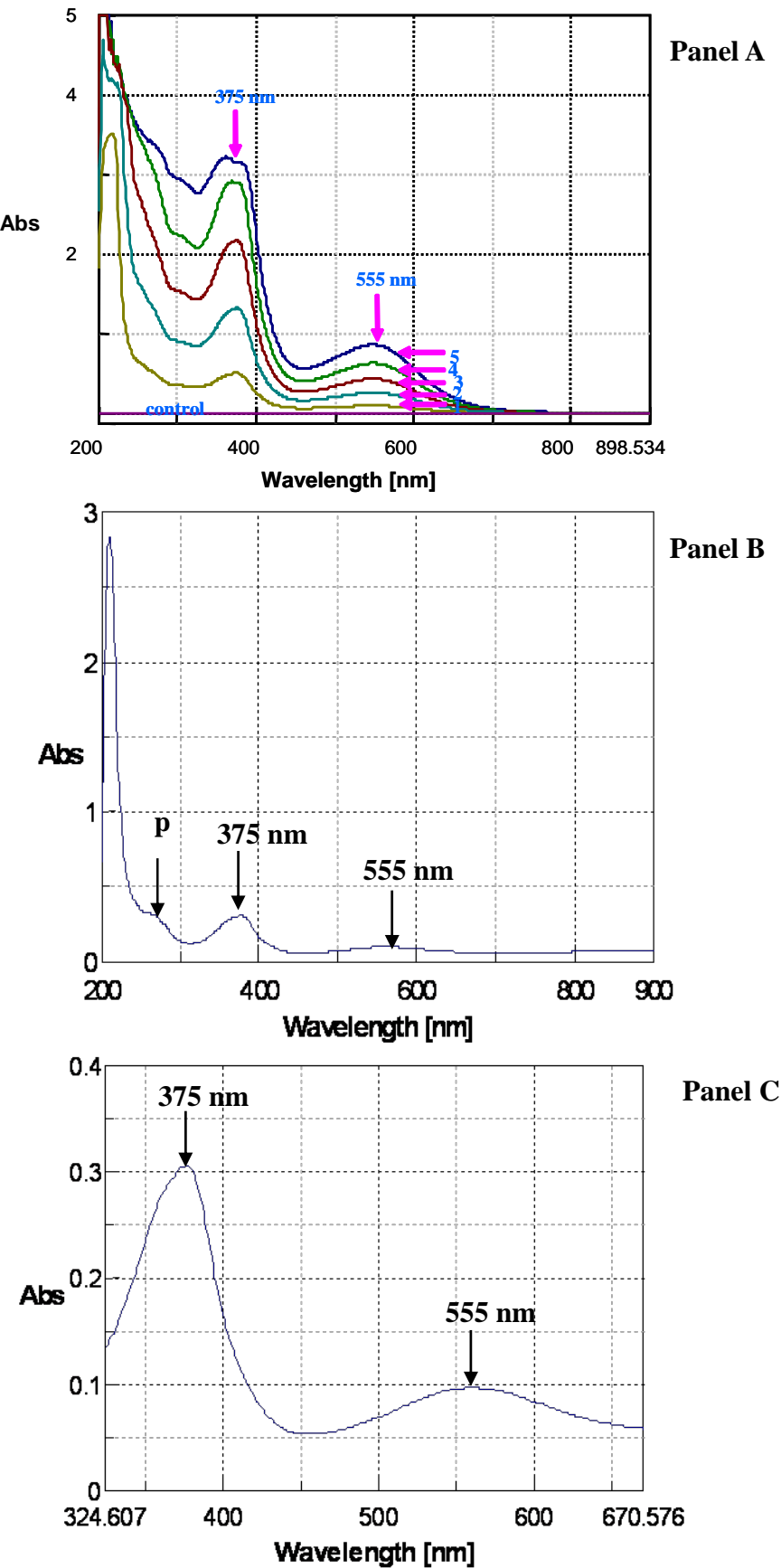
DISCUSSION

Polymers are excellent molecular systems that undergo phase separation under different solvent conditions. This property has been routinely used for separation, precipitation differential solubilisation of various polymeric substances. Based on these properties several research groups developed insoluble particulate matter composed of polymeric material made up of PLGA, PAA, chitin, BSA etc. Among such particulate forms are dendrimers and other molecular forms that could show particles of nano dimensions, which are referred as nanoparticles. In view of insoluble in nature these particles will be very stable and highly biocompatible. Further, due to nano dimension they exhibit negligible immunogenicity and can enter cells by diffusion. They attract wider application in delivery of various pharmaceutical agents. Though these are efficient in drug delivery but lack target specificity. It has been a practice to conjugate or coat such nanoparticles with a target specific ligand(s) such as apotransferrin and other such molecules. In this investigation, the results show that apotransferrin itself can be converted to nanoparticle. Apotransferrin nanoparticle can encapsulate the drug along with the protein. The morphological analysis of the particles using SEM, TEM and AFM (Figure 4.5, 4.6) show that these particles are of dimension below 100 nm and the surface of these particles is highly anisotropic. These anisotropic surface features indicate the possible exposure of epitopes of the protein on the surface, which is confirmed by the significant immunoreactivity of the particles to antihuman transferrin antibody (Figure 4.11). The recognition of the particle(s) is not due to the nonspecific binding of antibody as no such immune reactivity was observed with the BSA nanoparticles that were prepared under similar conditions.

These particles are indeed made of proteins, which are confirmed by their high sensitivity to the acidic pH and inert to the organic solvents (Figure 4.10), thus verifies any absence of any lipid layer on the particle surface for stabilization of particles, which is a novelty in these

98

particles. It is to be noted that in several nanoparticle preparations reported in the literature, additive like lipids, organic molecules, surfactants used to stabilize nanoparticles. While in the present study no additives were used and the particles were just made up of protein and the drug is encapsulated during the formation of nanoparticles

We hypothesize that drug is absorbed/adsorbed on to the protein. The drug absorption on to the protein is enhanced during partitioning of protein and drug complexes in oil phase. The partitioned protein-drug complexes undergo aggregation in oil phase leading to phase separation and induction of the formation of nanoparticles. These particles are size fractionated by the sonication. The aggregation of sized particles will be inhibited by freezing them in liquid nitrogen. These particles retain surface structural morphology of the protein that confers the recognition of cell surface receptor and biological activity. The absence of immune reactivity in BSA nanoparticles could be due to the inability of their recognition as they do not possess the structural motifs that are normally present in natural ligand apotransferrin.

In conclusion, the methodology used in this thesis could make particles of apotransferrin in nano dimensions. The particles can encapudate any drug during the preparation; hence this particle will become potential delivery vehicle for the drugs to the various cells, specifically to cancer cells.

CHAPTER V

Evaluation of efficacy of potent molecules in rat ascetic hepatocellular carcinoma

Nanoparticles are best characterized by their low immunogenicity and higher penetration into the cells through simple nonspecific diffusion or other mechanisms of active and passive transport. The results in chapter IV shows the formation of drug loaded nanoparticles. The present chapter aims at evaluation of the mechanism of cellular drug delivery of these nanoparticles and biological activity of the drug *in vitro* and *in vivo*. These studies were performed in cancer cell lines, SUP-T1, COLO-205, SK-N-SH and rat hepatocellular carcinoma model.

Cellular Localization of nanoparticles:

The results of these experiments show that the fluorescently labeled apotransferrin nanoparticles are found localized in cell membrane and were concentrated at some membrane locations, probably in the extra cellular space (shown by arrows Figure 5.1A). Whereas fluorescently labeled BSA nanoparticles, did not enter in the cells suggesting that the receptor binding is essential for the entry of the particles (Figure 5.1 B).

Receptor Mediates Transport of Nanoparticles:

The entry of drug loaded apotransferrin nanoparticles through transferrin receptor was assessed by competition experiments of cellular localization conducted using RITC labeled apotransferrin nanoparticles in the presence of increasing concentrations of unlabelled soluble apotransferrin. The results of these studies (Figure 5.2) showed that increasing concentrations of soluble apotransferrin compete out the fluorescently labeled apotransferrin nanoparticles, thus pointing out that the nanoparticles enter the cells by transferrin receptor mediated transport. The surface structural anisotropy of particles observed by AFM (Figure 4.6) may indeed contribute towards retaining the structural motifs required for recognition and binding to transferrin receptor. The inhibitory action of soluble apotransferrin at its high concentrations on the entry of nanoparticles suggests that they

Figure 5.1:

Cellular Localization of the Nanoparticles

SUP-T1 cells were incubated in serum free medium for 30 minutes. In the presence of RITC conjugated apotransferrin/BSA nanoparticles. The cells were washed extensively with serum free medium and washed thrice with PBS. The cells were observed in laser confocal microscopy using oil immersion objective. Panel A depicts localization of RITC apotransferrin particles in SUP-T1 cells. The arrow indicates the intense fluorescence localization of RITC conjugated apotransferrin in cells. A similar experiment was is carried out with RITC conjugated BSA and results are shown in panel B showing that BSA could not enter into cells.

Panel A: RITC labeled apotransferrin nanoparticles treated cells fluorescence and overlaid image

Panel B: RITC labeled BSA nanoparticles treated cells fluorescence and overlaid image

Figure 5.1

Cellular localization of the nanoparticles

Panel A

Fluorescence of apotransferrin nanoparticle localization in cell
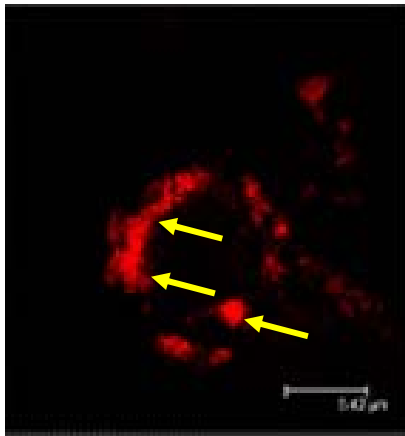
Fluorescence and phase images Over laid image
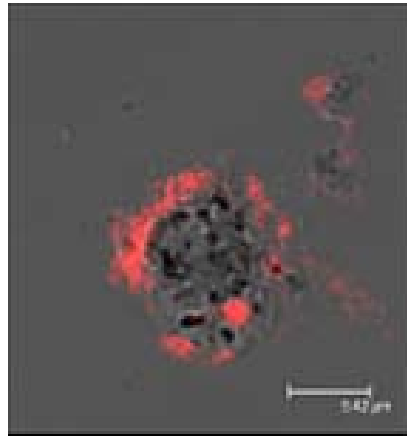
Panel B

Fluorescence of BSA nanoparticle localization in cell
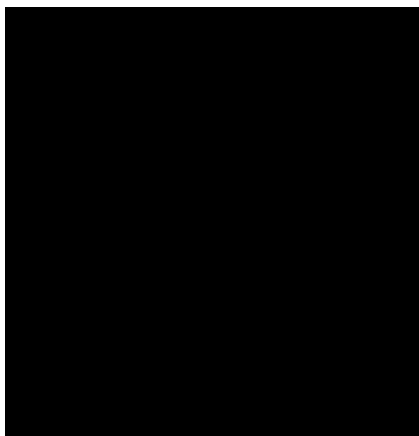
Fluorescence and phase images Over laid image
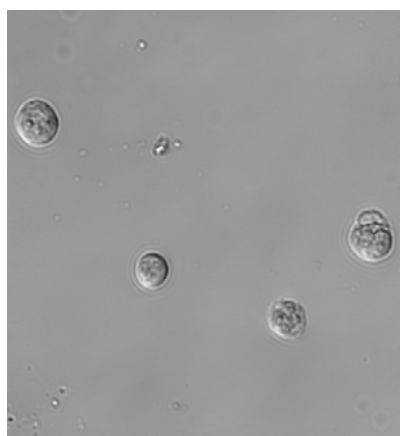
Figure 5.2:

Competition of Apotransferrin Nanoparticles with soluble Apotransferrin

SUP-T1cells were incubated with RITC conjugated apotransferrin in the presence of increasing concentrations of soluble apotransferrin. The cells were sorted using flow cytometer and the percentage of fluorescently labeled cells were plotted against amount of soluble apotransferrin.

Apotransferrin nanoparticles are able to compete with soluble apotransferrin and fluorescence of the cells decreased with increasing soluble apotransferrin, while cells treated with soluble doxorubicin, fluorescence of cells remain unchanged with increasing concentrations of soluble apotransferrin. These results suggest that the nanoparticles have apotransferrin on the surface which mediates the receptor mediated entry/endocytosis. In the presence of soluble apotransferrin competition for binding to transferrin receptor is enhanced and fluorescence of nanoparticles in cells decreased with increasing soluble unlabelled apotransferrin

Figure 5.2

Competition of Apotransferrin Nanoparticles with soluble Apotransferrin
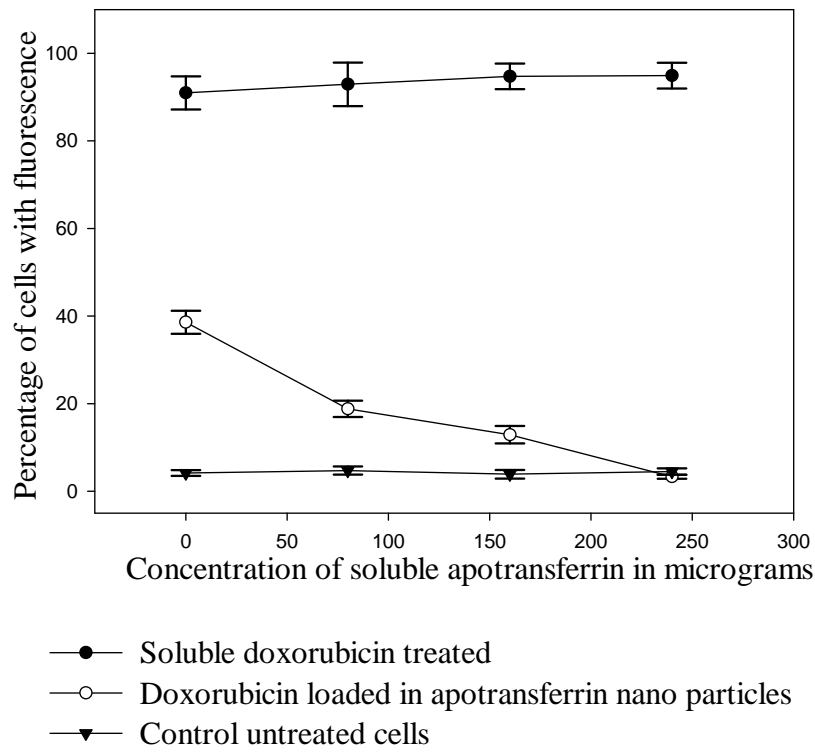
follow equilibrium binding and the nanoparticles enter the cells through equilibrium kinetics. Furthermore, the particles may not induce an iron deficiency state in the host unlike that observed in the case of irreversible binding transferrin mediated drug delivery systems (228).Since the fluorescence is not traceable in the cytosol, it may be inferred that the nanoparticle may be internalized through receptor and has migrated to the extra cellular spaces, from where it may be releasing drug through two alternative pathways viz., (I) the particles may be transported to an endosome vesicle that was still in fusion with the plasma membrane. That the drug may have been released from the particle from the membrane fused endosomal vesicle, which is leaked to the cytosol, while the protein in nanoparticle remained secreted/exocytosed or (ii) the particles enter through transferrin receptor and may remain in extra cellular spaces, where the conformational changes of apotransferrin in the nanoparticles may solublize protein leading to the release of drug into the cytosol and the protein is secreted out.

Localization of drug through apotransferrin mediated drug delivery:

To study the release of drug loaded in the nanoparticles, we monitored the intrinsic fluorescence of doxorubicin. The cytosol and nuclei are found to be highly localized with Doxorubicin (Figure 5.3) suggesting that while releasing the drug into the cytosol, the apotransferrin in nanoparticles remain in the cell membrane, and later secreted out after releasing the drug.

Delivery of drug localization in nanoparticles:

Doxorubicin was used for these studies. Intrinsic fluorescence of doxorubicin was monitored. Apotransferrin nanoparticles were loaded with doxorubicin (Apo-Doxo) SupT-1 cells were incubated with apo-doxo nanoparticles, the entry of drug localization was monitored by laser confocal microscopy. The results in Figure 5.3 show the localization of

Figure 5.3 :

Confocal Microscopy analysis of Nanoparticle Localization

SUP-T1 cells were incubated in the presence of 20 mg protein equivalent of indicated samples for a period of 30 min, 60 min, 16 hours and the cells were washed and the fluorescence localization in cells by using laser confocal microscopy (Leica). The reproducibility of the results was verified through three independent experiments.

Legends: C1: RITC conjugated apotransferrin nanoparticles; C2: RITC conjugated soluble apotransferrin, C3: Doxorubicin loaded nanoparticles; C4: Soluble doxorubicin and apotransferrin; C5 Soluble doxorubicin; C6: Soluble RITC; C7: Untreated cells

Figure 5.3

Confocal microscopy analysis of Nanoparticle Localization

Panel A

	C1	C2	C3	C4	
	A	D	G	J	30 min
	B	E	H	K	60 min
	C	F	I	L	16 hrs

Panel B

	C5	C6	C7
30 min	M	P	S
60 min	N	Q	T
16 hrs	O	R	
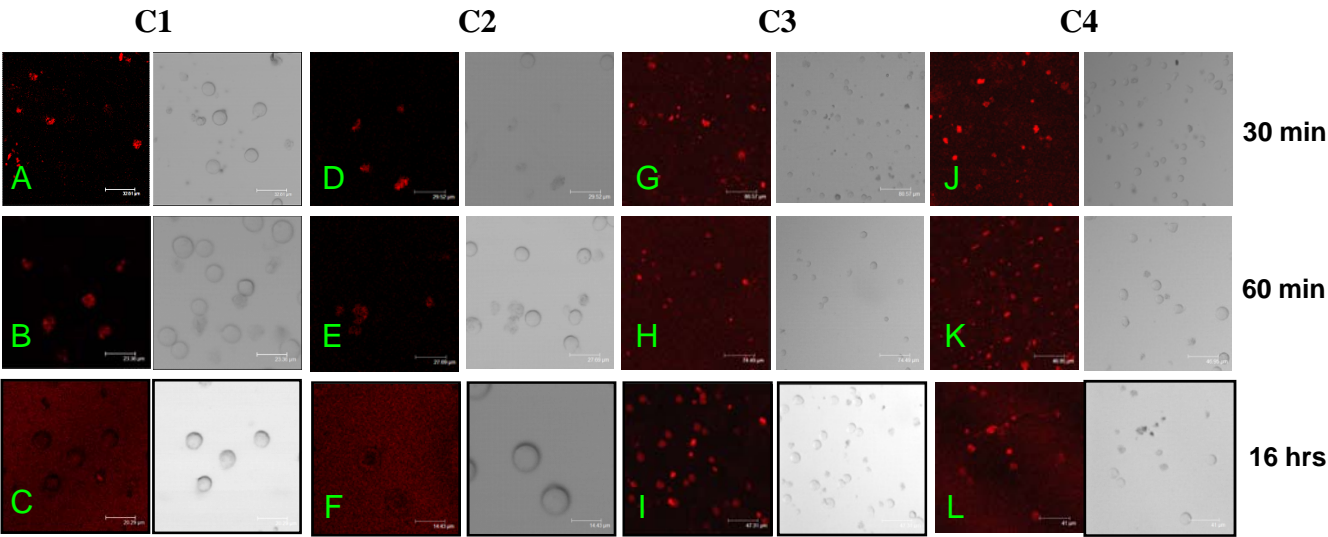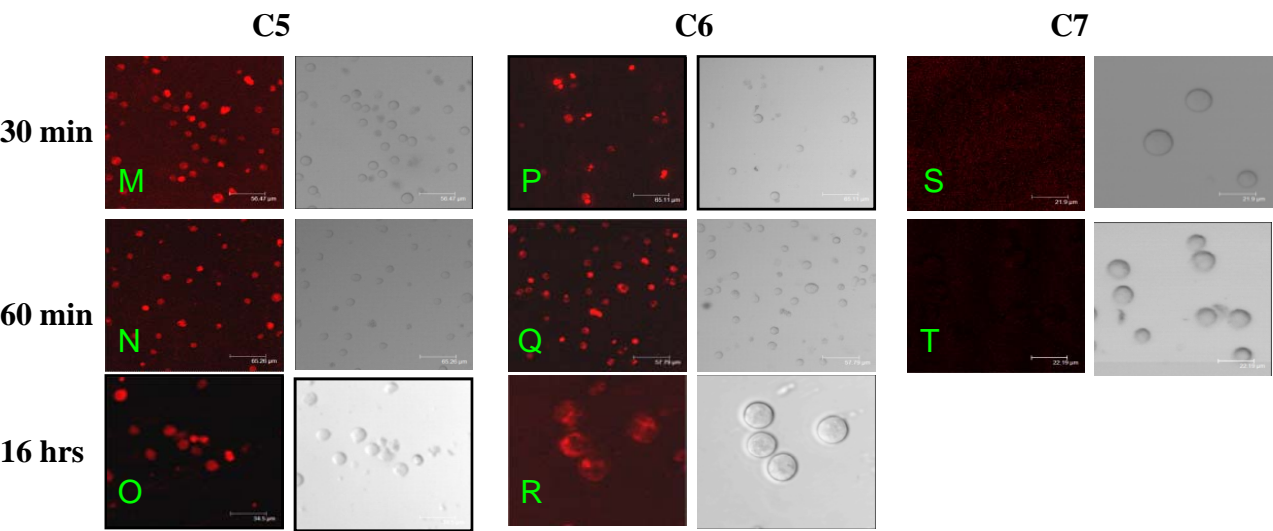
doxorubicin in cytosol and nuclei. These results suggest that the protein nanoparticles secreted in extracellular spaces, while the doxorubicin the drug into the cells.

5.17 Cellular recycling of Apotransferrin Protein present in Nanoparticles:-

The possible mechanism of exocytosis or secretion of the protein in the particles and release of drug into the cell was monitored by nanoparticle recycling assay. Nanoparticles made of RITC conjugated apotransferrin is used in the study. The cells were incubated with nanoparticles followed by monitoring of cellular fluorescence using flowcytometer analysis over a period of 4 hours. The results presented in Figure 5.4 show that the fluorescent labeled cells increases over a period of 30 minutes, then show a decrease in number of fluorescent cells reaching a minimum at 4 hours. Thus suggesting that RITC conjugated apotransferrin nanoparticles enter the cells and reach their saturation at 30 minutes followed by the secretion of protein over a period of four hours (229). A similar mechanism has been reported for apotransferrin mediated iron transport (229), the main difference being the apotransferrin enter the endosome for the release of iron in case of nanoparticle the protein in the nanoparticle is remained in the extracellular space while releasing the drug into the cytosol.

To know whether the protein in nanoparticles is secreted out after release of drug, intrinsic fluorescence of doxorubicin in the unlabelled apotransferrin nanoparticles was studied . Cells were incubated in the presence of apotransferrin doxorubicin nanoparticles and the cells localized with doxorubicin were monitored over a period of 4 hours. The results (Figure 5.5-5.6) show that majority of cell population were localized with doxorubicin intrinsic fluorescence reaching a maximum at 30 min, and remained at this level indicating that the fluorescent labeled cells reached saturation with their number remaining stable over a period of 4 hours, suggesting that the drug was indeed released into the cells. The biphasic

Figure 5.4

Cellular Recycle of Apotransferrin protein present in Nanoparticles

Experiments were conducted using RITC conjugated apotransferrin. The cells were incubated with indicated molecules in serum free medium for an indicated time. The number of fluorescently labeled cells were counted by FACS analysis (BD biosciences).

Legend: cells treated with A) no treatment , B) 80 ng of RITC labeled apotransferrin nanoparticles, C) 800 ng of RITC labeled apotransferrin nanoparticles, D) 80 ng of RITC labeled soluble apotransferrin treated cells, E) RITC soluble alone treated cells.

Figure 5.4

Cellular Recycle of apotransferrin protein present in nanoparticles

A	B	C	D	E	
					Control
					30 min
					60 min
					90 min
					2 hour
					3 hour
					4 hour
					16 hour
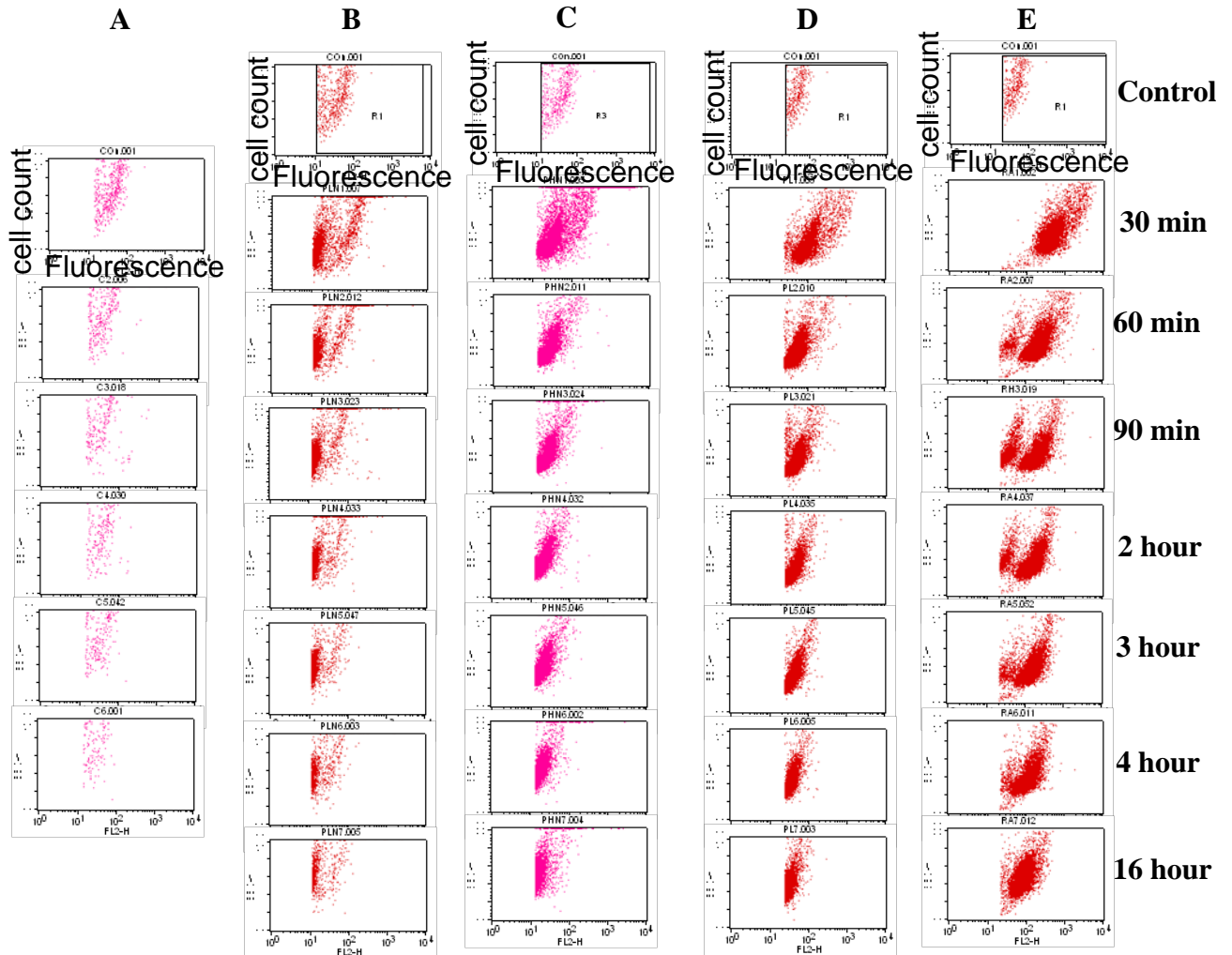
Figure 5.5:

Cellular Recycle of Apotransferrin protein present in Nanoparticles

Experiments were conducted with apotransferrin with doxorubicin (intrinsic fluorescence of doxorubicin is followed). **(A-F)** explains drug entry and drug localization in the cells. The cells were incubated in serum free medium for an indicated time the number of fluorescently labeled cells were counted by FACS analysis (BD biosciences).

Legends: A) untreated control cells ,B) 80 ng of apotransferrin-20 ng of doxorubicin nanoparticles, C) 800 ng of apotransferrin-200 ng of doxorubicin nanoparticles, D) 200 ng of doxorubicin alone treated, E) 80 ng of soluble apotransferrin-20 ng of doxorubicin soluble, F) 800 ng of soluble apotransferrin-200 ng of doxorubicin.

Figure 5.5

Cellular Recycle of Apotransferrin protein present in Nanoparticles
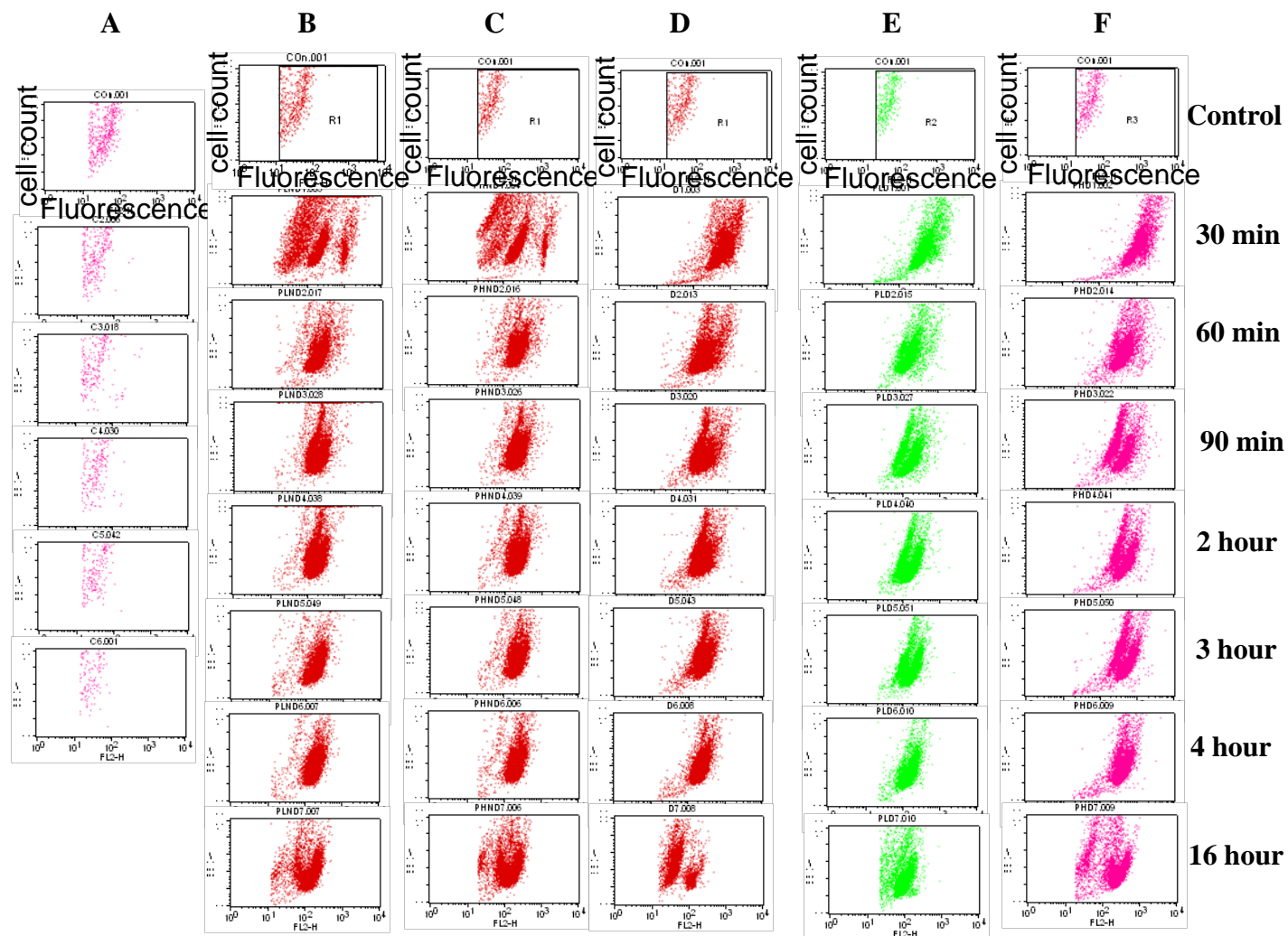
Figure 5.6:

Cellular Recycle of Apotransferrin protein present in Nanoparticles

The results in Fig 5.4 and 5.5 were replotted with % cells with fluorescence

Legends: cells treated with

      # 1: 80 ng of RITC labeled apotransferrin nanoparticles

      # 2: 800 ng of RITC labeled apotransferrin nanoparticles

      # 3: 80 ng of apotransferrin-20 ng of doxorubicin nanoparticles

      # 4: 800 ng of apotransferrin-200 ng of doxorubicin nanoparticles

      # 5: 200 ng of doxorubicin alone treated

      # 6: 80 ng of RITC labeled soluble apotransferrin treated cells

      # 7: 800 ng of RITC labeled soluble apotransferrin treated cells

      # 8: 80 ng of soluble apotransferrin-20 ng of doxorubicin

      # 9: 800 ng of soluble apotransferrin-200 ng of doxorubicin

      # 10: RITC soluble alone treated cells

Figure 5.6

Cellular Recycle of Apotransferrin protein present in Nanoparticles
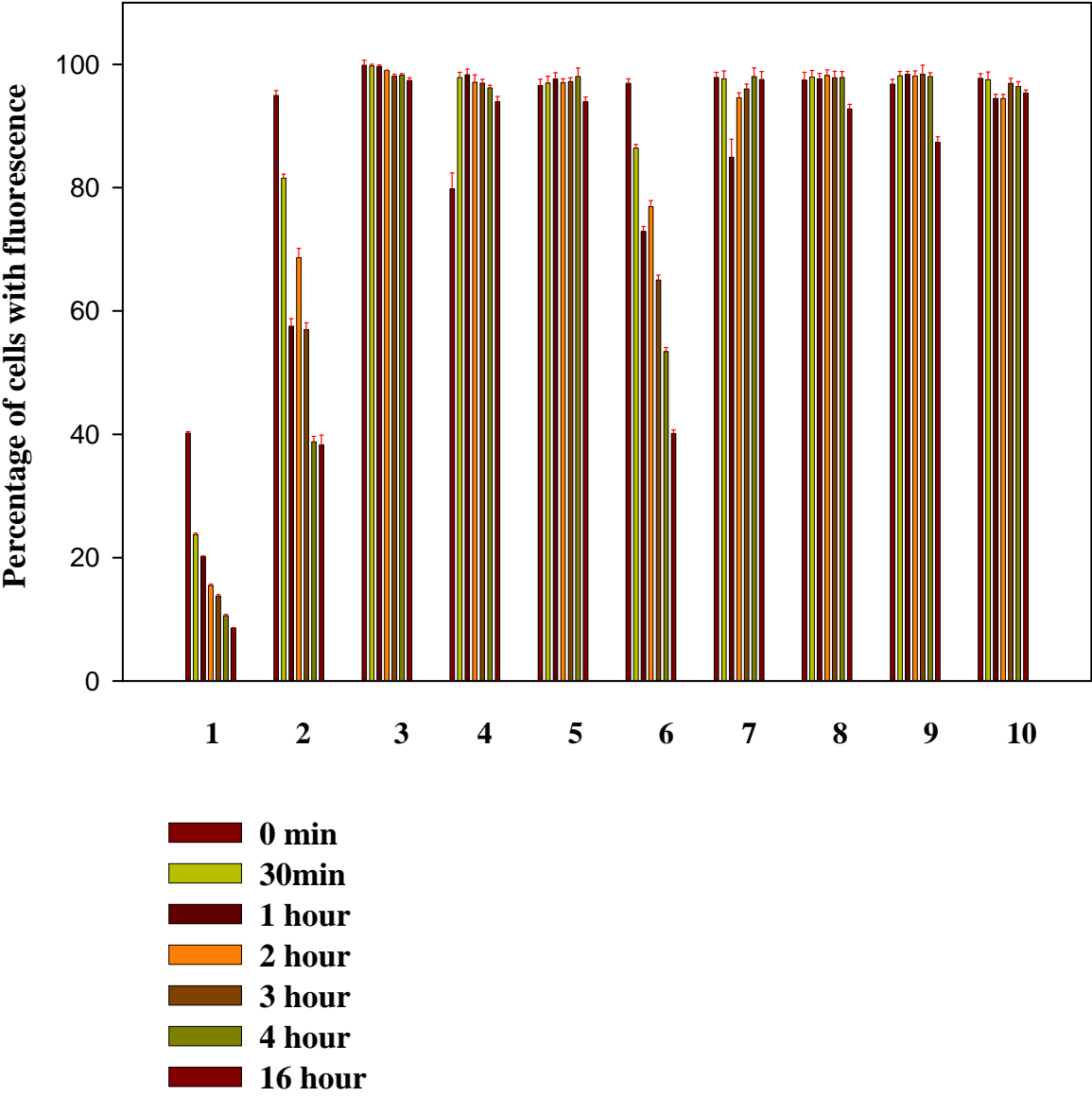
pattern of cell population observed at initial time points may be interpreted to be due to the presence of two different populations of cells characterized by differences in the rate of particle binding and internalization. This is supported by similar observations of biphasic population of cells in RITC conjugated nanoparticles as seen in Figure 5.5. These results demonstrate that apotransferrin in nanoparticles is secreted out after delivery of drug into the cytosol.

Bioactivity of nanoparticles: was studied using two independent assays. (1) Drug induced cytotoxicity in cultured cells by MTT assay and (2) regression of hepatoma in rat cancer model.

Antiproliferative activity of Apotransferrin-drug Nanoparticles:

The bioactivity of drug in apotransferrin-drug nanoparticle loaded with drug (nanodrug) was monitored by analysis of its action on the proliferation of T cell lymphoma (SUP-T1), neuroblastoma (SK-N-SH) and colon cancer (COLO-205) cell lines. The cells were cultured in presence of increasing concentrations of nanodrug for 16 hours and the cell viability was measured by MTT assay. The results (Figure 5.7) show that compared to soluble form of drug, nanoparticles of apotransferrin-doxorubicin can significantly inhibit the proliferation of these cell lines. Similar results were also obtained with apotransferrin-azalactone nanoparticles (Figure 5.7).

Evaluation of Nanoparticles in Rat Ascetic Hepatocellular Carcinoma Model:

Ascetic hepatocellular carcinoma was induced in a group of rats by administration of ZH5 cells intraperitoneally (zero days). This model induces ascetic cancer instantly that reaches a stage of metastasis and progresses to full blown stage in 4 days (Figure 5.8) and then the rat can survive only for seven days (Figure 5.8). The treatment was carried out by administering the protein-drug nanoparticles one dose per day from the 1st day of hepatoma

Figure 5.7:

Antiproliferation activity of drug loaded in Apotransferrin Nanoparticles

Cells were incubated for 16 hours in the presence of increasing concentration of nanodrug. The viable cells were quantified by MTT assay. O.D values in the absence of test samples was taken as 100% viable. The percentage inhibition of cell viability is estimated with reference to that in the absence of drug. Percentage viability is plotted against the concentration of drug in micrograms. Each data point is an average of three independent elutes. Standard deviations shown as error bars.

Figure 5.7

Antiproliferation activity of drug loaded in Apotransferrin Nanoparticles
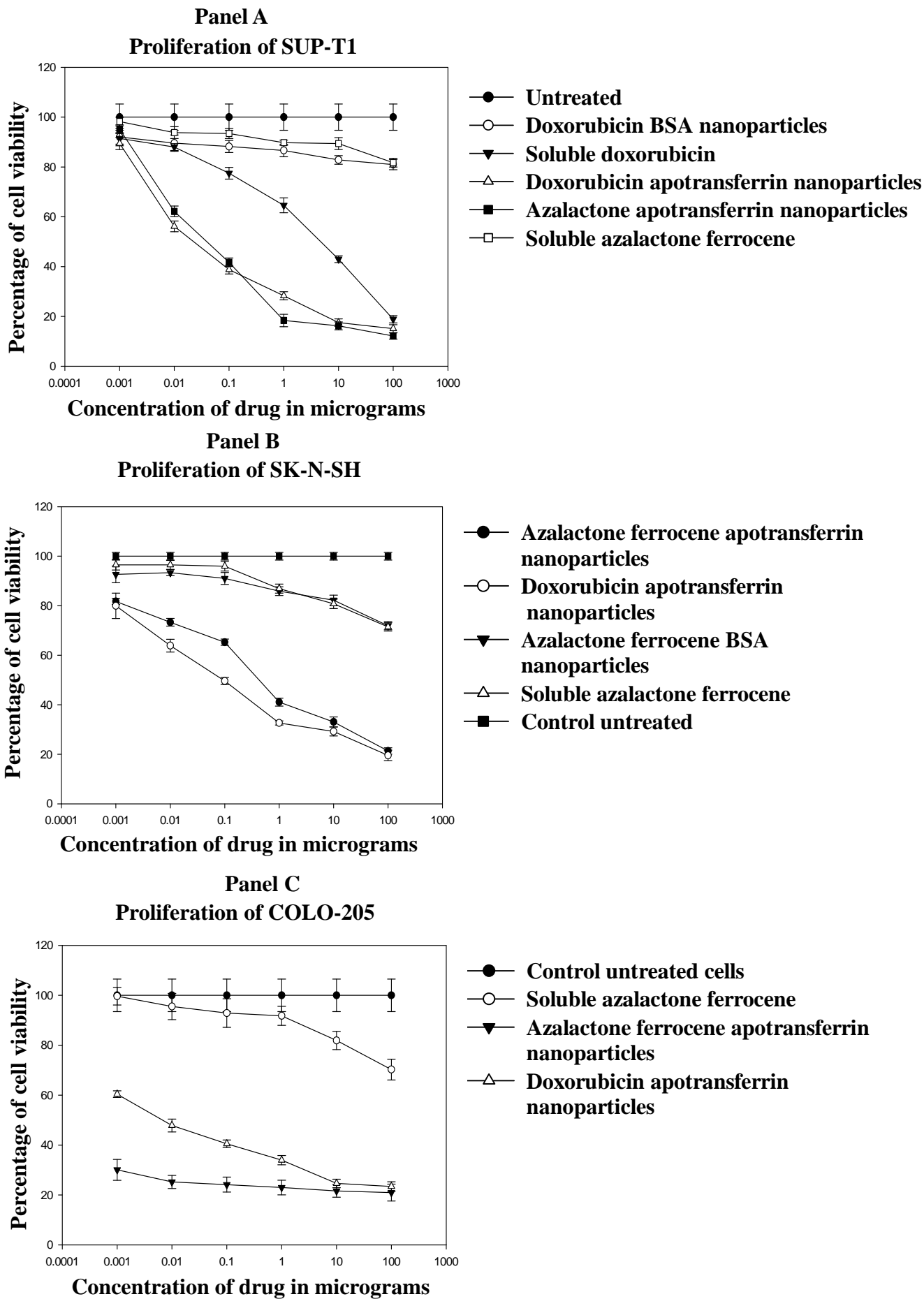
Figure 5.8:

Hepatocellular carcinoma induced Wistar rat Model generation

Rats aged 2 months were used for these studies 100 million cells per 0.5 ml cells were injected into intraperitoneal cavity of the rat on day zero. The induction of cancer was monitored by increase in volume of peritoneal cavity. Due to the multiple metastasis induced by the hepatocellular carcinoma the rats die on day 7.

Figure 5.8

**Hepatocellular carcinoma induced Wistar rat
Model generation**

1 day   2 day   3 day   4 day

5 day   6 day   7 day

DEAD

Figure 5.9

Treatment of Hepatocellular carcinoma with Azalactone ferrocene Apotransferrin Nanoparticle

Rats aged 2 months were used for these studies 100 million cells per 0.5 ml were injected into intraperitoneal cavity of the rat on day zero. Rats are photographed at the 1-72 days after injection of the 0.5 million ZH5 cells and treated with the azalactone ferrocene loaded apotransferrin nanoparticles and progression of the hepatoma is observed. In the figure rats are shown at different days of treatment. The various control rat as mentioned in the legends. Pictures showing on the corresponding days are collected. The control rat which is injected and untreated is dead on the 7th day. The nano delivery treated rat does not show any induction and was active. The azalactone ferrocene treated rat is further observed for 53 weeks.

Figure 5.9

Treatment of Hepatocellular carcinoma with Azalactone ferrocene Apotransferrin Nanoparticle
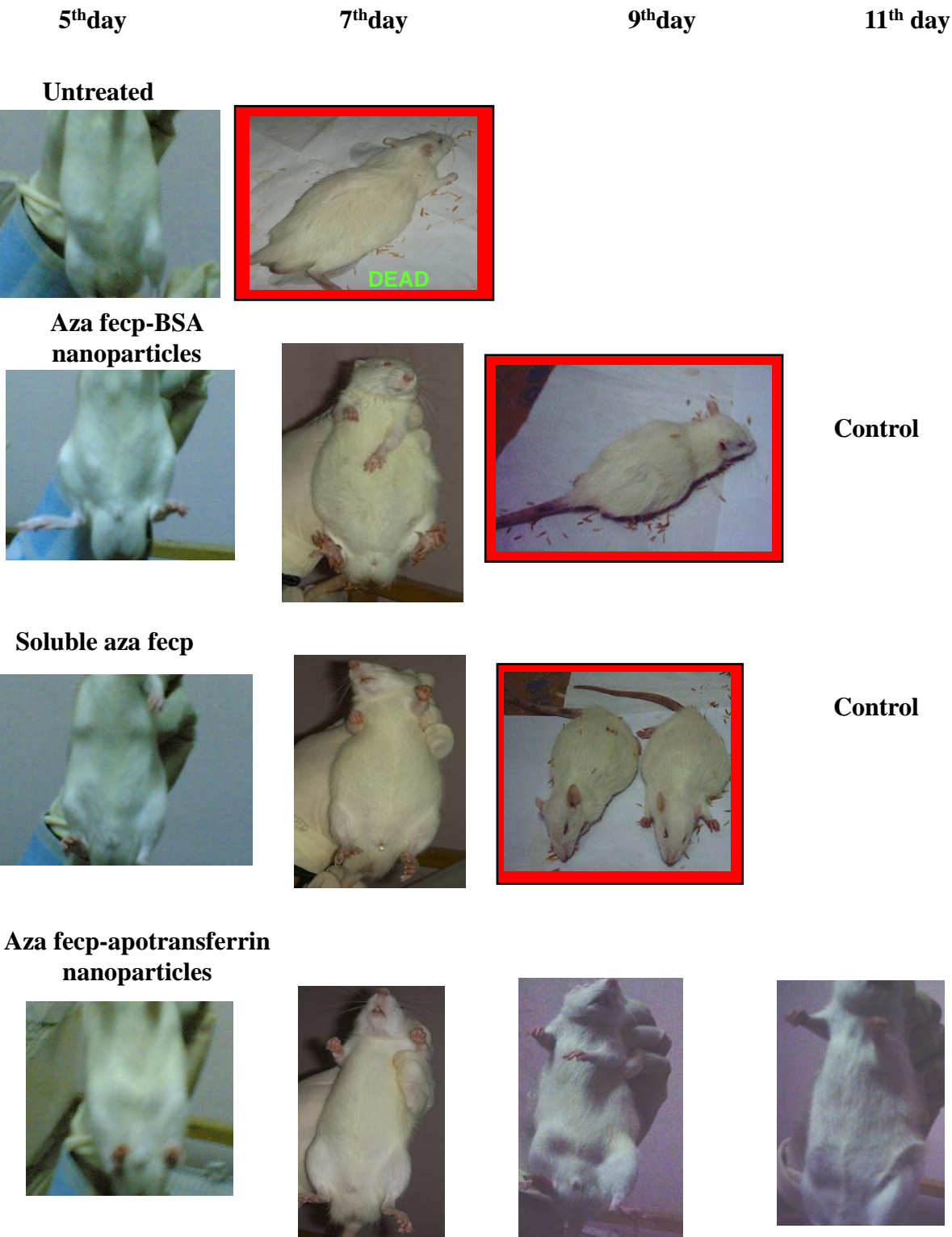
Figure 5.9 contd

Treatment of Hepatocellular carcinoma with Azalactone ferrocene Apotransferrin Nanoparticle

Azalactone ferrocene loaded nanoparticle treated rat observed at the corresponding day showing There is no significant change metabolic activity and the external volume of the peritoneal region of the rat indicating the regression of the cancer in dosage of the drug loaded apotransferrin nanoparticles. The experiment is done in the group of six rats, and the statistical value are given in the Table 5.1 .

Row 1: Untreated rat

Row 2: Azalactone ferrocene loaded BSA nanoparticles treated rat

Row 3: Soluble azalactone ferrocene treated rat

Row 4: Azalactone ferrocene loaded apotransferrin nanoparticles treated rat

Figure 5. 9 (contd)

Treatment of hepatocellular carcinoma with Azalactone ferrocene apotransferrin nanoparticle

| 16 day | 19 day | 21 day | 25 day | 27 day | 30 day |

| 49 day | 64 day | 73 day | 77 day |

Figure 5.10

Doxorubicin - Apotransferrin Nanoparticles treated rat

Rat are photographed at the 1-35 days after injection of the 0.5 million ZH5 cells and treated with the doxorubicin loaded apotransferrin nanoparticles and progression of the hepatoma is observed. In the figures rats are shown at different days of treatment. There is no significant change metabolic activity and the external volume of the peritoneal region of the rat indicating the regression of the cancer in dosage of the drug loaded apotransferrin nanoparticles. The experiment is done in the group of six rats and the statistical value are given in the Table 5.1 .

Figure 5.10

Doxorubicin - Apotransferrin Nanoparticles treated rat

1 day   2 day   3 day   4 day

9 day   10 day   13 day   35 day

Figure 5.11

A comparision of treated and untreated rat

Rats treated with azalactone ferrocene loaded apotransferrin nanoparticles was presented as comparative

       Panel A: Untreated rat

       Panel B: Treated rat

       Panel C: Comparsion of treated and untreated rats

Figure 5.11

A Comparison of Treated and Untreated rat

A   B
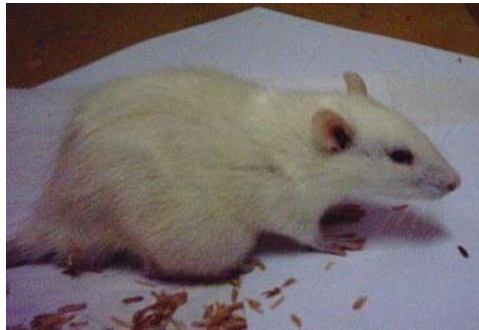
Nano treated rat   Untreated rat

C
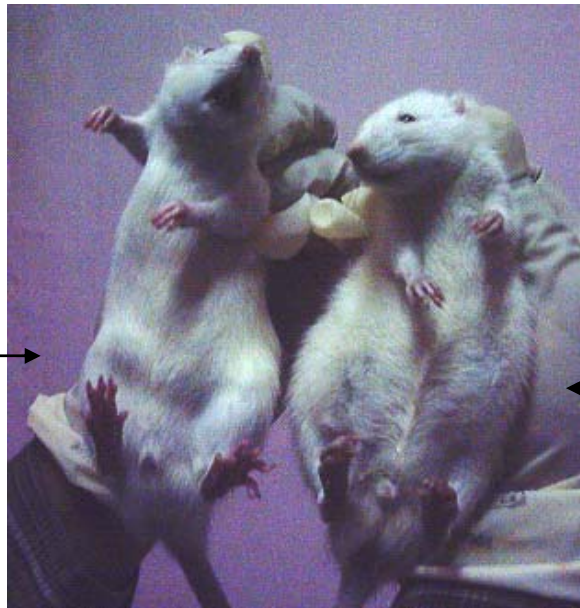
Azalactone ferrocene
loaded Nanoparticles
treated rat

Untreated rat

induction (Figure 5.9 -5.11). The progression of cancer was monitored by 1) survival time, and levels of 2) Alkaline phosphatase, 3) Lactate dehydrogenase, 4) urea, 5) creatinine, 6) α-feto protein, as given in Table 5.1 Figure 5.14. The liver sections were histochemically stained with Haematoxylin and Eosin and are shown in Figure 5.15. The results show a very significant regression of cancer in nano drug treated rats compared to those treated with soluble drug. The statistical significance of cancer regression in groups was analysed by ANOVA analysis and Tukey's Honestly significant difference (HSD) test (Appendix 2). The results showed that the differences of means among the groups are significant with a probability of above 95%. Furthermore treatment of full blown rats from 5th day of the injection of hepatocellular carcinoma showed very significant regression in cancer with survivability over 150 days for 4 rats in a group of rats (Figure 5.12)

Since serum alkaline phosphatase plays a significant role in tissue and cellular damage, and also since it is one of the important indicators that represent hepatocellular carcinoma progression, we have monitored its levels in untreated and treated rats. The results (Table 5.1) show that the levels of alkaline phosphatase in nanoparticle treated rats amounts to 60.49 ± 0.81 IU/L which comes to close to that for healthy ones, over 57.02 ± 0.04 IU/L (Tukey HSD difference 3.47 ± 10.43 between healthy and nano treated) suggesting that treatment through nanodrug can inhibit liver and cell damage that could occur due to cancer, where the enzyme level was four fold higher in untreated rat (252.01 ± 1.36 IU/L) (Tukey HSD difference is 191.51 ± 10.43).

Analysis of the prognostic hepatoma marker (225), the serum lactate dehydrogenase (LDH) in rats (Table 5.1) brought out that the nanodrug treated rats have shown significant decline in the levels of the LDH. While it was 206.48 ± 4 IU in untreated rats (Tukey HSD difference is 154.8 ± 10.76), it has decreased to, 51.68 ± 1 IU /L a value equivalent to that of

Table 5.1:

Prognosis of Hepatocellular Carcinoma in Nanodrug treated rats

Hepatocellular carcinoma is induced in rats. The rats were treated with indicated test compounds from day 1. The prognosis of hepatocellular carcinoma was monitored by various markers as given in the column 1.each data point was an average of values determined from six independent animals. Errors is presented in terms of standard deviation. Statistical evaluation was performed using Anova and Tukey HSD test. The parameters are presented in Appendix 2

[1]Each data is an average of 6 animal replicas and standard deviation is shown as errors.

[2]Statistical significance with and among the groups was carried out by ANOVA and Tukey HSD test the statistical parameters are presented in supporting data.

[3]The above parameters are monitored in rats these were treated from day 1 (Fig 5), the parameters were estimated on day 6 in group of 6 animals.

Table 5.1

Prognosis of Hepatocellular Carcinoma in Nanodrug treated rats[1,2,3]

Parameters	Untreated	Atr-doxo nano treated	Doxo soluble treated	Soluble Doxo Atr treated	BSA doxo nano treated	Saline / healthy rats
Serum Lactate Dehydrogenase (IU/L)	206.48 +/- 4.01	51.68 +/- 1.03	89.89 +/- 0.84	90.19 +/- 1.10	182.04 +/- 3.34	51 +/- 0.73
Serum Alkaline Phosphatase (IU/L)	252.01 +/- 1.36	60.49 +/- 0.81	71.33 +/- 0.52	123.97 +/- 4.09	184.86 +/- 3.05	57.02 +/- 0.04
Serum Creatinine (mg/dl)	0.23 +/- 0.01	0.19 +/- 0.02	0.20 +/- 0.01	0.20 +/- 0.01	0.20 +/- 0.006	0.21 +/- 0.01
Serum Urea (mg/dl)	26.05 +/- 0.86	4.66 +/- 0.04	3.63 +/- 0.007	4.58 +/- 0.007	19.21 +/- 0.53	4.62 +/- 0.13
Survival time (days)	7 +/- 1	No sign of death	16 +/- 1	16 +/- 1	8 +/- 1	No sign of death
Alpha feto protein (Image j quantitation)	17.337 +/- 4.78	1.2163 +/- 0.569	2.308 +/- 0.802	2.441 +/- 0.453	16.752 +/- 3.51	1.2163 +/-0.569

Figure 5.12

Regression of full blown hepatocellular carcinoma by drug loaded apotransferrin nanoparticles

Healthy rats are injected with ZH5 cells and kept untreated for 4 days and on the 5th day rats are treated with apotransferrin nanoparticles for 10 days as described in methodology. Rats are photographed from day 1-10 after the treatment. Regression of hepatoma is clearly seen from the photographs, the control untreated rat died on the 7th day while this full blown model treated rat survived for more than 150 days. These results suggest that the nanoparticles are delivered efficiently to the cancer cells and regression is observed in the *in vivo* model.

Figure 5.12

Regression of full blown Hepatocellular Carcinoma by drug loaded Apotransferrin Nanoparticles

Full blown model generated	Treated 1 day	Treated 5 day	Treated 9 day	Treated 10 day

a healthy rat (Tukey HSD difference 0.676 ± 10.76 between healthy and nano treated). It was observed that the LDH levels were significantly decreased in the case of rats subjected to apotransferrin nanoparticles treatment compared to that with that soluble form. To monitor, if any metabolic disorder was caused upon induction of hepatocellular carcinoma, we have estimated serum creatinine and urea in untreated rats as well and found that the creatinine in the treated groups of rats remained the same as that in healthy ones (Tukey difference less than 0.04) while the serum urea increased significantly by 5 fold (Tukey difference 21.43±1.92), and this suggests that treatment did not induce any toxicity to kidney. The observed absence of bioactivity of doxorubicin in BSA nanoparticles could be due to their inability in cellular binding and release of doxorubicin (Table 5.1), thus indicating that receptor recognition and binding of apotransferrin nanoparticles plays an important role in drug release. The results suggest that nanodrug can significantly and efficiently regress cancer in rat hepatoma model and this is also confirmed further by their survival rate. Apotransferrin nanoparticles treated rats were healthy and survived more than 53 weeks.(Figure 5.9 contd).

Activity of drug loaded apotransferrin nanoparticles on full blown hepatocellular carcinoma

Healthy rats are injected with ZAH cells and kept untreated for 4 days and on the 5th day rats are treated with drug loaded nanoparticles for 10 days as described in methodology. Rats are photographed from day 1-10 after the treatment. Regression of hepatoma is clearly seen form the photographs (Figure 5.12), the control untreated rat died on the 7th day while this full blown model treated rat survived for more than 150 days. These results suggest that the nanoparticles are delivered efficiently to the cancer cells and regression is observed in the in vivo model.

Figure 5.13:

Serum Alpha Feto protein levels in Treated and Untreated animals

Unhemolysed Plasma sample of the treated and untreated rats are collected on the 6th day and used for all the characterizations. The protein in the samples is estimated by Bradford's method. Protein Samples are resolved on 7% SDS PAGE and transferred to the nitrocellulose membrane as per the Western blotting methodology. The blot is probed with mouse anti human alpha feto protein monoclonal antibody and detected by goat antimouse IgG conjugated to alkaline phosphatase conjugated secondary antibody and stained with BCIP/NBT as per the methodology. The immunoprecipitated bands were quantified by densitometry, each experiment is conducted in triplicate and triplicate results are depicted as per the following description.

> #1-3: Untreated rat
>
> #4-6: Doxorubicin nanoparticles treated rat group
>
> # 7-9: Soluble doxorubicin treated rat group
>
> #10-12: Healthy rat group
>
> # 13-16: BSA doxorubicin nanoparticles treated rat group

Figure 5.13

Serum Alpha Feto protein levels in Treated and Untreated animals
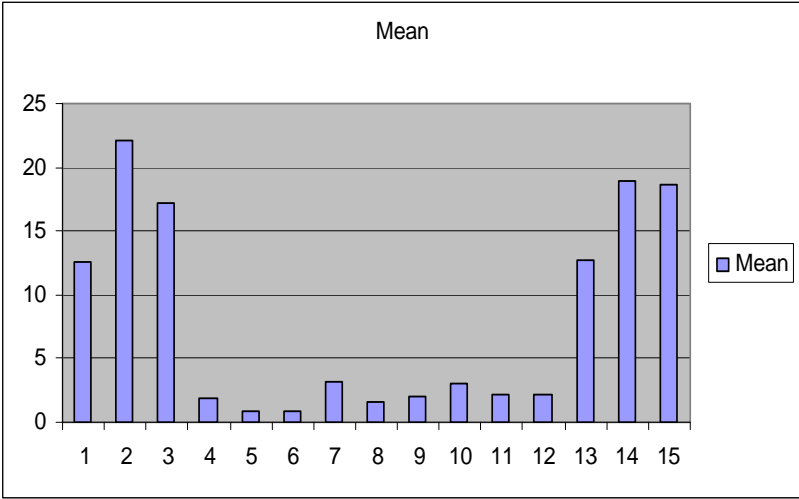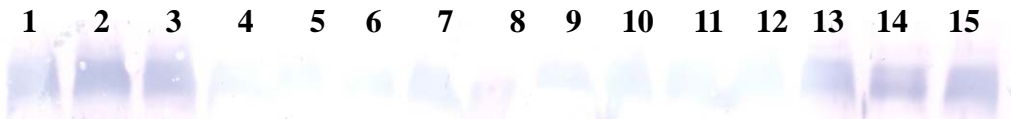
Analysis of prognosis hepatocellular carcinoma by monitoring Serum alpha feto protein

Unhemolysed Plasma sample of the treated and untreated rats are collected on the 6th day and used for all the characterizations. The protein in the samples is estimated by Bradfords method (355) and equal amount of Protein Samples were resolved on 7% SDS page and transferred to the nitrocellulose membrane as per the Western blotting methodology. The blot is probed with monoclonal antihuman Alpha feto protein antibody and alkaline phosphatase conjugated secondary antibody.The blots were developed with BCIP/NBT. The density of bands were quantified and shown on Fig 5.13 The plasma sample of untreated and BSA nano treated rats show significant elevation in the AFP protein levels, but the plasma sample of the soluble doxorubicin, healthy, doxorubicin apotransferrin nanoparticle treated rat did not show any elevation in the serum levels of the AFP, these results indicate the regression of hepatoma in the presence of soluble and drug loaded nanoparticles

In summary, the above results drugs loaded protein nanoparticles can be produced using the present method of preparation. The apotransferrin nanoparticles prepared in this method can retain their native conformation for transferrin receptor binding and localization of particles in cells through transferrin receptor mediated endocytosis. The drug is rapidly released into cytosol of cells and the apotransferrin protein is secreted out from cells. The drug in apotransferrin nanoparticles can enter the cells and the released drug can induce required biological activity namely antiproliferative activity. The drug loaded nanoparticles can significantly regress ascetic hepatocellular carcinoma in rats.

Figure 5.14

Unhemolysed Plasma sample of the treated and untreated rats are collected on the 6th day and used for all the characterizations. The protein in the samples is estimated by bradfords method. The marker are quantitated in the serum by the Sigma diagnostics kits as per the manufactures instructions. The results suggest that the urea, Alkaline phosphatase and Lactate dehydrogenase are elevated in the serum of the untreated and nano treated rats suggesting the prognosis of the cancer, and the levels are low in soluble doxorubicin treated rats and the levels are similar in the healthy, and doxorubicin loaded nanoparticles suggesting the regression in the cancer. While the serum creatinine levels are similar in all the treated and untreated groups indicate the proper functioning of the kidney and malfunctioning of the liver suggesting the liver cancer. The elevation of alkaline phosphatase and lactate dehydrogenase are general cancer makers in serum.

Bar 1:Untreated rat, Bar 2: Drug nano treated rat, Bar 3: Drug soluble alone treated rat, Bar 4: Drug transferrin soluble treated rat, Bar 5: BSA drug nano treated rat, Bar 6: Saline treated rat

Figure 5.14

Prognosis of Hepatocellular Carcinoma in Nanodrug treated rats
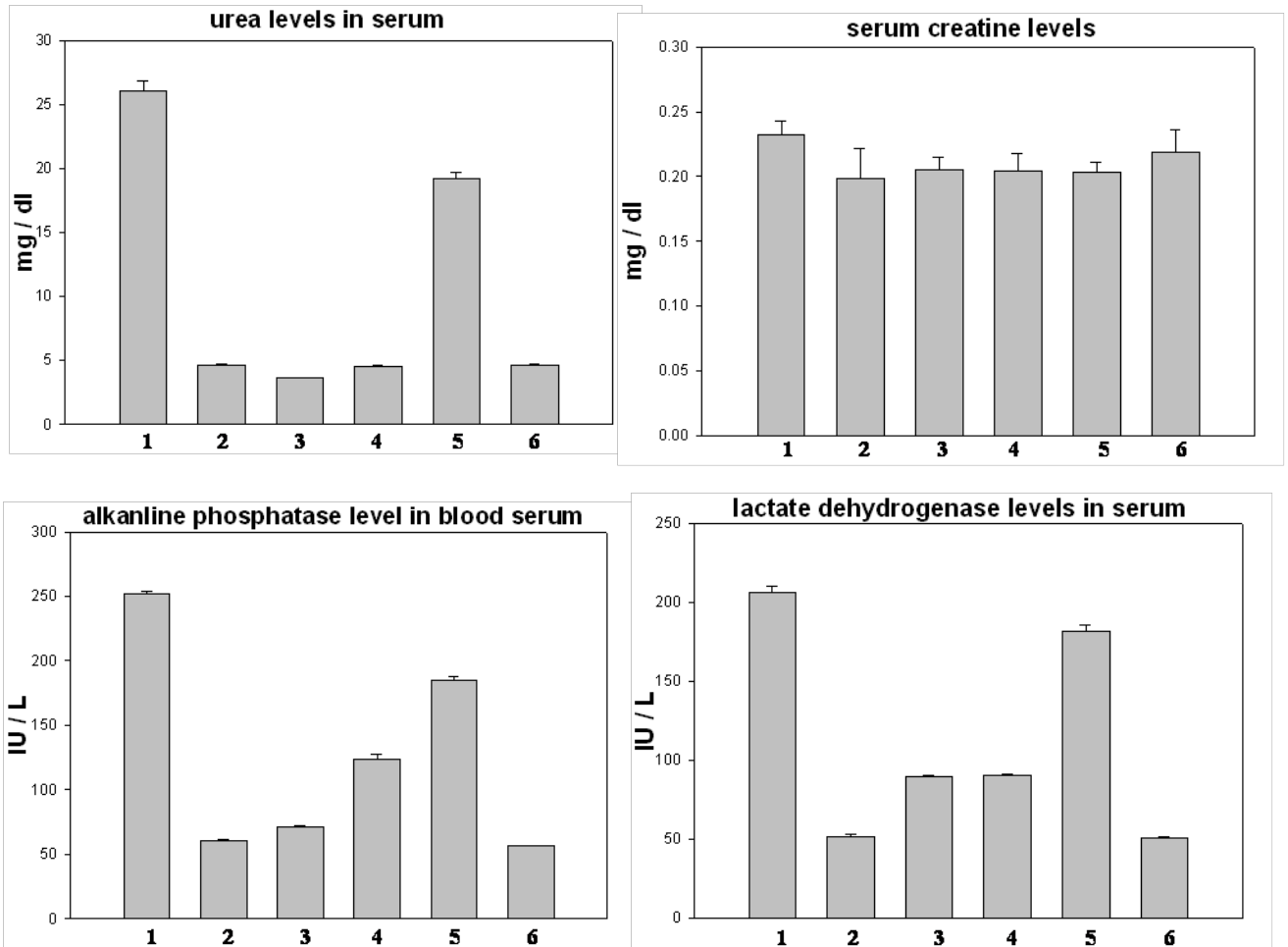
Figure 5.15:

Pathological analysis of Hepatocellular Carcinoma in Nanodrug treated rats

The treated and untreated rats are sacrificed on the 6th day by cervical dislocation as explained in the methodology. The liver sample was collected and fixed with 1% Para formaldehyde and histochemical analysis was done by Hematoxylin and Eosin staining. Microscopic analysis of these samples revealed the presence of the tumor lesions in the untreated rats while the rat group treated with doxorubicin loaded nanoparticles liver samples are clear of the lesions indicating the treatment is effective and able to regress the hepatoma in the rats. The arrows indicate the lesions. The results of animal experiments with control untreated shown.

Figure 5.15

Pathological analysis of Hepatocellular Carcinoma in Nanodrug treated rats

Untreated   **Treated**
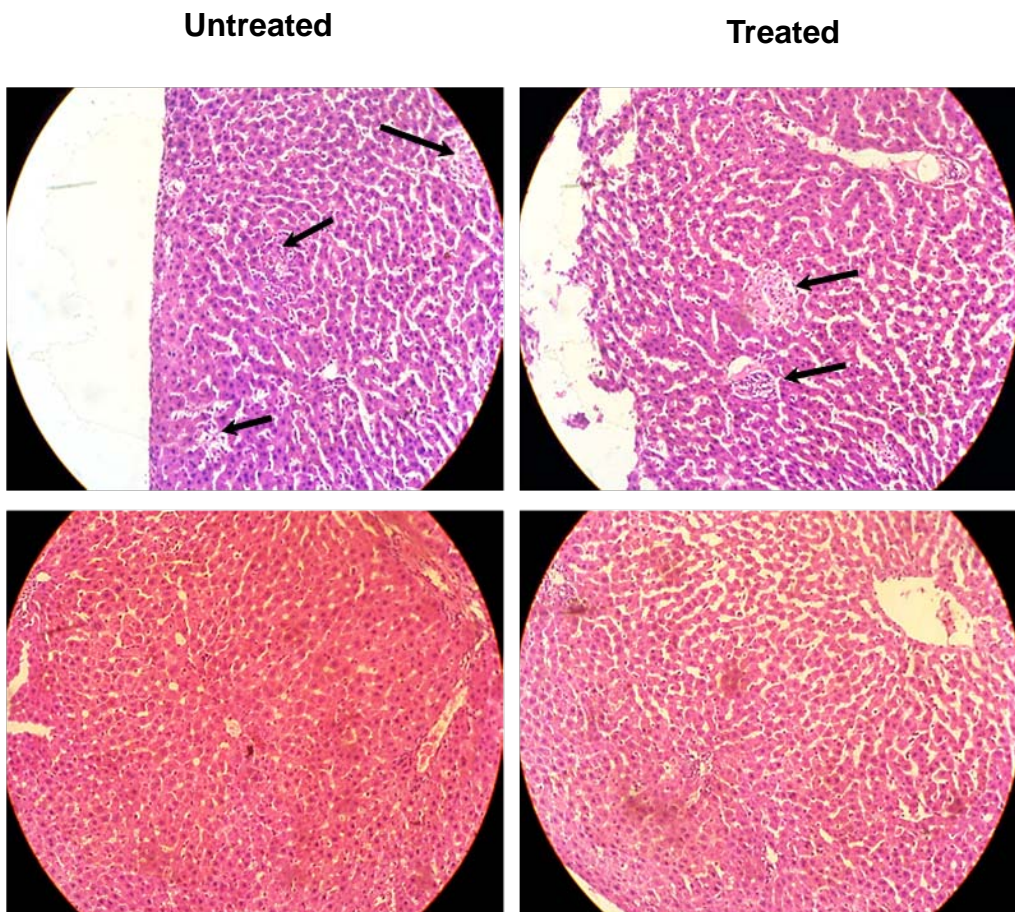
DISCUSSION:

Iron is an important micronutrient that is essential for the function of iron dependent proteins such as hemoglobin, myoglobin and cytochrome enzyme. Out of 4000 mg of iron in the human body, 3000 mg is mainly present in red blood cells (RBC) (230). This suggests the integral part of iron in RBC functioning. The deficiency of iron can lead to anemia that contributes to erythropoietin deficiency, a chronic disease that harbor inflammatory condition such as rheumatoid arthritis, chronic inflammatory bowl disease, HIV infection, cancer, pathogenic and metabolic diseases that demand iron uptake (230). Iron deficient tissues stimulate enhanced expression of receptor on the cell surface which mediates the accumulation of iron through an iron binding protein, apotransferrin and two types of iron receptors have been reported TfR1 and TfR2 (231). TfR-2 is present in two alternate spliced forms α and β, which possess the same molecular properties in transferrin binding, but their expression varies with the tissues (232).

Mechanism of apotransferrin recycle
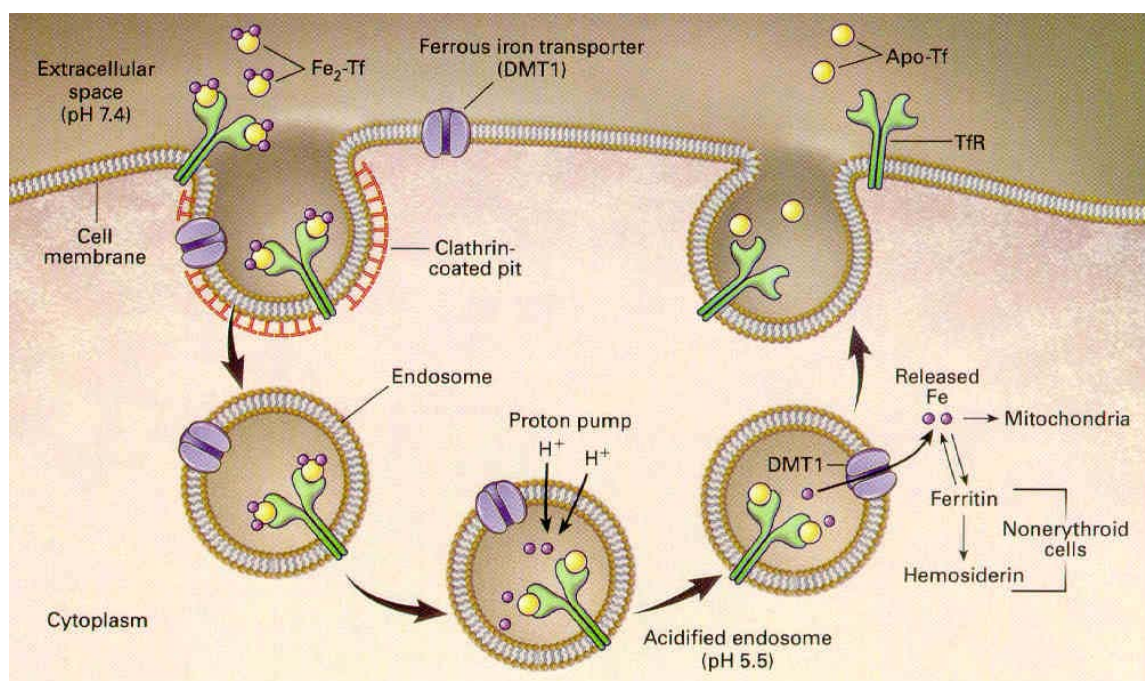
TfR1 level is seen to be low in liver, while TfR2 expression is exclusively seen to be present in liver of developed rats (232). TfR1 levels are significant in embryonic day-10 and start decreasing from embryonic day-17 to post natal day-1, while TfR2 expression starts from embryonic day-8 or 11, and remains high in liver throughout developmental stage (233). Though these receptors are differentially regulated, their molecular properties for apotransferrin binding and iron transport remain conserved. Such a feature makes apotransferrin an attractive drug carrier to various disease bearing cells, exploiting the higher TfR expression due to the requirement of essential micronutrient iron. It has been reported that the transferrin receptors are over expressed in cancer cells and tissue of liver, lung (234), breast (235), brain suggesting highly localization of drug targeted through apotransferrin mediated delivery.

The multi-drug resistant cancer cells are shown to be effectively targeted by apotransferrin-conjugate mediated delivery (236). Since apotransferrin is a highly stable and abundant protein in circulation for transport of iron, it is considered to be one of the best candidates for use in drug delivery. Several research groups have reported on the use of soluble apotransferrin and its conjugates for targeting specific delivery to cells such as cancer and brain (394). The present method as could be seen from the results presented will provide a new approach for protein based nanoparticle preparation and its application in delivery of drugs using a natural biological mode of transport. The method can be applied to any protein ligand for which specific receptor is expressed on target cell.

The water soluble drug can completely be encapsulated into the protein particles. While in the case of oil soluble drugs or water insoluble drugs, due to the inherent solubility of drug in oil phase, proportionately lesser amounts of drug could be encapsulated into nanoparticles. This novel methodology resembles a natural mode of receptor mediated

transportation of agents with negligible toxicity and can also help in rapid localization of drug in specific receptor expressed cells. Further, rapid releasing of drug into the cell can maintain an effective concentration of drug, (222) thus reducing the risk of developing drug resistance. The retarded drug release kinetics usually seen in drug conjugated polymeric and liposomal preparations (237) would provide low drug turnover that hinders the efficacy of drug and a prolonged suboptimum levels of drug in circulation may provide a possibility for development of drug resistance (238). Many of nanoparticle based drug delivery systems are facing challenges due to permanent localization of the delivery vehicle in the cells and tissue (239), which induce antigenic response and cellular damage (240), while apotransferrin delivery method can resolve such toxicity and drug release problems.

CONCLUSIONS

1. Substituent dependant molecular activity of ferrocene was analysed. The results showed a strong association of the structure and properties of the substituent with their ability in poisoning Topoisomerase II beta.

2. The molecular surface charge distribution plays an important role in conferring topoisomerase II inhibitory activity to the ferrocene molecules. The molecular volume determines the poisoning ability of the ferrocene derivatives.

3. Thiomorpholide amido methyl ferrocene inhibit topoisomerase II beta catalytic activity by interacting with the ATP binding domain without forming enzyme linked cleavable complexes.

4. Azalactone ferrocene exhibits topo II beta poisoning activity. In terms of IC_{50} values azalactone ferrocene show 2 fold lower activity compared to Thiomorpholide amido methyl ferrocene. Both the molecules do not posses affinity to DNA.

5. A novel apotransferrin nanoparticle drug delivery system is developed.

6. 20 to 40 nm protein nanoparticles assumed a dimension of 60 to 80 nm upon drug encapsulation.

7. Nanoparticles are made of protein alone without any lipid layer.

8. The nanoparticles show surface anisotropy that help in their immunoreactivity and affinity to transferrin receptors.

9. Analysis of drug localisation of nanoparticles showed that the protein and nanoparticles remain in extra cellular spaces and drug released in to the cytosol

10. Comparative analysis of antiproliferative activity of drug in soluble and nanoparticle form showed that apotransferrin nanoparticles can significantly proliferation of cancer cells.

11. A hepatocellular carcinoma has been used to evaluate *invivo* biological activity of drug in nanoparticles the result shows a significant regression of cancer by apotransferrin apotransferrin doxorubicin nanoparticles as well as Azalactone ferrocene nanoparticle, compared to that using BSA nanoparticles.

12. Apotransferrin nanoparticles completely cured the cancer and significantly decreased cancer associated liver toxicity and do not exhibit any toxicity to kidney

13. A stronger association of Alpha feto protein with the progression of Hepatocellular carcinoma is observed based on the analysis of AFP levels as well as immunohistochemistry we conclude that nanoparticles can efficiently regress Hepatocellular carcinoma in rats

In summary substituted ferrocenes Azalactone ferrocene and Thiomorpholide amido methyl ferrocene in apotransferrin nanoparticles delivery system can form potent formulation for future cancer chemotherapy.

References

1) Watson J.D., Crick F.H.C. Molecular structure of nucleic acids. Nature 171 (1953) 737–738.

2) Watson J.D., Crick F.H.C. Genetical implications of the structure of deoxyribonucleic acid. Nature 171 (1953) 964–967.

3) Cozzarelli N.R., and Wang, J.C. (eds). DNA Topology and its Biological Effects, Cold Spring Harbor Laboratory Press, Cold Spring Harbor. (1990)

4) Kanaar R., Cozzarelli N.R. Roles of supercoiled DNA structure in DNA transactions, Curr. Opin. Struct. Biol. 2 (1992) 369–379.

5) Wang J.C. DNA topoisomerases, Annu. Rev. Biochem. 65 (1996) 635–692.

6) Schvartzman J.B., Stasiak A. A topological view of the replicon, EMBO Rep. 5 (2004) 256–261.

7) Wang J.C. Cellular roles of DNA topoisomerases: a molecular perspective, Nat. Rev. Mol. Cell. Biol. 3 (2002) 430–440.

8) Brill S.J., DiNardo S., Voelkel-Meiman K., Sternglanz R. DNA topoisomerase activity is required as a swivel for DNA replication and for ribosomal RNA transcription, NCI Monogr. 4 (1987) 11–15.

9) Kim R.A., Wang J.C. Function of DNA topoisomerases as replication swivels in Saccharomyces cerevisiae, J. Mol. Biol. 208 (1989) 257–267.

10) Wang J.C., and Liu L.F. DNA Replication: Topological aspects and the roles of DNA topoisomerases. (1990) In: Cozzarelli, N. R., and Wang, J. C. (eds). DNA Topology and Its Biological Effects, Cold Spring Harbor Laboratory Press, Cold Spring Harbor

11) Peter B.J., Ullsperger C., Hiasa H., Marians K.J., Cozzarelli N.R. The structure of supercoiled intermediates in DNA replication, Cell 94 (1998) 819–827.

12) Drlica K. Control of bacterial DNA supercoiling., Mol Microbiol. Feb; 6 (4) (1992) 425-33.

13) Vologodskii A.V., Cozzarelli N.R. Conformational and thermodynamic properties of supercoiled DNA.., Annu Rev Biophys Biomol Struct.23 (1994) 609-43.

14) Tan R.K., Harvey S.C., Di Mauro E., Camilloni G., Venditti P. DNA topological context affects access to eukaryotic DNA topoisomerase I.., J Biomol Struct Dyn. Apr; 13 (5) (1996) 855-72.

15) Bates A.D., O'Dea M.H., Gellert M. Energy coupling in Escherichia coli DNA gyrase: the relationship between nucleotide binding, strand passage, and DNA supercoiling. Biochemistry. Feb 6; 35 (5) (1996) 1408-16.

16) Cozzarelli N.R. DNA gyrase and the supercoiling of DNA. Science. Feb 29; 207 (1980) 953-960.

17) Osheroff N. Biochim. Biophys. Acta 1400., DNA topoisomerases. (1998) (1-3), 1-2

18) Nitiss J.L. Investigating the biological functions of DNA topoisomerases in eukaryotic cells, Biochim. Biophys. Acta 1400 (1998) 63–81.

19) Champoux J.J. DNA topisomerases: structure, function, and mechanism, Annu. Rev. Biochem. 70 (2001) 369–413.

20) Fortune J.M., Osheroff N. Topoisomerase II as a target for anticancer drugs: when enzymes stop being nice, Prog. Nucleic Acid Res. Mol. Biol. 64 (2000) 221–253.

21) Wilstermann A.M., Osheroff N. Stabilization of eukaryotic topoisomerase II–DNA cleavage complexes, Curr. Top. Med.Chem. 3 (2003) 1349–1364.

22) Sabourin M., Osheroff N. Topoisomerases, in:Wiley Encyclopedia of Molecular Medicine, John Wiley & Sons, Inc., (2002) 3192–3197.

23) Velez-Cruz R., Osheroff N. DNA topoisomerases: type II, in: Encyclopedia of Biological Chemistry, Elsevier Inc., (2004) 806–811.

24) Forterre P., Gribaldo S., Gadelle D., Serre M.C. Origin and evolution of DNA topoisomerases. Biochimie. Apr; 89 (4) (2007) 427-46.

25) Wang J.C. Moving one DNA double helix through another by a type II DNA topoisomerase: the story of a simple molecular machine, Q. Rev. Biophys. 31 (1998) 107–144.

26) Wyckoff E., Hsieh T.S. Functional expression of a Drosophila gene in yeast: genetic complementation of DNA topoisomerase II, Proc. Natl. Acad. Sci. U.S.A. 85 (1988) 6272–6276.

27) Goto T., and Wang J.C. Yeast DNA topoisomerase II is encoded by a single-copy, essential gene. Cell 36 (1984) 1073-1080.

28) Drake F.H., Hofmann G.A., Bartus H.F., Mattern M.R., Crooke S.T., Mirabelli C.K. Biochemical and pharmacological properties of p170 and p180 forms of topoisomerase II, Biochemistry 28 (1989) 8154–8160.

29) Levine, C., Hiasa, H., and Marians, K.J. DNA gyrase and topoisomerase IV: biochemical activities, physiological roles during chromosome replication, and drug sensitivities. Biochim. Biophys. Acta 1400, (1998) 29-43.

30) Austin C.A., Marsh K.L. Eukaryotic DNA topoisomerase II β , Bioessays 20 (1998) 215–226.

31) Wasserman R.A., Austin C.A., Fisher L.M., Wang J.C. Use of yeast in the study of anticancer drugs targeting DNA topoisomerases: expression of a functional recombinant human DNA topoisomerase II alpha in yeast, Cancer Res. 53 (1993) 3591–3596.

32) Jensen S., Redwood C.S., Jenkins JR., Andersen A.H., Hickson I.D. Human DNA topoisomerases II alpha and II beta can functionally substitute for yeast TOP2 in chromosome segregation and recombination, Mol. Gen. Genet. 252 (1996) 79–86.

33) Meczes E.L., Marsh K.L., Fisher L.M., Rogers M.P., Austin C.A. Complementation of temperature-sensitive topoisomerase II mutations in Saccharomyces cerevisiae by a human TOP2 beta construct allows the study of topoisomerase II beta inhibitors in yeast, Cancer Chemother. Pharmacol. 39 (1997) 367–375.

34) Woessner R.D., Mattern M.R., Mirabelli C.K., Johnson R.K., Drake F.H. Proliferation- and cell cycle-dependent differences in expression of the 170 kD and 180 kD forms of topoisomerase II in NIH-3T3 cells, Cell Growth Differ. 2 (1991) 209–214.

35) Heck M.M., and Earnshaw W.C. Topoisomerase II: A specific marker for cell proliferation. J. Cell. Biol. 103 , (1986) 2569-2581.

36) Hsiang Y.H., Wu H.Y., Liu L.F. Proliferation-dependent regulation of DNA topoisomerase II in cultured human cells, Cancer Res. 48 (1988) 3230–3235.

37) Bauman M.E., Holden J.A., Brown K.A., Harker W.G., Perkins S.L. Differential immunohistochemical staining for DNA topoisomerase II alpha and beta in human tissues and for DNA topoisomerase II beta in non-Hodgkin's lymphomas, Mod. Pathol. 10 (1997) 168–175.

38) Isaacs R.J., Davies S.L., Sandri M.I., Redwood C., Wells N.J., Hickson I.D. Physiological regulation of eukaryotic topoisomerase II, Biochim. Biophys. Acta 1400 (1998) 121–137.

39) Dereuddre S., Delaporte C., Jacquemin-Sablon A. Role of topoisomerase II beta in the resistance of 9-OH-ellipticineresistant Chinese hamster fibroblasts to topoisomerase II inhibitors, Cancer Res. 57 (1997) 4301–4308.

40) Grue P., Grasser A., Sehested M., Jensen P.B., Uhse A., Straub T., Ness W., Boege F. Essential mitotic functions of DNA topoisomerase IIβ are not adopted by topoisomerase II in human H69 cells, J. Biol. Chem. 273 (1998) 33660–33666.

41) Berger J. M., and Wang J. C. Recent developments in DNA topoisomerase II structure and mechanism. Curr. Opin. Struct. Biol. 6, (1996) 84-90.

42) Berger J. M. Structure of DNA topoisomerases Biochim. Biophys. Acta 1400 . (1998) (1-3), 3-18.

43) Classen S., Olland S., Berger J.M. Structure of the topoisomerase II ATPase region and its mechanism of inhibition by the chemotherapeutic agent ICRF-187, Proc. Natl. Acad. Sci. U.S.A. 100 (2003) 10629–10634.

44) Wei H., Ruthenburg A.J., Bechis S.K., Verdine G.L. Nucleotide-dependent domain movement in the ATPase domain of a human type IIA DNA topoisomerase, J. Biol. Chem. 280 (2005) 37041–37047.

45) Worland S.T., Wang J.C. Inducible overexpression, purification, and active site mapping of DNA topoisomerase II from the yeast Saccharomyces cerevisiae, J. Biol. Chem. 264 (1989) 4412–4416.

46) Berger J.M., Gamblin S.J., Harrison S.C., Wang J.C. Structure and mechanism of DNA topoisomerase II, Nature 379 (1996) 225–232.

47) Shiozaki K., Yanagida M. Functional dissection of the phosphorylated termini of fission yeast DNA topoisomerase II, J. Cell. Biol. 119 (1992) 1023–1036.

48) Crenshaw D.G., Hsieh T. Function of the hydrophilic carboxyl terminus of type II DNA topoisomerase from Drosophila melanogaster. I. In vitro studies, J. Biol. Chem. 268 (1993) 21328–21334.

49) Mirski S.E., Cole S.P. Cytoplasmic localization of a mutant M(r) 160,000 topoisomerase II alpha is associated with the loss of putative bipartite nuclear localization signals in a drug resistant human lung cancer cell line, Cancer Res. 55 (1995) 2129–2134.

50) Wessel I., Jensen P.B., Falck J., Mirski S.E., Cole S.P., Sehested M. Loss of amino acids 1490Lys-Ser-Lys1492 in the COOH-terminal region of topoisomerase II alpha in human small cell lung cancer cells selected for resistance to etoposide results in an extranuclear enzyme localization, Cancer Res. 57 (1997) 4451–4454.

51) Adachi N., Miyaike M., Kato S., Kanamaru R., Koyama H., Kikuchi A. Cellular distribution of mammalian DNA topoisomerase II is determined by its catalytically dispensable C-terminal domain, Nucleic Acids Res. 25 (1997) 3135–3142.

52) Mirski S.E., Gerlach J.H., Cummings H.J., Zirngibl R., Greer P.A., Cole S.P. Bipartite nuclear localization signals in the C terminus of human topoisomerase II alpha, Exp. Cell Res. 237 (1997) 452–455.

53) Cowell I.G., Willmore E., Chalton D., Marsh K.L., Jazrawi E., Fisher L.M., Austin C.A. Nuclear distribution of human DNA topoisomerase II beta: a nuclear targeting signal resides in the 116-residue C-terminal tail, Exp. Cell Res. 243 (1998) 232–240.

54) DeVore R.F., Corbett A.H., Osheroff N. Phosphorylation of topoisomerase II by casein kinase II and protein kinase C: effects on enzyme-mediated DNA cleavage/religation and sensitivity to the antineoplastic drugs etoposide and 4'-(9- acridinylamino)methane-sulfon-m-anisidide, Cancer Res. 52 (1992) 2156–2161.

55) Cardenas M.E., Dang Q., Glover C.V., Gasser S.M. Casein kinase II phosphorylates the eukaryote-specific C-terminal domain of topoisomerase II in vivo, EMBO J. 11 (1992) 1785–1796.

56) Wells N.J., Addison C.M., Fry A.M., Ganapathi R., Hickson I.D. Serine 1524 is a major site of phosphorylation on human topoisomerase II alpha protein in vivo and is a substrate for casein kinase II in vitro, J. Biol. Chem. 269 (1994) 29746–29751.

57) Corbett K.D., Shultzaberger R.K., Berger J.M. The C-terminal domain of DNA gyrase adopts a DNA-bending beta-pinwheel fold, Proc. Natl. Acad. Sci. U.S.A. 101 (2004) 7293–7298.

58) Hsieh T.J., Farh L., Huang W.M., Chan N.L. Structure of the topoisomerase IV C-terminal domain: a broken beta-propeller implies a role as geometry facilitator in catalysis, J. Biol. Chem. 279 (2004) 55587–55593.

59) Corbett K.D., Schoeffler A.J., Thomsen N.D., Berger J.M. The structural basis for substrate specificity in DNA topoisomerase IV, J. Mol. Biol. 351 (2005) 545–561.

60) Schoeffler A. J., and Berger, J. M. Recent advances in understanding structure-function relationships in the type II topoisomerase mechanism. Biochem. Soc. Trans. 33 (Pt 6), (2005) 1465- 1470.

61) Osheroff N., Zechiedrich E.L., Gale K.C. Catalytic function of DNA topoisomerase II, BioEssays 13 (1991) 269-273.

62) Wang J.C. DNA topoisomerases, Annu. Rev. Biochem. 65 (1996) 635-692.

63) Watt P.M., Hickson I.D. Structure and function of type II DNA topoisomerases, Biochem. J. 303 (1994) 681-695.

64) Osheroff N., Shelton E.R., Brutlag D.L. DNA topoisomerase II from Drosophila melanogaster. Relaxation of supercoiled DNA, J. Biol. Chem. 258 (1983) 9536–9543.

65) Osheroff N. Eukaryotic topoisomerase II. Characterization of enzyme turnover, J. Biol. Chem. 261 (1986) 9944–9950.

66) Zechiedrich E.L., Osheroff N. Eukaryotic topoisomerases recognize nucleic acid topology by preferentially interacting with DNA crossovers, EMBO J. 9 (1990) 4555-4562.

67) Roca J., Berger J.M., Wang J.C. On the simultaneous binding of eukaryotic DNA topoisomerase II to a pair of double stranded DNA helices, J. Biol. Chem. 268 (1993) 14250-14255.

68) Roca J., Wang J.C. The capture of a DNA double helix by an ATP-dependent protein clamp: a key step in DNA transport by type II DNA topoisomerases, Cell 71 (1992) 833–840.

69) Madden K.R., Stewart L., Champoux J.J. Preferential binding of human topoisomerase I to superhelical DNA, EMBO J. 14 (1995) 5399-5409.

70) Corbett A.H., DeVore R.F., Osheroff N. Effect of casein kinase II-mediated phosphorylation on the catalytic cycle of topoisomerase II. Regulation of enzyme activity by enhancement of ATP hydrolysis. J. Biol. Chem. 267 (1992) 20513-20518.

71) Dang Q., Alghisi G.C., Gasser S.M. Phosphorylation of the C-terminal domain of yeast topoisomerase II by casein kinase II a¡ects DNA-protein interaction, J. Mol. Biol. 243 (1994) 10-24.

72) Liu L.F., Rowe T.C., Yang L., Tewey K.M., Chen G.L. Cleavage of DNA by mammalian DNA topoisomerase II,J. Biol. Chem. 258 (1983) 15365-15370.

73) Sander M., Hsieh T. Double strand DNA cleavage by type II DNA topoisomerase from Drosophila melanogaster,J. Biol. Chem. 258 (1983) 8421-8428.

74) Osheroff N. Role of the divalent cation in topoisomerase II mediated reactions, Biochemistry 26 (1987) 6402-6406.

75) Roca J., Wang J.C. The capture of a DNA double helix by an ATP-dependent protein clamp: a key step in DNA transport by type II DNA topoisomerases, Cell 71 (1992) 833–840.

76) Sander M., Hsieh T.S. Drosophila topoisomerase II doublestrand DNA cleavage: analysis of DNA sequence homology at the cleavage site, Nucleic Acids Res. 13 (1985) 1057-1072.

77) Spitzner J.R., Muller M.T. A consensus sequence for cleavage by vertebrate DNA topoisomerase II, Nucleic Acids Res.16 (1988) 5533-5556.

78) Muller M.T., Spitzner J.R., DiDonato J.A., Mehta V.B., Tsutsui K. Single-strand DNA cleavages by eukaryotic topoisomerase II, Biochemistry 27 (1988) 8369-8379.

79) Lindsley J.E., Wang J.C. Proteolysis patterns of epitopically labeled yeast DNA topoisomerase II suggest an allosteric transition in the enzyme induced by ATP binding, Proc. Natl. Acad. Sci. USA 88 (1991) 10485-10489.

80) Roca J., Wang J.C. The capture of a DNA double helix by an ATP-dependent protein clamp: a key step in DNA transport by type II DNA topoisomerases, Cell 71 (1992) 833–840.

81) Burden D.A, Osheroff N., Mechanism of action of eukaryotic topoisomerase II and drugs targeted to the enzyme. Biochim Biophys Acta. 1;1400(1-3) (1998) 139-54

82) Robinson M.J., Osheroff N. Effects of antineoplastic drugs on the post-strand-passage DNA cleavage/religation equilibrium of topoisomerase II. Biochemistry 30 (1991) 1807-1813.

83) Miller K.G., Liu L.F., Englund P.T. A homogeneous type II DNA topoisomerase from HeLa cell nuclei, J. Biol. Chem. 256 (1981) 9334-9339.

84) Benedetti P., Baldi M.I., Mattoccia E., Tocchini-Valentini G.P. Purification and characterization of Xenopus laevis topoisomerase II, EMBO J. 2 (1983) 1303-1308.

85) Corbett A.H., Fernald A.W., Osheroff N. Protein kinase C modulates the catalytic activity of topoisomerase II by enhancing the rate of ATP hydrolysis: evidence for a common mechanism of regulation by phosphorylation, Biochemistry 32 (1993) 2090-2097.

86) McClendon A.K, Osheroff N., DNA topoisomerase II, genotoxicity, and cancer. Mutat Res. 1;623(1-2) (2007) 83-97

87) Mouchel N.A., Jenkins JR. The identification of a functional interaction between PKC and topoisomerase II. FEBS Lett. Jan 9; 580 (1) (2006) 51-7

88) Pommier Y., Pourquier P., Fan Y., Strumberg D. Mechanism of action of eukaryotic DNA topoisomerase I and drugs targeted to the enzyme, Biochim. Biophys. Acta 1400 (1998) 83– 106.

89) Liu L.F., D'Arpa P. Topoisomerase-targeting antitumor drugs: mechanisms of cytotoxicity and resistance, Important Adv. Oncol. (1992) 79–89.

90) Li T.K., Liu L.F. Tumor cell death induced by topoisomerasetargeting drugs, Annu. Rev. Pharmacol. Toxicol. 41 (2001) 53–77.

91) Lockshon D. and Morris. Positively supercoiled plasmid DNA is produced by treatment of Escherichia coli with DNA gyrase inhibitors. Nucleic Acids Res 11, (1983) 2999-3017.

92) Liu L.F. and Wang J.C. Supercoiling of the DNA template during transcription. Proc.Natl. Acad.Sci. USA. 84, (1987) 7024-7027.

93) Kim R.A., Wang J.C. Function of DNA topoisomerases as replication swivels in Saccharomyces cerevisiae, J. Mol. Biol. 208 (1989) 257–267.

94) Ishida R., Sato M., Narita T., Utsumu K.R., Nishimoto T., Morita T., Nagata H., Andoh T. Inhibition of DNA topoisomerase II by ICRF-193 induces polyploidization by uncoupling chromosome dynamics from other cell cycle events. J. Cell. Biol 126, (1994) 1341-1351.

95) Dinardo S., Voelkel K., Rosenberg S.A. (eds) . DNA topoisomerase II mutant of Saccharomyces cerevisiae: topoisomerase II is required for segregation of daughter molecules at the termination of DNA replication. Proc. Natl. Acad.Sci. USA. 81, (1985) 2616-2620.

96) Uemura T. and Yanadiga M . Mitotic spindle pulls but fails to separate chromosomes in type II DNA topoisomerase mutants: uncoordinated mitosis. EMBO J (1986) 1003-1010.

97) Holm C., Goto T. , Wang J.C. and Botstein D. DNA topoisomerase II is required at the time of mitosis in yeast. Cell 41, (1985) 553-563.

98) Christman M.G., Dietrich F.S., and Fink G.R. Mitotic recombination in the rDNA of S. cerevisiae is suppressed by the combined action of DNA topoisomerases I and II. Cell 55, (1988) 413-425.

99) Kim R.A. and Wang J.C . Appendix. I: An introduction to DNA supercoiling and DNA topoisomerase-catalyzed linking number changes of supercoiled DNA. J. Mol. Biol 208, (1989) 257-267.

100) Sweldow JR., Sedat J.W., and Agard D.A. Multiple chromosomal populations of topoisomerase II detected in vivo by time-lapse, three-dimensional wide-field microscopy. Cell 73, (1993) 97-108.

101) Earnshaw W.C. and Heck M.M. Localization of topoisomerase II in mitotic chromosomes. J Cell Biol 100, (1985) 1716-1725.

102) Gasser S.M., Laemmli U.K. Improved methods for the isolation of individual and clustered mitotic chromosomes. Trends Genet 3, (1987) 16-22.

103) Hirano T. and Mitchison T.J. Topoisomerase II does not play a scaffolding role in the organization of mitotic chromosomes assembled in Xenopus egg extracts. J Cell Biol 120, (1993) 601-612.

104) Adachi Y., Luke M. and Laemmuli U.K. Chromosome assembly in vitro: topoisomerase II is required for condensation. Cell 64, (1991) 137-148.

105) Wood E.R., and Earnshaw W.C. Mitotic chromatin condensation in vitro using somatic cell extracts and nuclei with variable levels of endogenous topoisomerase II. J Cell Biol 111, (1990) 2839-2850.

106) Ma X., Saitoh N., and Curtis P.J. Purification and characterization of a nuclear DNA-binding factor complex containing topoisomerase II and chromosome scaffold protein 2. J Biol. Chem 268, (1993) 6182-6188.

107) Saitoh N., Goldberg I.G., Wood E.R., and Earnshaw W.C. ScII: an abundant chromosome scaffold protein is a member of a family of putative ATPases with an unusual predicted tertiary structure. J Cell Biol 127, (1994) 303-318.

108) Cardenas M.E. and Gasser S.M. Regulation of topoisomerase II by phosphorylation: a role for casein kinase IIJ Cell Sci 104, (1993) 219-225.

109) Hsiang Y.H., Wu J.Y., and Liu L.F. Proliferation-dependent regulation of DNA topoisomerase II in cultured human cells. Cancer Res, 48, (1988) 3230-3235.

110) Corbett A.H., and Osheroff N. When good enzymes go bad: conversion of topoisomerase II to a cellular toxin by antineoplastic drugs.., Chem Res Toxicol 6, (1993) 585-597.

111) Isaacs R.J., Davies S.L. Sandri M.I., Redwood C., Wells N.J., Hickson I.D. Physiological regulation of eukaryotic topoisomerase II.., Biochim Biophys Acta. Oct 1; 1400 (1-3) (1998) 121-37

112) Kaufmann W.K. Human topoisomerase II function, tyrosine phosphorylation and cell cycle checkpoints.., Proc Soc Exp Biol Med. Mar; 217 (3) (1998) 327-34.

113) Larsen A.K., Skladanowski A., Bojanowski K. The roles of DNA topoisomerase II during the cell cycle., Prog Cell Cycle Res. 2 (1996) 229-39.

114) Cardenas M.E., Gasser S.M. Regulation of topoisomerase II by phosphorylation: a role for casein kinase II. J Cell Sci. Feb; 104 (Pt 2) (1993) 219-25.

115) Watabe M., Nakajo S., Yoshida T., Kuroiwa Y., Nakaya K. Treatment of U937 cells with bufalin induces the translocation of casein kinase 2 and modulates the activity of topoisomerase II prior to the induction of apoptosis. Cell Growth Differ. Aug; 8 (8) (1997) 871-879.

116) Matsumoto Y., Kunishio K., Nagao S. Increased phosphorylation of DNA topoisomerase II in etoposide resistant mutants of human glioma cell line. J Neurooncol. 45 (1) (1999) 37-46.

117) Plo I., Hernandez H., Kohlhagen G., Lautier D., Pommier Y., Laurent G. Overexpression of the atypical protein kinase C zeta reduces topoisomerase II catalytic activity, cleavable complexes formation, and drug-induced cytotoxicity in monocytic U937 leukemia cells. J Biol Chem. Aug 30; 277 (35) (2002) 31407-15.

118) Reeca R.J., and Maxwell A. DNA gyrase: structure and function. Crit Rev Biochem Mol Biol 26, (1991) 335-375.

119) Gupta M., Fujimori A., and Pommier Y. Eukaryotic DNA topoisomerases I. Biochem Biophys Acta 1262, (1995) 1-14.

120) Byl J.A., Cline S.D., Utsugi T., Kobunai T., Yamada Y., Osheroff N. DNA topoisomerase II as the target for the anticancer drug TOP-53: mechanistic basis for drug action. Biochemistry. Jan 23; 40 (3) (2001) 712-718.

121) Anderson R.D., and Berger N.A. International Commission for Protection Against Environmental Mutagens and Carcinogens. Mutagenicity and carcinogenicity of topoisomerase-interactive agents. Mutat Res 309, (1994) 109-142.

122) Ferguson L.R., and Baguley B.C. Topoisomerase II enzymes and mutagenicity. Environ .Mol. Mutagen 24, (1994) 245-261.

123) Nelson E.M., Tewey K.M ., Liu L.F. Mechanism of antitumor drug action: poisoning of mammalian DNA topoisomerase II on DNA by 4'-(9-acridinylamino)-methanesulfon-m-anisidide. Proc.Natl. Acad. Sci. USA. 81, (1984) 1361-1365.

124) Chen A.Y., and Liu L.F. DNA topoisomerases: essential enzymes and lethal targets. Annu Rev Pharmacol Toxicol 34, (1994) 191-218.

125) Smith P.J. DNA topoisomerase dysfunction: a new goal for antitumor chemotherapy. BioEssays 12, (1990) 167-172.

126) Liu L.F. DNA topoisomerase poisons as antitumor drugs. Annu Rev Biochem 58, (1989) 351-375.

127) Binaschi M., Zunino F., Capranico G. Mechanism of action of DNA topoisomerase inhibitors. Stem Cells. Jul; 13 (4) (1995) 369-79.

128) Wilstermann A.M., Osheroff N. Stabilization of eukaryotic topoisomerase II-DNA cleavage complexes. Curr Top Med Chem. 3 (3) (2003) 321-38.

129) Pommier Y. DNA topoisomerase I and II in cancer chemotherapy: update and perspectives. Cancer Chemother Pharmacol 32, (1993) 103-108.

130) Tricoli J.V., Sahai B.M., Mccormick P.J., Jarlinski S.J., Bertram J.S., and Kowalski D. DNA topoisomerase I and II activities during cell proliferation and the cell cycle in cultured mouse embryo fibroblast (C3H 10T1/2) cells. Exp Cell Res 158, (1985) 1-14.

131) Capranico G., Binaschi M. DNA sequence selectivity of topoisomerases and topoisomerase poisons. Biochim Biophys Acta. Oct 1; 1400 (1-3) (1998) 185-194.

132) Beck W.T., Kim R., and Chen M. Novel actions of inhibitors of DNA topoisomerase II in drug-resistant tumor cells. Cancer Chemother Pharmacolo 34, (1994) 14-18.

133) Velez-Cruz R., and Osheroff N. DNA topoisomerases: type II. In.Encyclopedia of Biological Chemistry, Elsevier Inc. (2004)

134) Alisi A., Balsano C. Enhancing the efficacy of hepatocellular carcinoma chemotherapeutics with natural anticancer agents. Nutr Rev. Dec; 65 (2007)

135) Hande K.R. Clinical applications of anticancer drugs targeted to topoisomerase II. Biochim. Biophys. Acta 1400 (1-3), (1998) 173-184.

136) Hande K.R. Etoposide: four decades of development of a topoisomerase II inhibitor. Eur. J. Cancer 34 (10), (1998) 1514-1521.

137) Takimoto C.H., Wright J., and Arbuck S.G. Clinical applications of the camptothecins. Biochim. Biophys. Acta1400 (1-3), (1998) 107-119.

138) Baldwin E.L., and Osheroff N. Etoposide, topoisomerase II and cancer., Curr. Med. Chem. Anti-Cancer Agents 5 (4), (2005) 363-372.

139) McClendon A.K., Osheroff N. DNA topoisomerase II, genotoxicity, and cancer. Mutat Res. Oct 1; 623 (1-2) (2007) 83-97.

140) Baguley B.C., Leteurtre F., Riou J.F., Finlay G.J., and Pommier Y. A carbamate analogue of amsacrine with activity against non-cycling cells stimulates topoisomerase II cleavage at DNA sites distinct from those of amsacrine. Eur. J. Cancer 33 (2), (1997) 272-279.

141) Sehested M., Holm B., and Jensen P.B. Dexrazoxane for protection against cardiotoxic effects of anthracyclines. J. Clin. Oncol. 14 (10), (1996) 2884.

142) Walker J.V., and Nitiss J.L. DNA topoisomerase II as a target for cancer chemotherapy. Cancer Invest. 20 (4), (2002) 570-589.

143) Utsugi T., Shibata J., Sugimoto Y., Aoyagi K., Wierzba K., Kobunai T., Terada T., Ohhara T., Tsuruo T., and Yamada Y. Antitumor activity of a novel podophyllotoxin derivative (TOP-53) against lung cancer and lung metastatic cancer. Cancer Res. 56 (12), (1996) 2809-2814.

144) Byl J.A., Cline S.D., Utsugi T., Kobunai T., Yamada Y., and Osheroff N. DNA topoisomerase II as the target for the anticancer drug TOP-53: mechanistic basis for drug action., Biochemistry 40 (3), (2001) 712-718.

145) Barnes S., Peterson T. G., and Coward L. Rationale for the use of genistein-containing soy matrices in chemoprevention trials for breast and prostate cancer. J. Cell. Biochem. Suppl. 22, (1995) 181-187.

146) Lamartiniere C.A. Protection against breast cancer with genistein: a component of soy. Am. J. Clin. Nutr. 71(6 Suppl), (2000) 1705S-1707S.

147) Spitzner Jr., Chung I.K., Gootz T.D., McGuirk P.R., and Muller M.T. Analysis of eukaryotic topoisomerase II cleavage sites in the presence of the quinolone CP-115,953 reveals drug-dependent and -independent recognition elements. Mol. Pharmacol. 48 (2), (1995) 238-249.

148) Bromberg K.D., Burgin A.B., and Osheroff N. Quinolone action against human topoisomerase IIalpha: stimulation of enzyme-mediated double-stranded DNA cleavage., Biochemistry 42 (12), (2003) 3393-3398.

149) Elsea S.H., McGuirk P.R., Gootz T.D., Moynihan, M., and Osheroff N. Drug features that contribute to the activity of quinolones against mammalian topoisomerase II and cultured cells: correlation between enhancement of enzyme-mediated DNA cleavage in

vitro and cytotoxic potential.., Antimicrob. Agents Chemother. 37 (10), (1993) 2179-2186.

150) Utsugi T., Aoyagi K., Asao T., Okazaki S., Aoyagi Y., Sano M., Wierzba K., and Yamada Y. Antitumor activity of a novel quinoline derivative, TAS-103, with inhibitory effects on topoisomerases I and II. Jpn. J. Cancer Res. 88, (1997) 992-1002.

151) Fortune J.M., Velea L., Graves D.E., and Osheroff N. DNA topoisomerases as targets for the anticancer drug TAS-103: DNA interactions and topoisomerase catalytic inhibition. Biochemistry 38, (1999) 15580-15586.

152) Nelson E.M., Tewey K.M., and Liu L.F. Mechanism of antitumor drug action: poisoning of mammalian DNA topoisomerase II on DNA by 4'-(9-acridinylamino)-methanesulfon-m-anisidide. Proc. Natl. Acad. Sci. USA 81 (5), (1984) 1361-1365.

153) Pommier Y., Minford J.K., Schwartz R.E., Zwelling L.A., and Kohn K.W. Effects of the DNA intercalators 4'-(9-acridinylamino)methanesulfon-m-anisidide and 2-methyl-9-hydroxyellipticinium on topoisomerase II mediated DNA strand cleavage and strand passage. Biochemistry 24 (23), (1985) 6410-6416.

154) Maxwell A. DNA gyrase as a drug target. Trends Microbiol. 5, (1997) 102-109.

155) Osheroff N. Effect of antineoplastic agents on the DNA cleavage/religation reaction of eukaryotic topoisomerase II: inhibition of DNA religation by etoposide. Biochemistry 28 (15), (1989) 6157-6160.

156) Robinson M.J., and Osheroff N. Effects of antineoplastic drugs on the post-strand-passage DNA cleavage/religation equilibrium of topoisomerase II. Biochemistry 30 (7), (1991) 1807-1813.

157) You Y. Podophyllotoxin derivatives: current synthetic approaches for new anticancer agents. Curr Pharm Des. 11 (13) (2005) 1695-1717

158) Corbett A.H., Hong D., and Osheroff N. Exploiting mechanistic differences between drug classes to define functional drug interaction domains on topoisomerase II. Evidence that several diverse DNA cleavage-enhancing agents share a common site of action on the enzyme. J. Biol. Chem. 268 (19), (1993) 14394-14398.

159) Froelich-Ammon S.J., and Osheroff N. Topoisomerase poisons: harnessing the dark side of enzyme mechanism. J. Biol. Chem. 270, (1995) 21429-21432.

160) Burden D.A., Kingma P.S., Froelich-Ammon S.J., Bjornsti M.A., Patchan M.W., Thompson R.B., and Osheroff N. Topoisomerase II.etoposide interactions direct the formation of drug-induced enzyme-DNA cleavage complexes. J. Biol. Chem.271, (1996) 29238-29244.

161) Tse-Dinh Y.C. Exploring DNA topoisomerases as targets of novel therapeutic agents in the treatment of infectious diseases. Infect Disord Drug Targets. Mar; 7 (1) (2007) 3-9

162) Beck W.T., Danks M.K., Wolverton J.S., Kim R., and Chen M. Drug resistance associated with altered DNA topoisomerase II. Adv. Enzyme Reg. 33, (1993) 113-127

163) Vassetzky Y.S., Alghisi G.C., and Gasser S.M. DNA topoisomerase II mutations and resistance to anti-tumor drugs. Bioessays 17, (1995) 767-774.

164) Kingma P.S., Burden D.A., and Osheroff N. Binding of etoposide to topoisomerase II in the absence of DNA: decreased affinity as a mechanism of drug resistance. Biochemistry 38, (1999) 3457-3461.

165) Leroy D., Kajava A.V., Frei, C., and Gasser, S.M. Analysis of etoposide binding to subdomains of human DNA topoisomerase II alpha in the absence of DNA. Biochemistry 40 (6), (2001) 1624-1634.

166) Pommier Y., and Marchand C. Interfacial inhibitors of protein-nucleic acid interactions. Curr. Med. Chem. Anti-CancerAgents 5 (4), (2005) 421-429.

167) Waring M. Variation of the supercoils in closed circular DNA by binding of antibiotics and drugs: evidence for molecular models involving intercalation. J. Mol. Biol. 54 (2), (1970) 247-279.

168) Waring M.J. Drugs and DNA: uncoiling of the DNA double helix as evidence of intercalation. Humangenetik 9 (3), (1970) 234-236.

169) Pommier Y. DNA Topoisomerase II inhibitors. In: Teicher, B. A.(ed). Cancer Therapeutics: Experimental and Clinical Agents, Humana Press,Totowa, New Jersey (1997)

170) Cooney D.A., Covey J.M., Kang G.J., Dalal M., McMahon J.B., and Johns D.G. Initial mechanistic studies with merbarone (NSC 336628). Biochem. Pharmacol. 34 (18), (1985) 3395-3398.

171) Andoh T, and Ishida R. Catalytic inhibitors of DNA topoisomerase II. Biochim. Biophys. Acta 1400 (1-3), (1998) 155-171.

172) Gellert M., O'Dea M.H., Itoh T., and Tomizawa J. Novobiocin and coumermycin inhibit DNA supercoiling catalyzed by DNA gyrase. Proc. Natl.Acad. Sci., USA 73, (1976) 4474-4478.

173) Sugino A., Higgins N.P., Brown P.O., Peebles C.L., and Cozzarelli N.R. Energy coupling in DNA gyrase and the mechanism of action of novobiocin. Proc. Natl. Acad. Sci. USA 75 (10), (1978) 4838-4842.

174) Drake F.H., Hofmann G.A., Mong S.M., Bartus J.O., Hertzberg R.P., Johnson R.K., Mattern M.R., and Mirabelli C.K. In vitro and intracellular inhibition of topoisomerase II by the antitumor agent merbarone. Cancer Res.49 (10), (1989) 2578-2583.

175) Fortune J.M., and Osheroff N. Merbarone inhibits the catalytic activity of human topoisomerase IIalpha by blocking DNA cleavage. J. Biol. Chem. 273 (28), (1998) 17643-17650.

176) Larsen A.K., Escargueil A.E., and Skladanowski A. Catalytic topoisomerase II inhibitors in cancer therapy. Pharmacol.Ther. 99 (2), (2003) 167-181.

177) Downes C.S., Clarke D.J., Mullinger A.M., Gimenez-Abian J.F., Creighton A.M., and Johnson R.T. A topoisomerase II-dependent G2 cycle checkpoint in mammalian cells/. Nature 372 (6505), (1994) 467-470.

178) Anderson H., and Roberge M. Topoisomerase II inhibitors affect entry into mitosis and chromosome condensation in BHK cells. Cell Growth Differ. 7 (1), (1996) 83-90.

179) Hartmann J.T., Lipp H.P. Camptothecin and podophyllotoxin derivatives: inhibitors of topoisomerase I and II - mechanisms of action, pharmacokinetics and toxicity profile.., Drug Saf.; 29 (3) (2006) 209-30.

180) Kealy T.J., Pauson P.L. Nature, 168, (1951) 1039.

181) Miller S.A., Tebboth J.A., Tremaine J.F. J.Chem. Soc. (1952) 632.

182) Wilkinson G., Rosenblum M., Whiting M.C., Woodward R.B. The structure of iron bis –cyclopentadienyl J. Am. Chem. Soc.74, (1952) 2125.

183) Fischer E.O., Pfab W.Z. A cationic bis-fulven complex of cobaltNaturforsch., 7b, (1952) 377.

184) Woodward R.B., Rosenblum M., Whiting M.C. A new aromatic system., J.Am. Chem.Soc. 74, (1952) 3458.

185) Jaouen G., Vessieres A., Butler I.S. Acc. Chem. Res.26, (1993) 361.

186) Fish R.H., Jaouen G. Organometallics, 22, (2003) 2166.

187) Metzler-Nolte N. Labeling of Biomolecules for Medicinal Applications-Bioorganometallic ChemistryAngew. Chem. 113, (2001) 1072; Angew. Chem., Int. Ed., 40, (2001) 1040.

188) Shago R.F., Swarts J.C., Kreft E., Van Rensburg C.E. Antineoplastic activity of a series of ferrocene-containing alcohols., Anticancer Res. 27 (2007) 3431-3.

189) Kollmann M., Sourjik V., In silico biology: from simulation to understanding. Curr Biol. 20;17(4) (2007) 132-134.

190) Michielin O. Application of molecular modeling to new therapeutic cancer approaches., Bull Cancer. 1; 94 (9) (2007) 763-768.

191) Peltason L., Bajorath J., SAR index: quantifying the nature of structure-activity relationships., J Med Chem. 15; 50 (23) (2007) 5571-5578

192) Dahl S.G., Sylte I., Molecular modelling of drug targets: the past, the present and the future. Basic Clin Pharmacol Toxicol. 96(3) (2005)151-155.

193) Ernesto E. and Enrique M. 3D Connectivity Indices in QSPR/QSAR Studies., J. Chem. Inf. Comput. Sci., 41 (3), (2001) 791 -797.

194) Philip P. and Saxena Anil K. Evaluation of Binary QSAR Models Derived from LUDI and MOE Scoring Functions for Structure Based Virtual Screening., J. Chem. Inf. Model., 46 (1), (2006) 39 -51.

195) Stanton David T. On the Physical Interpretation of QSAR Models., J. Chem. Inf. Comput. Sci., 43 (5), (2003) 1423 -1433.

196) Rajarshi G. and Jurs Peter C. Determining the Validity of a QSAR Model - A Classification Approach., J. Chem. Inf. Model., 45 (1), (2005) 65 -73.

197) Yukio T. and Iwao F. Prediction-Weighted Partial Least-Squares Regression Method (PWPLS) 2: Application to CoMFA., J. Chem. Inf. Comput. Sci., 37 (6), (1997) 1152 - 1157.

198) Yi F., Shi Leming M., Kohn Kurt W., Yves P., and Weinstein John N. Quantitative Structure-Antitumor Activity Relationships of Camptothecin Analogues: Cluster Analysis and Genetic Algorithm-Based Studies., J. Med. Chem., 44 (20), (2001) 3254 - 3263.

199) Laura M., Matteo M., Giovannella S., Federico C., Maurizio B., and Fabrizio M. A Genetic-Function-Approximation-Based QSAR Model for the Affinity of Arylpiperazines toward 1 Adrenoceptors., J. Chem. Inf. Model., 46 (3), (2006) 1466 - 1478.

200) Taha Mutasem O. and AlDamen Murad A. Effects of Variable Docking Conditions and Scoring Functions on Corresponding Protein-Aligned Comparative Molecular Field Analysis Models Constructed from Diverse Human Protein Tyrosine Phosphatase 1B Inhibitors., J. Med. Chem., 48 (25), (2005) 8016 -8034.

201) Subhash A., Kamalakar J., and Kulkarni Sudhir A. Three-Dimensional QSAR Using the k-Nearest Neighbor Method and Its Interpretation., J. Chem. Inf. Model., 46 (1), (2006) 24 -31.

202) Kunal R., and Thomas Leonard J. QSAR Analyses of 3-(4-Benzylpiperidin-1-yl)-N-phenylpropylamine Derivatives as Potent CCR5 Antagonists., J. Chem. Inf. Model., 45 (5), (2005) 1352 -1368.

203) Robinson Daniel D., Lyne Paul D., and Graham Richards W. Alignment of 3D-Structures by the Method of 2D-Projections., J. Chem. Inf. Comput. Sci., 39 (3), (1999) 594-600.

204) Lemmen C., Lengauer T. Computational methods for the structural alignment of molecules. J Comput Aided Mol Des. Mar; 14 (3) (2000) 215-232.

205) Roberta B., Thuy D., Theovan W., Marcel de G., Edwin K., and Paul V. Comparative Spectra Analysis (CoSA): Spectra as Three-Dimensional Molecular Descriptors for the Prediction of Biological Activities., J. Chem. Inf. Comput. Sci., 39 (5), (1999) 861 -886.

206) Ernesto E., Enrique M., and Perdomo-Lopez I. Can 3D Structural Parameters Be Predicted from 2D (Topological) Molecular Descriptors?., J. Chem. Inf. Comput. Sci., 41 (4), (2001) 1015-1021.

207) Shu-Shen L., Chun-Sheng Y., and Lian-Sheng W. Combined MEDV-GA-MLR Method for QSAR of Three Panels of Steroids, Dipeptides, and COX-2 Inhibitors., J. Chem. Inf. Comput. Sci., 42 (3), (2002) 749-756.

208) Thierry L. and Hoffmann Remy D. On the Use of Chemical Function-Based Alignments as Input for 3D-QSAR., J. Chem. Inf. Comput. Sci., 38 (2), (1998) 325-330.

209) Mello Castanho Amboni Renata D., Berenice da Silva J., Rosendo Augusto Y., and Vilma Edite Fonseca H. Quantitative Structure-Odor Relationships of Aliphatic Esters Using Topological Indices., J. Agric. Food Chem., 48 (8), (2000) 3517-3521.

210) Tropsha A., Golbraikh A. Predictive QSAR modeling workflow, model applicability domains, and virtual screening. Curr Pharm Des. 13(34) (2007) 3494-3504.

211) Jaworska J., Nikolova-Jeliazkova N., Aldenberg T. QSAR applicabilty domain estimation by projection of the training set descriptor space: a review. Altern Lab Anim. Oct. 33(5) (2005) 445-459.

212) Akamatsu M. Current state and perspectives of 3D-QSAR. Curr Top Med Chem. Dec. 2 (12) (2002) 1381-1394.

213) Seville P.C., Li H.Y., Learoyd T.P. Spray-dried powders for pulmonary drug delivery. Crit Rev Ther Drug Carrier Syst.24 (4) (2007) 307-360.

214) N Tosi G., Costantino L., Ruozi B., Forni F., Vandelli M.A. Polymeric nanoparticles for the drug delivery to the central nervous system., Polymeric nanoparticles for the drug delivery to the central nervous system. Expert Opin Drug Deliv. Feb. 5 (2) (2008) 155-174.

215) Hsieh P.C., Davis M.E., Gannon J., MacGillivray C., Lee R.T. Controlled delivery of PDGF-BB for myocardial protection using injectable self-assembling peptide nanofibers. J Clin Invest. Jan. 116 (1) (2006) 237-248

216) Sawyer A.J., Piepmeier J.M., Saltzman W.M. New methods for direct delivery of chemotherapy for treating brain tumors., Yale J Biol Med. Dec.79 (3-4) (2006) 141-152.

217) Baker A.H., Sica V., Work L.M., Williams-Ignarro S., de Nigris F., Lerman L.O., Casamassimi A., Lanza A., Schiano C., Rienzo M., Ignarro L.J., Napoli C. Brain

protection using autologous bone marrow cell, metalloproteinase inhibitors, and metabolic treatment in cerebral ischemia.., Proc Natl Acad Sci U S A. 104 (9) (2007) 3597-602.

218) Brigger I., Dubernet C., Couvreur P. Nanoparticles in cancer therapy and diagnosis. Adv Drug Deliv Rev. 13;54 (5) (2002) 631-651.

219) Wilkinson J.M. Nanotechnology applications in medicine. Med. Device Technol. 14 (5), (2003) 29–31.

220) Roco M.C. Nanotechnology: convergence with modern biology and medicine. Curr. Opin. Biotechnol. 14, (2003) 337–346.

221) Brigger I. et al. Nanoparticles in cancer therapy and diagnosis. Adv. Drug Deliv. Rev. 54, (2002) 631–651.

222) Panyam J. et al. Biodegradable nanoparticles for drug and gene delivery to cells and tissue. Adv. Drug Deliv. Rev. 55, (2003) 329–347.

223) Lamprecht A. et al. Biodegradable nanoparticles for targeted drug delivery in treatment of inflammatory bowel disease. J. Pharmacol. Exp. Ther. 299, (2001) 775–781.

224) Passirani C. et al. Long-circulating nanoparticles bearing heparin or dextran covalently bound to poly(methyl methacrylate). Pharm. Res. 15, (1998) 1046–1050.

225) Desai M.P. et al. Gastrointestinal uptake of biodegradable microparticles: effect of particle size. Pharm. Res. 13, (1996) 1838–1845.

226) Desai M.P. et al. The mechanism of uptake of biodegradable microparticles in Caco-2 cells is size dependent. Pharm. Res. 14, (1997) 1568–1573.

227) Panyam J. et al. Fluorescence and electron microscopy probes for cellular and tissue uptake of poly(D,L-lactide-co-glycolide) nanoparticles. Int. J. Pharm. 262, (2003) 1–11.

228) Thomas M. et al. Conjugation to gold nanoparticles enhances polyethylenimine's transfer of plasmid DNA into mammalian cells. Proc. Natl. Acad. Sci. U. S. A. 100, (2003) 9138–9143.

229) Scherer F. et al. Magnetofection: enhancing and targeting gene delivery by magnetic force in vitro and in vivo. Gene Ther. 9, (2002) 102–109.

230) Monsky W.L. et al. Augmentation of transvascular transport of macromolecules and nanoparticles in tumors using vascular endothelial growth factor. Cancer Res. 59, (1999) 4129–4135.

231) Maeda H. The enhanced permeability and retention (EPR) effect in tumor vasculature: the key role of tumor-selective macromolecular drug targeting. Adv. Enzyme Regul. 41, (2001) 189–207.

232) Sahoo S.K. et al. Pegylated zinc protoporphyrin: a water-soluble heme oxygenase inhibitor with tumor-targeting capacity. Bioconjugate Chem. 13, (2002) 1031–1038.

233) Panyam J. et al. Efficiency of Dispatch® and Infiltrator® cardiac infusion catheters in arterial localization of nanoparticles in a porcine coronary model of restenosis. J. Drug Target. 10, (2002) 515–523.

234) Guzman L.A. et al. Local intraluminal infusion of biodegradable polymeric nanoparticles. A novel approach for prolonged drug delivery after balloon angioplasty. Circulation 94, (1996) 1441–1448.

235) Lanza G.M. et al. Targeted antiproliferative drug delivery to vascular smooth muscle cells with a magnetic resonance imaging nanoparticle contrast agent: implications for rational therapy of restenosis. Circulation 106, (2002) 2842–2847.

236) Lockman P.R. et al. Nanoparticle technology for drug delivery across the blood–brain barrier. Drug Dev. Ind. Pharm. 28, (2002) 1–13.

237) Fisher R.S. et al. Potential new methods for antiepileptic drug delivery. CNS Drugs 16, (2002) 579–593.

238) Kastin A.J. et al. Interleukin-10 as a CNS therapeutic: the obstacle of the blood–brain/blood–spinal cord barrier. Mol. Brain Res. 114, (2003) 168–171.

239) Sun H. et al. Drug efflux transporters in the CNS. Adv. Drug Deliv. Rev. 55, (2003) 83–105.

240) Kreuter J. et al. Direct evidence that polysorbate-80-coated poly(butylcyanoacrylate) nanoparticles deliver drugs to the CNS via specific mechanisms requiring prior binding of drug to the nanoparticles. Pharm. Res. 20, (2003) 409–416.

241) Cherian A.K. et al. Self-assembled carbohydrate-stabilized ceramic nanoparticles for the parenteral delivery of insulin. Drug Dev. Ind. Pharm. 26, (2000) 459–463.

242) Jain T.K. et al. Nanometer silica particles encapsulating active compounds: a novel ceramic drug carrier. J. Am. Chem. Soc. 120, (1998) 11092–11095.

243) Roy I. et al. Calcium phosphate nanoparticles as novel non-viral vectors for targeted gene delivery. Int. J. Pharm. 250, (2003) 25–33.

244) Lal M.L. et al. Silica nanobubbles containing an organic dye in a multilayered organic/inorganic heterostructure with enhanced luminescence. Chem. Mater. 19, (2000) 2632–2639.

245) Badley R.D. et al. Surface modification of colloidal silica. Langmuir 6, (1990) 792–801

246) Nishiyama N. et al. Polymeric micelle drug carrier systems: PEG-PAsp(Dox) and second generation of micellar drugs. Adv. Exp. Med. Biol. 519, (2003) 155–177.

247) Kataoka K. et al. Block copolymer micelles for drug delivery: design, characterization and biological significance. Adv. Drug Deliv. Rev. 47, (2001) 113–131.

248) Rosler A. et al. Advanced drug delivery devices via self-assembly of amphiphilic block copolymers. Adv. Drug Deliv. Rev. 53, (2001) 95–108.

249) Jones M. et al. Polymeric micelles – a new generation of colloidal drug carriers. Eur. J. Pharm. Biopharm. 48, (1999) 101–111.

250) Savic R. et al. Micellar nanocontainers distribute to defined cytoplasmic organelles. Science 300, (2003) 615–618.

251) Nakanishi T. et al. Development of the polymer micelle carrier system for doxorubicin. J. Control. Release 74, (2001) 295–302.

252) Yokoyama M. et al. Selective delivery of adriamycin to a solid tumor using a polymeric micelle carrier system. J. Drug Target. 7, (1999) 171–186.

253) Matsumura Y. et al. Reduction of the side effects of an antitumor agent, KRN5500, by incorporation of the drug into polymeric micelles. Jpn. J. Cancer Res. 90, (1999) 122–128.

254) Sessa G. et al. Formation of artificial lysosome in vitro. J. Clin. Invest. 48, (1969) 76–77.

255) Bangham A.D. et al. Diffusion of univalent ions across the lamellae of swollen phospholipids. J. Mol. Biol. 13, (1965) 238–252.

256) Gabizon A. et al. Development of liposomal anthracyclines: from basics to clinical applications. J. Control. Release 53, (1998) 275–279.

257) Allen T.M. Liposomes. Opportunities in drug delivery. Drugs 54, (1997) 8–14.

258) Lasic D.D. et al. Sterically stabilized liposomes in cancer therapy and gene delivery. Curr. Opin. Mol. Ther. 1, (1999) 177–185.

259) Quintana A. et al. Design and function of a dendrimer-based therapeutic nanodevice targeted to tumor cells through the folate receptor. Pharm. Res. 19, (2002) 1310–1316.

260) Padilla De Jesus O.L. et al. Polyester dendritic systems for drug delivery applications: in vitro and in vivo evaluation. Bioconjugate Chem. 13, (2002) 453–461.

261) Kihara F. et al. Effects of structure of polyamidoamine dendrimer on gene transfer efficiency of the dendrimer conjugate with alpha-cyclodextrin. Bioconjugate Chem. 13, (2002) 1211–1219.

262) Tripathi P.K. et al. Dendrimer grafts for delivery of 5- fluorouracil. Pharmazie 57, (2002) 261–264.

263) Emerich D.F. et al. Nanotechnology and medicine. Expert Opin. Biol. Ther. 3, (2003) 655–663.

264) Han M. et al. Quantum-dot-tagged microbeads for multiplexed optical coding of biomolecules. Nat. Biotechnol. 19, (2001) 631–635.

265) Clark H.A. et al. Optical nanosensors for chemical analysis inside single living cells. 2. Sensors for pH and calcium and the intracellular application of PEBBLE sensors. Anal. Chem. 71, (1999) 4837–4843.

266) Sumner J.P. et al. A fluorescent PEBBLE nanosensor for intracellular free zinc. Analyst 127, (2002) 11–16.

267) Peira E. et al. In vitro and in vivo study of solid lipid nanoparticles loaded with superparamagnetic iron oxide. J. Drug Target. 11, (2003) 19–24.

268) Ito A. et al. Tumor regression by combined immunotherapy and hyperthermia using magnetic nanoparticles in an experimental subcutaneous murine melanoma. Cancer Sci. 94, (2003) 308–313.

269) Chemla Y.R. et al. Ultrasensitive magnetic biosensor for homogeneous immunoassay. Proc. Natl. Acad. Sci. U. S. A. 97, (2000) 14268–14272.

270) Lubbe A.S. et al. Preclinical experiences with magnetic drug targeting: tolerance and efficacy. Cancer Res. 56, (1996) 4694–4701.

271) Babincova M. et al. High-gradient magnetic capture of ferrofluids: implications for drug targeting and tumor embolization.Z. Naturforsch. (Sect. C) 56, (2001) 909–911.

272) Tsavellas G. et al. Flow cytometry correlates with RT-PCR for detection of spiked but not circulating colorectal cancer cells. Clin. Exp. Metastasis 19, (2002) 495–502.

273) Collarini E.J. et al. Comparison of methods for erythroblast selection: application to selecting fetal erythroblasts from maternal blood. Cytometry 45, (2001) 267–276.

274) Martin Malmsten., Soft drug delivery systems. Soft Matter, 2, (2006) 760–769.

275) Xiu-Lian D., Kui W., Ya K., Lan Y., Rong-Chang L., Zhong Y., Kwok Ping H., Zhong Ming Q. Apotransferrin is internalized and distributed in the same way as holotransferrin in K562 cells. J Cell Physiol 201 (1) (2004) 45-54.

276) Zhong M.Q., Hongyan L., Hongzhe U., Kwokping H. Targeted drug delivery via the transferrin receptor-mediated endocytosis pathway. Pharmacol Rev; 54 (2002) 561–587.

277) Kratz F., Roth T., Fichiner I., Schumacher P., Fiebig H.H., Unger C. In vitro and in vivo efficacy of acid-sensitive transferrin and albumin doxorubicin conjugates in a human xenograft panel and in the MDA-MB-435 mamma carcinoma model. J Drug Target;8 (5) (2000) 305-318.

278) Von Bonsdorff L. et al. Development of a pharmaceutical apotransferrin product for iron binding therapy. Biologicals 29, (2001) 27–37.

279) Parkkinen J. et al. Function and therapeutic development of apotransferrin. Vox Sang. 83 (Suppl. 1), (2002) 321–326.

280) MacGillivray R.T. et al. Two highresolution crystal structures of the recombinant N-lobe of human transferrin reveal a structural change implicated in iron release. Biochemistry 37, (1998) 7919–7928.

281) Hirose M. The structural mechanism for iron uptake and release by transferrins. Biosci. Biotechnol. Biochem. 64, (2000) 1328–1336.

282) Davis S.S. Biomedical applications of nanotechnology – implications for drug targeting and gene therapy. Trends Biotechnol. 15, (1997) 217–224.

283) Li H. and Qian, Z.M. Transferrin/transferrin receptor-mediated drug delivery. Med. Res. Rev. 22, (2002) 225–250.

284) Van Campenhout A. et al. Transferrin modifications and lipid peroxidation: Implications in diabetes mellitus. Free Radic. Res. 37, (2003) 1069–1077.

285) Rice-Evans C. Oxidised low density lipoproteins. In Free Radicas: From Basic Science to Medicine (Poli, G. et al., eds), Birhäuser Verlag, Basel, (1993) 323–339.

286) Wolff S.P. and Dean R.T. Glucose autooxidation and protein modification. The potential role of 'autooxidive glycosylation' in diabetes. Biochem. J. 245, (1987) 243–250.

287) He Q.Y. et al. The chloride effect is related to anion binding in determining the rate of iron release from the human transferring N-lobe. Biochem. J. 350, (2000) 909–915.

288) Beutler E. et al. Molecular characterization of a case of atransferrinemia. Blood 96, (2000) 4071–4074.

289) Lecureuil C. et al. Transgenic mice as a model to study the regulation of human transferrin expression in Sertoli cells. Hum. Reprod. 6, (2004) 1300–1307.

290) Suire S. et al. Transferrin gene expression and secretion in rat Sertoli cells. Mol. Reprod. Dev. 48, (1997) 168–175.

291) Tsutsumi M. et al. Transferrin gene expression and synthesis by cultured choroid plexus epithelial cells. Regulation by serotonin and cyclic adenosine 3′,5′-monophosphate. J. Biol. Chem. 264, (1989) 9626–9631.

292) Bloch B. et al. Transferrin gene expression visualised in oligodendrocytes of the rat brain by using in situ hybridization and immunohistochemistry. Proc. Natl. Acad. Sci.U. S. A. 82, (1985) 6706–6710.

293) Nicolson G.L. et al. Differential expression of a Mr approximately 90,000 cell surface transferrin receptor-related glycoprotein on murine B16 metastatic melanoma sublines selected for enhanced brain or ovary colonization. Cancer Res. 50, (1990) 515–520.

294) Inoue T. et al. Differences in transferrin response and numbers of transferrin receptors in rat and human mammary carcinoma lines of different metastatic potentials. J. Cell. Physiol. 156, (1993) 212–217.

295) Qian Z.M. et al. Targeted drug delivery via the transferrin receptor-mediated endocytosis pathway. Pharmacol. Rev. 54, (2002) 561–587.

296) Hayashi A. et al. Studies on familial hypotransferrinemia: unique clinical course and molecular pathology. Am. J. Hum. Genet. 53, (1993) 201–213.

297) Hemadi M. et al. Transferrin's mechanism of interaction with receptor 1. Biochemistry 43, (2004) 1736–1745.

298) Paterson S. et al. Intravesicular pH and iron uptake by immature erythroid cells. J. Cell. Physiol. 120, (1984) 225–232.

299) Harford J.B. et al. Molecular mechanisms of iron metabolism. In The Molecular Basis of Blood Diseases (Stamatoyannopoulos, G.A. et al. eds), (1994) 351–378, Philadelphia: W.B. Saunders Co.

300) Fleming R.E. et al. Transferrin receptor 2: continued expression in mouse liver in the face of iron overload and in hereditary hemochromatosis. Proc. Natl. Acad. Sci. U. S. A.97, (2000) 2214–2219.

301) Kaminski K.A. et al. Oxidative stress and neutrophil activation–the two keystones of ischemia/reperfusion injury. Int. J. Cardiol. 86, (2002) 41–59.

302) Koc M. et al. Levels of some acute-phase proteins in the serum of patients with cancer during radiotherapy. Biol. Pharm. Bull. 26, (2003) 1494–1497.

303) Kruger W. et al. Early infections in patients undergoing bone marrow or blood stem cell transplantation–a 7 year single centre investigation of 409 cases. Bone Marrow Transplant. 23, (1999) 589–597.

304) Durken M. et al. Nontransferrin-bound iron in serum of patients receiving bone marrow transplants. Free Radic. Biol. Med. 22, (1997) 1159–1163.

305) Okamoto T. et al. Effects of insulin and transferrin on the generation of lymphokineactivated killer cells in serum-free medium. J. Immunol. Methods 195, (1996) 7–14.

306) Sadava D., Phillips T., Lin C., Kane S.E. Transferrin overcomes drug resistance to artemisinin in human small-cell lung carcinoma cells. Cancer Lett. May 28;179 (2) (2002) 151-156.

307) Cavanaugh P.G., Jia L., Zou Y., Nicolson G.L. Transferrin receptor overexpression enhances transferrin responsiveness and the metastatic growth of a rat mammary adenocarcinoma cell line. Breast Cancer Res Treat. Aug;56 (3) (1999) 203-217.

308) Yang D.C., Wang F., Elliott R.L., Head J.F. Expression of transferrin receptor and ferritin H-chain mRNA are associated with clinical and histopathological prognostic indicators in breast cancer. Anticancer Res. Jan-Feb;21 (1B) (2001) 541-549.

309) Walker R.A., Day S.J. Transferrin receptor expression in non-malignant and malignant human breast tissue., J Pathol. Mar;148 (3) (1986) 217-224.

310) Racz A., Brass N., Heckel D., Pahl S., Remberger K. and Meese E. Expression analysis of genes at 3q26-q27 involved in frequent amplification in squamous cell lung carcinoma., Eur J Cancer. Apr;35 (4) (1999) 641-646.

311) Whitney J.F., Clark J.M., Griffin T.W., Gautam S., Leslie K.O. Transferrin receptor expression in nonsmall cell lung cancer. Histopathologic and clinical correlates., Cancer. Jul 1;76 (1) (1995) 20-25.

312) Kayser K., Ernst M., Bubenzer J. Expression of transferrin- and interleukin-2-receptors, and HLA-DR in human lung carcinoma., Exp Pathol.;41 (1) (1991) 37-43.

313) Kondo K., Noguchi M., Mukai K., Matsuno Y., Sato Y., Shimosato Y., Monden Y. Transferrin receptor expression in adenocarcinoma of the lung as a histopathologic indicator of prognosis., Chest. Jun;97 (6) (1990) 1367-1371.

314) Drewinko B., Moskwa P., Reuben J. Expression of transferrin receptors is unrelated to proliferative status in cultured human colon cancer cells. Anticancer Res. Mar-Apr;7 (2) (1987) 139-141.

315) Alessia C., Isabella O., Silvia D., Gualtiero M., Mauro B., Nadia Maria S., Fabio M., Cesare P. and Ugo T. Transferrin receptor 2 is frequently expressed in human cancer cell lines., Blood Cells Mol Dis. Jul-Aug;39 (1) (2007) 82-91.

316) Wen Dennis Y. M.B., B.S., Hall Walter A. M.D. Conrad John B.S. Godal A., Florenes V., Fodstad Oystein M.D., In Vitro and In Vivo Variation in Transferrin Receptor Expression on a Human Medulloblastoma Cell Line. Neurosurgery. June 36 (6) (1995) 1158-1164.

317) Prior R., Reifenberger G., Wechsler W. Transferrin receptor expression in tumours of the human nervous system: relation to tumour type, grading and tumour growth fraction., Virchows Arch A Pathol Anat Histopathol.416 (6) (1990) 491-496

318) Kobayashi T., Ishida T., Okada Y., Ise S., Harashima H., Kiwada H. Effect of transferrin receptor-targeted liposomal doxorubicin in P-glycoprotein-mediated drug resistant tumor cells., Int J Pharm. Feb 1;329 (1-2) (2007) 94-102.

319) Fritzer M., Szekeres T., Szüts V., Jarayam H.N., Goldenberg H. Cytotoxic effects of a doxorubicin-transferrin conjugate in multidrug-resistant KB cells., Biochem Pharmacol. Feb 23;51 (4) (1996) 489-493.

320) Wang F., Jiang X., Yang D.C., Elliott R.L., Head J.F., Doxorubicin-gallium-transferrin conjugate overcomes multidrug resistance: evidence for drug accumulation in the nucleus of drug resistant MCF-7/ADR cells., Anticancer Res. Mar-Apr;20 (2A) (2000) 799-808.

321) Kondapi A.K., Mulpuri N., Mandraju R.K., Sasikaran B., Subba Rao K., Int. J. Dev. Neurosci. 22 (2004) 19–30.

322) Cohn et al, von Bonsdorff L., Tolo H., Lindeberg E., Nyman T., Harju A., Parkkinen J. Development of a pharmaceutical apotransferrin product for iron binding therapy. Biologicals. Mar; 29 (1) (2001) 27-37.

323) Bradford M.M. A rapid and sensitive method for the quantitation of microgram quantities of protein utilizing the principle of protein-dye binding.Anal. Biochem. 72 (1976) 248–254.

324) Broadhead G.D., Osgerby J.M., Pauson P.L. J. Chem. Soc. 77 (1958) 650–656.

325) Graham P.J., Lindsey R.V., Parshall G.W., Peterson M.L., Whitman G.M. Some Acyl Ferrocenes and their Reactions. J. Am. Chem. Soc. 79 (1957) 3416–3420.

326) Osgerby J.M., Pauson P.L. J. Chem. Soc. 77 (1958) 650–656.

327) Osgerby J.M., Pauson P.L. part IX some disubstituted derivatives. (1961) 4604 4615.

328) Pauson P.L., Sandhu M.A, and Watts W.E. J. Chem. Soc. (1966) 251–255.

329) Weinmayr V.J. Hydrogen Fluoride as a Condensing Agent. V. Reactions of Dicyclopentadienyliron in Anhydrous Hydrogen FluorideJ. Am. Chem. Soc. 77 (1955) 3009–3011.

330) Knox G.R. and Pauson P.L. Ferrocene derivatives. Part VII . some sulphur derivatives JCS (1958) 692-696.

331) Rausch M.D. Convenient Synthesis of Ferrocenyl Aryl Sulfides J. Org. Chem. 26 (1961) 3579.

332) Kennethl Rinehart Jr., Motz Kayel M. and Sung M. Organic Chemistry of Ferrocene, I. JACS The Acetylation of Dialkylferrocenes volume 79. (1957) 2749-2754.

333) Tomonori Katada, Munehiro Nishida, Shinzi Kato and Masateru Mizuta., The preparation of ferrocenethiocarboxylic acid derivatives and their spectral properties. .j. Organo metallic chem. (1977) 129, 189-196.

334) Roberts D.T., Little W.F., Bursey M.M. Organic Chemistry of Ferrocene. II. The Preparation of Ferrocenyl Aliphatic. J. Am. Chem. Soc. 79 (1957) 3420–3424.

335) Sevenaidra Nnyh John P., Lewis and Ponde W. The Reaction of Acylferrocenes with Dimethyloxosulfonium Methylide and Dimethylsulfonium Methylide., J. Org. Chem., Vol. 37, No. 66,(1972) 4061-4063.

336) Combs C.S., Ashmore C., Bridges A.F., Swanson C.R.., Stephens W.D. Reactions of hydroxymethylferrocene. II. Sulfides. J. Org. Chem. 34 (1969) 1511–1512.

337) Myornr O., Woodward R.B. The Structure and Chemistry of Ferrocene.. Evidence Pertaining to the Ring Rotational Barrier., (1958) 5443-5449.

338) Hauser C.R., Lindsay J.K. Certain Alkylations with the Methiodide of N,N-Dimethylaminomethylferrocene. Synthesis of an a-Amino Acid Having the Ferrocene Group' J. Org. Chem. 22 (1957) 1246–1247.

339) Weliky N., Gould E.S. Studies in the Ferrocene Series. I. Some Reactions of Compounds Related to Monobenzoylferrocene. J. Am. Chem. Soc. 79 (1957) 2742–2746.

340) Kenneth L., Rinehart JR., Ronald J., Cursu JR. and Phillipe S. Organic Chemistry of Ferrocene. 11. The Preparation of w-Ferrocenyl Aliphatic Acids., JACS 79, (1957) 3420-3424.

341) Thomas T. Tidwell, T. G. Traylor ., Nucleophilic Substitution on Ferrocenylmethyl Chloride . J. Am. Chem. Soc. 88(14), (1966) 3442-3444.

342) Booth D.J., Rockett B.W. J. Chem. Soc., Section C (1968) 656–659.

343) Cerius2. A program suite for molecular modeling activities,Molecular Simulations, Scranton Road, Diego, USA

344) Tropsha A, Zheng W., Identification of the descriptor pharmacophores using variable selection QSAR: applications to database mining. Curr Pharm Des. 7(7) (2001) 599-612.

345) Sammi T., Silakari O., Ravikumar M. Three-dimensional quantitative structure-activity relationship modeling of gamma-secretase inhibitors using molecular field analysis. Chem Biol Drug Des Feb; 71 (2) (2008) 155-66.

346) Richard D. Cramer., Topomer CoMFA: A Design Methodology for Rapid Lead Optimization., J. Med. Chem., 46 (3) (2003) 374 -388.

347) Jonathan J. S., A. Daniel Jones, and Kenneth K. Tanji., QSAR Treatment of Electronic Substituent Effects Using Frontier Orbital Theory and Topological Parameters., J. Chem. Inf. Comput. Sci., 40 (5) (2000) 1113 -1127.

348) Khan M.T., Sylte I. Predictive QSAR modeling for the successful predictions of the ADMET properties of candidate drug molecules. Curr Drug Discov Technol. (3) (2007) 141-9.

349) Tropsha A., Golbraikh A. Predictive QSAR modeling workflow, model applicability domains, and virtual screening. J Pharm Pharmacol. Jul 59 (7) (2007) 935-40. Des.13 (34) (2007) 3494-504.

350) Rohrbaugh R.H., Jurs P.C. Anal. Chim. Acta 199 (1987) 99–109.

351) Osheroff N., Shelton E.R., Brutlag D.L. DNA topoisomerase II from Drosophila melanogaster. Relaxation of supercoiled DNA.J. Biol. Chem. 258 (1983) 9536–9543.

352) Robinson M.J., Osheroff N. Stabilization of the topoisomerase II-DNA cleavage complex by antineoplastic drugs: inhibition of enzyme-mediated DNA religation by 4'-(9-acridinylamino)methanesulfon-m-anisidide Biochemistry 29 (1990) 2511–2515.

353) Jayaraju D., Kondapi A.K. Curr. Sci. 81 (2001) 787–792.

354) Vashist Gopal Y.N., Jayaraju D., Kondapi A.K. Topoisomerase II poisoning and antineoplastic action by DNA-nonbinding diacetyl and dicarboxaldoxime derivatives of ferrocene.Arch. Biochem.Biophys. 376 (2000) 229–235.

355) Milman N., Cohn J. Serum iron, serum transferrin and transferrin saturation in healthy children without iron deficiency. Eur J Pediatr. Dec; 143 (2) (1984) 96-8.

356) Graham P.J., Lindsey R.V., Parshall G.W., Peterson M.L., Whitman G.M. Some Acyl Ferrocenes and their Reactions J. Am. Chem. Soc. 79 (1957) 3416–3420.

357) Matteini P., Rossi F., Menabuoni L., Pini R. , Microscopic characterization of collagen modifications induced by low-temperature diode-laser welding of corneal tissue. : Lasers Surg Med. 39(7) (2007) 597-604.

358) Cruz G.A., Toledo S., Sallum E.A., Lima A.F., Morphological and chemical analysis of bone substitutes by scanning electron microscopy and microanalysis by spectroscopy of dispersion energy. Braz Dent J.; 18(2) (2007) 129-133.

359) Teeranachaideekul V., Souto E.B., Müller R.H., Junyaprasert V.B.,, Physicochemical characterization and in vitro release studies of ascorbyl palmitate-loaded semi-solid nanostructured lipid carriers (NLC gels).., Microencapsul. 25(2) (2008) 111-120.

360) Rotomskis R, Streckyte G, Karabanovas V.Nanoparticles in diagnostics and therapy: towards nanomedicine. Medicina (Kaunas).42(7) :(2006)542-58.

361) Gupta Y., Jain A., Jain S.K. Transferrin-conjugated solid lipid nanoparticles for enhanced delivery of quinine dihydrochloride to the brain. J Pharm Pharmacol. 59 (7) (2007) 935-940.

362) Correa JR., Atella G.C., Vargas C., Soares M.J. Transferrin uptake may occur through detergent-resistant membrane domains at the cytopharynx of Trypanosoma cruzi epimastigote forms. Mem Inst Oswaldo Cruz. Nov; 102 (7) (2007) 871-876.

363) Smith T.A. Human serum transferrin cobalt complex: stability and cellular uptake of cobalt. Bioorg Med Chem Jul 15; 13 (14) (2005) 4576-4579.

364) Tim M. Rapid colorimetric assay for cellular growth and survival: Application to proliferation and cytotoxicity assays., J. Immuno. Methods 65, Issues 1-2, 16 (1983) 55-63.

365) Gopal P., Joshi D.S., Sundaram K., Das M.R. Isolation and Characterization of the Two Subpopulations of Cells with Different Lethalities from Zajdela Ascitic Hepatoma. Cancer research; 46 (1986) 1673-1678.

366) Berthelot M.E., report , chim Appl, 1, (1859) 284.

367) Young D.S. effects of drugs on clinical laboratory tests, third edition, AACC press, Washinton DC 3 122-3, (1990) 131.

368) Sayler G.S., Puziss M., Silver M. Alkaline Phosphatase Assay for Freshwater Sediments: Application to Perturbed Sediment Systems., Appl Environ Microbiol. 38 (5) (1979) 922-927.

369) Buhl S.W., and Jackson K.Y. Optimal conditions for assaying human lactate dehydrogenase , pyruvate to lactate at 25, 30, and 37^0C. Clin.Chem, 24, (1978) 261.

370) Ayroles J.F., Gibson G. Analysis of variance of microarray data., Methods Enzymol; 411 (2006) 214-233.

371) Garey J., Paule M.G., Effects of chronic low-dose acrylamide exposure on progressive ratio performance in adolescent rats., Neurotoxicology. 28(5) (2007) 998-1002.

372) Ssaq H.J., Veenstra T.D. The role of electrophoresis in disease biomarker discovery. Electrophoresis28(12) (2007) 1980-1988.

373) McDonagh P.F., Williams S.K. The preparation and use of fluorescent-protein conjugates for microvascular research. Microvasc Res. 27 (1) (1984) 14-27.

374) Zeller R., Fixation, embedding, and sectioning of tissues, embryos, and single cells.., Curr Protoc Mol Biol. (2001) 14 Unit 14.1.

375) Pedrera M., Sanchez-Cordon P.J., Romero-Trevejo J.L., Raya A.I., Nunnez A., Gomez-Villamandos J.C., Cytokine expression in paraffin wax-embedded tissues from conventional calves. J Comp Pathol. 136(4) (2007) 273-278.

376) Ito M., Moriya T., Ishida T., Usami S., Kasajima A., Sasano H., Ohuchi N., Significance of pathological evaluation for lymphatic vessel invasion in invasive breast cancer., Breast Cancer. 14(4) (2007)381-387.

377) Vashisht Gopal Y.N., Jayaraju D., Kondapi A.K., Topoisomerase II poisoning and antineoplastic action by DNA-nonbinding diacetyl and dicarboxaldoxime derivatives of ferrocene. Arch Biochem Biophys. Apr 1;376 (1) (2000) 229-35.

378) Fernandes D.J., Qiu J., and Catapano C.V. DNA topoisomerase II isozymes involved in anticancer drug action and resistance.Adv Enzyme Regul., 35 (1995) 265-81

379) Sai Krishna A.D, Panda G, Kondapi A.K., Mechanism of action of ferrocene derivatives on the catalytic activity of topoisomerase IIalpha and beta--distinct mode of action of two

derivatives. Arch Biochem Biophys. 15;438(2) (2005) 206-16.

380) Pritchard K.I, Messersmith H, Elavathil L, Trudeau M, O'Malley F, Dhesy-Thind B., HER-2 and topoisomerase II as predictors of response to chemotherapy. J Clin Oncol. 10;26(5): (2008) 736-44

381) Barthelmes, H.U., Niederberger E., Roth T., Schulte K., Tang W.C., Boege F., Fiebig H.H., Eisenbrand G., Marko D. Lycobetaine acts as a selective topoisomerase II beta poison and inhibits the growth of human tumour cells. Br J Cancer.85 (2001)1585-1591.

382) Park K., Kim J., Lim S., and Han S. Topoisomerase II-alpha (topoII) and HER2 amplification in breast cancers and response to preoperative doxorubicin chemotherapy. Eur J Cancer. 39 (2003) 631-634.

383) Kobayashi K., Nishioka M., Kohno T., Nakamoto M., Maeshima A., Aoyagi K., Sasaki H., Takenoshita S., Sugimura H., Yokota M. Identification of genes whose expression is upregulated in lung adenocarcinoma cells in comparison with type II alveolar cells and bronchiolar epithelial cells in vivo. J. Oncogene., 23(17) (2004) 3089-96.

384) Brustmann H. Expression of cellular apoptosis susceptibility protein in serous ovarian carcinoma: a clinicopathologic and immunohistochemical study.Gynecol Oncol.,92 (1) (2004) 268-276.

385) Houlbrook S., Addison C.M., Davies S.L., Carmichael J., Stratford I.J., Harris A.L., and Hickson I.D. Relationship between expression of topoisomerase II isoforms and intrinsic sensitivity to topoisomerase II inhibitors in breast cancer cell lines.Br J Cancer,74 (1996) 1154

386) Hazlehurst L.A., Foley N.E., Gleason-Guzman M.C., Hacker M.P., Cress A.E., Greenberger L.W., and De Jong M.C., Dalton W.S. Multiple mechanisms confer drug

resistance to mitoxantrone in the human 8226 myeloma cell line.Cancer Res., 9 (5), (1999) 1021-1028.

387) Gao H., Huang K.C., Yamasaki E.F., Chan K.K., Chohan L., and Snapka R.M. XK469, a selective topoisomerase IIbeta poison.Proc. Natl. Acad. Ssci., 96 (1999) 12168-12173.

388) Drlica K., and Franco R.J. Inhibitors of DNA topoisomerases, Inhibitors of DNA topoisomerases. Biochemistry, 27 (1988) 2253-2259.

389) Kratz F., Hartmann M., Keppler B., Messori L. The binding properties of two antitumor ruthenium(III) complexes to apotransferrin. J Biol Chem. Jan 28; 269 (4) (1994) 2581-8.

390) Aisen P. Entry of iron into cells: a new role for the transferrin receptor in modulating iron release from transferrin. Ann Neurol. 32 (1992)

391) Hogemann D., Josephson L., Weissleder R., Basilion J.P. Improvement of MRI probes to allow efficient detection of gene expression. Bioconjug Chem. Nov-Dec; 11 (6) (2000) 941-6.

392) Pardridge W.M. Drug targeting to the brain. Pharm Res. Sep; 24 (9) (2007) 1733-44.

393) Aktas Y., Yemisci M., Andrieux K., Gursoy R.N., Alonso M.J., Fernandez-Megia E., Novoa-Carballal R., Quinoa E., Riguera R., Sargon M.F., Celik H.H., Demir A.S., Hincal A.A., Dalkara T., Capan Y., Couvreur P. Development and brain delivery of chitosan-PEG nanoparticles functionalized with the monoclonal antibody OX26. Bioconjug Chem. Nov-Dec; 16 (6) (2005) 1503-11.

394) Rivest V., Phivilay A., Julien C., Belanger S., Tremblay C., Emond V., Calon F. Novel liposomal formulation for targeted gene delivery. Pharm Res. May; 24 (5) (2007) 981-90.

Appendix I

Ferrocene IR spectra

IR Spectra: bands at 1105 and 999 cm^{-1} confirm the Ferrocene unsubstituted ring
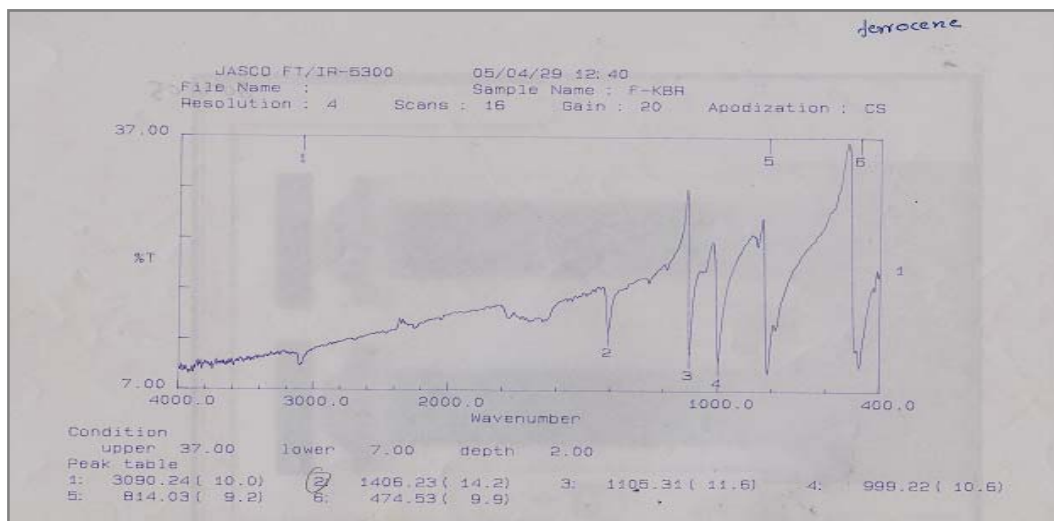
Ferrocene NMR spectra

Proton NMR spectra: singlet peak at 4.18 PPM, corresponding to the cyclopentadiene ring hydrogen's
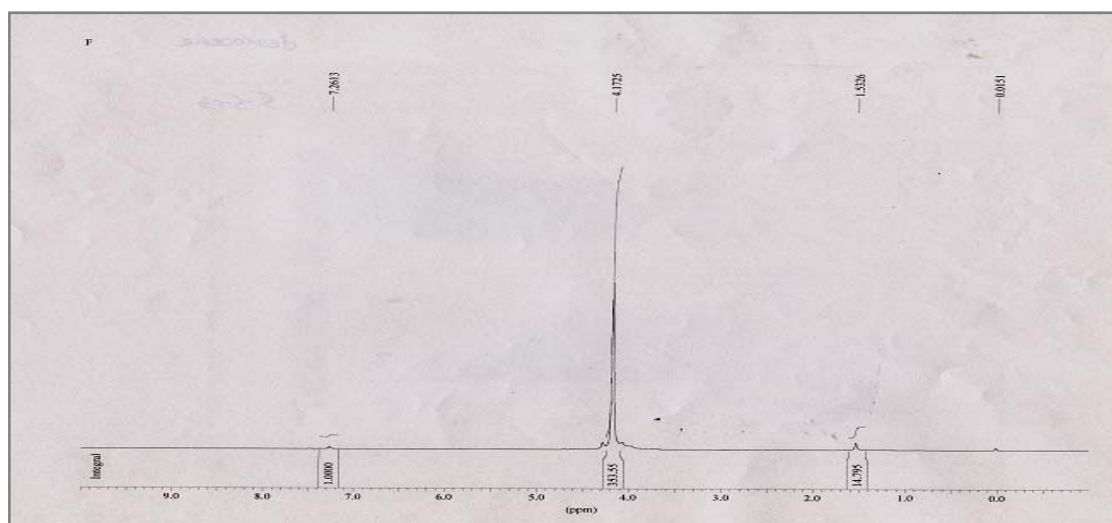
Appendix II

Ferrocene carboxyaldehyde IR spectra

IR Spectra: band at 1682 cm^{-1} confirm the presence of aldehyde C=O, bands at1105 and 1033 cm^{-1} confirm the Ferrocene unsubstituted ring
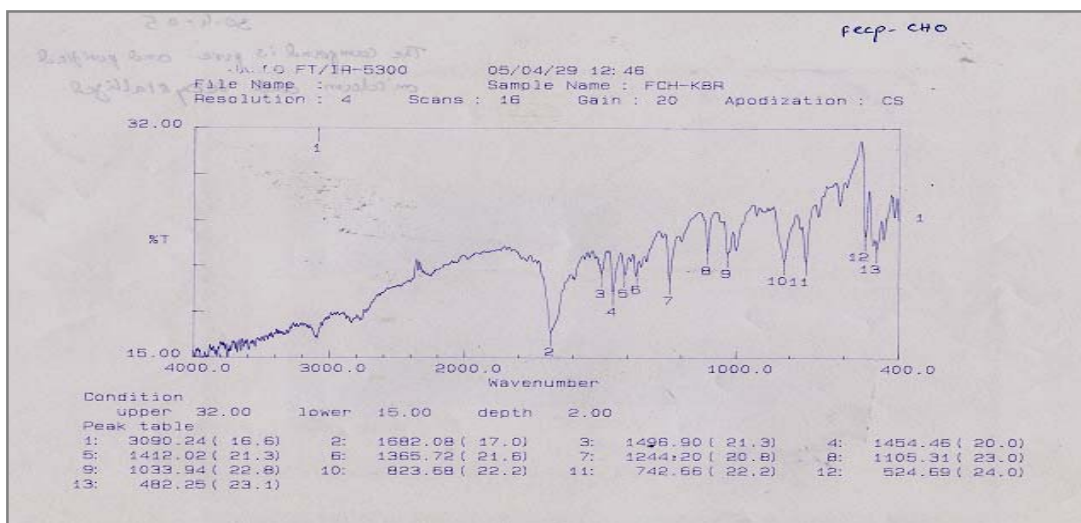
Ferrocene carboxyaldehyde NMR spectra

Proton NMR spectra: 4.2 PPM corresponding to the un-substituted lower ring hydrogen's, 2.42 PPM corresponding to methyl group hydrogen's, 9.959 PPM corresponding to the shifted hydrogen's in the CHO substituted ring
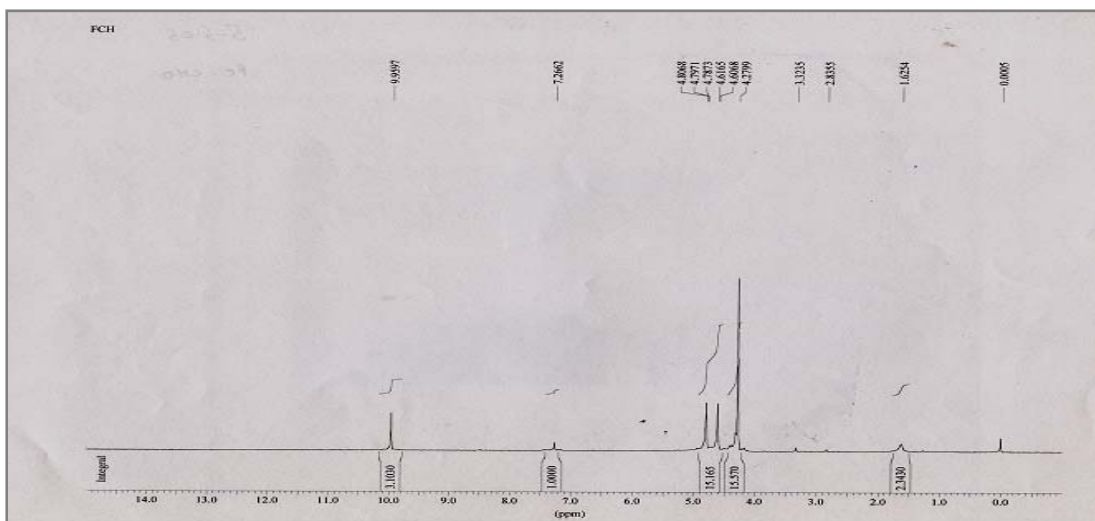
Appendix III

Azalactone ferrocene IR spectra

IR Spectra: bands at 1491, 1645 cm^{-1} confirm the presence of phenyl, band at 1780 cm^{-1} confirm the presence of C=O, bands at 3414 cm^{-1} confirm the presence of -NH and bands at 1103, 975 cm^{-1} confirm the presence of Ferrocene unsubstituted ring .

Azalactone ferrocene NMR spectra

Proton NMR spectra: 4.2 PPM corresponding to the unsubstituted lower ring hydrogen's, 2.42 PPM corresponding to methyl group hydrogen's, 4.68, 7.25, 1.25, 1.43 PPM corresponding to the shifted hydrogen's in the azalactone substituted ring
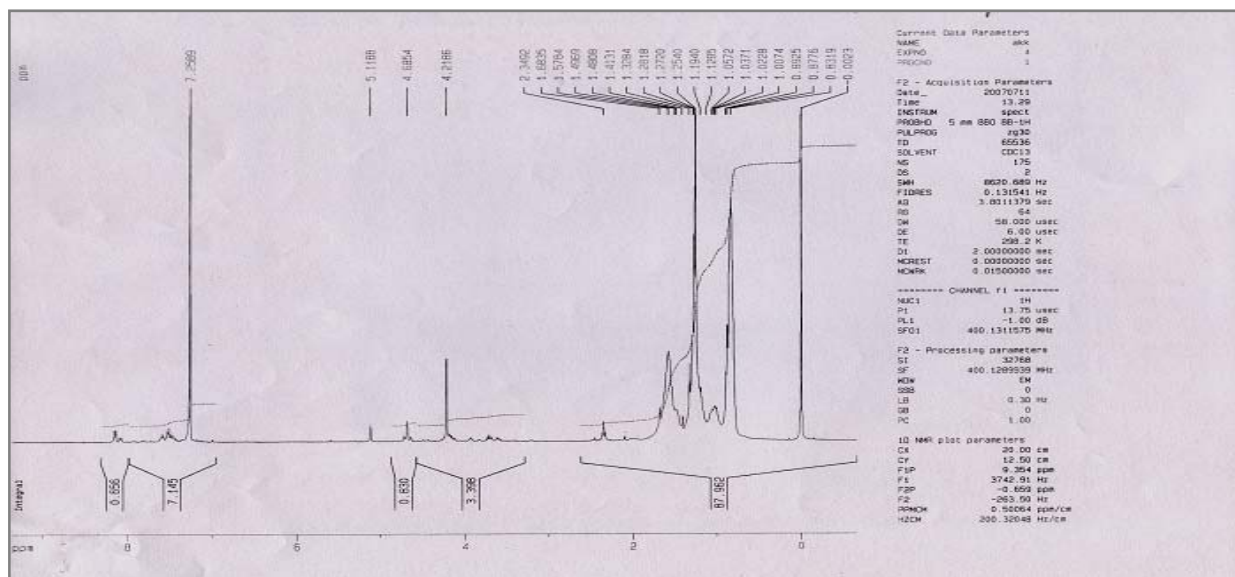
Appendix IV

Acetyl ferrocene IR spectra

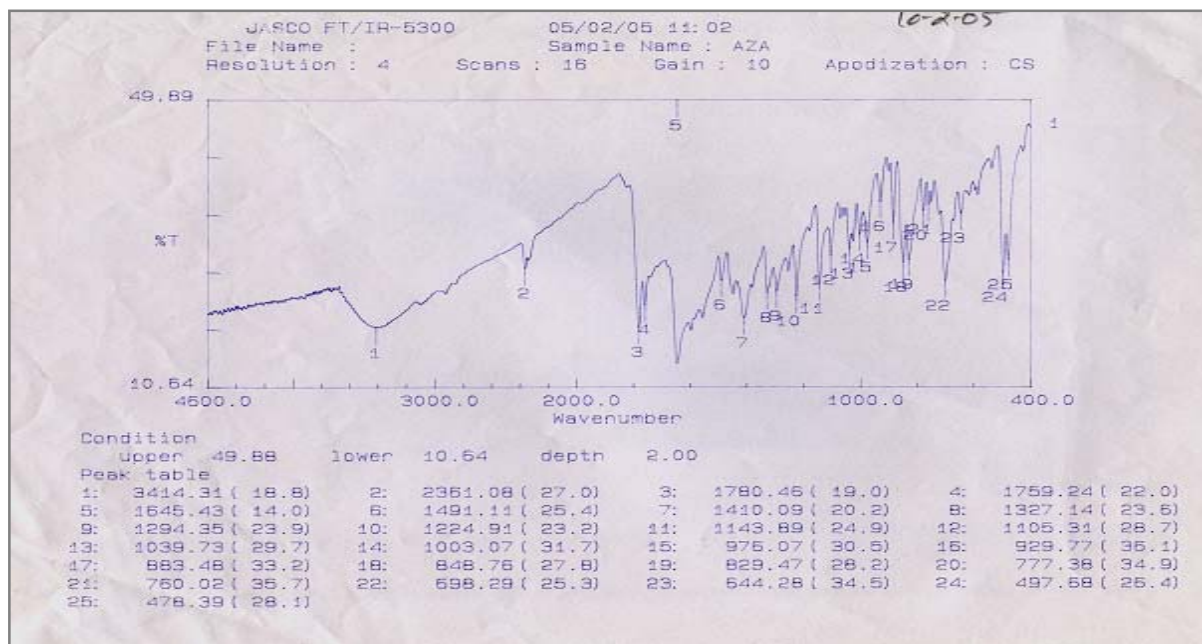**IR Spectra:** bands at 1651   cm^{-1} confirm the presence of aldehyde C=O, bands at 1101 and 960 cm^{-1} confirm the presence of Ferrocene unsubstituted ring

Fecp - acetyl
(acetyl ferrocene)

JASCO FT/IR-5300   05/04/29 12:34
File Name ;   Sample Name :FAC-KBR
Resolution : 4   Scans : 16   Gain : 20   Apodization : CS

Condition								
upper 33.45	lower 6.50	depth 2.00						

Peak table
1:	3080.60 (11.8)	2:	1551.22 (10.1)	3:	1454.46 (13.5)	4:	1373.44 (15.2)
5:	1278.92 (12.6)	6:	1101.45 (17.6)	7:	1041.65 (19.1)	8:	1003.07 (17.5)
9:	960.64 (20.4)	10:	891.19 (20.3)	11:	846.83 (18.7)	12:	821.75 (15.6)
13:	621.13 (22.2)	14:	532.40 (17.7)	15:	499.61 (16.4)	16:	480.32 (16.6)
17:	461.03 (17.5)						

Acetyl ferrocene NMR spectra

Proton   NMR spectra: 4.2 PPM corresponding to the un-substituted lower ring hydrogen's, 4.4, 4.7 PPM corresponding to the shifted hydrogen's in the acetyl substituted ring
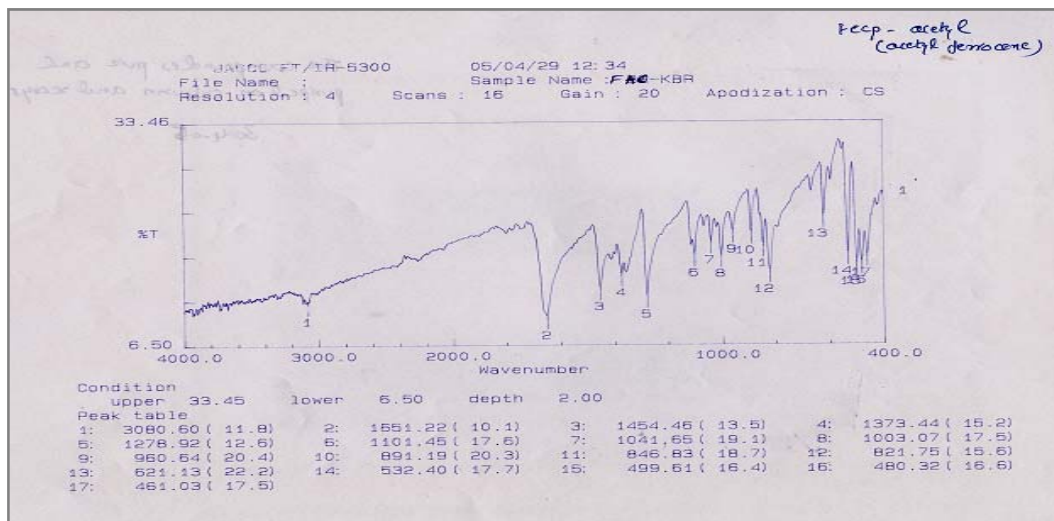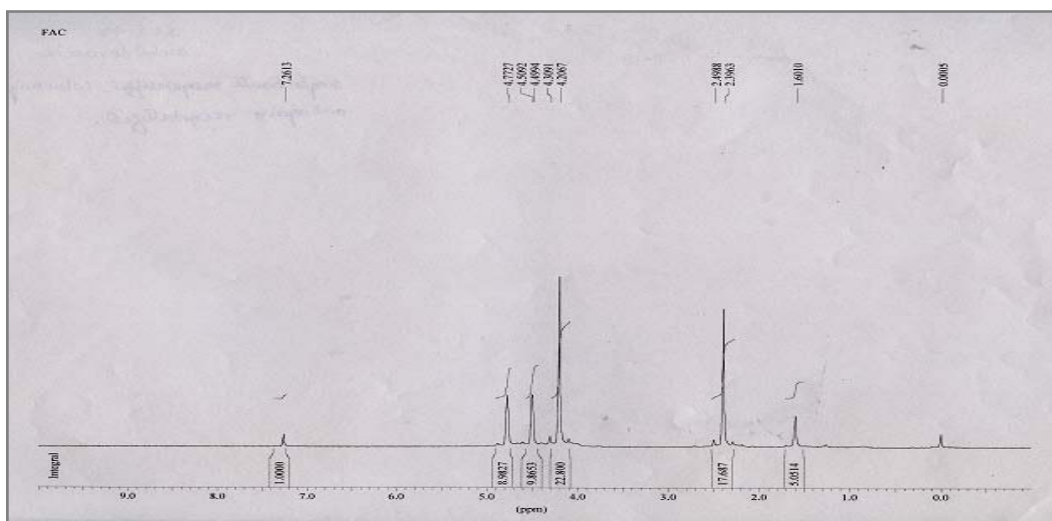
Thiomorpholide amido methyl ferrocene IR spectra

IR Spectra: bands at 1493 cm^{-1} confirm the presence of –CSN=, band at 1068 and 864 cm^{-1} confirm the presence of -SH , bands at 1660 cm^{-1} confirm the presence of (C=O) of -COOH and bands at 1113, 997cm^{-1} confirm the presence of Ferrocene unsubstituted ring

Thiomorpholide amido methyl ferrocene NMR spectra

Proton NMR spectra: 4.2 PPM corresponding to the un-substituted lower ring hydrogen's, 4.27, 4.29 ,7.25 , 1.25,1.43 PPM corresponding to the shifted hydrogen's in the thiomorpholide amido methyl substituted ring
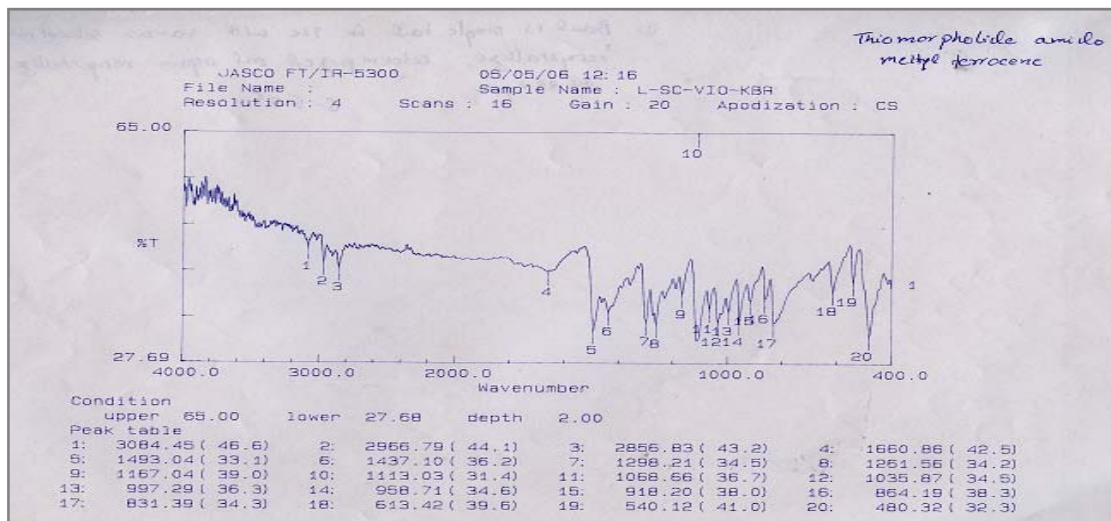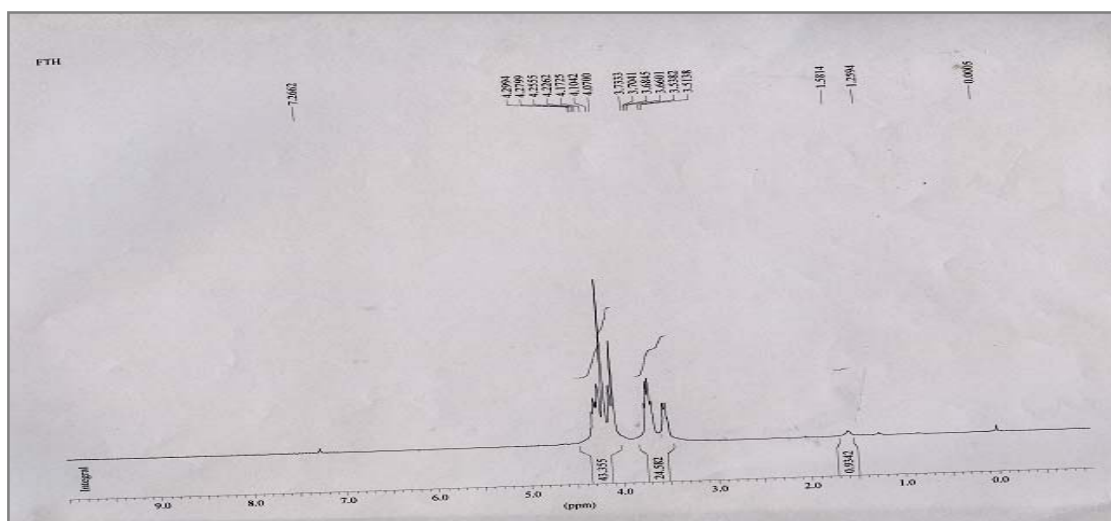
Appendix VI: Alkaline phosphatase activity in rat groups, analysis by ANOVA and Tukey HSD test Table

Panel A: ANOVA Table

Source	Sum of Squares	Df	Mean Square	F-Ratio	P-Value
Between groups	**94133.9**	**5**	**18826.8**	**1302.29**	**0.0000**
Within groups	**173.48**	**12**	**14.4567**		
Total (Corr.)	**94307.4**	**17**			

Panel B: Multiple Range Tests:- Method: 95.0 percent Tukey HSD

* denotes a statistically significant difference.

	Count	Mean	Homogeneous Groups
healthy	6	57.022	X
nano treated	6	60.4973	X
doxo trea	6	71.3393	X
doxo atr	6	123.977	X
bsa nan o	6	184.869	X
untreated	6	252.01	X

Contrast	Sig.	Difference	+/- Limits
untreated - nano treated	*	**191.513**	10.4291
untreated - doxo trea	*	180.671	10.4291
untreated - doxo atr	*	128.033	10.4291
untreated - bsa nan o	*	67.1407	10.4291
untreated - healthy	*	194.988	10.4291
nano treated - doxo trea	*	-10.842	10.4291
nano treated - doxo atr	*	-63.48	10.4291
nano treated - bsa nan o	*	-124.372	10.4291
nano treated - healthy		**3.47533**	10.4291
doxo trea - doxo atr	*	-52.638	10.4291
doxo trea - bsa nan o	*	-113.53	10.4291
doxo trea - healthy	*	14.3173	10.4291
doxo atr - bsa nan o	*	-60.892	10.4291
doxo atr - healthy	*	66.9553	10.4291
bsa nan o - healthy	*	127.847	10.4291

Appendix VII: Creatinine activity in rat groups, analysis by ANOVA and Tukey HSD test Table

Panel A: ANOVA Table

Source	Sum of Squares	Df	Mean Square	F-Ratio	P-Value
Between groups	0.00238761	5	0.000477522	0.73	0.6141
Within groups	0.007844	12	0.000653667		
Total (Corr.)	0.0102316	17			

Panel B: Multiple Range Tests:- Method: 95.0 percent Tukey HSD

	Count	Mean	Homogeneous Groups
nano tre	6	0.198333	X
bsa nano tre	6	0.203667	X
doxo atr tre	6	0.204	X
doxo trea	6	0.205	X
healthy	6	0.218667	X
untrea	6	0.232	X

* denotes a statistically significant difference.

Contrast	Sig.	Difference	+/- Limits
untrea - nano tre		0.0336667	0.0701279
untrea - doxo trea		0.027	0.0701279
untrea - doxo atr tre		0.028	0.0701279
untrea - bsa nano tre		0.0283333	0.0701279
untrea - healthy		0.0133333	0.0701279
nano tre - doxo trea		-0.00666667	0.0701279
nano tre - doxo atr tre		-0.00566667	0.0701279
nano tre - bsa nano tre		-0.00533333	0.0701279
nano tre - healthy		-0.0203333	0.0701279
doxo trea - doxo atr tre		0.001	0.0701279
doxo trea - bsa nano tre		0.00133333	0.0701279
doxo trea - healthy		-0.0136667	0.0701279
doxo atr tre - bsa nano tre		0.000333333	0.0701279
doxo atr tre - healthy		-0.0146667	0.0701279
bsa nano tre - healthy		-0.015	0.0701279

Appendix VIII: Urea activity in rat groups, analysis by ANOVA and Tukey HSD test Table

Panel A: ANOVA Table

Source	Sum of Squares	Df	Mean Square	F-Ratio	P-Value
Between groups	1406.1	5	281.221	**539.15**	**0.0000**
Within groups	6.2592	12	0.5216		
Total (Corr.)	1412.36	17			

Panel B: Multiple Range Tests:-Method: 95.0 percent Tukey HSD

	Count	Mean	Homogeneous Groups
doxo trea	6	3.63267	X
doxo atr	6	4.58467	X
healthy	6	4.62367	X
nano treated	6	4.66033	X
bsa nan o	6	19.21	X
untreated	6	26.0583	X

* denotes a statistically significant difference.

Contrast	Sig.	Difference	+/- Limits
untreated - nano treated	*	**21.398**	1.98099
untreated - doxo trea	*	22.4257	1.98099
untreated - doxo atr	*	21.4737	1.98099
untreated - bsa nan o	*	6.84833	1.98099
untreated - healthy	*	21.4347	1.98099
nano treated - doxo trea		1.02767	1.98099
nano treated - doxo atr		0.0756667	1.98099
nano treated - bsa nan o	*	-14.5497	1.98099
nano treated - healthy		**0.0366667**	1.98099
doxo trea - doxo atr		-0.952	1.98099
doxo trea - bsa nan o	*	-15.5773	1.98099
doxo trea - healthy		-0.991	1.98099
doxo atr - bsa nan o	*	-14.6253	1.98099
doxo atr - healthy		-0.039	1.98099
bsa nan o - healthy	*	14.5863	1.98099

Appendix IX : Survivality in rat groups, analysis by ANOVA and Tukey HSD test Table

Panel A: ANOVA Table

Source	Sum of Squares	Df	Mean Square	F-Ratio	P-Value
Between groups	1.00274E6	5	200549.	**293486.19**	**0.0000**
Within groups	20.5	30	0.683333		
Total (Corr.)	1.00276E6	35			

Panel B: Multiple Range Tests:-Method: 95.0 percent Tukey HSD

	Count	Mean	Homogeneous Groups
untre	6	6.33333	X
bsa nano tre	6	7.16667	X
doxo tre	6	14.5	X
doxo atr	6	16.1667	X
helthy	6	365.0	X
nano tre	6	365.0	X

* denotes a statistically significant difference.

Contrast	Sig.	Difference	+/- Limits
untre - nano tre	*	**-358.667**	1.45185
untre - doxo tre	*	-8.16667	1.45185
untre - doxo atr	*	-9.83333	1.45185
untre - bsa nano tre		-0.833333	1.45185
untre - helthy	*	-358.667	1.45185
nano tre - doxo tre	*	350.5	1.45185
nano tre - doxo atr	*	348.833	1.45185
nano tre - bsa nano tre	*	357.833	1.45185
nano tre - helthy		**0.0**	1.45185
doxo tre - doxo atr	*	-1.66667	1.45185
doxo tre - bsa nano tre	*	7.33333	1.45185
doxo tre - helthy	*	-350.5	1.45185
doxo atr - bsa nano tre	*	9.0	1.45185
doxo atr - helthy	*	-348.833	1.45185
bsa nano tre - helthy	*	-357.833	1.45185

Appendix X: LDH activity in rat groups, analysis by ANOVA and Tukey HSD test Table

Panel A: ANOVA Table

Source	Sum of Squares	Df	Mean Square	F-Ratio	P-Value
Between groups	66473.0	5	13294.6	862.93	0.0000
Within groups	184.875	12	15.4063		
Total (Corr.)	66657.9	17			

Panel B: Multiple Range Tests:-Method: 95.0 percent Tukey HSD

	Count	Mean	Homogeneous Groups
healthy	6	51.0033	X
nano treated	6	51.68	X
doxo trea	6	89.89	X
doxo atr	6	90.1933	X
bsa nano	6	182.047	X
untreated	6	206.487	X

* denotes a statistically significant difference.

Contrast	Sig.	Difference	+/- Limits
untreated - nano treated	*	154.807	10.7662
untreated - doxo trea	*	116.597	10.7662
untreated - doxo atr	*	116.293	10.7662
untreated - bsa nan o	*	24.44	10.7662
untreated - healthy	*	155.483	10.7662
nano treated - doxo trea	*	-38.21	10.7662
nano treated - doxo atr	*	-38.5133	10.7662
nano treated - bsa nan o	*	-130.367	10.7662
nano treated - healthy		0.676667	10.7662
doxo trea - doxo atr		-0.303333	10.7662
doxo trea - bsa nan o	*	-92.1567	10.7662
doxo trea - healthy	*	38.8867	10.7662
doxo atr - bsa nan o	*	-91.8533	10.7662
doxo atr - healthy	*	39.19	10.7662
bsa nan o - healthy	*	131.043	10.7662

Mechanism of action of ferrocene derivatives on the catalytic activity of topoisomerase IIα and β—Distinct mode of action of two derivatives ☆

A.D. Sai Krishna, Gayatri Panda, Anand K. Kondapi *

Department of Biochemistry, University of Hyderabad, Hyderabad 500 046, India

Abstract

Topoisomerase II is found to be present in two isoforms α and β, and both the isoforms are regulated in cancerous tissue. Development of isoform-specific topoisomerase II poisons has been of great interest for cancer-specific drug targeting. In the present investigation using quantitative structure–activity analysis of ferrocene derivatives, we show that two derivatives of ferrocene, azalactone ferrocene and thiomorpholide amido methyl ferrocene, can preferentially inhibit topoisomerase IIβ activity. Thiomorpholide amido methyl ferrocene shows higher inhibition of catalytic activity ($IC_{50} = 50\ \mu M$) against topoisomerase IIβ compared to azalactone ferrocene ($IC_{50} = 100\ \mu M$). The analysis of protein DNA intermediates formed in the presence of these two compounds suggests that azalactone ferrocene readily induces formation of cleavable complex in a dose-dependent manner, in comparison with thiomorpholide amido methyl ferrocene. Both the compounds show significant inhibition of DNA-dependent ATPase activity of enzyme. These results suggest that azalactone ferrocene inhibits DNA passage activity of enzyme leading to the formation of cleavable complex, while thiomorpholide amido methyl ferrocene competes with ATP binding resulting in the inhibition of catalytic activity of enzyme. In summary, thiomorpholide amido methyl ferrocene and azalactone ferrocene show distinctly different mechanisms in inhibition of catalytic activity of topoisomerase IIβ.
© 2005 Elsevier Inc. All rights reserved.

Keywords: Topoisomerase IIα; Topoisomerase IIβ; Ferrocene; Quantitative structure–activity relationship; Anti-cancer; Topo II poisons

Eukaryotic topoisomerase II is present in two isoforms, viz., 170 kDa α isoform and 180 kDa β isoform [1]. Both exhibit similar catalytic activities in relaxation of supercoiled DNA; decatenation and catenation; and unknotting and knotting of double-stranded DNA [2,3]. Topoisomerase IIα is largely localized in proliferating cells and tissues [4], while β isoform is predominantly localized in brain especially in cerebellum [5]. In normal cells, the activity of topoisomerase IIα is highly regulated, while it is present at high levels in rapidly proliferating cancerous cells [6]. Both the isoforms are shown to be differentially regulated in cancerous tissue [4]. Thus, both topoisomerase IIα and β assume significance as anti-cancer targets for development of cancer-specific chemotherapeutics [6].

The catalytic cycle of topoisomerase II involves the binding of the enzyme as a dimer in a segment of DNA [7]. The DNA bound dimeric enzyme undergoes a conformational change upon binding to ATP leading to breakage of DNA segment with 5′-overhangs bound to the enzyme through a phosphotyrosyl linkage. This allows the opening of a transient gate, through which the second segment of DNA is passed following ATP hydrolysis and religation of broken strands [8]. If an inhibitor binds to the enzyme and halts, the formation of the phosphotyrosyl

linkage and/or ATP binding can block enzymatic activity without the formation of such a cleavable complex. Thus, the covalently linked DNA–protein transient intermediates formed during the catalytic cycle have been recognized as the targets for various topoisomerase II inhibitors [8]. The topoisomerase II inhibitors can be classified into two major classes: the one that induces the formation of "cleavage complexes" making the enzyme as DNA cleaving enzyme, and these are referred to as topoisomerase II poisons [9]; the other one "which does not induce formation of any cleavage complexes," and these are named as topoisomerase II inhibitors [10].

Among topoisomerase II poisons two types of molecules are reported—one, the DNA binding Topo II poisons ex: m-AMSA [11], doxirubicine [10], ruthenium (ben) derivatives [12,13], and the other type, the poisons that do not bind to DNA ex: Etoposide [10], some ferrocene derivatives [14].

The topoisomerase II inhibitors that do not form cleavage complexes may interact with enzymatic active site especially at ATP binding region and/or at the region involved in the formation of phosphotyrosyl linkage thus interfering with the ATP binding associated conformational changes.

In the present investigation, we have synthesized a series of ferrocene derivatives and studied their inhibitory properties against topoisomerase IIα and β. Based on the structure–activity analysis, we arrived at two compounds, azalactone ferrocene and thiomorpholide amido methyl ferrocene, that show significant activity against topoisomerase IIβ activity. We have characterized the molecular mechanism of action of these two compounds against topoisomerase II isoforms, and the results showed that these two compounds inhibit topoisomerase II catalytic activity through distinctly different modes of action.

Experimental procedure

The negatively supercoiled plasmid DNA pBR 322 and pRYG was purified as described in [5]. Mouse anti-human topoisomerase IIα and topoisomerase IIβ monoclonal antibodies were obtained from BD Bioscience USA, and γ-^{32}P were obtained from Brit India. Other chemicals and biochemicals were of analytical grade.

Synthesis of ferrocene derivatives

Ferrocene was purchased from Merck. Substitutions were done on this compound using published procedures with minor modifications.

Synthesis of azalactone ferrocene

Azalactone derivative was synthesized from ferrocene carboxyaldehyde. Ferrocene carboxyaldehyde was initially prepared through refluxing with phosphoric oxychloride and N-methyl formanilide as described in [15]. The ferrocene carboxyaldehyde was used to prepare azalactone using hippuric acid and sodium acetate [16]. The synthesized dark purple coloured compound was re-crystallized, and was characterized by IR spectroscopy and melting temperature studies (188 °C).

Synthesis of thiomorpholide amido methyl ferrocene

Acetyl ferrocene was synthesized using acetic anhydride [17]. It was then refluxed with morpholine and sulphur at 130 °C for 2 h 30 min to form thiomorpholide amido methyl ferrocene as described in [17]. The compound was purified by re-crystallization to get the dark orange crystalline thiomorpholide amido methyl ferrocene; that was confirmed by IR and from its melting point (129 °C).

Enzyme source

Rat brain cerebellar region was used as enzyme source. Topoisomerase IIα and β were isolated using two sequential steps, first by MONO S and then by MONO Q ion exchange chromatography. The bound protein was eluted at 0.25 M NaCl. The α and β isoforms present in the preparation were further affinity purified using corresponding antibody coupled agarose matrix. Mouse anti-human topoisomerase IIα and topoisomerase IIβ monoclonal antibodies were used. The antibody bound protein was eluted using buffer containing 20 mM Tris–HCl (pH 8.0), 1 M KCl, 0.5 mM EDTA, 10 mM mercaptoethanol, and 10% glycerol, followed by dialysis using the same buffer containing 100 mM KCl. The purity of protein was confirmed by Western blot analysis. The protein was estimated using Bradford's method [18]. The catalytic activity was assayed using supercoiled pRYG DNA [5].

QSAR equation generation

QSAR[1] equation was generated as described in Accelrys Cerius^2 tutorials [19]. Ferrocene models were sketched using 3D sketchers and models were minimized by smart minimizations in offset methods, while atomic charges were calculated by offset up method. The models were superimposed using the iron axis and the upper

---

[1] *Abbreviations used:* QSAR, quantitative structure–activity relationship; PRESS, predicted sum of squares (it is the root mean square error of all target predictions); MFA, molecular field analysis; r^2, square of correlation coefficient; r^2_{cv}, cross validation square of correlation coefficient; topoisomerase IIα, topoisomerase II alpha; topoisomerase IIβ, topoisomerase II beta; m-AMSA, N-[4-(9-acridinylamino)-3-methoxy-phenyl] methane sulphonamide; SDS, sodium dodecyl sulphate; IC$_{50}$, inhibitory concentration 50%; G/PLS, genetic partial least squares; EDTA, ethylenediaminetetraacetic acid.

cyclopentadiene ring as the basic skeleton. These models were entered into QSAR study table, with the negative log value of the IC_{50} entered into study table, while the descriptors were added in default mode, the probing was done using H^+ and CH_3^+ probes and the grid was developed. The QSAR equation was generated using G/PLS [20]. The above equation is further tuned to get a better QSAR equation by selecting appropriate training and test set. 3D points were generated by default. The models were used in receptor module of Cerius[2] and the interactions were computed.

Relaxation assay

This assay was performed following the procedure of Osheroff et al. [21]. The reaction mixture contained 0.6 μg of negatively supercoiled pRYG plasmid DNA with increasing concentrations of ferrocene drugs in relaxation buffer (50 mM Tris–HCl (pH 8.0), 120 mM KCl, 0.5 mM EDTA, 0.5 mM DTT, 10 mM MgCl₂, 30 μg/ml BSA, and 1 mM ATP). The reaction was initiated by adding 2 U of topoisomerase IIα or β and incubated at 37 °C for 30 min. The reaction was stopped by adding 2 μl of 10% SDS and 3 μl of loading dye (0.5% bromophenol blue, 0.5% xylenol cyanol, and 30% glycerol in water), and the products were separated on a 1% agarose gel in TAE (20 mM Tris–acetate and 0.5 mM EDTA) at 50 V for 10 h. The gel was stained with ethidium bromide (1 μg/ml) and was observed in photodyne UV transilluminator and photographed.

Cleavage assay

The formation of cleavage complex was assayed following the procedure of Robinson and Osheroff [22]. The reaction mixture contained 0.6 μg of negatively supercoiled pBR 322 DNA with increasing concentrations of ferrocene compounds in cleavage buffer [10 mM Tris–HCl (pH 7.9), 50 mM NaCl, 50 mM KCl, 0.1 mM EDTA, 2.5% glycerol, and 5 mM MgCl₂]. The reaction was initiated by adding 10 U of topoisomerase II and incubated at 37 °C for 15 min, then stopped with addition of 2 μl each of 0.5 M EDTA and 10% SDS. The DNA bound protein was proteolyzed by incubating the reaction mixture with 2 μl Proteinase K (2 mg/ml) at 45 °C for 1 h. The products were separated on 1% agarose gel for 2 h at 50 V in TAE buffer, ethidium bromide (1 μg/ml) stained, and photographed under UV.

ATPase assay

This assay was conducted as described in Jayaraju and Kondapi [23]. The reaction mixture containing 1 ml of reaction buffer (20 mM Tris–HCl, pH 7.5, 0.1 mg NADH, 100 μM DTT, 1 mM ATP, 2 mM of phosphoenol pyruvate, and 4 mM MgCl₂), 12.5 U of pyruvate kinase, and 12.5 U of lactate dehydrogenase was incubated at 37 °C for 5 min. The incubation was continued further with addition of 0.3 μg DNA with increasing concentrations of the ferrocene drugs and 4 U of topoisomerase II for 30 min and the absorbance was recorded at 340 nm. In control study, the reaction was also carried out without topoisomerase II.

DNA thermal denaturation assay

Calf thymus DNA (sodium salt) was dissolved in 1 mM of sodium phosphate buffer containing 1 mM sodium chloride and 1 mM EDTA. DNA concentration was adjusted to give an absorbance of 1.0 in 1 cm pathlength cuvette at 260 nm [14]. The ferrocene drugs were added to DNA at concentrations, which gave drug to nucleotide ratio of 1:10, 1:5, 1:2, and 1:1, respectively. The samples were incubated in 1 cm pathlength cuvette for 2 min to allow drug–DNA binding. A JASCO 550 spectrophotometer was set to give a 1 °C rise in temperature per minute with ETC 505 T thermo programmer and temperature controller. Increase in absorbance at 260 nm was recorded from 40 to 90 °C

Drug interaction assay

The interaction of drug with enzyme was done in two ways. In the first, the enzyme was immunoprecipitated using protein A–agarose method as described in [5]. Immunoprecipitated enzyme was incubated with azalactone ferrocene at 50 and 100 μM for 15 min. The unbound drug was removed by washing three times with TBS buffer containing 0.1% Tween 20. The drug treated enzyme immunoprecipitate was mixed with supercoiled DNA and the relaxation assay was conducted.

In the second approach, pRYG DNA was preincubated at 50, 100 μM of azalactone ferrocene. The complex was incubated for 15 min at 37 °C. After incubation, the drug was diluted by 10-fold to get drug concentrations of 5 and 10 μM. The reaction mixture containing diluted drug–DNA was added to immunoprecipitated topoisomerase IIβ isoform and the relaxation assay was conducted.

Results

Quantitative structure and activity analysis of ferrocene derivatives

Our earlier studies suggest that inhibitory activity of ferrocene derivatives is dependent on the substituent present on cyclopentadiene ring [14]. An interesting property of ferrocene derivatives is that these possess

no affinity to DNA, and this property has reduced non-specific action of these drug molecules against DNA. Furthermore, the presence of organic cyclopentadiene ring will provide caging to iron, thus stabilizing it from redox environment. These considerations led us to choose ferrocene derivatives for the present study. We have synthesized a series of 25 substituted ferrocene derivatives using the published procedures. We have studied the inhibitory activity of each derivative against the catalytic activity of topoisomerase IIβ and IC$_{50}$ values were determined. The structures of these compounds were modeled using Accelrys Cerius^2 [19]. The structures obtained were superimposed pointing towards iron ferrocene axis. The overlaid structures were analyzed using quantitative structure–activity relationship (QSAR) methodology as per Accelrys. The molecular field analysis (MFA) [20] yielded good fit of data, with cross-validation square of correlation coefficient (r^2_{cv}) of 0.943, square of correlation coefficient r^2 of 0.985, predicted sum of squares (PRESS) of 0.083, outliers of 4.0. This model has been generated with the following linear regressed equation:

$$\begin{aligned} \text{Activity} = {} & 3.47383 - 0.005202(\text{H}^+/373) + 0.005198 \\ & \times (\text{CH}_3/216) + 0.00866(\text{H}^+/455) - 0.0088 \\ & \times (\text{CH}_3/527) + 0.01219(\text{CH}_3/226) \\ & - 0.00552(\text{H}^+/215) + 0.011875(\text{CH}_3/375). \end{aligned}$$
$$(1)$$

As the equation suggests, the steric 216, 226, 375 and electrostatic probes 455 have positive contributions to the activity (Fig. 1).

The QSAR analysis yielded a linear relation between the predicted activities from Eq. (1) versus experimental activity as per Table 1. These results predicted two compounds, azalactone ferrocene and thiomorpholide ferrocene, containing active structural features. To test this, we have further analyzed these two compounds for their molecular mode of action (Fig. 2).

Azalactone ferrocene and thiomorpholide amido methyl ferrocene exhibit enhanced inhibition of catalytic activity of topoisomerase IIβ

Topoisomerase IIα and β-catalyzed relaxation activity was analyzed with increasing concentrations of azalactone ferrocene and thiomorpholide methyl ferrocene. The results show that azalactone ferrocene inhibits catalytic activity of topoisomerase IIβ at 100 μM (Fig. 3B) while it requires 300 μM for inhibition of catalytic activity of topoisomerase IIα catalytic activity (Fig. 3A). Thiomorpholide amido methyl ferrocene could inhibit catalytic activity of topoisomerase IIβ at 50 μM (Fig. 3D), while 200 μM was required for inhibition of topoisomerase IIα (Fig. 3C). These results suggest that azalactone ferrocene is threefold higher potent against topoisomerase IIβ compared to α isoform, while thiomorpholide amido methyl ferrocene exhibits fourfold higher activity against topoisomerase IIβ isoform compared to that of topoisomerase IIα. Further, thiomorpholide amido methyl ferrocene shows a twofold higher activity against topoisomerase IIβ compared to that observed for azalactone ferrocene. The DNA when incubated with increasing concentrations of the drug in the absence of enzyme, the results showed no nicking activity of the drugs against DNA alone (data not shown).

Thiomorpholide amido methyl ferrocene and azalactone ferrocene show distinct mode of mechanism of action against topoisomerase IIβ

To investigate the mechanism of action of the two compounds, thiomorpholide amido methyl ferrocene and azalactone ferrocene, we have carried out cleavage assay to monitor the ability of these two compounds in inducing the formation of enzyme-linked DNA complexes. The cleavage assay was conducted with increasing concentrations of drug and the cleavable complexes
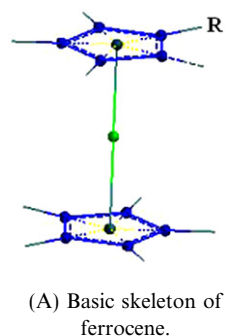

(A) Basic skeleton of ferrocene.

(B) Alignment of ferrocene derivatives.

Fig. 1. Structure alignment of ferrocene derivatives towards iron cyclopentadiene ring axis using 3D alignment procedure of Cerius^2. A view of the molecular rectangular field grid around the superposed molecular units was presented. Both steric (CH$_3$) and electrostatic (H$^+$) grid points in the final QSAR equation are depicted.

Table 1
Structures and experimental and calculated inhibitory activities against enzyme-catalyzed relaxation of supercoiled DNA, $-(\log IC_{50})$, of the molecules used in the training set based on the molecular skeleton
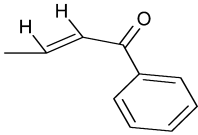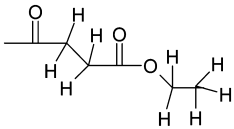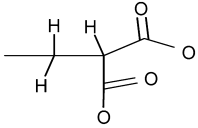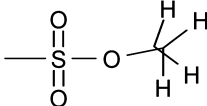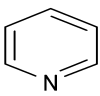
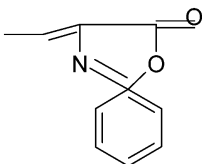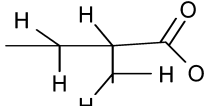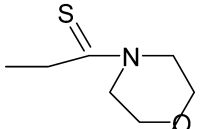|	Substitution, R	Negative (logIC$_{50}$)	Predicted activity MFA	Reference from which the compound was synthesized and characterized
1	CH$_3$	3.455	3.551	[33]
2	CHO	3.522	3.614	[34]
3		3.522	3.518	[43]
4	C$_2$H$_5$	3.522	3.626	[33]
5	CH$_2$CH$_2$COOH	3.522	3.522	
6	COCH$_3$	3.560	3.615	[34]
7	CH$_2$OH	3.602	3.612	[17]
8	CH$_2$Cl	3.602	3.748	[33]
9		3.698	3.694	[15]
10	CH$_2$CHO	3.698	3.730	[35]
11		3.698	3.716	[36]
12		3.823	3.763	[37]
13	CH$_2$–SH	3.823	3.667	[38]
14	CH$_2$COOH	3.823	3.685	[39]
15	CH$_2$(OH)$_2$	3.823	3.841	[17]
16	COOH	3.823	3.742	[36]
17	CH$_2$(COOH)$_2$	3.823	3.885	[40]
18	–CH$_2$CH$_2$OH	3.886	3.880	[17]
19	COSH	3.920	3.877	[41]
20	CHCHCOOH	4.000	3.946	[40]
21	SH	4.000	3.452	[41]
22		4.000	3.971	[42]
23		4.096	4.029	[16]

Table 1 (*continued*)

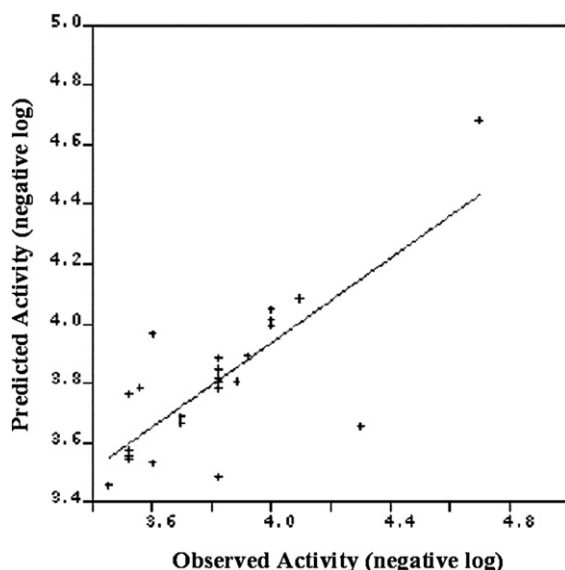|	Substitution, R	Negative (logIC$_{50}$)	Predicted activity MFA	Reference from which the compound was synthesized and characterized
24		4.301	4.332	[15]
25		4.698	4.744	[17]

Fig. 2. Plot of theoretically predicted activity versus experimentally determined enzyme inhibition activity. The theoretical activity in terms of negative log of IC$_{50}$ plotted on the *Y*-axis, which was computed using regression Eq. (1) obtained from the Cerius^2 QSAR methodology based on molecular shape analysis of the ferrocene derivatives. The *X*-axis shows the experimentally measured activity in terms of IC$_{50}$ values for the inhibition of topoisomerase IIβ-catalyzed relaxation of DNA as per Table 1.

formed were analyzed through formation of linear DNA on agarose gel. The results presented in Fig. 4A show that azalactone ferrocene induces formation of linear double-stranded DNA intermediates in a dose-dependent manner. On the other hand, the results of cleavage assay conducted in the presence of thiomorpholide amido methyl ferrocene show that it cannot mediate formation of cleavable complex as intermediate (Fig. 4A). The experiments were repeated using topoisomerase IIα (Fig. 4B), the results suggest that azalactone ferrocene also poisons topoisomerase IIα through formation of cleavage complex, where as thiomorpholide amido methyl ferrocene cannot form cleavage complex and does not induce enzyme-linked cleavable complex. The concentration at which the

cleavable complex formed by azalactone ferrocene with topoisomerase IIα was ~2-fold lower compared to that of topoisomerase IIβ. These results thus suggest distinct different modes of mechanism for the two compounds. The highly potent thiomorpholide amido methyl ferrocene which does not induce formation of drug induced enzyme associated DNA double strand breaks, may be classified as a "catalytic inhibitor," while the azalactone ferrocene that induces formation of enzyme associated double strand breaks may be classified as "Topoisomerase II poison."

Affinity of azalactone ferrocene and thiomorpholide amido methyl ferrocene to calf thymus DNA

The DNA melting experiment was carried out at drug-to-nucleotide ratios of 1:10, 1:5, 1:2, and 1:1. The results show that both the compounds do not protect melting of calf thymus DNA, and hence are classified as non-DNA binding molecules (data not shown).

The mechanism of drug interaction with the enzyme

Since both the drugs do not bind to DNA and azalactone ferrocene can only induce the formation of cleavable complexes, we have investigated whether azalactone ferrocene binding to enzyme alone is adequate to account for its activity.

We have conducted two sets of experiments. In one set, the enzyme incubated with drug, and then the enzyme was immunoprecipitated and washed three times with TBS. The activity of the immunoprecipitated enzyme was assayed in the presence of supercoiled DNA using relaxation assay. The results presented in Fig. 5 at lanes 5 and 6 show that pretreatment of enzyme with azalactone ferrocene is indeed adequate for inhibition of catalytic activity of topoisomerase IIβ.

In the second set of experiments, the azalactone ferrocene was preincubated at 37 °C for 15 min and the drug concentration was reduced by diluting 10 times to bring below its inhibitory concentration. The diluted mixture containing DNA and drug was incubated with topoiso-

Panel A. Topoisomerase alpha.

Panel B. Topoisomerase beta.

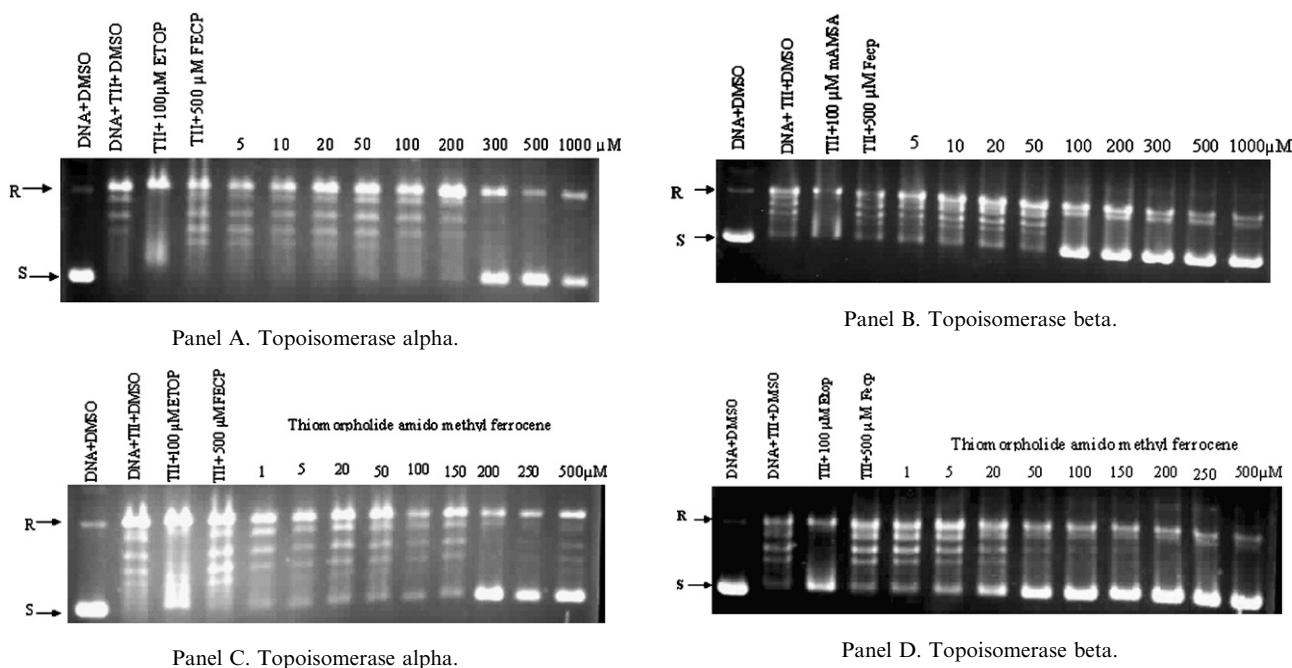Panel C. Topoisomerase alpha.

Panel D. Topoisomerase beta.

Fig. 3. Action of azalactone ferrocene and thiomorpholide amido methyl ferrocene on the catalytic activity of topoisomerase IIα isoform and β isoform: DNA relaxation activity of topoisomerase IIα or β was studied in presence of indicated concentrations of ferrocene derivatives. The relaxing DNA intermediates were separated on agarose gel and stained with ethidium bromide and photographed (S: supercoiled form, R: relaxed form). The data show the activity of azalactone ferrocene against topoisomerase IIα (A), topoisomerase IIβ (B), and the activity of thiomorpholide amido methyl ferrocene against topoisomerase IIα (C), and topoisomerase IIβ (D) as indicated.

merase IIβ and the relaxation assay was conducted. The results for lanes 7 and 8 presented in Fig. 5 show that the relaxation of DNA is not affected when DNA is pre-treated with the drug. This suggests that the drug does not form complexes with DNA, confirming our earlier results of DNA melting studies. These findings clearly show that azalactone ferrocene interacts with the enzyme and induces the formation of enzyme-linked cleavable complexes. Analysis of the interaction of these two compounds against topoisomerase IIα isoform also shows a similar mode of interactions observed with topoisomerase IIβ (data not shown).
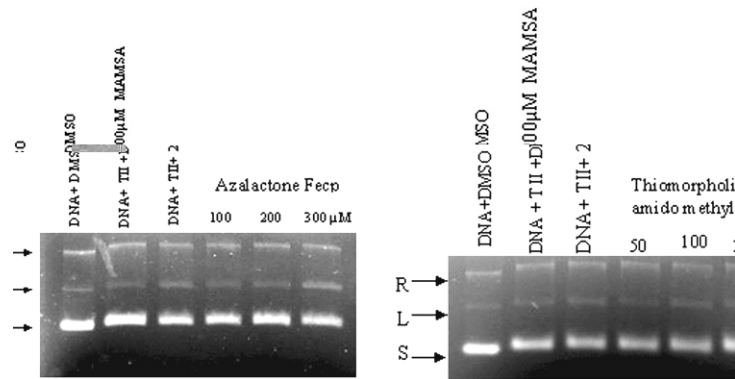
Action of thiomorpholide amido methyl ferrocene and azalactone ferrocene on DNA-dependent ATPase activity of the enzyme

The DNA-dependent ATPase activity of enzyme was monitored with increasing concentrations of thiomorpholide amido methyl ferrocene and azalactone ferrocene using spectrophotometric assay. The results (Fig. 6) show that both the compounds are potent inhibitors of DNA-dependent ATPase activity of enzyme. To further investigate whether the inhibition of ATPase activity of enzyme is due to competitive inhibition of ATP binding to the enzyme or due to the drug associated inhibition of DNA passage activity, we have carried out ATP binding experiments using $[\gamma\text{-}^{32}P]ATP$. In this experiment, the enzyme was incubated with

DNA and $[\gamma\text{-}^{32}P]ATP$ at increasing concentrations of the drug. The enzyme was immunoprecipitated and washed three times, and the amount of ATP bound in terms of incorporated ^{32}P was monitored in immunoprecipitated topoisomerase II. The results of these experiments showed that the ATP binding in terms of ^{32}P incorporation increased in a dose-dependent manner in the presence of increasing concentrations of azalactone ferrocene, while the thiomorpholide amido methyl ferrocene completely inhibited $[\gamma\text{-}^{32}]ATP$ incorporation into the enzyme. These results suggest that azalactone ferrocene binding do not competitively inhibit ATP and it will rather increase ATP binding in a concentration-dependent manner (data not shown). Thus, azalactone ferrocene may block DNA passage activity of enzyme leading to the formation of enzyme-linked cleavable complexes, while thiomorpholide amido methyl ferrocene inhibits catalytic activity of enzyme through blocking of ATP interaction with the enzyme.

Discussion

Topoisomerase IIα and β are known to be potential targets for the cancer chemotherapy [24–26]. The levels of topoisomerase IIα isoform were shown to be up-regulated in certain cancers, lung [27] ovarian [28], prostate [29], where as topoisomerase IIβ levels are up-regulated

Panel A. Topoisomerase II beta.
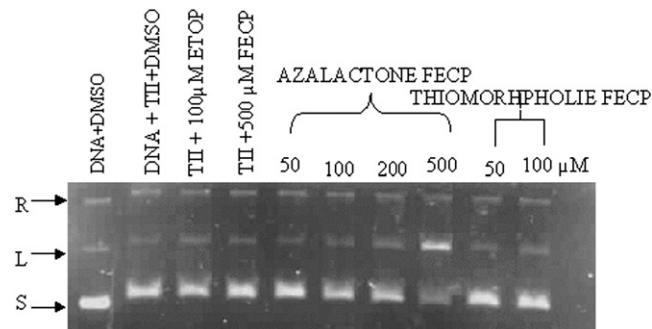
Panel B. Topoisomerase alpha.

Fig. 4. Azalactone ferrocene induces the formation of enzyme-linked cleavable complexes, while thiomorpholide amido methyl ferrocene does not. Cleavage assay was carried out using topoisomerase IIα isoform (A) and β isoform (B). The assay was done in the presence of indicated concentrations of azalactone ferrocene and thiomorpholide amido methyl ferrocene. The cleaved DNA intermediates were digested with Proteinase K, separated on agarose gel, stained with ethidium bromide, and photographed (S: supercoiled form, L: linear, R: relaxed form).
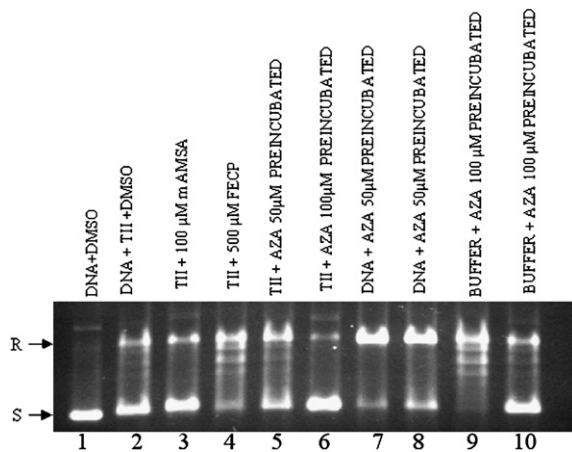

Fig. 5. Analysis of azalactone–Fecp interaction with protein and DNA. The assay was carried out at two concentrations of azalactone–Fecp 50 μM (non-inhibitory dose) and 100 μM (inhibitory dose). Azalactone–Fecp interaction with topoisomerase IIβ (TII) was assessed by pre-incubation of drug with enzyme followed by immunoprecipitation of enzyme using mouse anti-topoisomerase IIβ monoclonal antibody and the free drug is washed off, the activity of immunoprecipitated enzyme was assayed in presence of DNA as shown at lane #5 (50 μM) and #6 (100 μM). While azalactone–Fecp interaction with DNA was assessed by pre-incubation of drug with enzyme followed by 10-fold dilution of drug (to bring down drug to inactive dose), then the DNA relaxation activity was studied with topoisomerase IIβ as shown at lane #7 (50 μM) and #8 (100 μM).
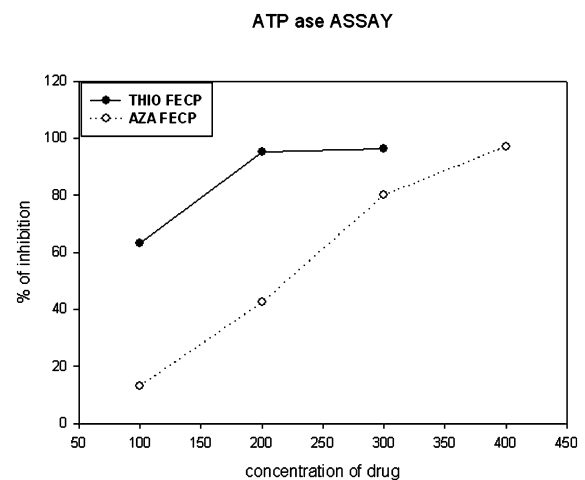

Fig. 6. Inhibition of DNA-dependent ATPase activity of topoisomerase II by azalactone ferrocene and thiomorpholide amido methyl ferrocene. ATPase assay was conducted using spectrophotometer method. ATP hydrolysis in the absence of drug was taken as 100% and the ATP hydrolysis in the presence of increasing concentrations of the drug was calculated and presented. Each data value is an average of three experiments.

in breast [30] and brain cancer [31]. This differential expression of topoisomerase II isoforms in different cancers prompted efforts towards development of topoisomerase II isoform-specific poisons or inhibitors for targeting against cancer tissue of interest.

XK469 was the first, topoisomerase IIβ-specific poison reported from screening of large library of various compounds [32], and it was found to poison the activity of topoisomerase IIβ. Other topoisomerase II poisons namely etoposide [10] and quinoline derivatives poison both the isoforms of the topoisomerase II. In the present study, we used QSAR methodology in finding topoisomerase IIβ-specific poisons from derivatives of ferrocene. The two active ferrocene derivatives, namely azalactone ferrocene and thiomorpholide amido methyl ferrocene, do not possess affinity to DNA. This could be due to the absence of a planar ring system that has been shown to be involved in DNA binding in other topoisomerase II inhibitors. Also, the caged iron is not directly available for DNA interaction. But the positive electrostatic potential induced by iron through cyclopentadiene ring may provide weak interaction of the ferrocene with the negatively charged phosphate backbone, when the ferrocene derivative interacts with the enzyme (Fig. 8).

The inhibition of topoisomerase IIβ isoform by thiomorpholide amido methyl ferrocene is higher than azalactone ferrocene. The action of thiomorpholide amido methyl ferrocene is found to be due to inhibition of

ATP–enzyme interaction without forming cleavable complexes, whereas the azalactone ferrocene allows ATP binding to the enzyme and induces the formation of cleavable complexes. Comparison of structure of XK469 with those of azalactone amido ferrocene and thiomorpholide amido methyl ferrocene shows that the latter possesses largely charged surfaces on the interacting face, as shown in Fig. 8. This may be one of the structural features that these compounds possess which might be enhancing their ability in topoisomerase IIβ interaction. The higher molecular volume containing hydrophobic groups may allow azalactone ferrocene in freezing enzyme–DNA covalent intermediates.

The comparison of structural features of these two compounds shows that the distance and orientation of the interacting atom of the substituent from iron cyclopentadiene ring may play a key role in modulating the activity of the drug (Figs. 7A and B). This analysis suggests that the orientation of interacting groups away from the ferrocene axis and above and below the plane of cyclopentadiene ring is important for affecting the activity of the enzyme. The difference between azalactone ferrocene and thiomorpholide amido methyl ferrocene in inducing cleavable complex could be due to the difference in orientation of the substituent, while the thiomorpholide amido methyl ferrocene orients towards the iron axis and lies in the plane of the second cyclopentadiene ring (Fig. 7B), the azalactone ferrocene
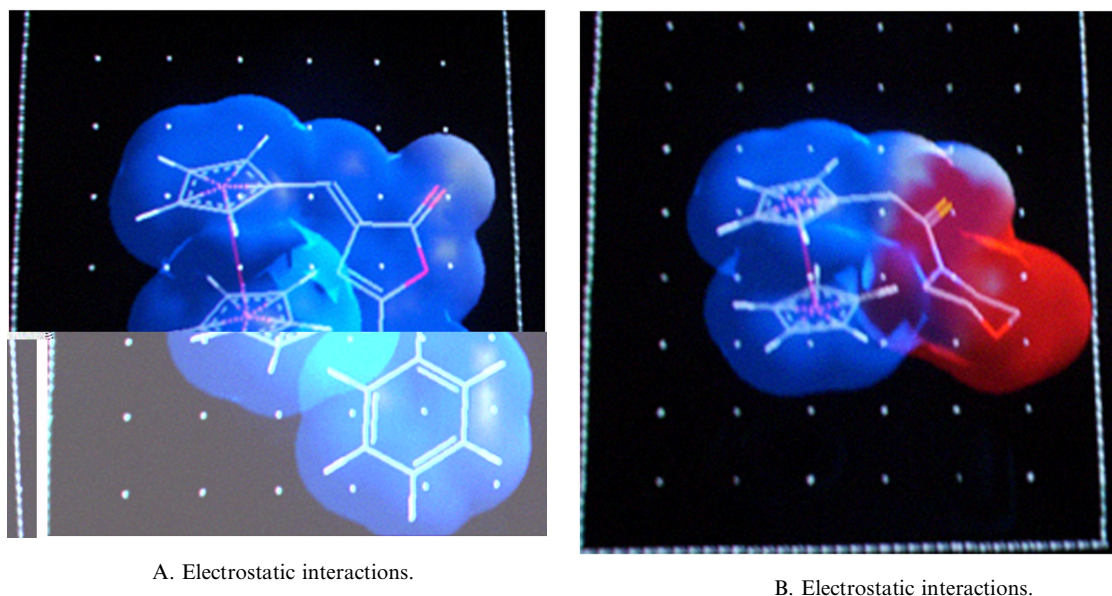

A. Electrostatic interactions.

B. Electrostatic interactions.

Fig. 7. (A) Azalactone ferrocene showing various receptor interactions. Receptor model for azalactone ferrocene was done using Accelrys cerius[2]. The surface with red area is negatively electrostatic potential, the blue area is positively electrostatic potential, and the white area is neutral potential. The positive electrostatic potential side chain of azalactone ferrocene may be forming bonding with negative electrostatic potential of the phosphate group exposed during catalytic assay and form cleavage complex. (B) Thiomorpholide amido methyl ferrocene showing various receptor interactions. The surface with red area is negatively electrostatic potential, the blue area is positively electrostatic potential, and the white area is neutral potential. The negative electrostatic potential side chain of the thiomorpholide amido methyl ferrocene (similar to ATP phosphate group which also have negative electrostatic potential group) may be forming linkage with the ATP binding site and inhibiting the reaction. (For the interpretation of the references to colour in this figure legend, the reader is referred to the web version of this paper.)
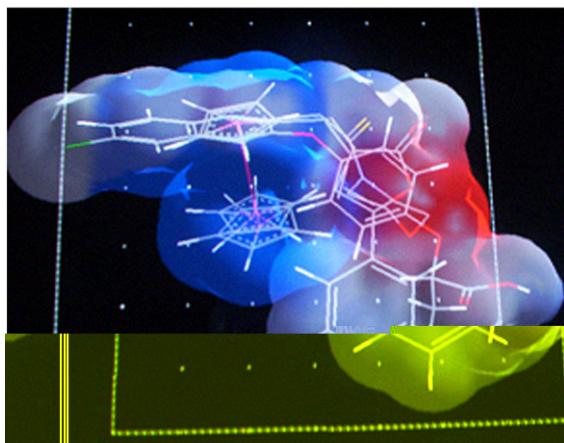
ELECTROSTATIC INTERACITONS

Fig. 8. The closely overlaid structures of the azalactone ferrocene and thiomorpholide amido methyl ferrocene, and XK469 showed conserved electrostatic features among these molecules that may be involved in topoisomerase IIβ interaction. The molecules are analyzed using the cerius^2 receptor module. Data shown are the various interactions of molecules with receptor. The surface with red area is negatively electrostatic potential, the blue area is positively electrostatic potential, and the white area is neutral potential. (For the interpretation of the references to colour in this figure legend, the reader is referred to the web version of this paper.)

moves away from the iron axis and lies above the substituted cyclopentadiene ring (Fig. 7A). These findings indicate that the structural requirement of ferrocene drugs for inhibition of catalytic activity of topoisomerase IIβ and substitutions away from iron axis may play a role in blocking the DNA passage activity of enzyme. In addition, substitution towards iron axis may be important in blocking ATP binding domain of the enzyme. Further analysis of a few more structurally distinct ferrocene derivatives may provide critical details of conformational molecular changes that ferrocene derivatives confer upon enzyme. In summary, both azalactone ferrocene and thiomorpholide amido methyl ferrocene are found to be potent inhibitors of topoisomerase II with preferential action against β isoform, and the two compounds show distinctly different modes of action against enzyme.

Acknowledgments

Appendix A. Supplementary material

Supplementary data associated with this article can be found, in the online version, at doi:10.1016/j.abb. 2005.04.014.

References

[1] E. Prosperi, E. Sala, C. Negri, R. Supino, G.B. Astraldi Ricotti, G. Bottiroli, Anticancer Res. 12 (1992) 2093–2099.

[2] W.C. Earnshaw, M.M.S. Heck, J. Cell Biol. 100 (1985) 1716–1725.

[3] W.C. Earnshaw, B. Hallifan, C.A. Cooke, M.M.S. Heck, L.F. Liu, J. Cell Biol. 100 (1985) 1706–1715.

[4] H. Turley, M. Comley, S. Houlbrook, N. Nozaki, A. Kikuchi, I.D. Hickson, K. Gatter, A.L. Harris, Br. J. Cancer. 75 (1997) 1340–1346.

[5] A.K. Kondapi, N. Mulpuri, R.K. Mandraju, B. Sasikaran, K. Subba Rao, Int. J. Dev. Neurosci. 22 (2004) 19–30.

[6] A.K. Larsen, A.E. Escargueil, A. Skladanowski, Pharmacol Ther. 99 (2003) 167–181.

[7] J.M. Berger, S.J. Gamblin, S.C. Harrison, J.C. Wang, Nature 379 (1996) 225–232.

[8] J. Roca, Trends Biochem. Sci. 20 (4) (1995) 156–160.

[9] G.L. Chen, T.C. Yang, T. Rowe, B.D. Halligan, K.M. Tewey, L.F. Liu, J. Biol. Chem. 259 (1984) 13560–13566.

[10] K. Drlica, R.J. Franco, Biochemistry 27 (1988) 2253–2259.

[11] M. Eric, K. Nelson, M. Tewey, L.F. Liu, Proc. Natl. Acad. Sci. USA 81 (1984) 1361–1365.

[12] Y.N. Vashisht gopal, D. Jayaraju, A.K. Kondapi, Biochemistry 38 (1999) 4382–4388.

[13] Y.N. Vashisht gopal, N. Konuru, A.K. Kondapi, Arch. Biochem. Biophys. 401 (2002) 53–62.

[14] Y.N. Vashist Gopal, D. Jayaraju, A.K. Kondapi, Arch. Biochem. Biophys. 376 (2000) 229–235.

[15] G.D. Broadhead, J.M. Osgerby, P.L. Pauson, J. Chem. Soc. 77 (1958) 650–656.

[16] J.M. Osgerby, P.L. Pauson, J. Chem. Soc. 77 (1958) 650–656.

[17] P.J. Graham, R.V. Lindsey, G.W. Parshall, M.L. Peterson, G.M. Whitman, J. Am. Chem. Soc. 79 (1957) 3416–3420.

[18] M.M. Bradford, Anal. Biochem. 72 (1976) 248–254.

[19] Cerius^2. A program suite for molecular modeling activities, Molecular Simulations, Scranton Road, Diego, USA.

[20] R.H. Rohrbaugh, P.C. Jurs, Anal. Chim. Acta 199 (1987) 99–109.

[21] N. Osheroff, E.R. Shelton, D.L. Brutlag, J. Biol. Chem. 258 (1983) 9536–9543.

[22] M.J. Robinson, N. Osheroff, Biochemistry 29 (1990) 2511–2515.

[23] D. Jayaraju, A.K. Kondapi, Curr. Sci. 81 (2001) 787–792.

[24] D.J. Fernandes, J. Qiu, C.V. Catapano, Adv. Enzyme Regul. 35 (1995) 265–281.

[25] H.U. Barthelmes, E. Niederberger, T. Roth, K. Schulte, W.C. Tang, F. Boege, H.H. Fiebig, G. Eisenbrand, D. Marko, Br. J. Cancer 85 (2001) 1585–1591.

[26] K. Park, J. Kim, S. Lim, S. Han, Eur. J. Cancer 39 (2003) 631–634.

[27] K. Kobayashi, M. Nishioka, T. Kohno, M. Nakamoto, A. Maeshima, K. Aoyagi, H. Sasaki, S. Takenoshita, H. Sugimura, J. Yokota, Oncogene 23 (17) (2004) 3089–3096.

[28] H. Brustmann, Gynecol. Oncol. 92 (1) (2004) 268–276.

[29] R.S. DiPaola, E.S. Chenven, W.J. Shih, Y. Lin, P. Amenta, S. Goodin, A. Shumate, T. Capanna, M. Cardiella, K.B. Cummings, J. Aisner, M.B. Todd, Cancer 92 (2001) 2065–2071.

[30] S. Houlbrook, C.M. Addison, S.L. Davies, J. Carmichael, I.J. Stratford, A.L. Harris, I.D. Hickson, Br. J. Cancer 74 (1996) 1154.

[31] L.A. Hazlehurst, N.E. Foley, M.C. Gleason-Guzman, M.P. Hacker, A.E. Cress, L.W. Greenberger, M.C. De Jong, W.S. Dalton, Cancer Res. 9 (5) (1999) 1021–1028.

[32] H. Gao, K.-C. Huang, E.F. Yamasaki, K.K. Chan, L. Chohan, R.M. Snapka, Proc. Natl. Acad. Sci. USA 96 (1999) 12168–12173.

[33] P.L. Pauson, W.E. Watts, J. Chem. Soc. (1962) 3880–3886.

[34] G. Wilkinson, F.A. Cotton, J.M. Biermaingham, J. Inorg. Nucl. Chem. 2 (1956) 95–99.

[35] J.P. Sevenair, D.H. Lewis, B.W. Ponder, J. Org. Chem. 37 (66) (1972) 4061–4063.

[36] R.A. Benkeser, D. Goffin, G. Schroll, J. Am. Chem. Soc. 76 (1954) 4025–4026.

[37] V.J. Weinmayr, J. Am. Chem. Soc. 77 (1955) 3009–3011.

[38] C.S. Combs, C. Ashmore, A.F. Bridges, C.R. Swanson., W.D. Stephens, J. Org. Chem. 34 (1969) 1511–1512.

[39] D.T. Roberts, W.F. Little, M.M. Bursey, J. Am. Chem. Soc. 79 (1957) 3420–3424.

[40] C.R. Hauser, J.K. Lindsay, J. Org. Chem. 22 (1957) 1246–1247.

[41] M.D. Rausch, J. Org. Chem. 26 (1961) 3579.

[42] D.J. Booth, B.W. Rockett, J. Chem. Soc., Section C (1968) 656–659.

[43] N. Weliky, E.S. Gould, J. Am. Chem. Soc. 79 (1957) 2742–2746.

A study of the Topoisomerase II activity in HIV-1 replication using the ferrocene derivatives as probes ☆

Anand K. Kondapi *, Nathamu Satyanarayana, A.D. Saikrishna

Department of Biochemistry, University of Hyderabad, School of Life Sciences, Hyderabad 500 046, India

Abstract

Human Topoisomerase II is present in two isoforms, 170 KDa α and 180 KDa β. Both the isoforms play a crucial role in maintenance of topological changes during DNA replication and recombination. It has been shown that Topoisomerase II activity is required for HIV-1 replication and the enzyme is phosphorylated during early time points of HIV-1 replication. In the present study, we have studied the molecular action of Topoisomerase II inhibitors, azalactone ferrocene (AzaFecp), Thiomorpholide amido methyl ferrocene (ThioFecp), and Ruthenium benzene amino pyridine (Ru(ben)Apy) on cell proliferation and also on various events of HIV-1 replication cycle. The Topoisomerase II β over-expressing neuroblastoma cell line shows a higher sensitivity to these compounds compared to the Sup-T1 cell line. All the three Topoisomerase II inhibitors show significant anti-HIV activity at nanomolar concentrations against an Indian isolate of HIV-$1_{93IN101}$ in Sup-T1 cell line. An analysis of action of these compounds on proviral DNA synthesis at 5 h of post-infection shows that they inhibit proviral DNA synthesis as well as the formation of pre-integration complexes completely. Further analysis, using polymerase chain reaction and western blot, showed that both the Topoisomerase II α and β isoforms are present in the pre-integration complexes, suggesting their significant role in HIV-1 replication.
© 2006 Elsevier Inc. All rights reserved.

Keywords: HIV infection; Topoisomerase II α; Topoisomerase II β; Proviral DNA; Organometallic compounds; Ferrocene derivatives; Ruthenium derivatives; Topoisomerase II poisons; Anti proliferation; Anti-HIV activity

Human Topoisomerase II is a ubiquitous enzyme present in two isoforms that are originated from two distinct genetic loci, a 170 KDa α isoform and a 180 KDa β isoform [1]. Both the isoforms exhibit similar molecular activities in vitro [2]. While the α isoform is known to play a crucial role in cell division [2], the exact function of β isoform is still not clear and is a subject of intense study. The localization studies of Topoisomerase II α and Topoisomerase II β in proliferating and non-proliferating tissues showed that the α isoform is predominantly present in replicating cells and β isoform is present in both the replicating and non-replicating cell types [3,4]. This suggests the dual functional role of β isoform in both the replicating and differentiated cells, in contrast to the function of the α isoform which is limited to replicating cells. Since retroviruses are shown to be replicating in both dividing and non-dividing cells [5–7], they form best model systems in understanding the function of Topoisomerase II α and β in these cell types. The activity of Topoisomerase II has been shown to be associated with the retroviral infections namely HIV-1[1] [8–10],

[1] *Abbreviations used:* Topo II, Topoisomerase II; PCR, polymerase chain reaction; p.i, HIV-1 post-infection period; PBS, phosphate-buffered saline; TBS, Tris buffer saline; SDS, sodium dodecyl sulphate; NBT, nitro blue tetrazoleum; BCIP, 5-bromo, 4-chloro 3-indolyl phosphate; AzaFecp, azalactone ferrocene; ThioFecp, thiomopholide amido methyl ferrocene; Ru(ben)Apy, [(η^6-benzene) (3-Aminopyridine)-N1-ruthenium (II)]; AZT, azidothymidine; HIV, human immunodeficiency virus; CMV, cytomegalo virus; MMLV, moloney murine leukemia virus.

MMLV [10,11], CMV [10,12,13], though the exact nature of molecular action of Topoisomerase II in replication cycle of these viruses is not clear.

Howard and Griffith [14] showed that the Topoisomerase II binding and cleavage sites are present both in HIV-1 viral genome as well as in Human genome at the upstream of HIV-1 integration site suggesting a potential interaction of Topoisomerase II at these sites of HIV-1 proviral DNA [5,15,16]. The down regulation of Topoisomerase II can decrease the HIV-1 replication suggesting the requirement of Topoisomerase II activity in HIV-1 replication [8,9]. Topoisomerase II undergoes phosphorylation during HIV-1 replication [9,17]. The virus itself is shown to be associated with Topoisomerase II α and β-specific kinase activity [17]. The main aim of the present study is to investigate the role of Topoisomerase II α and β in HIV-1 replication and evaluate the anti-HIV-1 potential of some of the Topoisomerase II β poisons. Accordingly in the present investigation, we have examined the molecular action of Topoisomerase II α and β poisons in progression of HIV-1 replication. The organometallic compounds may exhibit low frequency of resistance due to their irreversible binding to the biomacromolecules (DNA/protein). Hence, the organometallic compounds of Ferrocene were developed as potential Topoisomerase II poisons [18,19]. Amongst these compounds, we have chosen non-DNA binding Topoisomerase II β inhibitors from the class of substituted ferrocene, viz. azalactone ferrocene (AzaFecp), thiomorpholide amido methyl ferrocene (ThioFecp). AzaFecp can induce the formation of enzyme linked cleavable complexes, whereas ThioFecp can not induce the formation of enzyme linked cleavable complexes [19]. Thus, the action of Aza-Fecp and ThioFecp on the early events of HIV replication can probe the requirement of molecular activity of Topoisomerase II β during HIV-1 early replication cycle. Ru(ben)Apy shows preferential poisoning of the catalytic activity of Topoisomerase II α isoform [18]. Hence, its effect on the progression of HIV-1 replication could help inferring about the requirement of Topoisomerase II α isoform in HIV-1 replication cycle.

In the present investigation, we studied the inhibition activity of these compounds on the cellular proliferation as well as HIV-1 replication. We have also analyzed the action of these compounds on proviral DNA synthesis and the formation of pre-integration complexes. The results show that the molecular activity of both Topoisomerase II α and β isoforms is required in the progression of HIV-1 early replication events namely proviral DNA synthesis and pre-integration complex formation.

Materials and methods

Materials

The following reagents were obtained from AIDS Research and Reference Reagent Program, Division of AIDS, National Institute of Allergy and Infectious Dis-

eases, National Institutes of Health, USA. The contributor's name is given in parenthesis. Recombinant HIV-1$_{NL4-3}$ integrase (Dr. R. Craigie), SupT1 cell line (Dr. J. Hoxie). HIV-1 virus (subtype C), HIV-1$_{93IN101}$ (Dr. R. Bollinger), Anti-serum to HIV-1$_{NL4-3}$ Vpr (Dr. Jeffrey Kopp), HIV-1 RT Monoclonal Antibody (Dr. Stephen Hughes), pNL4-3 (Dr. Malcolm Mortin), SKNSH (Neuroblastoma), cell line was obtained from NCCS, Pune, India.

Mouse anti-human Topoisomerase II α and Mouse anti-human Topoisomerase II β were from BD biosciences. Protein A agarose was from Bangalore genei. India. The secondary antibodies were from US Biological.

Topoisomerase II inhibitors

Azalactone ferrocene (AzaFecp) and Thiomorpholide amido methyl ferrocene (ThioFecp) were synthesized and characterized as explained in Saikrishna et al. [19]. Ruthenium benzene amino pyridine (Ru(ben)Apy) was synthesized and characterized as described in [18]. Etoposide and azidothymdine (AZT) were purchased from Sigma Chemical Company.

Topoisomerase II activity assay

DNA relaxation by Topoisomerase II was performed as mentioned in Kondapi et al. [4]. About 0.6 mg of supercoiled plasmid DNA was incubated with the immunoprecipitated Topoisomerase II captured on to a Protein A Agarose beads in relaxation buffer (50 mM Tris–HCl, pH 8.0, 120 mM KCl, 0.5 mM EDTA, 0.5 mM DTT, 10 mM MgCl$_2$, 30 mg/ml BSA, and 1 mM ATP) for 30 min at 37 °C. The beads were spun down at 300g for 5 min and supernatants were collected separately. The reaction was stopped by addition of 10% SDS and the DNA products were resolved on 1% agarose gel and stained with ethidium bromide and photographed.

Anti-HIV activity

Anti-HIV activity was assayed out as explained in Kondapi et al. [20]. In brief, SupT-1 cells (0.2×10^6) in RPMI1640, 10%FCS was seeded in 96-well plate. Increasing concentrations of ferrocene derivatives were added to the cells and were challenged with HIV-1$_{93IN101}$ at a final concentration of 1 ng of p24 per ml. In one set, the infected cells were incubated at 37 °C for 96 h in a CO$_2$ incubator with 5%CO$_2$. In the second set, the virus and drug were incubated for 5 h and cells were washed twice and re-cultured in fresh medium without drug and virus and incubated for 96 h at 37 °C in a CO$_2$ incubator. The cells were analyzed for the viability using MTT as explained in the cytotoxicity assay. The supernatants were collected at 96 h post-infection and analyzed using p24 antigen capture assay kit (SAIC Frederic). The inhibition of infection, in the absence of the drug was considered to be 0% and the % inhibition of HIV replication was calculated based on this

control. Each compound was analyzed in triplicates at increasing concentrations on a logarithmic scale and standard deviation was also shown. In control infection study, in the absence of drugs, the virus replicated was 10 ng/ml of p24 equivalent. Azidothymidine (AZT) and Etoposide were used as positive controls.

Cytotoxicity assay

Reduction of 3-(4,5-dimethylthiozol-2-yl)-2,5-diphenyltetrazolium bromide (MTT, Sigma) is chosen as an optimal endpoint of cell viability measurement [21–23]. SupT-1 cells or Neuroblastoma (0.2×10^6 cells per well) in RPMI 1640, 10% FCS were seeded in 96-well plates. Increasing concentrations of compounds were added to the cells and incubated at 37 °C for 14 h in a CO_2 Incubator with 5% CO_2. The media was replaced with a fresh growth medium along with 20 μl of 3-(4,5-dimethylthiozol-2-yl)-2,5-diphenyltetrazolium bromide (MTT, Sigma). After incubation for 4 h in a humidified atmosphere, the media was removed and 200 μl of 0.1 N acidic isopropyl alcohol was added to the wells to dissolve the MTT-formazan crystals. The absorbance was recorded at 570 nm, immediately after the development of purple colour. Each experiment was conducted in triplicate and the data are represented as average, with standard deviation.

Preparation of cell extracts

Human SupT1 cells (2×10^6 cells per ml) were challenged with HIV-$1_{93IN101}$ (10 ng of p24 viral core protein per ml). Infected cells were washed twice with buffer A (20 mM Hepes, pH 7.4/150 mM KCl/5 mM $MgCl_2$/1 mM dithiothreitol/2 mM aprotinin) at 5 h p.i. and permeabilized with 0.025%Triton X-100. Cells were incubated for 10 min at room temperature, and then lysate was centrifuged at 1000*g* for 10 min at room temperature. The supernatant was clarified by centrifugation at 8000*g* for 3 min and was defined as "cytosolic fraction" [24–29]. Cytosolic extracts were frozen in 2 ml aliquots at −70 °C

Purification of pre-integration complexes

Pre-integration complexes (PICs) were purified as described earlier [28,30]. In brief, Crude cytosolic extracts were thawed and diluted with an equal volume of Buffer K (20 mM Hepes (pH 7.4), 5 mM $MgCl_2$, 1 mM DTT, and 10 U/ml aprotinin) to bring the KCl concentration to 75 mM (150 mM). The diluted extracts were incubated at room temperature for 10 min and then centrifuged at 2000*g* for 10 min. Under these conditions, more than 95 percent of PICs were pelleted. Pelleted complexes were resuspended in a volume equivalent to the original extract volume (before dilution) of Buffer K with Tris (pH 8.0), instead of Hepes and 30% glycerol. The purified PICs were frozen at −70 °C until they were used.

Isolation of proviral DNA

SupT1 cells (0.4×10^6) were challenged with HIV-$1_{93IN101}$ (100 pg of p24 viral core protein) in the presence of increasing concentrations of drugs as indicated at 5% CO_2 and 37 °C. The cells were harvested at 5 h. post-infection and washed with phosphate-buffered saline. They were then lysed with 50 μl lysis buffer containing 10× Solution A (1 M KCl, 100 mM Tris–HCl (pH 8.3), 2.5 mM $MgCl_2$), 10× Solution B (100 mM Tris–HCl (pH 8.3), 2.5 mM $MgCl_2$, 0.45% Tween 20, 0.45% Nonidet P 40, and 50 mM NaCl). The cell lysates were treated with RNaseI (10 μg/ml) and incubated at 37 °C for 30 min. Proteinase K (60 μg/ml) was added to the lysates and incubated at 56 °C for 2 h followed by the inactivation of Proteinase K at 95 °C for 10 min. The lysates were then stored at −20 °C, for their subsequent use for PCR analysis.

PCR analysis of proviral DNA

The Cell lysates were added to the 50 μl of reaction mixture comprising of 10× PCR buffer, 0.2 mM of each deoxynucleotide triphosphates (dNTPs), 2.5 mM $MgCl_2$, 0.40 μM SK38 (5′-ATAATCCACCTATCCCAGTAGGAGAAA T-3′), SK39 (5′-TTTGGTCCTTGTCTTATGTCCAGAA TGC-3′) primers [31] (Synthesized by Integrated DNA Technologies (IDT), USA) and 0.5 U of *Taq* DNA Polymerase (Biogene, USA) [31,32]. The mixtures were heated to 94 °C for denaturation for 2 min and then subjected to amplification for 30 cycles of PCR (1 min 94 °C, 1.30 min 60 °C, and 2 min 72°), and a final step for extension at 72 °C for 5 min. Control amplification was done using β-actin specific primers (Forward: 5′-GGCCCAGAGCAAGAG AGGTATCC-3′, Reverse-5′-ACGCACGATTTCCCTCT CAG C-3′) [33]. The products were resolved on 2% agarose gel electrophoresis, ethidium bromide stained, and photographed.

Analysis of pre-integration complexes

HIV-1 pre-integration complexes were immunoprecipitated [4,25,34,35] and amplified by PCR to know the effect of the drugs on the formation as well as to monitor the presence of various proteins in pre-integration complexes. Cell extracts were two fold diluted with the buffer K with 1% Triton X-100 and incubated at 37 °C for 1 h with 10 μl of each monoclonal antibody, Topoisomerase II α, Topoisomerase II β (Pharmingen group of Becton–Dickinson), HIV-1 RT, and Vpr anti-serum (1:100 ratio each) (NIH-AIDS Research and Reference Reagent program, USA). Protein A agarose (25 μl of 10 mg/ml stock), (Bangalore genei, India) was added to the samples and incubated at 4 °C for 15 min followed by centrifugation at 2000*g* for 5 min to precipitate the immunocomplexes. The beads were washed thrice with 0.5%Triton X-100 followed by digestion with Proteinase K (60 mg/ml) at 56 °C for one hour and inactivation at 94 °C for 15 min. The DNA in the extracts

was amplified using SK38, SK39 primers as described earlier.

Western blot analysis

Western blots were performed as described in Toubin et al. [36]. Pre-integration Complexes isolated from infected cells were boiled with buffer containing SDS and resolved on 7.5, 12% SDS–PAGE. The proteins on the gel were transferred to nitrocellulose membrane, then immunoblotted [37] with a 1 ng dilution of mouse anti-human Topoisomerase II α, β, HIV-1 RT monoclonal antibodies, and incubated with alkaline phosphatases (ALP) conjugated goat anti-mouse IgG antibody (1:2000 dilutions in TBS) for 60 min at room temperature and washed with TBS. The blots were developed with NBT-BCIP substrate in ALP buffer and documented.

Integrase catalyzed endonuclease assay

This assay was carried out as described in [38]. Endonuclease cleavage of heterologous DNA substrate was measured by monitoring the conversion of supercoiled (C) plasmid DNA to linear (L) DNA. Ten microliters of reaction mixture containing 0.2 µg of supercoiled DNA in a buffer containing 20 mM Tris–HCl (pH 8), 5 mM 2-mercaptoethanol, 2 mM $MnCl_2$, and 0.5 µg of integrase. The reaction was carried out in the absence as well as in the presence of 1 femto molar (fM) and 1 micro molar (1 µM) of drug. The reaction mixture was incubated for 30 min at 37 °C and reaction was stopped by the addition of 1 µl of 0.5 M EDTA plus 2 µl of 15% Ficoll 400 and 0.2% bromophenol blue in TAE buffer (40 mM Tris/20 mM acetic acid/1 mM EDTA). The DNA products were separated on 1% agarose gel and ethidium bromide stained and visualized under UV.

Results and discussion

Topoisomerase II α plays an important role in cellular proliferation, while the exact role of Topoisomerase II β is not yet clearly understood [3]. Interestingly in some cancer tissues, either the Topoisomerase II α isoform or the Topoisomerase II β isoform is predominantly up regulated [50], thus suggesting that the cell types in these tissues possess a distinct signaling process in organization of various cell division functions by corresponding isoform. Topoisomerase II poisons azalactone ferrocene (AzaFecp) and thiomorpholide amido methyl ferrocene (ThioFecp) show preferential inhibition against Topoisomerase II β [19], while etoposide show preferential inhibition against α isoform.

Since α and β isoforms are specifically expressed in different cancer tissues, they become important for selective application in cancer chemotherapy. The enzymatic activity and protein levels of Topo II α and β were analyzed in both neuroblastoma and SupT1 cell lines. The results showed that neuroblastoma cells expressed higher levels of Topo II β protein as seen in western blot analysis (Fig. 1A). In concurrence with the protein levels, a higher catalytic activity of Topo II β isoform was observed in neuroblastoma cells (Fig. 1B); the analysis of Topo II α and β isoforms in Sup T1 cells using western blot (Fig. 1C) show that these cells possess equal amounts of both the isoforms and these results were consistent with the corresponding levels of catalytic activity of these isoforms (Fig. 1D). Hence, the results of these studies suggest the enhanced expression of Topo II β in neuroblastoma cells, and an equal expression of Top II α and β in SupT1 cells. An analysis of anti-proliferation activity of AzaFecp and ThioFecp in both neuroblastoma and Sup-T1 cell lines show that Topoisomerase II β over-expressing neuroblastoma cell line is highly sensitive to both AzaFecp and ThioFecp (Fig. 2A), while Topoisomerase II α and β equally expressing cell line, namely the Sup-T1 cell line is comparatively less sensitive to both AzaFecp and ThioFecp, with more than 65% cells viable at 10nM concentration (Fig. 2B). Further, we observed that neuroblastoma is highly sensitive to Azidothymidine (AZT) (Fig. 2A).
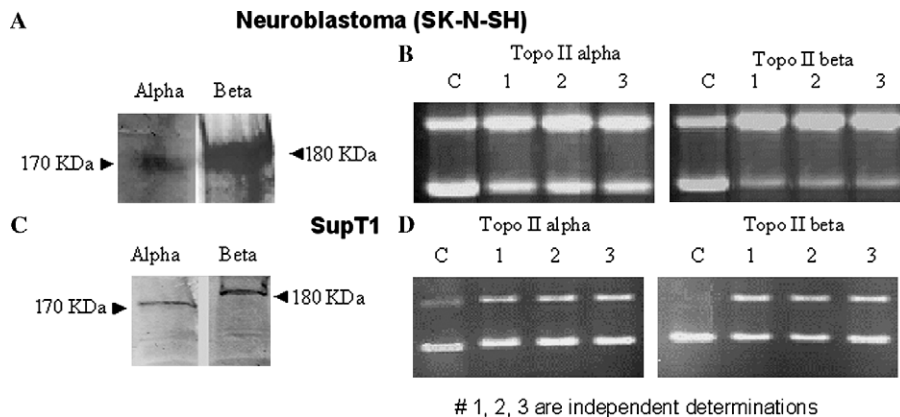

Fig. 1. Differential levels of protein and activity of Topoisomerase II α and β in neuroblastoma and SupT-1 cells. The protein levels were monitored in 100 µg of total protein using Western blot. Catalytic activity of Topo II isoform in 100 mg total protein was monitored by enzyme catalyzed relaxation of supercoiled pRYG DNA. (A) Western blot of SK-N-SH cell protein. (B) Relaxation assay of immunoprecipitated indicated Topo II isoform in SK-N-SH cell protein. (C) Western blot of Sup-T1 cell protein. (D) Relaxation assay of immunoprecipitated indicated Topo II isoform in Sup-T1 cell protein.
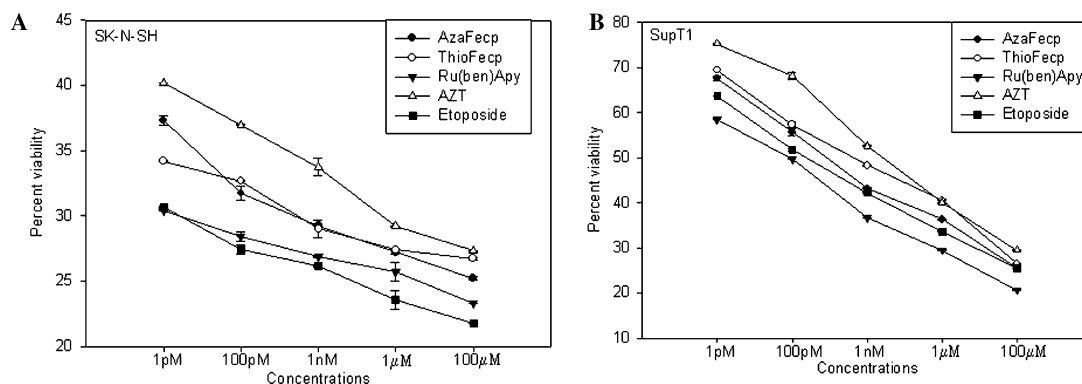
Fig. 2. Anti-proliferation activity of ferrocene derivatives: Neuroblastoma (A) and Sup-T1 (B) cells were incubated in presence of increasing concentrations of indicated inhibitors for 16 h and the cytotoxicity was determined by MTT assay. The cell viability is determined based on the control cells in absence of inhibitor.

Anti-HIV activity of AzaFecp and ThioFecp

Since AzaFecp and ThioFecp exhibit preferential Topoisomerase II β poisoning activity [19], these drugs may inhibit Topoisomerase II β associated viral replicative function. To test whether poisoning of Topoisomerase II β activity can inhibit HIV-1 viral replication, the HIV-1 infection was carried out in the presence of increasing concentrations of AzaFecp, ThioFecp, Ru(ben)Apy AZT, and Etoposide. The results show (Fig. 3A) that AzaFecp and ThioFecp and Ru(ben)Apy significantly inhibit HIV-1 replication even at nanomolar concentrations. Since the above infectivity assay involves incubation of compounds for 96 h, the cells were exposed to the cytotoxicity of the compounds during the time period. When we studied the cytotoxicity of these compounds against
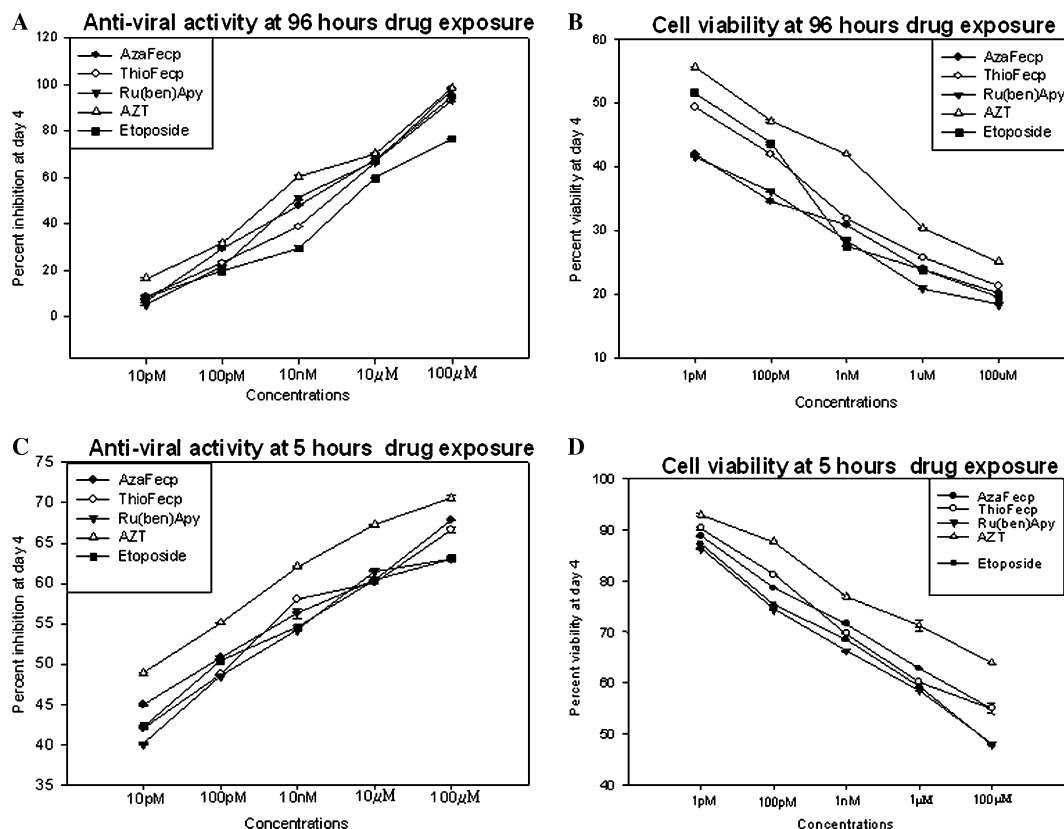

Fig. 3. Topoisomerase II inhibitors can affect HIV-1 replication. (A) Sup-T1 cells were challenged with HIV-1$_{93IN101}$ in presence of increasing concentrations of indicated inhibitors and the virus replicated on the day 4 was quantified. The control cells produced 10 ng/ml equivalent of HIV-1 p24. The percent of inhibition was calculated and plotted on *Y* axis and indicated concentrations of compounds on the *X* axis. (B) The viability of infected cells when they were incubated with the inhibitors for 96 h. (C) The infection was conducted at increasing concentrations of indicated inhibitors for 5 h. After 5 h the cells were washed twice and re-cultured in complete medium without inhibitor and virus. The amount of virus replicated at Day 4 was quantified and % inhibition was calculated based on the virus replicated in the absence of inhibitors, which was 11.6 ng/ml of p24 equivalent. The viability of the same cells was monitored using MTT assay and given in (D).

infected and non-infected cells at 96 h, we found that these compounds are 50% cytotoxic to the cells (Fig. 3B). Hence, the observed anti-viral activity in Fig. 3A may have cytotoxicity component in addition to the ability of the compounds in inhibition of proviral DNA synthesis. To address this problem we have incubated the cells with the virus and inhibitors for a period of 5 h (over 5 h of post-infection the proviral DNA is shown to be synthesized). Then, the cells were washed twice and re-cultured in fresh complete medium without virus and medium. The amount of virus replicated at 96 hours was quantified and results presented in Fig. 3C, show that exposure of compounds to the virus for 5 h is adequate for the significant anti-HIV activity. Further, the analysis of cytotoxicity of

these inhibitors in the infection conducted for 5 h exposure, cells showed ~20% cytotoxicity (Fig. 3D). These results infer that the inhibition of Topo II α and β catalytic activity may block proviral DNA synthesis and inhibit HIV-1 replication. A specific targeting of inhibitors to the HIV-1 infected cells can help in reducing the drug induced cytotoxicity to the uninfected cells.

Action of Topoisomerase II β poisons on HIV-1 proviral DNA formation

Topoisomerase II promotes inter-conversion of various topological isoforms of nucleic acids in maintaining the torsional integrity and thermodynamic stability of nucleic acid
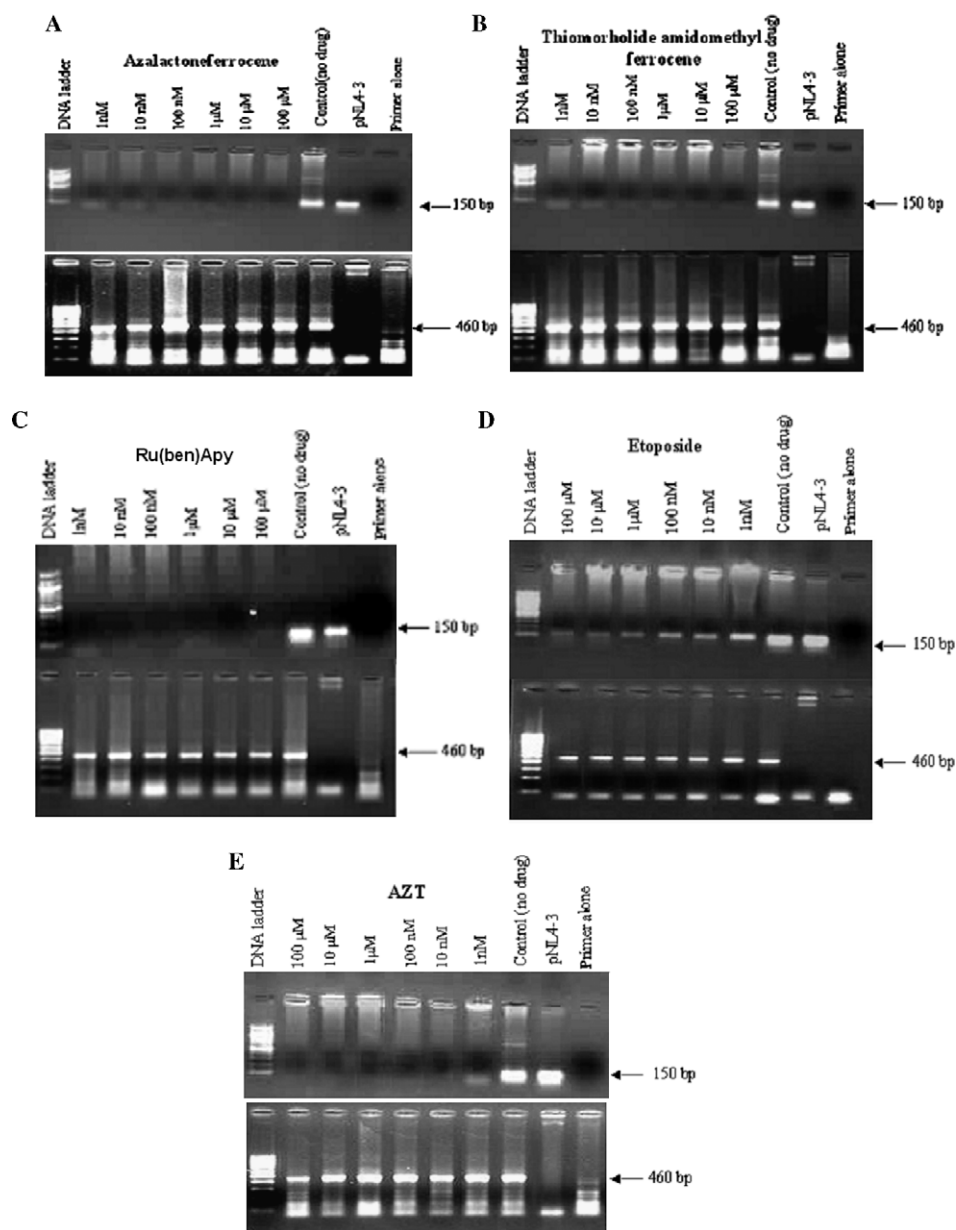

Fig. 4. Topoisomerase II inhibitors interfere with HIV-1 proviral DNA formation. (A–E) HIV-1 infection was conducted in presence of increasing concentrations of indicated inhibitors. The infection was stopped at 5 h post-infection, the proviral DNA was purified and analyzed by PCR using gag-specific primers, SK38 and SK39. Bottom gel in (A–E) indicates the PCR amplification for β-actin as loading control.

intermediates [51]. Such nucleic acid intermediates reported to be transiently formed during the course of HIV-1 early replication cycle [52]. The resolution of such viral nucleic acid topological intermediates may be promoted by Topoisomerase II isoforms. Since the proviral DNA is the stable intermediate formed during HIV-1 replication, we have studied the action of Topoisomerase II α and β poisoning on the formation of the proviral DNA. Results of analysis at 5 h post-infection in the presence of increasing concentrations of Topoisomerase II inhibitors show (Fig. 4) that Topoisomerase II β preferential poisons AzaFecp (Fig. 4A), ThioFecp (Fig. 4B) and Topo II α poison Ru(ben)Apy (Fig. 4C) produce significant inhibition of proviral DNA synthesis at drug concentrations as low as 1 nM, while the etoposide shows comparatively lower inhibition of proviral DNA synthesis (Fig. 4D). These observations suggest a strong association of Topoisomerase II α and β with the formation and stabilization of proviral
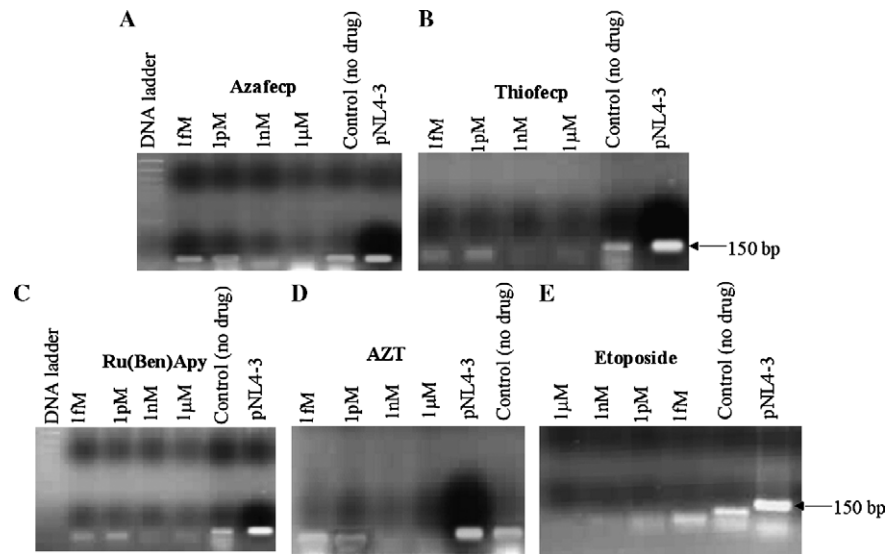

Fig. 5. Topoisomerase II α inhibition can block the formation of pre-integration complexes. HIV-1 infection was carried out in presence of increasing concentrations (as indicated) of AzaFecp (A), ThioFecp (B), Ru(Ben)Apy (C), Etoposide (E), and AZT (D). The pre-integration complexes were isolated from cytosolic fraction and were immunoprecipitated with mouse anti-human Topoisomerase II α monoclonal antibody. The proviral DNA in the immunoprecipitate was PCR amplified using gag-specific primers followed by resolution on 2% Agarose gel electrophoresis. Ethidium bromide stained and photographed under UV.
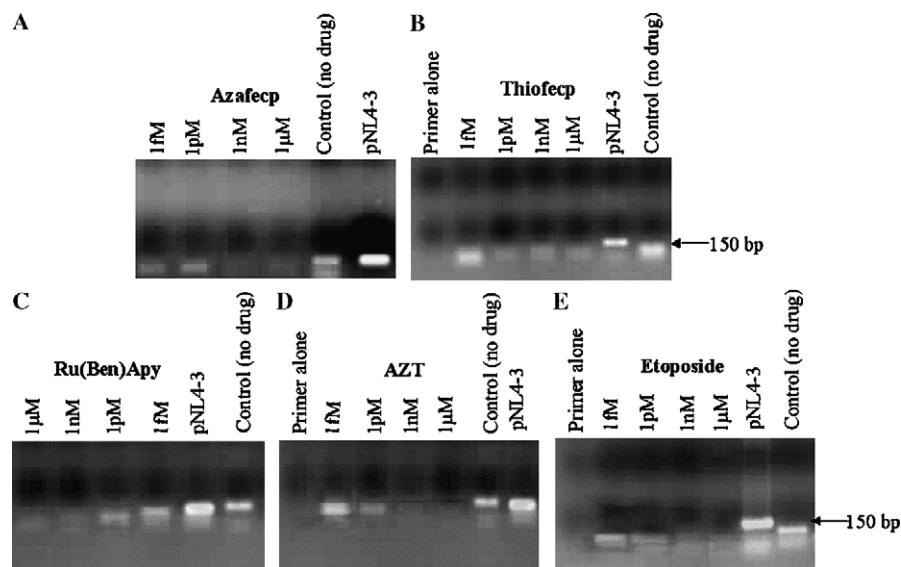

Fig. 6. Topoisomerase II β inhibition can block the formation of pre-integration complexes. HIV-1 infection was carried out in presence of increasing concentrations (as indicated) of AzaFecp (A), ThioFecp (B), Ru(Ben)Apy (C), Etoposide (E), and AZT (D). The pre-integration complexes were isolated from cytosolic fraction and were immunoprecipitated with mouse anti-human Topoisomerase II β monoclonal antibody. The proviral DNA in the immunoprecipitate was PCR amplified using gag-specific primers followed by resolution on 2% Agarose gel electrophoresis. Ethidium bromide stained and photographed under UV.

DNA synthesis and the importance of Topoisomerase II α as well as β poisons as inhibitors to interfere with HIV-1 early replication.

Association of Topoisomerase II α and β isoforms with pre-integration complex

The HIV-1 infection was conducted in the presence of increasing concentrations of drugs for 5 h and the cytosolic fraction of cells was fractionated. The pre-integration complexes (PICs) in the cytosolic fraction were isolated and immunoprecipitated using mouse anti-human Topoisomerase II α as well as Topoisomerase II β. The proviral DNA in immunoprecipitated PICs was analyzed by amplification of gag region. The results show that AzaFecp, ThioFecp, Ru(ben)Apy, and etoposide can inhibit the association of Topoisomerase alpha (Fig. 5) as well as Topoisomerase II β

(Fig. 6) isoforms in pre-integration complexes. This suggests that ferrocene derivatives can be used to inhibit the catalytic activity of Topoisomerase II α and β and their association with the formation of proviral DNA synthesis and pre-integration complexes. The inhibition of pre-integration complex formation could also be attributed to the reduced/inhibited proviral DNA intermediate in the presence of the inhibitor.

To further confirm whether proviral DNA is associated with both Topoisomerase II α and β to form pre-integration complexes, the infection was conducted in the absence of inhibitors. The isolated pre-integration complexes were immunoprecipitated with antibodies against Topoisomerase II α, Topoisomerase II β, Reverse Transcriptase, and Vpr. The immunoprecipitates were PCR analyzed for the proviral DNA to assess its association with the corresponding antigens. The results showed (Fig. 7A) that the proviral
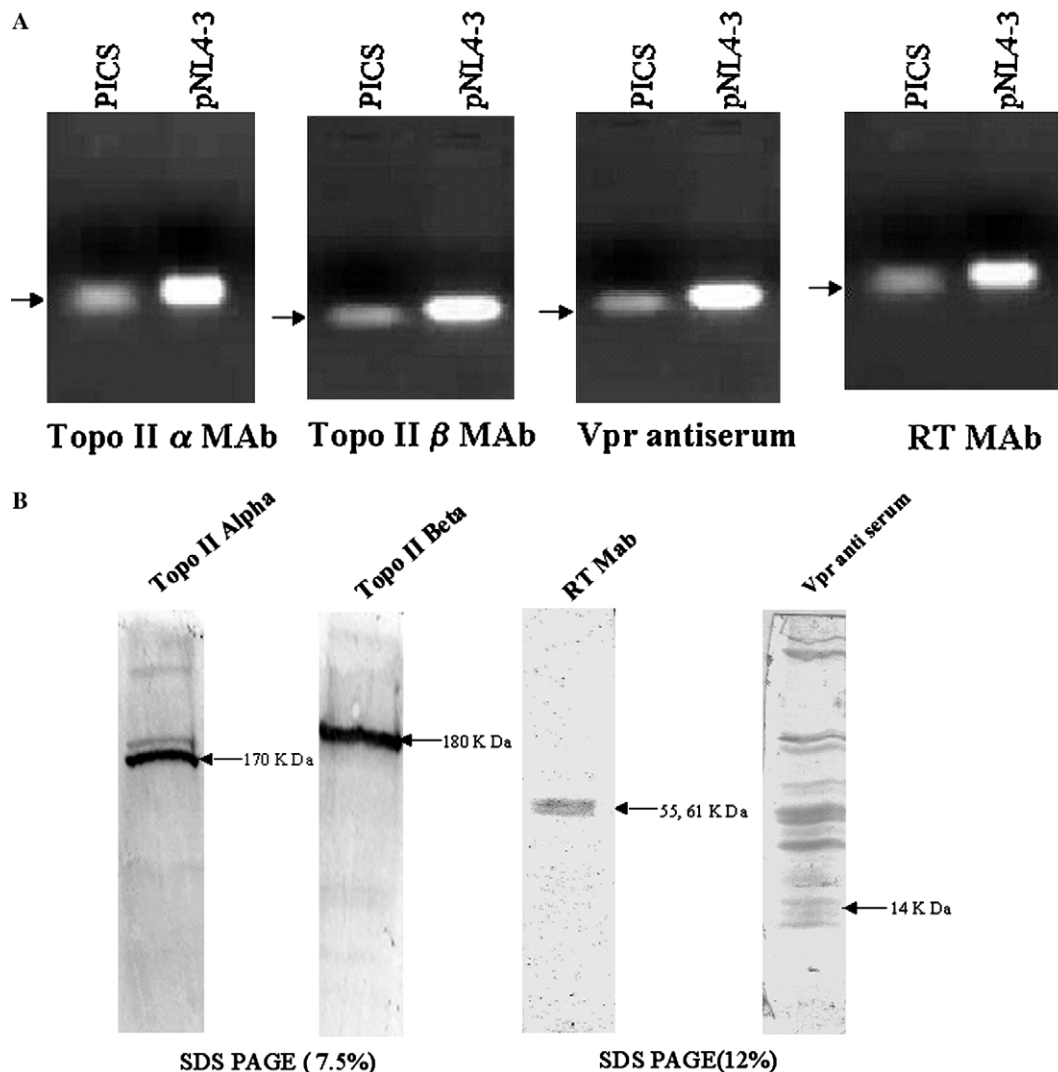

Fig. 7. Topoisomerase II isoforms are associated with pre-integration complexes. The pre-integration complexes were isolated from cytosolic fraction of 5 h HIV-1 infected cells. (A) Pre-integration complexes were immunoprecipitated with indicated antibody, washed and proteinase K treated. The proviral DNA was analyzed with gag-specific primers. An arrow indicates the amplified product of 150 bp. (B) The pre-integration complexes were boiled with buffer containing SDS and proteins were analyzed on SDS–PAGE and western transferred and probed using indicated antibodies. Since Vpr was analyzed with an anti-serum, may have some non-specificity, hence multiple proteins developed in pre-integration complexes, this clearly show the presence of other proteins in pre-integration complexes. Vpr and RT were used as positive controls.

DNA was present in the immunoprecipitates of pre-integration complexes. The results suggest that both Topoisomerase α and β are associated with the pre-integration complexes along with the reverse transcriptase and Vpr. Results of analysis of the isolated pre-integration complexes by western blot (Fig. 7B), confirm the presence of both the isoforms of Topoisomerase II. Reverse transcriptase and Vpr were used as positive controls in this study. Similar results were reported for the association of reverse transcriptase and other cellular and viral factors in pre-integration complexes [29,34,39].

The possibility of molecular action of these Ferrocene derivatives on the catalytic activity of HIV-1 integrase was studied by monitoring the endonuclease activity of recombinant HIV-1 integrase in the presence of these inhibitors. The results shown in (Fig. 8) suggest that the Topoisomerase II inhibitors used in the study do not interfere with the integrase catalyzed endonuclease activity against pBR322 supercoiled DNA. This indicate that the inhibition of proviral DNA synthesis and the formation of pre-integration complexes were only due to their action on the catalytic activity of Topoisomerase II, but not due to their non-specific action on HIV-1 integrase.

These observations conclusively show that both Topoisomerase II α and Topoisomerase II β are indeed associated with pre-integration complexes. Further studies are warranted to understand the exact nature of molecular function of Topoisomerase II isoforms in the formation and stabilization of pre-integration complex and proviral DNA rearrangements in cytosol and nuclei of the infected cells.

HIV-1 nucleic acid replication involves reverse transcription during which HIV-1 RNA is converted into the proviral DNA [40,41]. During reverse transcriptase catalyzed synthesis of DNA from single stranded RNA molecule, the LTR may be formed either through rearrangement of U3, R, U5 or by reverse transcriptase upward movement to form U3–R–U5 [28,42–45]. The rearrangements of the newly formed proviral DNA intermediates would encounter certain topological restrictions that need to be removed to maintain the thermodynamic stability of the proviral DNA. Such a stability of double stranded DNA can be provided by DNA Topoisomerase II isoforms. Based on our earlier findings on the activation of Topoisomerase II β during early time-points of HIV-1 post-infection [17] as well as the results of the present study, we propose that Topoisomerase II β activity may be required to maintain the stability of the proviral DNA during its formation from viral RNA. The proviral DNA formed may undergo an entanglement during proviral DNA synthesis and the formation of pre-integration complexes by the bound host and viral factors. Such entanglements or torsional stresses are required to be resolved and removed continuously so as to keep the ~10 kbp proviral DNA in pre-integration complexes stable against the strand breakage. Results of the present study, (1) Blockage of proviral DNA formation in presence of Topoisomerase II poisons/inhibitors; (2) Inhibition of pre-integration complex formation by poisoning of Topoisomerase II β; (3) The association of both the isoforms of Topoisomerase II with pre-integration complexes, point out that the DNA Topoisomerase II isoforms associated with pre-integration complexes may be involved in maintenance of the torsional integrity of proviral DNA in pre-integration complexes, to stabilize the DNA during its translocation to nucleus. The presence of both isoforms poses intriguing questions about the distinct activity of the individual isoforms in the pre-integration complexes and other DNA rearrangements reported [34,43,44,46–48]. Thus both the isoforms of Topoisomerase II could be potential targets for inhibition of HIV early replication events.
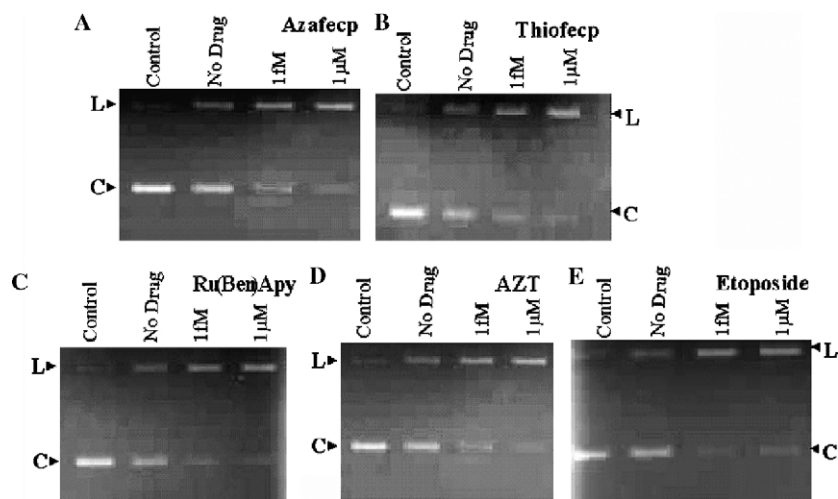

Fig. 8. Topoisomerase II inhibitors did not interfere catalytic activity of HIV-1 integrase. The DNA endonuclease activity of the recombinant integrase was monitored using supercoiled pBR 322 (indicated as C) in the presence of AzaFecp (A), ThioFecp (B), Ru(Ben)Apy (C), AZT (D), and etoposide (E). The cleaved DNA product (indicated as L) was resolved on 1% agarose gel electrophoresis and ethidium bromide stained and photographed under UV.

The novel strategies to interfere with pre- and post-integration steps of viral replication [49] clearly point out that the viral entry, viral reverse transcription and transcription, pre-integration complex formation, nuclear export, viral assembly, and maturation as potential targets for control of HIV-1 replication. The present investigation suggests proviral DNA as a potential target through poisoning of Topoiosmerase II isoforms to inhibit viral replication.

Acknowledgments

Appendix A. Supplementary data

Supplementary data associated with this article can be found, in the online version, at doi:10.1016/j.abb.2006.04.003.

References

[1] M. Tsai-Pflugfelder, L.F. Liu, A.A. Liu, K.M. Tewey, J. Whang-Peng, T. Knutson, K. Huebner, C.M. Croce, J.C. Wang, Proc. Natl. Acad. Sci. USA 19 (1988) 7177–7181.
[2] P.E. Warburton, W.C. Earnshaw, BioEssays 19 (1997) 97.
[3] K.N. Meyer, E. Kjeldren, T. Straub, B.K. Knudsen, A. Kikuchi, I.D. Hickson, H. Kreipe, F. Beoge, J. Cell Biol. 136 (1997) 775–778.
[4] A.K. Kondapi, N. Mulpuri, R.K. Mandraju, B. Sasikaran, K. Subba Rao, Int. J. Dev. Neurosci. 22 (2004) 19–30.
[5] H. Rohdewohld, H. Weiber, W. Reik, R. Jaenisch, M. Breindl, J. Virol. 61 (1987) 336–343.
[6] C. Cartier, B. Hemonnot, B. Gay, M. Bardy, C. Sanchiz, C. Devaux, L. Briant, J. Biol. Chem. 278 (2003) 35211–35219.
[7] E. Devroe, P.A. Silver, A. Engelman, Virology 331 (2005) 181–189.
[8] P. Bouielle, F. Subra, J.F. Mouscadet, C. Auclair, J. Mol. Biol. 285 (1999) 945–954.
[9] E. Mathes, P. Langer, H. Brachwitz, H.C. Schrader, A. Maidhof, B.E. Weiler, K. Renneisen, W.E. Muller, Antiviral Res. 13 (1990) 273–286.
[10] A. Cereseti, M. Giacca, AIDS Rev. 6 (2004) 13–21.
[11] C.N. Johnson, L.S. Levy, Virology 2 (2005) 68.
[12] J.D. Benson, E.S. Huang, J. Virol. 64 (1990) 9–15.
[13] E.S. Huang, J.D. Benson, S.M. Huang, B. Wilson, C. van der Horst, Antiviral Res. 17 (1992) 17–32.
[14] M.T. Howard, J.D. Griffith, J. Mol. Biol. 232 (1993) 1060–1068.
[15] Y. Pommier, B. Paddenvin, M. Gupta, J. Jenkins, Biochem. Biophys. Res. Commun. 205 (1994) 1601–1609.
[16] M. Stevenson, T.L. Stanwick, M.P. Dempsy, C.A. Lamonica, EMBO J. 9 (1990) 1551–1560.
[17] A.K. Kondapi, G. Padmaja, N. Satyanarayana, R. Mukhopadyaya, M.S. Reitz, Arch. Biochem. Biophys. 441 (2005) 41–55.
[18] Y.N.V. Gopal, N. Konuru, A.K. Kondapi, Arch. Biochem. Biophys. 401 (2002) 53–62.
[19] A.D. Sai Krishna, G. Panda, A.K. Kondapi, Arch. Biochem. Biophys. 438 (2005) 206–216.
[20] A.K. Kondapi, M.A. Hafiz, T. Sivaram, Antiviral Res. 54 (2002) 47–57.
[21] T. Mosmann, J. Immunol. Methods 65 (1983) 55–63.
[22] S.P.C. Cole, Cancer Chemother. Pharmacol. 17 (1986) 259–263.
[23] M.C. Alley, D.A. Scudiero, A. Monks, M.L. Hursey, M.J. Czerwiniski, D.L. Fine, B.J. Abbot, J.G. Mayo, R.H. Shoemaker, M.R. Boyd, Cancer Res. 48 (1988) 589–601.
[24] F. Lejbkowicz, C. Goyer, A. Darveau, S. Neron, R. Lemieux, Proc. Natl. Acad. Sci. USA 89 (1992) 9612–9616.
[25] Y.L. Lu, P. Spearman, L. Ratner, J. Virol. 67 (1993) 6542–6550.
[26] P.O. Brown, B.H. Bowerman, H.E. Varmus, J.M. Bishop, Cell 49 (1987) 347–356.
[27] C.M. Farnet, W.A. Haseltine, Proc. Natl. Acad. Sci. USA 87 (1990) 4164–4168.
[28] C.M. Farnet, B. Wang, J.R. Lipford, F.D. Bushman, Proc. Natl. Acad. Sci. USA 93 (1996) 9742–9747.
[29] M. Bukrinsky, N. Sharova, T.L. McDonald, T. Pushkarskaya, W.G. Tarpley, M. Stevenson, Proc. Natl. Acad. Sci. USA 93 (1993) 6125–6129.
[30] T. Fujiwara, K. Muzuuchi, Cell 54 (1988) 497–504.
[31] R.K. Saiki, D.H. Gelfand, S. Stoffel, S.J. Scharf, R. Higuchi, G.T. Horn, K.B. Mullis, H.A. Erlich, Science 239 (1988) 487–491.
[32] S. Sonza, A. Maerz, N.Deacon.J. Meanger, J. Mills, S. Crowe, J. Virol. 70 (1996) 3863–3869.
[33] K.Y. Kwan, J.C. Wang, Proc. Natl. Acad. Sci. USA 98 (2001) 5717–5721.
[34] C.M. Farnet, W.A. Haseltine, J. Virol. 65 (1991) 1910–1915.
[35] K. Hansen, L. Rönnstand, L. Claesson-welsh, H. Carl-henrik, FEBS Lett. 409 (1997) 195–200.
[36] H. Towbin, J.S. Staehelin, J. Gordon, Proc. Natl. Acad. Sci. USA 76 (1979) 4350–4354.
[37] A. Lazaris-Karatzas, K.S. Montine, N. Sonenberg, Nature (London) 345 (1990) 544–547.
[38] P.A. Sherman, J.A. Fyfe, Proc. Natl. Acad. Sci. USA 87 (1990) 5119–5123.
[39] M.J. Tremblay, J.F. Fortin, R. Cantin, Immunol. Today 19 (1998) 346–351.
[40] J. Zack, S.J. Arrigo, S.R. Weitsman, A.S. Go, A. Haislip, I.S.Y. Chen, Cell 61 (1990) 213–222.
[41] J.M. Coffin, Retroviruses and their replication, in: Fields, Knipe (Eds.), Virology, Rever press, NY, 1990, pp. 645–708.
[42] M. Negroni, H. Buc, Annu. Rev. Genet. 35 (2001) 275–302.
[43] M. Götte, X. Li, M.A. Wainberg, Arch. Biochem. Biophys. 365 (1999) 199–210.
[44] M.D. Miller, C.M. Farnet, F.D. Bushman, J. Virol. 71 (1997) 5382–5390.
[45] W.-S. Hu, M.T. Howard, Science 250 (1990) 1227–1233.
[46] B. Berkhout, J.V. Wamel, B. Klaver, J. Mol. Biol. 252 (1995) 59–69.
[47] S. Zennou, C. Petit, D. Guetard, U. Nerhbass, L. Montegnier, P. Charneau, Cell 101 (2000) 173–185.
[48] Y. Wu, Retrovirology 1 (2004) 13.
[49] M.H. Nielsen, F.S. Pedersen, J. Kjems, Retrovirology 2 (2005) 10.
[50] M.I. Sandri, D. Hochhauser, P. Ayton, R.C. Camplejohn, R. Whitehouse, H. Turley, K. Gatter, I.D. Hickson, A.L. Harris, Br. J. Cancer 73 (1996) 1518–1524.
[51] A.V. Vologodskii, W. Zhang, V.V. Rybenkov, A.A. Podtelezhnikov, D. Subramanian, J.D. Griffith, N.R. Cozzarelli, Proc. Natl. Acad. Sci. USA 98 (2001) 3045–3049.
[52] J.M. Kilzer, T. Stracker, B. Beitzel, K. Meek, M. Weitzman, F.D. Bushman, Virology 314 (2003) 460–467.